The Feasibility of Traffic Data Collection Using Satellite Imagery

Mark R. McCord
Department of Civil Engineering

Carolyn J. Merry
Department of Civil Engineering

John D. Bossler
Center for Mapping

The Ohio State University

Prepared for:
Federal Highway Administration
Washington, D.C.

under ODOT Agreement No. 6952

Final Report

Research Foundation Project 769863/726108

April 1995

TABLE OF CONTENTS

Page

APPENDICES

ILLUSTRATIONS

Figure

TABLES

Table

Executive Summary

Purpose

The decrease of international tensions due to recent geopolitical events brings with it the potential for decreased restrictions on civilian satellite data. Civilian satellite imagery is presently restricted to 10 m resolution or coarser. However, missions are being designed now to fly at 1 m resolution. Technologically, these resolutions are already feasible. At the same time, three issues – the demands on traffic data collection that are being imposed by economic and safety considerations and recent legislation (e.g., the Clean Air Act Amendments of 1990), the flexibility that is being encouraged in the general transportation field by the Intermodal Surface Transportation Efficiency Act (ISTEA), and the vision that is being promoted in the Intelligent Vehicle/Highway Systems (IVHS), now Intelligent Transportation Systems (ITS) efforts – raise the question of the potential for complementing existing traffic data collection programs with satellite data.

Evaluating and monitoring traffic characteristics is becoming increasingly important as worsening congestion, declining economic situations, and increasing environmental sensitivities are forcing states and municipalities to make better use of existing roadway capacities. There is no doubt that a large shift has occurred from adding more roadways and facilities to one of maximizing the use of existing facilities with improved and more comprehensive management techniques. Likewise, the upgrading and maintenance of existing infrastructures are growing concerns, since much of the infrastructure is nearing, or even past, time for repair and replacement. In addition, the Clean Air Act Amendments requires states and municipalities to conduct before and after project measurements of traffic parameters, and to do so at finer spatial levels than are currently required. Other specific needs for a continual gathering of traffic data include: (1) inputs to traffic and pavement deterioration models for highway management and maintenance programs, (2) better surveillance of the roadways to satisfy federal requirements to monitor compliance with speed limits, which is an ongoing task because of increasing concerns with clean air, safety and litigation, and (3) better estimates of volume-delay functions at specific sites because of increasing problems with capacity/congestion management.

The present system of using automatic counters at selected points on highways works well from a temporal point of view (i.e., during a specific period of time at one location). However, the present system does not cover the spatial aspects of the entire road system (i.e., for every location during specific periods of time); the counters are employed only at *points* and only on *selected* highways. This lack of spatial coverage is due, in part, to the cost of the automatic counter systems (fixed procurement and maintenance costs) and of the personnel required to deploy them, and is evidenced by the fact that of Ohio's 112,000 miles of roadway by example, there are only 200 detectors located along these roads. This same type of problem is also present in other states.

The current procedure is believed to work fairly well in the aggregate mode, at the macro level (U.S. coverage). However, at the micro level (state and local), the numbers are more suspect. In addition, the statistics only work when assuming a certain homogeneity among characteristics (trucks, volumes, speed limit adherence) of highways in the same class, an assumption that is impossible to test when little or no data is gathered on many of the highways for a given class.

Given these observations, it is clear that a remote sensing system to include improved spatial coverage and resolution would complement the existing system. Synoptic coverage provided by a satellite would be worth exploring. Satellite information would allow more coverage of a region and provide improved estimates at more disaggregate levels. If a satellite could provide repetitive coverage for a wide swath area, while counters are providing temporal data on vehicle movement, the spatial coverage of the existing system might be greatly improved. For example, satellite *snapshots* at specific times could tie traffic characteristics on segments with no automatic counters to those segments with counters to develop the spatial variability among roads. If this spatial variability were assumed constant in time, the satellite data could be used to extrapolate traffic characteristics from the segments with continuous ground counts to those without ground counts during periods when there is not satellite coverage. Satellite views could also be used to test whether sampled roadways (i.e., roads and locations along these roads using mechanical counters) are representative of the roads in the class; if they are not, the categories could be refined. Satellite measurements are also safer, since fewer personnel would be required to interfere with vehicle traffic to install and operate ground measurements. These *snapshots* could also be used to identify troublespots for either temporary or permanent deployment of traffic counters.

Technical Issues

The principal question addressed by this study is: What is the potential to complement existing traffic data collection programs with image data acquired from a satellite platform *in the future*, given what we know from an aircraft platform *today?* We identified three major technical issues that needed to be addressed.

ISSUE 1: The performance capabilities of remote sensing data need to be estimated to determine what vehicle types could be classified and counted against a background of pavement types. Initial tests of remote sensing data could be performed using digitized panchromatic imagery acquired from an aircraft platform.

ISSUE 2: Once the spatial resolution was defined to count and classify vehicle types, the characteristics of the orbital coverage for such a satellite sensor to meet these requirements need to be defined. In this way we could determine the spatial and temporal coverage that could be expected from various satellite orbit configurations.

ISSUE 3: The availability of and a recommendation of the characteristics for a satellite sensor system to meet traffic data collection requirements need to be defined.

We studied these three technical issues in detail. Specifically, Section 3 describes a mathematical model developed to work with digital panchromatic imagery from a remote sensing instrument used to image vehicles against pavements. We were led to such a model, since there is no imagery available to us at the resolutions required to identify vehicles and since such a model would allow us the flexibility to control and vary different parameters (e.g., imaging resolution, vehicle class distribution, vehicle sizes, angle of pixel grid, and composition of pavement) for efficient analysis. Although subsequent analysis showed that two of the inputs to this model (the vehicle and pavement reflectances) were distributed in such a way as to make this model unworkable at this stage, the model did lead us to first approximations of required resolutions. Specifically, as a first cut, we considered that we would want at least 50% of some pixel to be covered by the vehicle with 0.85 probability. The resolutions required to achieve this performance were between 3 m and 4 m for trucks and between 1 m and 2 m for cars. The model also showed that knowing the rotation angle between the pixel grid and the centerline of the pavement could provide useful information.

We evaluated several types of digital imagery in an attempt to understand the characteristics that might be expected in a digital image of vehicles on pavement background. We investigated infrared images of pavements and vehicles at the Vicksburg, Mississippi airport, the spectral reflectance curve data bases recently made available by the National Photographic Interpretation Center, and simulated panchromatic representations of aerial photographs at various resolutions. These analyses led us to believe that panchromatic reflectances of vehicles and pavements would be distributed so similarly that it would be difficult to use the type of mathematical model developed to systematically and analytically investigate the performance of remotely sensing vehicles on pavement within the panchromatic range. Although these results were discouraging in terms of our modeling efforts, we believe that they are valuable, since to our knowledge they were unknown in the remote sensing literature and they imply that vehicle detection might have to be accomplished through indirect means. Analysis of the aerial photographs showed that the shadows of the vehicles could be one such means.

We present the results of a systematic study designed to investigate the ability to count and classify vehicles using panchromatic images (0.5-0.9 μm) at roughly 1 m, 2 m and 4 m resolutions. We first did this in a manual mode, using a subjective analysis, and then automated the process in an image processing procedure. We used traditional remote sensing concepts of correct classification, errors of omission, and errors of commission, but had to modify the definitions for use in our study. Based on these modified definitions, it appears that we can count vehicles and classify smaller vehicles at 1 m resolution and that we may be able to classify trucks at a coarser resolution than 2 m. These are conservative estimates of requirements, since we used relatively unsophisticated procedures and criteria for a first-cut analysis. We discuss qualitative results based on our experiences with analyzing the digital representations of the aerial photographs and how we incorporated them into the image processing procedures. We witnessed problems associated with local variability in pavement types, traffic congestion on a highway segment, and with shadows from highway signs, tall buildings, and trees.

We believe, however, that these problems could be greatly reduced with relatively straightforward techniques.

In Section 4 we describe the orbital coverage problem. Several design variables were considered. These included the satellite altitude, repeat period, number of orbits per repeat period, number of pixels (detectors) in the sensor array, physical size of the pixel on the detector array, number of spectral bands, and the data compression rate. We determined that the resolutions required would not allow the use of geo-stationary or geosynchronous orbits, and that the resulting coverage would imply that satellite data would augment, rather than replace the traffic data collection task. We formulated the orbital parameter problem as a nonlinear program to determine the orbital parameters that would maximize coverage over the continental United States. A series of mathematical formulations were developed so as to easily evaluate various satellite designs that allowed for circular orbits. Our mathematical analysis showed that we can cover approximately 1% of the highways in the United States per day.

In Sections 5 and 6 we addressed the commercial feasibility of such a satellite design and describe other potential remote sensing sensors. Several commercial companies are designing satellites that will achieve 1-m resolution in the very near future. One system, Eyeglass™, will be launched and operational by 1997. The only drawback to Eyeglass™ is that it is planned to be in a sun-synchronous orbit. However, with its design of fore-and-aft and side-to-side image coverage at an angle of ±45°, it will be possible to achieve additional times of satellite coverage.

Recommendations

We offer several recommendations for a satellite design for traffic data collection. We also offer a recommendation to carry forth the research addressed in this study. This future work is discussed in detail in Section 7.

1. From our image processing tests with several highway segments we could count and classify vehicles at excellent levels of accuracy with 1-m resolution. Based on our tests, we recommend that the resolution from a satellite platform be 1 m to count and classify vehicles.

2. To maximize coverage, a circular, non-sun-synchronous satellite orbit is recommended. We determined that the resolutions required would not allow the use of geo-stationary or geosynchronous orbits.

3. To achieve 1 m resolution a swath width of 15 km (using a pixel array of 15,000) is recommended for the satellite altitudes under consideration. To achieve the maximum coverage per day over the continental United States, an inclination angle of 130° is recommended.

4. The next step in determining the feasibility of using satellite data for traffic data collection should be to use Eyeglass™ and any other near-term satellite missions offering fine resolution image data for testing purposes.

Conclusions

We were tasked to determine the possibility of using satellite remote sensing data to collect highway traffic data. We determined that the resolutions required would not allow the use of geo-stationary or geosynchronous orbits, and that the resulting coverage would imply that satellite data would augment, rather than replace the traffic data collection task. We investigated the resolution, the orbital parameters, and the commercial feasibility of a satellite system that could count and classify vehicles.

From our analyses, we determined that a 1-m resolution is necessary to count and classify vehicles (cars and trucks) with greater than a 90% accuracy. With a satellite design using an inclination angle of 130° for a swath width of 15 km to achieve a 1-m resolution, our mathematical analysis showed that we can cover approximately 1% of the highways in the United States per day. Systematic analysis showed that the primary limiting constraint to increasing coverage would be data transmission rate when acquiring data at 1-m resolution.

Before satellite data could be used routinely to count and classify traffic data on an operational basis, the infrastructure required to process and use the satellite data must be considered. The Eyeglass™ system, which will provide 1-m resolution satellite data, will be launched and operational in 1997. This provides an excellent opportunity to develop the infrastructure required to process and use the satellite data on an operational basis for traffic data collection parameters.

Section 1. Introduction

Quantifying the efficiency and effectiveness of existing traffic systems and facilities is essential and requires continual estimation and measurement of traffic characteristics. The principal parameters that require measurement and data collection are volumes, speeds, densities, and compositions, along with the resultant measures of flow efficiency and safety of travel times and headways. These data allow for assessing existing situations and levels of service and provide the required inputs for evaluating alternative improvements to operations, maintenance, and more efficient utilization of the facilities.

Evaluating and monitoring traffic characteristics is becoming increasingly important as worsening congestion, declining economic situations, and increasing environmental sensitivities are forcing states and municipalities to make better use of existing roadway capacities. There is no doubt that a large shift has occurred from adding more roadways and facilities to one of maximizing the use of existing facilities with improved and more comprehensive management techniques. Likewise, the upgrading and maintenance of existing infrastructures are growing concerns, since much of the infrastructure is nearing, or even past, time for repair and replacement. In addition, the recently enacted Clean Air Act Amendments of 1990 require states and municipalities to conduct before and after project measurements of traffic volumes, speeds, concentrations and compositions, and to do so at finer spatial levels than are currently required. Other specific needs for a continual gathering of traffic data include: (1) inputs to traffic and pavement deterioration models for highway management and maintenance programs, (2) better surveillance of the roadways to satisfy federal requirements to monitor compliance with speed limits, which is an ongoing task because of increasing concerns with clean air, safety and litigation, and (3) better estimates of volume-delay functions at specific sites because of increasing problems with capacity and congestion management.

The present system of using automatic counters at selected points on highways works well from a temporal point of view (i.e., during a specific period of time at one location). However, the present system does not cover the spatial aspects of the entire road system (i.e., for every location during specific periods of time); the counters are employed only at *points* and only on *selected* highways. This lack of spatial coverage is due, in part, to the cost of the automatic counter systems (fixed procurement and maintenance costs) and of the personnel required to deploy them, and is evidenced by the fact that of Ohio's 112,000 miles (180,000 km) of roadway, there are only 200 detectors located along these roads. This same type of problem is also present in other states.

The current procedure is believed to work fairly well in the aggregate mode, at the national level. However, at the state and local levels, the numbers are more suspect. In addition, the statistics only work when assuming a certain homogeneity among characteristics (trucks, volumes, speed limit adherence) of highways in the same class, an assumption that is impossible to test when little or no data is gathered on many of the highways for a given class.

Given these observations, it is clear that a remote sensing system providing improved spatial coverage and resolution would complement the existing system. Synoptic coverage provided by a satellite would be worth exploring, since it would allow more coverage of a region and provide improved estimates at more disaggregate levels. If a satellite could provide repetitive coverage for a wide swath area, while counters are providing temporal data on vehicle movement, the spatial coverage of the existing system might be greatly improved. For example, satellite "snapshots" at specific times could tie traffic characteristics on segments with no automatic counters to those segments with counters to estimate spatial variability among roads. If this spatial variability were assumed constant in time, the satellite data could be used to extrapolate traffic characteristics from the segments with continuous ground counts to those without such counts during periods when there is no satellite coverage. Satellite views could also be used to test whether sampled roadways (i.e., roads and locations along these roads where data are gathered using mechanical counters) are representative of the roads in the class; if they are not, the categories could be refined. Satellite measurements are also safer, since fewer personnel would be required to interfere with vehicle traffic to install and operate ground measurements. These "snapshots" could also be used to identify troublespots for either temporary or permanent deployment of traffic counters.

The purpose of this report is to summarize what we have done over the past two years on the project entitled "Feasibility of Satellite-Based Traffic Data Collection." The objectives of our research consist of four parts:

(1) estimate the performance capabilities of remote sensor technologies to determine vehicle types against a background of pavement types,
(2) evaluate the feasibility of determining vehicle types from a simulated data set (digitized aircraft photography),
(3) investigate the availability of and specify an ideal satellite sensor system to meet these requirements, and
(4) analyze the spatial and temporal coverage that could be expected from various satellite orbit configurations.

Section 2. Background on Traffic Data Collection

2.1 Current Traffic Data Collection Efforts

2.1.1 Traffic Flow Data

Traffic data is currently gathered via traffic engineering studies that obtain empirical facts about existing roadway conditions and vehicular traffic movements. Such studies involve obtaining data by measurements in the field. These field measurements then add to existing databases at the federal, state and local levels.

There are two broad categories of data: system inventory data and traffic flow data. Inventories represent static conditions at the time of measurement. For example, these may include the numbers and types of roadways, land uses and zoning controls, traffic generators (e.g., businesses, schools, shopping centers, parking structures and spaces), or traffic control devices (e.g., signs, markings and signals). The inventory study consists of an accounting of the existing infrastructures and associated elements. The second category of traffic data – traffic flow data – represents the dynamic or quickly changing patterns and characteristics of the movement of traffic and individual vehicles within the system. By quickly changing, we mean anything from on the order of seconds to days to even seasonal patterns. In one way, the existing infrastructure may be thought of as system supply, while the traffic flow data is the realization of the demand on the system supply.

Inventory data are usually obtained from two sources. The first is through existing data that are already in office files and records in a number of locations and departments within agencies. However, this data may be incomplete or require periodic updating through field collection efforts. Many of these efforts require manual observation while driving through the system and recording the required items.

Traffic flow data can be considered from an aggregated perspective of the movement of the *stream* of vehicles, drivers and passengers. This is a *macroscopic* view that is concerned primarily with averages, e.g., the average speed of vehicles or the average number of vehicles on a section or past a point of roadway over a period of time. Data may also be collected on the dynamics of movements of individual vehicles in the traffic stream. This is a *microscopic* view and yields information on individual vehicle behavior. Since this individual data can later be aggregated to provide averages, if collection and storage costs were not an issue, this microscopic data would always be preferable to macroscopic data.

2.1.2 Uses of Traffic Flow Data

The collection of dynamic or changing traffic conditions requires traffic studies and provides for *needs* at the federal, state, and local levels. These needs may represent internal or external requests. Internal needs or requirements refer to data obtained for the internal use of the collecting agency, usually the state, while external needs refer to data

provided for external uses, usually for federal reporting requirements. For example, federal reporting requests include vehicle miles traveled (VMT) for different classes of roadways from each state. The miles of each type of road – e.g., urban freeway, arterial, etc. – are required to provide VMT and may be obtained from the existing inventory of road data. Furthermore, to estimate the vehicle miles traveled requires an estimate of the traffic volume during the considered time period.

We propose that traffic data needs or requirements may be classified into three broad areas: operations, planning and design, and research. Operations consist of the day-to-day operations, maintenance and management of roadways and facilities. Examples of operations include maintenance of pavement and hardware, such as signs, pavement markings, channelization and signalization. These are the daily routine operations that are well defined and have a tendency to lend themselves to manual or handbook collection procedures. Volume counts and vehicle classification data are required for operations and system management and maintenance. Estimates of daily volumes are normally obtained at specific locations. That is, they are site-specific. Vehicle classification data, on the other hand, may be site-specific, but they are usually averaged by functional class of roadway. Volume data are required at specific sites to quantify the operating conditions at the site, since averages over similar facilities in the area would not be applicable. This is because volume measures the specific existing demand, which can then be compared with the existing *supply* or ability to handle the demand. The system may be able to handle the average demand, but specific sites may not adequately handle demands at critical times such as peak periods or during special events.

Data requirements for planning and design, both short and long range, require priorities, trade-offs, and perhaps less routine collection, although there may be much overlap with daily operational data. This data is used for future system improvements and additions. It includes VMT, average daily traffic (ADT) and design hourly volumes (DHV), which are used as measures in planning and operations.

ADT is the average 24-hr volume at a given location for some period of time less than a year. It may be measured for a period of time, such as a few days, a week, or some other period less than a year. It is valid only for the period over which it is measured. The average 24-hr traffic volume measured at a given location over a full 365-day year is referred to as the average annual daily traffic (AADT). It is the total number of vehicles past a given location in a year divided by 365.

Traffic volume varies considerably over a 24-hr day and usually includes morning and evening rush hours. The highest hour of the day is called the peak hour volume and is of interest in design and operations.

Design hourly volumes may be estimated from the relation between DHV and AADT as DHV = AADT x K, where K represents the proportion of AADT occurring during the 30th highest peak hour of the year for rural roads or 15th highest peak hour for urban areas. An example may be used to illustrate DHV. Suppose the projected future AADT in 20 years is 21,000 vehicles per day per direction for a given highway and location, and 20% of this volume occurs during the current peak hour (i.e., K = 0.20). If K

does not change over time, then DHV = 21,000 x 0.20 = 4,200 vehicles per day, a figure used for planning purposes.

An estimate of VMT is obtained by assuming that a vehicle counted on a specific segment of road travels the entire length of that segment. Then VMT is obtained by multiplying the volume by the segment length. For example, if the ADT was 1,124 vehicles and the segment length is 0.5 miles, VMT is 1,124 x 0.5 = 562 miles traveled over that segment.

The third broad area of traffic data requirements is research. This includes model building and calibration primarily through the comparison of empirical data on traffic movement to output of theoretical models. The research results may eventually be incorporated into operations, control, management, design, and planning models, but when the data are collected, the goal is to provide a better description of traffic conditions, regardless of the eventual application.

The data collected for research may be more specific or comprehensive than the data required for operations and planning. Examples include the density of vehicles within a section of roadway or the time headways between vehicles. (Density is defined as the number of vehicles per distance of road and is usually expressed as vehicles per kilometer or mile. Time headway, or just headway, is defined as the time between consecutive vehicles, measured from front to front of vehicles and normally expressed in seconds.) Other examples of data that may be collected for research include the characteristics of platoons of vehicles as they move in the traffic stream. This requires observation from a vantage point above the roadway.

2.1.3 Traffic Parameters

For each of these three classes of data collection there are specific categories of aggregated traffic data that are currently collected and often required by state and federal agencies. Of particular interest in this study are traffic counts or volumes, classification of types of vehicles, and vehicle speeds. Other aggregated measures may be obtained from these measures by making use of the relationship that connect volume, density and speed. This relationship is defined as density (expressed in vehicles per kilometer), which is equal to the volume (vph) divided by average speed (km/hr). In addition, the average distance spacing between vehicles is the inverse of density, the average time headway between vehicles is the inverse of the volume, and the average travel time is the inverse of average speed.

Finer or microscopic traffic flow information on individual vehicular movement and the observation of traffic stream disturbances require different means of data collection than those that are routinely encountered. Since this type of data is not collected in a routine or established manner, it would be difficult to base operations and planning and design procedures on these parameters. Therefore, the data currently fall into the research area. Such data might eventually fall into the operational area, if it were more easily collected. The collection of density, which measures the congestion of the traffic, and speed distributions, which indicates individual travel times, should be considered. Both of

these parameters measure the *quality* of traffic movement, and they are readily sensed by drivers and passengers. Traditional measures, such as volume, are not sensed by the driver or passenger and, therefore, may be of less relevance in determining user satisfaction. Still, volume can indicate the system demand and, perhaps, performance at the aggregate level.

The principal traffic volume measures are AADT and VMT. AADT gives an indication of the average annual number of vehicles on the facility per day. (ADT, on the other hand, is a 24-hr average and only represents the period for which it is collected.) AADT may be either directly measured or estimated from shorter counts using estimated relations between ADT and AADT that account for day of week and monthly or seasonal variations. Directly measured data requires continuous counting during 24-hr periods. This may not be possible for all desired collection locations and times. It may also not be necessary if shorter collection periods can be used to estimate 24-hr volumes. The estimates of AADT are based on shorter counting periods, on the other hand, and they are only as good as the day-of-the-week, monthly and seasonal correction factors.

To obtain VMT, it is assumed that vehicles counted on any link or section of roadway travel the entire length of that section. Then VMT is obtained by multiplying the length of the segment by the volume traversing that segment. VMT data are further stratified by highway functional classes, by regions, and by specific sites that may be of interest. Aggregated VMT is required by vehicle type and by roadway functional class to provide state and national statistics that are used in analysis. It has been determined that statewide annual traffic monitoring programs should provide VMT by functional class of highway and, optionally, by region.

Functional classes of roadways are divided into rural and urban areas, which are further broken into the classes shown in Table 2.1.

Table 2.1 Functional classes of roadways for rural and urban areas.

Rural Classes	*Urban Classes*
Rural Principal Arterial – Interstate	Urban Principal Arterial – Interstate
Rural Other Principal Arterial	Urban Other Principal Arterial
Rural Minor Arterial	Urban Minor Arterial
Rural Major Collector	Urban Collector
Rural Minor Collector	Urban Local
Rural Local	

Since traffic characteristics may vary significantly within a given classification due to terrain or region, a state may choose to further stratify some groups. For example, in rural areas, mountainous Principal Arterials may display different traffic flow characteristics from non-mountainous Principal Arterials. In addition to characteristic differ-

ences due to topographical areas, such roads may also contain significantly different percentages of vehicle classes.

2.1.4 The Highway Performance Monitoring System (HPMS)

Traffic counts, speeds, vehicle classification and truck weight data are submitted to the Federal Highway Administration (FHWA) for use in assessing the extent of the roadway system, the movement of people and goods, the physical condition of the roadways, and in determining national travel trends. Such data are also used to assist in preparing reports requested by Congress and to assess the impacts of existing national programs and policies and potential impacts of proposed programs and policies. As an example, Congress may be interested in the impact of raising the gasoline tax on the VMT and, subsequently, on consumption and pollutant emissions.

The Highway Performance Monitoring System (HPMS) was introduced in 1978 at the federal level, with the goal of consolidating previous federal data requirements and strengthening the methods at the state level (FHWA, 1987; FHWA, 1992; Peat Marwick, Mitchell and Co., 1984). The HPMS is a program management tool for annual monitoring of highway performance and represents a joint effort of federal, state and local governments. Data reporting is the task of state highway agencies. They are assisted in this task by local government units and Metropolitan Planning Organizations (MPOs).

Data reported under the HPMS include "limited data that are reported for all mileage of a given highway system." This is referred to as *universe* data. The universe data includes identification of the type of roadway, jurisdiction, operation type (toll, non-toll) and length of highway section. In contrast to this data is *sample* data, which is reported for a smaller portion, or sample, of the highway system. The sampled sections are monitored from year to year, with a statistically designed sample plan based on a random selection of road sections within predetermined AADT volume groups. These groups are chosen to represent each functional roadway class in rural and urban areas of the state. Four summary areas are submitted: (1) mileage and daily travel, (2) accidents, (3) local functional system mileage, and (4) travel activity by vehicle type and functional system.

This HPMS program provides a base set of locations where traffic volumes are collected on a continuous basis, i.e., over 24 hours per day and 365 days per year. Actual data collection by the states may vary due to economic considerations and sampling strategies to semi-annually or perhaps once every three years for a given location as opposed to yearly sampling. The time duration of data collection may also vary to 48 hours instead of 24 hours.

Trade-offs between precision and available resources (costs, time and personnel) to obtain data must be considered by the states when determining their data collection efforts and the subsequent frequency and amount of data to be collected. The continuous counts or 24-hr volume counts are used to obtain data for control and coverage counts. Control counts provide the *controls* used to define a common basis for estimating ADT at other locations within a roadway system. They are used in areawide and statewide

programs to monitor and quantify daily, monthly and seasonal volume changes. AADT is obtained from ADT by adjusting with the daily, monthly and seasonal variation factors. Specifically, AADT = ADT x DF x MF, where DF is the daily variation factor and MF is the monthly variation factor. For example, suppose that a 24-hr count records an ADT of 2,000 vehicles on Monday in June. Further suppose the daily variation factor for Monday is 1.07 and the monthly variation factor for June is 0.91. That is, Monday has 7% more traffic than an average day and June has 9% less traffic then an average month. Thus AADT = 2,000 x 1.07 x 0.91 = 1,947 vehicles per day.

Data for these control counts are obtained at permanent-count sites or at sites that are counted periodically throughout the year with portable counters. Permanent-count stations use continuous automatic traffic recorders that record data 24 hours a day, 365 days per year. They are distributed geographically and over functional classes of roadways within the states. The portable control count stations are used to supplement these permanent station counts. Usually the portable counters are used at a different location in the same functional roadway class, continuously during one week of each month of the year or continuously during five days every other month, depending on resources available. The data collected serve as the control data for expanding other shorter counts and are adjusted for hourly, daily and seasonal variations.

Coverage counts are *broader* in space, but not as *deep* through time as the permanent counts. They are used to estimate AADT on the roadway system within the state. AADT is obtained from ADT by multiplying by the daily and monthly variation factors, as previously illustrated. The roadway sections used for coverage counts in urban areas are more closely spaced than those in nonurban areas, where AADT is usually estimated for a two-mile (3-km) segment or a segment where flow is considered to be reasonably constant. The urban section is usually taken as a link between intersections or interchanges.

2.1.5 Other Data

Vehicle classification data for HPMS reporting is selected as a subset of the volume estimation samples. Vehicle classification data is used to determine the percentage of passenger vehicles and trucks within the traffic stream. The FHWA has defined 13 classes of vehicle types as shown in Table 2.2.

The average weight or equivalent axle load by vehicle and functional class is usually desired for planning future system improvements, project design, reporting and research. Such information is required and used for public policy, taxation and funding allocations.

Speed data is normally not required for reporting at the national level for planning and operational purposes. Data may be required, however, for special studies concerning conformance to national speed limits. Although not required, this data may be useful in estimating fuel consumption and emissions outputs. Instantaneous or spot speeds can be obtained and then an average speed over these calculated to obtain the time mean speed of vehicles in the stream. If the average speed is calculated over a section of road, this

Table 2.2 FHWA definitions of vehicle types.

Class	*Class Definition*
1	Motorcycles (optional)
2	Passenger cars
3	Other 2-axle, 4-tire single unit such as pick-ups, panels, vans, campers, motor homes, and those pulling recreational or light trailers
4	Buses – traditional and school buses
	Trucks
5	2-axle, 6-tire, single unit trucks
6	3-axle, single unit trucks
7	4 or more axle single unit trucks
8	4 or fewer axle single trailer trucks (2-units, tractor and trailer)
9	5-axle single trailer trucks
10	6 or more axle single unit trailer trucks
11	5 or less axle multitrailer trucks (3 or more units, tractor and trailer)
12	6-axle multitrailer trucks
13	7 or more axle multitrailer trucks

gives what is referred to as the space mean speed. It is this space mean speed that is required to describe traffic stream flow as a whole or on the average. It gives more weight to slower vehicles, as they are on any given section of roadway longer than faster moving vehicles. It may be obtained from knowing all the individual spot speeds of vehicles or directly calculated if volume and density is known.

2.2 Methodologies Used to Collect and Monitor Traffic Data

Traffic studies require collecting, reducing and analyzing data. These three elements overlap, due to the fact that the collection methodology may influence subsequent reduction techniques and have an effect on the type of analysis performed. The collection consists of observing and recording data in the field. This effort involves personnel and equipment. The recording or observation can be done manually or with some sort of "automatic" collection technology. The automatic technology may be either electronic or mechanical and may be set up either as a permanent or portable installation.

2.2.1 Manual Collection of Data

Volume data, for example, is collected both manually and automatically, depending on the situation. At locations such as intersections, where turning movements, approach volumes and queues are required, volumes are collected manually. Observers tally and write down the required data. When volumes are to be recorded for short periods (e.g., on the order of a few hours), manual collection is frequently preferred.

Normally, the short duration does not justify the installation of automatic recording equipment. Manual collection still involves some equipment, such as watches with pencil and paper, pre-printed field sheets showing the site geometrics, tally sheets, or mechanical tally counters arranged on a clipboard that allow one person to count traffic from all directions. Electronic intersection assemblies with memories that record and store total counts on manually-operated counters for later playback or direct input into computers are also available.

Manually collecting data represents a problem with accuracy of recording when writing on field sheets or entering data into laptop computers, due to human error. Direct entry of data into a laptop computer does, however, offer the potential for easier data reduction. Forms are prepared to assist in making this task easier. Data may also be recorded on audio tapes for transcription later. This also offers a possibility of error when transcribing the data from the audio tape. The principal disadvantage of manually recording data is the amount of people required and the associated expenses in personnel time to cover a large number of locations. Moreover, there is a necessary amount of down time involved when transporting the manual collector from one location to another.

Manual counts do, however, offer some advantages. Manual collection allows information on travel directions and turning movements at intersections. It also can provide classification of vehicles by type, size and occupancy. Also, queue lengths and delays can be observed and recorded. Manual collection also allows for the possibility of observing unanticipated conditions that may explain other observations. For example, an accident or occurrence of an incident may explain a recorded decrease in volume or average speed.

2.2.2 Automatic Vehicle Recording

Mechanical or automatic recording devices are used when data are to be collected over extended periods of time longer than a few hours, usually for collecting data for 24 hours or longer. One method is to use a road tube on the road surface across the width of the roadway. The tube utilizes the pneumatic pulse of air created when vehicle wheels pass over it, closing an electric circuit. The count records the number of axles. Since not all vehicles have just two axles, multi-axle vehicles produce an overcount that must be accounted for by correction factors. For example, since in most cases a vehicle passage is represented by the recording of two axles, if more than two axles are recorded, an overestimate of the number of vehicles will occur. A correction factor is used, which would estimate the percentage of multi-axle vehicles in the traffic stream. This percentage would be obtained from manual counts or adjustment factors. A sample manual count is taken to classify vehicles by the number of axles. The average number of axles per vehicle is obtained for the sample and is assumed to be the same for the entire count.

If vehicles arrive simultaneously in adjacent lanes, an undercount may also be produced. Moreover, road tubes can be damaged by the impact of vehicle wheels and other physical damage. They also do not function when a vehicle is stopped with its wheels on the tube and are not usable on gravel roads due to possible damage. The

placement of the tube is also limited, since a fixed object such as a pole or tree is required to anchor the recorder.

Other portable counters may be actuated by tape switches, which consist of wires taped to the roadway surface. When a vehicle crosses the wire, it closes a low current circuit or disturbs an electromagnetic field, which in turn actuates the detector. These tape switches are usually connected to computers in vehicles on the roadside. These computers record the data automatically for later reduction and analysis. The tape switches can also be damaged, since they are on the surface of the road. A time clock may also be part of the equipment, which may be set to turn on and turn off after a period of time. On some recording devices, a printout may transfer the accumulated counts at predetermined intervals; for example, 15-minute subtotals may be printed and registered in the counter, and the counter can be automatically reset to zero every hour.

Permanent automatic counters are installed at the permanent stations that are established at urban and rural locations. These continuous recordings of volumes provide hourly data for every day of the year. Such counts are used to compare hourly volumes among different weekdays, weekends, months and seasons to obtain volume variation factors. They also provide the volumes for each hour of the year and can be used to obtain the 15th, 30th, or other highest hourly volume, which is used for design purposes.

Underpavement detectors are loop or magnetic detectors. Loop detectors are commonly used on high volume, multi-lane roads, since loop detectors can distinguish vehicles in separate lanes. They are often used at intersections to detect the passage of vehicles for use in the operation of actuated signals. These detectors, which are wire loops embedded in the pavement surface connected to a weak power source, carry a predetermined frequency signal. Vehicles passing over the loop change the inductance and, thus, the frequency of the signal. This change is then detected. This is the most common detector because of its reliability and low cost. Magnetic detectors consist of a wire coil embedded in the roadway surface. The detector measures the difference in the level of the Earth's magnetic forces caused by the presence of a vehicle. The constant lines of flux from the Earth's magnetic field are deflected by the passage of a vehicle, causing a voltage drop.

Another type of detector is the pressure sensitive detector. A pressure plate detector consists of a metal plate installed in the pavement that is insulated by rubber springs and buffers from a second plate below it. When a vehicle crosses the plate, the weight of the vehicle causes the two plates to connect. This connection completes a circuit, and an impulse is recorded.

A sonic detector consists of a sonic meter, that, like radar, operates on the Doppler principle. These detectors are located at the side of the road or above the road over a lane. They emit sonic waves that are reflected back by vehicles and detected by the meter. Also, a photoelectric light beam may be emitted (e.g., electric eye) from either the roadside or above the road. The interruption of this beam operates a relay and causes detection.

In addition, optical and video cameras mounted above or to the side of the roadway may be used to obtain vehicle data. These may be mounted permanently or in a portable set-up. An advantage of this type of recording traffic data is that it allows several parameters to be observed simultaneously and can be used to create a permanent record of the observations.

In addition to obtaining video data from fixed locations, this method of data collection can be used with cameras mounted in airplanes or helicopters. This allows for surveillance and monitoring situations where real time information on the traffic flow is desired. Reporting and visually portraying conditions at rush hour on the radio and TV are typical situations of these uses of aerial observation. This type of data collection also allows flexibility and movement of data collection locations. Volumes, speeds and densities may be extracted automatically via computer. Since data reduction has tended to be expensive and time consuming, applications have thus far been limited to research, except for monitoring in traffic surveillance centers. This may change, however, if done on a large scale and if automatic data reduction programs become available at a reasonable cost.

Video imagery has been used to assist in logging information on roadway conditions. A photolog laser videodisc viewing system was developed for the Connecticut Department of Transportation (ConnDOT) to film the entire state highway system. A photograph is taken every 0.01 mile (16 m) from a moving vehicle with the camera oriented slightly down and to the right for optimum coverage of the highway and roadside development. While filming is occurring, on-board sensors record route numbers, direction of travel, cross slope, compass reading, date, time, horizontal and vertical curvature, long-term and short-term roughness, grade, side friction and vehicle speed. In addition to Connecticut, the states of Delaware, Iowa, Minnesota and Wisconsin and Montgomery County, Maryland and Columbia, Missouri make use of video logging technology (King, 1990; Whited and McCall, 1991). Typically, these systems are integrated into a geographic information system (GIS). Applications include pavement management, safety analysis, bridge management and sign inventory.

A review of existing video image processing systems for roadway monitoring is provided in Hockaday (1991) and Hockaday *et al.* (1992). Their study evaluated eight different systems for 28 different traffic sets. In their evaluation they categorized the vehicle detection technique to be a *tracking* or *tripwire* model. Tripwire models are the simplest type and detect a vehicle by watching for a significant deviation in light intensity measured along a narrow band transverse to the direction of travel. An estimate of vehicle speed is derived using speed traps constructed using two adjacent tripwires. The tracking model is used to locate a vehicle in a detection zone by correlating generalized vehicle templates to digital images recorded of the detection zone. This technology is based on standard image processing techniques and uses a time series of template locations to count and estimate the speed of vehicles passing through the detection zone. A new tracking model for video-based vehicle detection was developed by Bullock *et al.* (1993) and is based on neural networks. Their work does not rely on developing or calibrating

rigid templates, but instead learns to recognize vehicle shapes by "learning" from a human operator who locates example vehicles.

Data transmission of traffic information also occurs in northwest Chicago. Information from 1,800 6-ft by 6-ft (1.8-m by 1.8-m) wire loops embedded in 118 miles (189 km) of expressway pavement is transmitted to the Illinois Department of Transportation (IDOT) Traffic System Center in Oak Park, Illinois. The information is processed by a computer program to determine estimates of travel times between various points throughout the city.

Time lapse films to measure speed, headways and delays have been replaced by video tape recordings (Ashworth, 1976; Polus *et al.*, 1978). Analyzing these data can be quite slow and labor-intensive. Application of ime-lapse aerial photography to origin-and-destination survey has also been reported by Ashwood and Inglis (1975) and Garner and Mountain (1978). Traffic routes were determined for an area 0.7-km by 0.5-km by using still photos acquired at 15-second intervals from a helicopter at an altitude of 100 m. Again, this involved a lot of time (four weeks of effort) to track 1,500 vehicles through the road system.

2.3 Potential of Remote Sensing Techniques

Remote sensing is defined "as the technique of obtaining information about objects through the analysis of data collected by special instruments that are not in physical contact with the objects of investigation" (Avery and Berlin, 1992, p. 1). In this way remote sensing takes advantage of sensors – such as photographic cameras, mechanical line scanners and radar systems – that record images at given wavelengths taken at some distance away from an object. Normally platforms such as aircraft or satellites are used to mount the remote sensing instruments.

The energy sensed in remote sensing is electromagnetic radiation, which is either reflected or emitted in varying amounts depending on the surface material. The major spectral regions used in remote sensing are shown in Figure 2.1. Electromagnetic radiation both inside and outside the range of wavelengths seen by the human eye can be recorded with these instruments. Remote sensing sensors that are used to record the radiation in various wavelength regions are also listed. The instruments are designed to capture and record the amount of energy, sometimes called reflectance, from the earth's surface. The data collected by the sensors is interpreted either visually or by image processing methods. Computer equipment has been developed with accompanying software that provide for the display, enhancement, processing, and automatic classification of image data.

There are generally two types of remote sensing systems – passive and active systems. Passive sensors record reflected and emitted energy from an object, whereas active sensors provide their own energy source and record the reflected signal from the object.

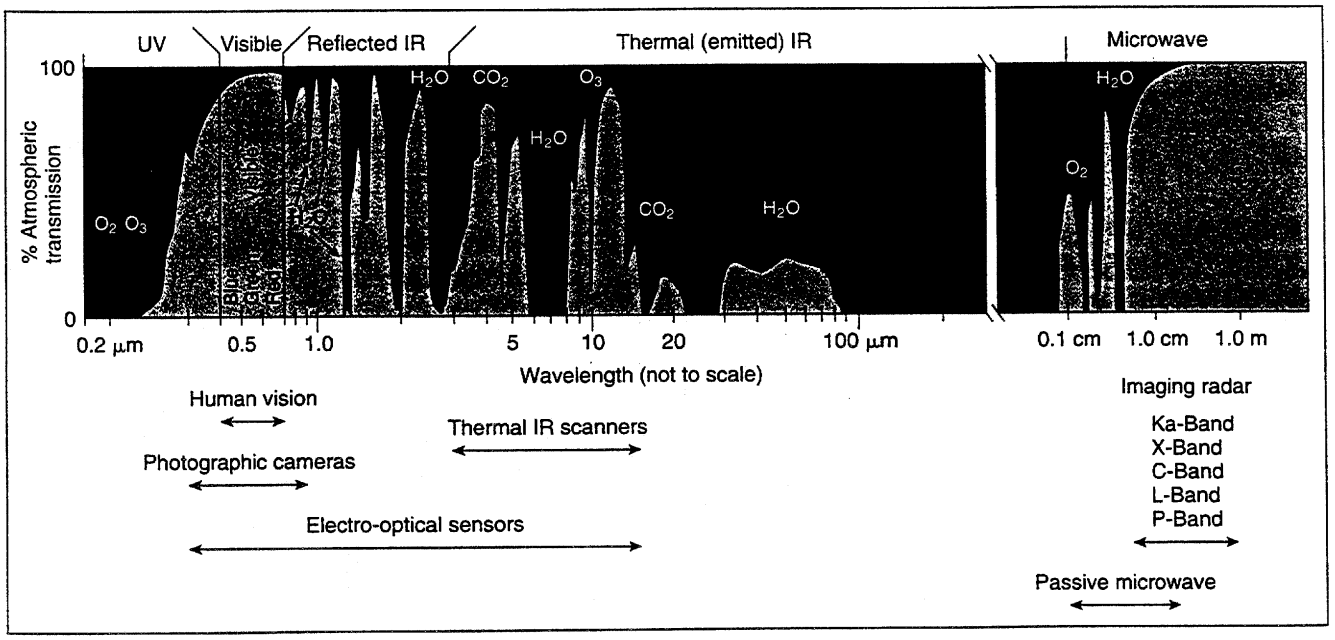

Figure 2.1 Major spectral regions used in remote sensing with the operational range of remote sensing systmes (from Avery and Berlin, 1992).

Photographic cameras were the first type of remote sensing systems. Typically, these cameras can record energy in wavelengths ranging from 0.3 to 0.9 μm. The cameras produce a film emulsion product, in which a frame, typically 9- by 9-inch (22.9 by 22.9 cm), is exposed in one instant of time. Visual photointerpretation of the product can be performed. Recognition elements, such as shape, size, pattern, shadow, tone or color, texture, association and site, are used in the photointerpretation process to classify the photograph into categories of interest to the user.

Most remote sensing imagery used today is in a digital format. This allows for easy incorporation into a digital data base, such as a geographic information system (GIS). Electromagnetic radiation is recorded by photon detectors in electro-optical sensors. These detectors are sensitive to predefined wavelengths. Normally data is recorded in 8 bits or 256 shades of gray that correspond to reflectance levels on the ground.

Present commercial satellite systems include the U.S. Landsat and the French Satellite Pour l'Observation de la Terre (SPOT). These two systems are sun-synchronous and polar-orbiting with coverage limited to the morning hours. Landsat will only allow repeat coverage every 16 days over a given site. SPOT has a 26-day repeat cycle. However, the off-nadir pointing capability allows additional days of coverage within the 26 days. For example, at a latitude of 40°N, the potential repeat coverage would be 11 days within the 26-day time period.

The 30-m and 80-m data from Landsat is too coarse for our purposes. The 10-m or 20-m spatial resolution from the SPOT satellite would be more detailed. Although the 10-m panchromatic imagery could be used for mapping the road network system, the imagery is not detailed enough for identifying vehicle types. Thus, current satellite systems (1994 time frame) cannot be used to measure vehicle counts and speeds.

Satellite technology should be at a stage to attain higher-resolution data capabilities within the next five years. For example, four commercial companies have been awarded licenses by the U.S. Department of Commerce to market high-resolution satellite data. Worldview Imaging Corporation of Livermore, California plans to market 3-m resolution data by 1995. Worldview's system includes a panchromatic sensor and a three-color sensor (sensing in the green, red and near infrared part of the electromagnetic spectrum). Eyeglass International, Inc. (an alliance of Orbital Sciences Corporation of Dulles, Virginia, Litton's Itek Optical Systems division in Lexington, Massachusetts, and GDE Systems Inc. of San Diego, California) intends to launch and operate a satellite by early 1997 for a 1-m panchromatic imagery system. Construction of their system is planned for 1994. Lockheed Missiles and Space Company of Sunnyvale, California plans a 1-m system. Ball Corporation's Aerospace and Communications group in Broomfield, Colorado was recently granted a commercial remote sensing license to provide 1-m panchromatic and 5-m multispectral imagery. Just recently, Ball Aerospace merged with WorldView Imaging Corporation to form a new company called EarthWatch.

An objective of our effort for this study is to define the sensor requirements necessary for distinguishing vehicle types from a satellite platform *in the future*, given what we know from an aircraft platform *today*. Most traffic monitoring tasks being done today involve monitoring the traffic flow on a continuous basis. This is done using high-resolution video cameras. However, in this study we are evaluating the potential of using satellite images acquired at various instants of time to provide an image that would be integrated with point measurements of the traffic conditions. Therefore, another objective of our research is to define what the design constraints would be on such a system to obtain imagery that could be usable for monitoring a traffic situation.

2.4 Deficiencies in Current Data Collection and Advantages for Collecting Spatially Rich Data

Current data collection provides valuable traffic flow data to use as inputs to current analysis and design procedures. The procedures are often developed to accommodate limitations of collection methodologies. However, it is enlightening to consider traffic data collection from an idealized point of view. What data would we choose to have for operations, planning and design, and research, if there were no constraints on the costs, technology or levels of efforts required to collect the data?

Both quantity and quality of data collected should be considered. Data coverage is a quantitative concept. Ideally, we would like to have data at all possible locations and at all times. This is disregarding the ability to store and analyze such information and the costs associated with such storage and analysis.

Coverage of traffic movement requires consideration over the dimensions of both time and space. Current procedures obtain data over time at a finite number of locations on a road network. This temporal data is quite useful, but in practice it is limited in spatial coverage to a relatively small number of locations. It is also limited in the type or variety of data obtained. When an observer or automatic data recorder is located at a fixed point, no upstream or downstream traffic information is observed or recorded. It is as if the observer has tunnel vision and cannot see upstream or downstream. This is one reason why the morning and evening helicopter traffic reports are so popular; they speak to the driver or passenger by providing information on the overall traffic movement.

The available data collected at a point location along a road consist of volumes (vehicles per hour) and spot speeds of vehicles passing a point. Although the volumes provide a quantitative measure of current demand on the system at the point of measurement, they provide no immediate information on the quality of traffic flow and, thus the level of service that is being provided on the facility. A driver or passenger within a vehicle has no feel for this volume. It is an operational measure of the amount of traffic moving through the system. For any volume measured, the actual average traffic speed may be fairly high or low, depending on how many vehicles are occupying the road section "around" the point of measurement. Thus, the speed or density of traffic must also be known at the same time to estimate the quality of flow.

It is the number of vehicles on the road (i.e., density or number of vehicles per mile) that is much more important to the driver or passenger. This is a spatial measurement that shows how crowded a segment of road is and provides a measure of congestion and level of service being provided. The speed is also a measure of quality of flow, and is directly available to the driver and passengers. Anyone inside a vehicle "feels" the speed and density of traffic flow, and can thus associate with it as a real time measure of the quality of traffic movement.

Data obtained alongside of the road may also provide the arrival times of vehicles, if either manually recorded or "time stamped" with automatic recorders. From this data, averages of speeds and volume may be found. Density may then be calculated, assuming steady state conditions of flow around the collection point, since density is volume divided by the space mean speed. (Space mean speed is the harmonic mean speed of all the individual spot speeds past a point over time.)

What is not obtained using this temporal data is the density at any instant in time and the occurrences of disturbances in the traffic stream and their movements through the stream. They provide no immediate information on the conditions around a bottleneck, lane restrictions, entrance or exit movements on freeways, lane weaving, traffic composition, and incident detection. This is for both uninterrupted flow on freeways and arterials, as well as for interrupted flow on collector streets. For interrupted flow at intersections, data on stop and start-up times, intersection clearance time, delay, and turning movements require observation and vehicle identification.

There are a number of advantages that would be possible if spatially rich data could be obtained. One is the ability to observe the traffic situation over a physical area of

road section at a point in time. This allows observation of the entire area or network section. If we consider looking down on the movement of traffic from above, then by counting the number of vehicles within any section of road and measuring the length of road, we know the density of traffic. This instantly provides a picture of the situation and the quality of flow. Another observation, say one second later, could then provide data on the distances traveled by individual vehicles. From this, speeds can be calculated and also volumes. Such data provide not only averages or aggregated measures, but also individual movement of vehicles, if observations are obtained over time.

Section 3. Imagery Performance and Evaluation

3.1 Introduction

We developed a mathematically-based model of digital vehicle imaging from a satellite sensor, anticipating that such a model would give us the capability of objectively investigating the performance of design parameters (e.g., the sensing resolution) under different conditions representing the state of the system (e.g., traffic conditions, pavement type). The characteristics of the pavement and vehicle spectral reflectances (two inputs to our model), which were only discovered later, limited the usefulness of the analytical model. We were not able to use the model to perform the large-scale simulation of performance originally envisioned. Descriptions of the mathematical model (Appendix A) and results (Appendix B) are provided.

The analytical model did give useful insights into certain aspects of the problem, however. Specifically, we saw that we would require a 1-m to 2-m resolution to image cars and between a 3-m and 5-m resolution to image trucks, if the criterion was one of having the vehicle cover at least 50% of some pixel with a probability of at least 0.85. Also, the angle that the vehicle makes with the pixel grid axes would be a parameter influencing the imaging performance.

In parallel to our modeling efforts, we investigated the literature and current research to determine what imagery was available to derive vehicle and pavement reflectance values. We researched four sources of information. The reflectance data that we needed for vehicles and pavements were not available in the published literature. Reflectances available from the National Photographic Interpretation Center (NPIC) are principally for military paints and materials. There is a remote sensing instrument available from Daedalus to measure true reflectances, but using this instrument would have required an extensive field effort that we were not willing to take on at this stage. A REMIDS scanner has been used by the U.S. Army Corps of Engineers to detect mines, but the instrument operates at wavelengths that would probably not be available on a satellite platform. Therefore, we scanned several low-altitude aerial photographs to simulate a wide band panchromatic sensor at various resolutions. These data sets were used to estimate vehicle counts from simulated satellite resolution imagery.

The vehicle reflectances R_{veh} and pavement reflectances R_{pvt} resulting from the scanned representations of the aerial photographs were so similar that we were not able to use the mathematical model presented in Appendix A. However, the scanned representations did provide a product that simulates an image of traffic conditions that would be obtained by digitally sensing in the panchromatic region of the electromagnetic spectrum. We discuss our use of the scanned representations to simulate the performance of a panchromatic sensor for imaging vehicles on highways in this section. We analyzed the performance of each traffic segment using photointerpretation techniques and then developed an image processing method to automatically process the images, thus providing a

more objective image analysis procedure. Image processing tools developed to perform these tests could be adapted for an operational system.

These scanned representations simulated reflectance values and served as inputs to our systematic investigation of sensing performance for the purposes of vehicle classification at various resolutions. The disadvantage of this approach, compared to the mathematically-based simulation developed in Appendix A, is that it lacks the experimental control that we would have been able to exert in that type of study. We were limited to the data sets of the four aerial photographs. These data sets were rather time-consuming to obtain and process. They offered no control of the traffic characteristics, e.g., the spacing between successive vehicles, the numbers and distributions of trucks and cars, but we had to accept those characteristics that existed in the photos. Moreover, they could only yield imperfect estimates of the true traffic characteristics in the photographs, due to the limited ability of the aerial photograph to portray the actual characteristics and our limited ability to interpret the photographs.

Still, the tests discussed in this section were useful in two ways. First, they gave us a feel for the issues that would arise in remotely sensing traffic conditions in the manner envisioned in this study. They showed, for example, that vehicle shadows, rather than complicating the task, appear to be the principal means of identifying the presence of a vehicle. Given the importance of the shadows for detecting the vehicles, a knowledge of the sun angle is an important parameter for future interpretation and even design. The sun angle parameter was incorporated into the image processing method to use in future tests where the sun angle would be different.

The second way in which the tests based upon scanned representations of aerial photographs proved useful was in their ability to allow quantitative analysis of the expected performance of remotely sensing vehicles at various resolutions. Based on the studies described below, we believe that a 2 m resolution would be sufficient for detecting large trucks, yet 1 m resolution would probably be required for detecting cars.

3.2 WES REMIDS Scanner Data

Dr. Ernie Cespedes (Electrical Engineer, U.S. Army Engineer Waterways Experiment Station – WES) has developed a scanner called REMIDS. The multisensor line scanner was developed to help in the detection of surface mine explosives. The instrument is used in a helicopter platform. Typical altitude is 30 to 125 m (100 to 400 ft), with the helicopter moving at 50 to 195 km/hr (30 to 120 mph). These parameters result in a resolution of 4 to 15 cm (1.5 to 6 in.). The scanner transmits a beam of linearly polarized laser energy (1.053 μm) and senses reflected electromagnetic energy parallel and perpendicular to transmitted polarization. The magnitude of the two components depends on the depolarization, directional and reflectance properties of the surface. The scanner also includes a thermal channel (8-12 μm). An example photographic image from this scanner showing vehicles on a pavement area is shown in Figure 3.1. Although the REMIDS images are outside the electromagnetic spectral region for which we performed our simulations, they do provide information on how vehicles appear against a pavement background.

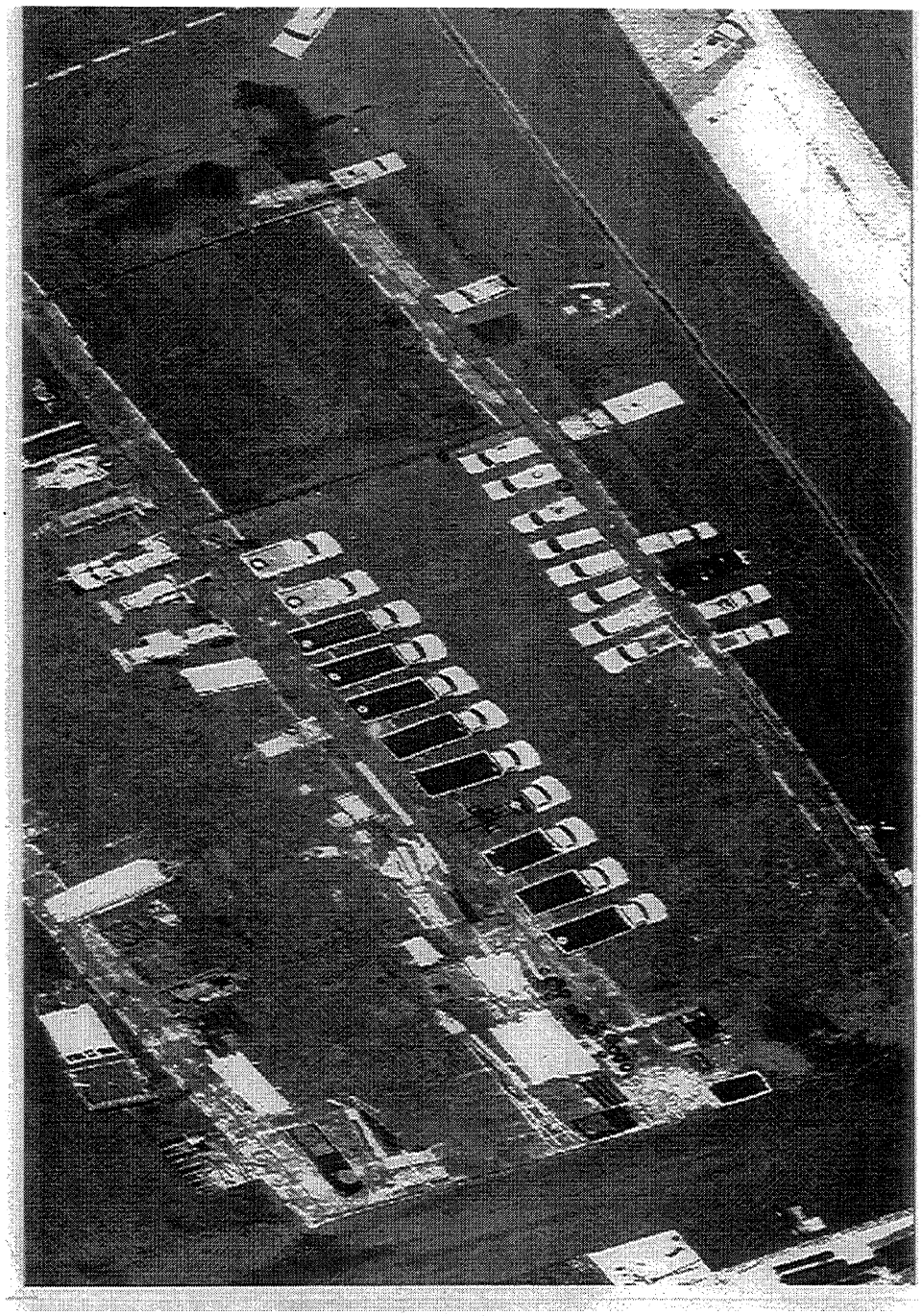

Figure 3.1 Reflectance channel measurements (sum of the parallel channel [laser return having the same polarization as the transmitted beam] and the cross-polarized channel from the REMIDS scanner) of a parking lot showing different vehicle types.

Example digital images from the REMIDS scanner were provided by WES. Analysis of these images for vehicle and pavement reflectances was performed. The cumulative distribution of the reflectance values for a large patch of asphalt pavement is shown in Figure 3.2a, and those for four smaller patches of pavement at different locations are shown in Figure 3.2b. We also present the cumulative distribution in which the theoretical reflectance value of a typical asphalt pavement (R_{pvt}=18) is represented by a Gamma distribution with mean and standard deviation of reflectance values of 18.2 and 3.8, respectively. To develop the Gamma distribution, we examined a theoretical reflectance value of an "asphalt " pavement from a typical reflectance curve developed by Colwell (1966). In the infrared part of the spectrum, we found the asphalt curve rising, and therefore, we would expect the infrared reflectances to be higher.

The results are encouraging. Specifically, as expected, the infrared values are slightly above our calculated panchromatic values, i.e., the "pavement" curves lie to the right of the "Gamma" curve. Moreover, the variances of the different pavement patches are low. The statistics show that each patch had lower standard deviations than what we assumed would be "low" (3.6 counts). The variance across the patches would, of course, be higher. Recall, however, that the resolution of these WES images (6 in. or 15 cm) is much smaller than that which we expect from a satellite platform (1 m, perhaps).

The infrared reflectances of the parked vehicles showed much higher variances (Fig. 3.3a, b). It appears that some vehicles have a bi- or tri-modal frequency distribution, perhaps representing the windshields, cabs, and truck beds at the fine resolution of the image. We had no theoretical results to make relevant comparisons to the cars or trucks.

Figure 3.4 contains several asphalt and concrete surfaces from another location (the Vicksburg, Mississippi airport), as well as additional areas of grass and water. We processed selected samples of these images through OSU-MAP-for-the-PC (a GIS computer program available at The Ohio State University) and produced the cumulative distributions shown in Figure 3.5a-c. As with Figure 3.2 above, there was very little variability in asphalt for the specific patches of pavement analyzed. The small variability is represented by the steep cumulative distributions. (Each distribution represents between 2,500 and 5,000 observations of approximately 7.6 cm by 7.6 cm.) On the other hand, there is more variability in concrete (Fig. 3.5c) than for the east and north sections of the asphalt curves (i.e., when comparing Figures 3.5a and 3.5b). This variability in the pavement surfaces may not allow us to get a unique characteristic distribution for R_{pvt}.

We worked with these digital data sets to get some feel for R_{pvt} and R_{veh}, but felt that the spectral channels would not be suitable for a satellite platform. Laser energy could probably not achieve the fine spatial resolution that we would need to detect vehicles.

3.3 NPIC Data Sets

We contacted Leon Hicks (National Photographic Interpretation Center, Washington, DC), who sent us the Spectral Catalog, which is a reference collection of

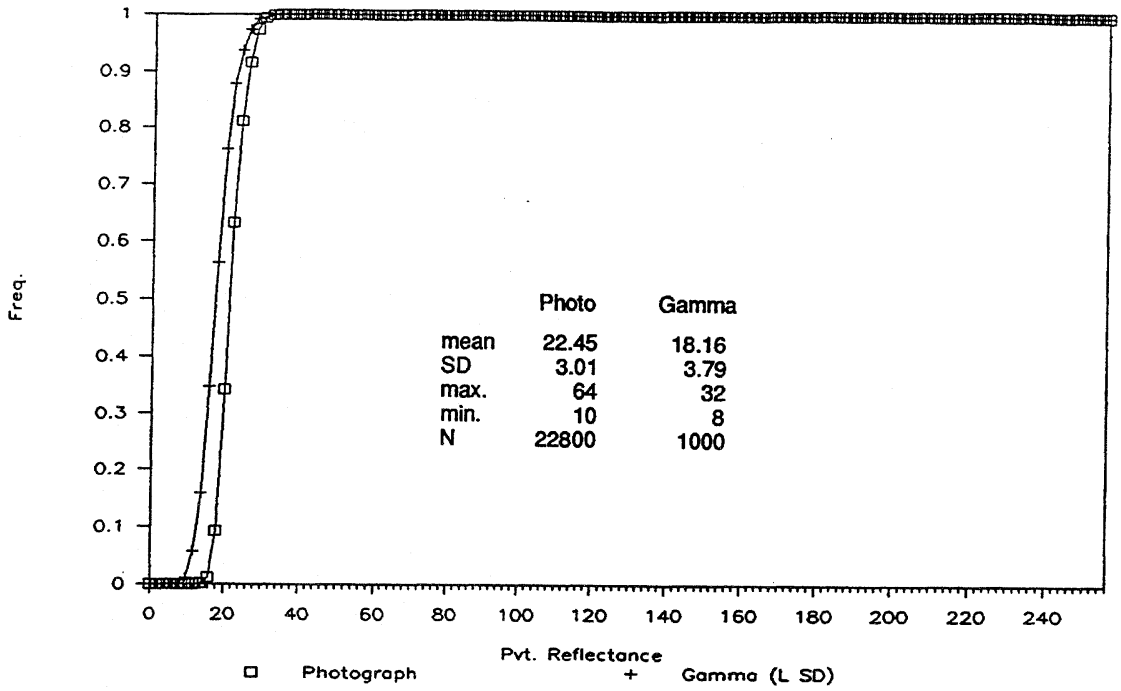

a. Large patch of WES-imaged pavement ("photo") and theoretical asphalt pavement with "low" variance

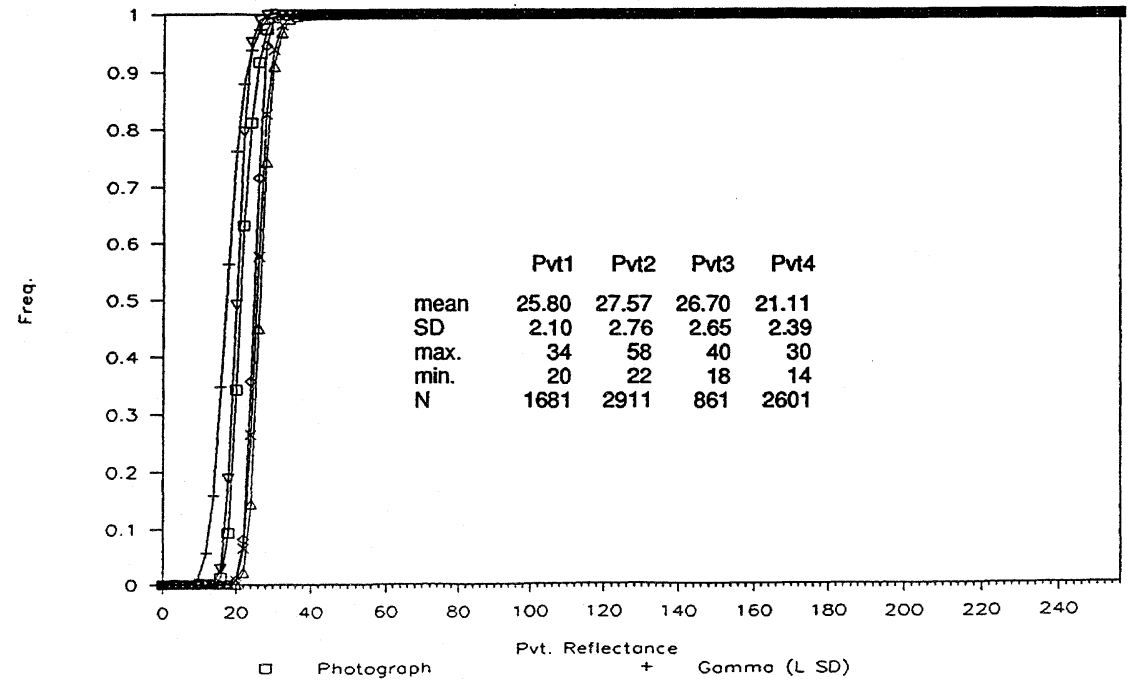

b. Four patches of of WES-imaged pavement (Pvt1-Pvt2) at distinct locations and theoretical asphalt pavement with "low" variance

Figure 3.2 Cumulative distributions of infrared pavement reflectances in WES image and theoretically calculated asphalt pavement with "low" variance.

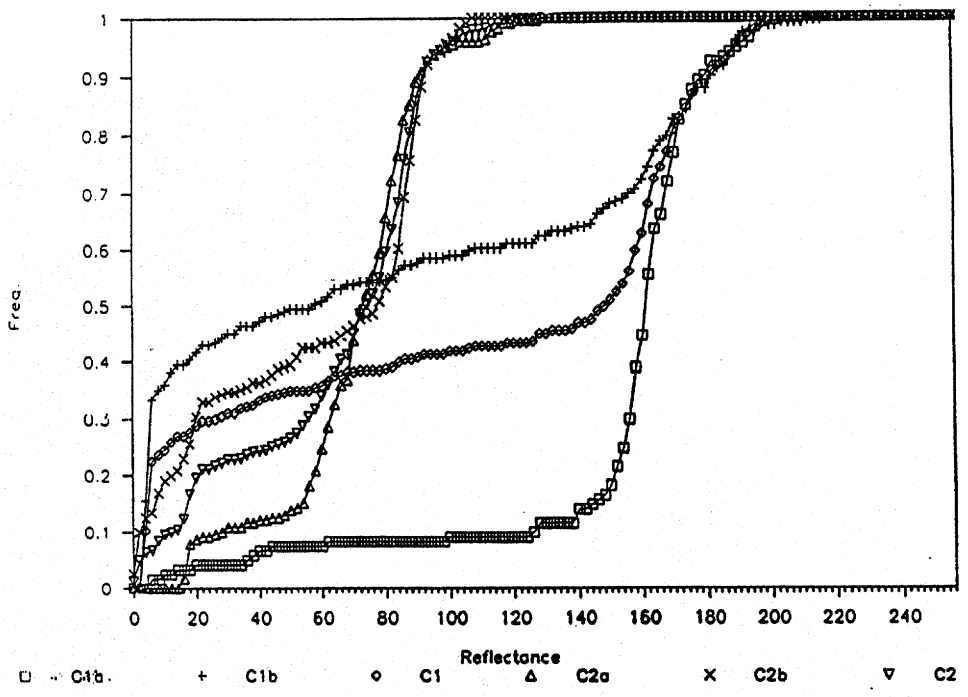

a. Cars

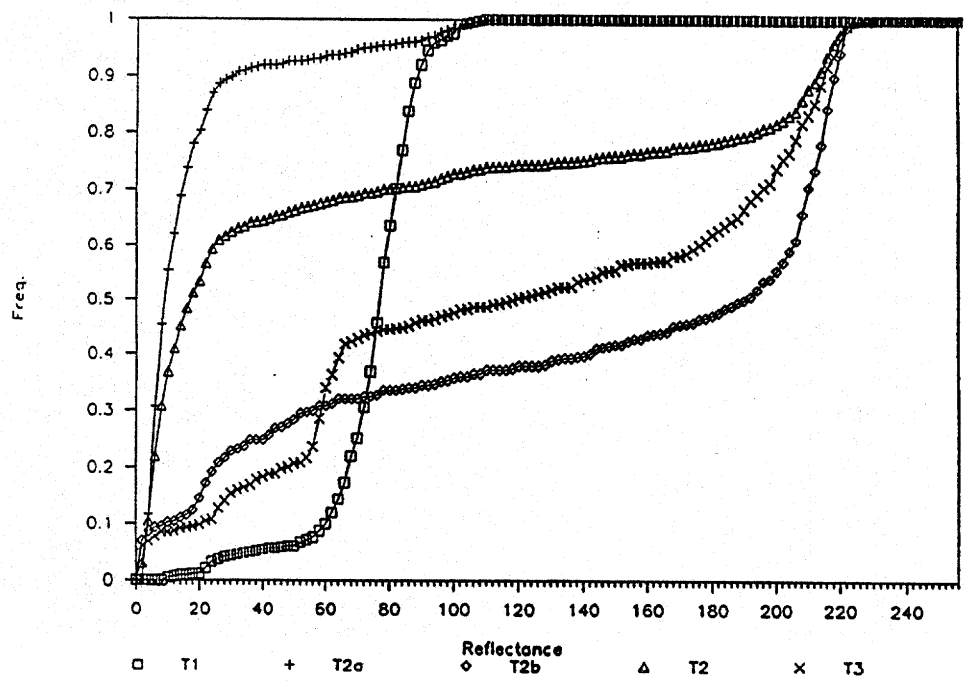

b. Trucks

Figure 3.3 Cumulative distributions of infrared reflectances for portions of parked vehicles in WES imagery.

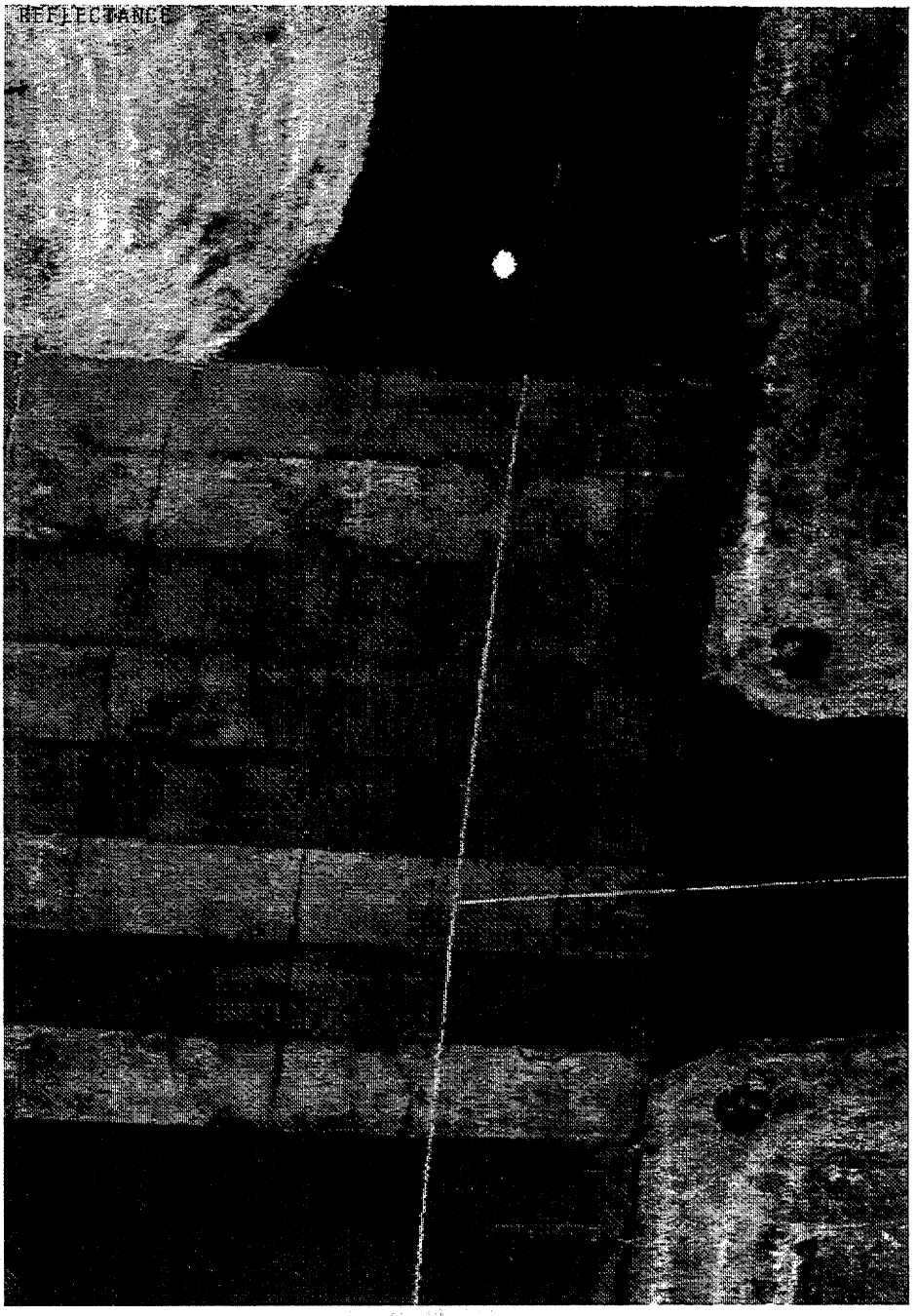

Figure 3.4 Reflectance channel measurements (sum of the parallel channel[laser return having the same polarization as the transmitted beam] and the cross-polarized channel from the REMIDS scanner) of various pavement types at the Vicksburg, Mississippi airport.

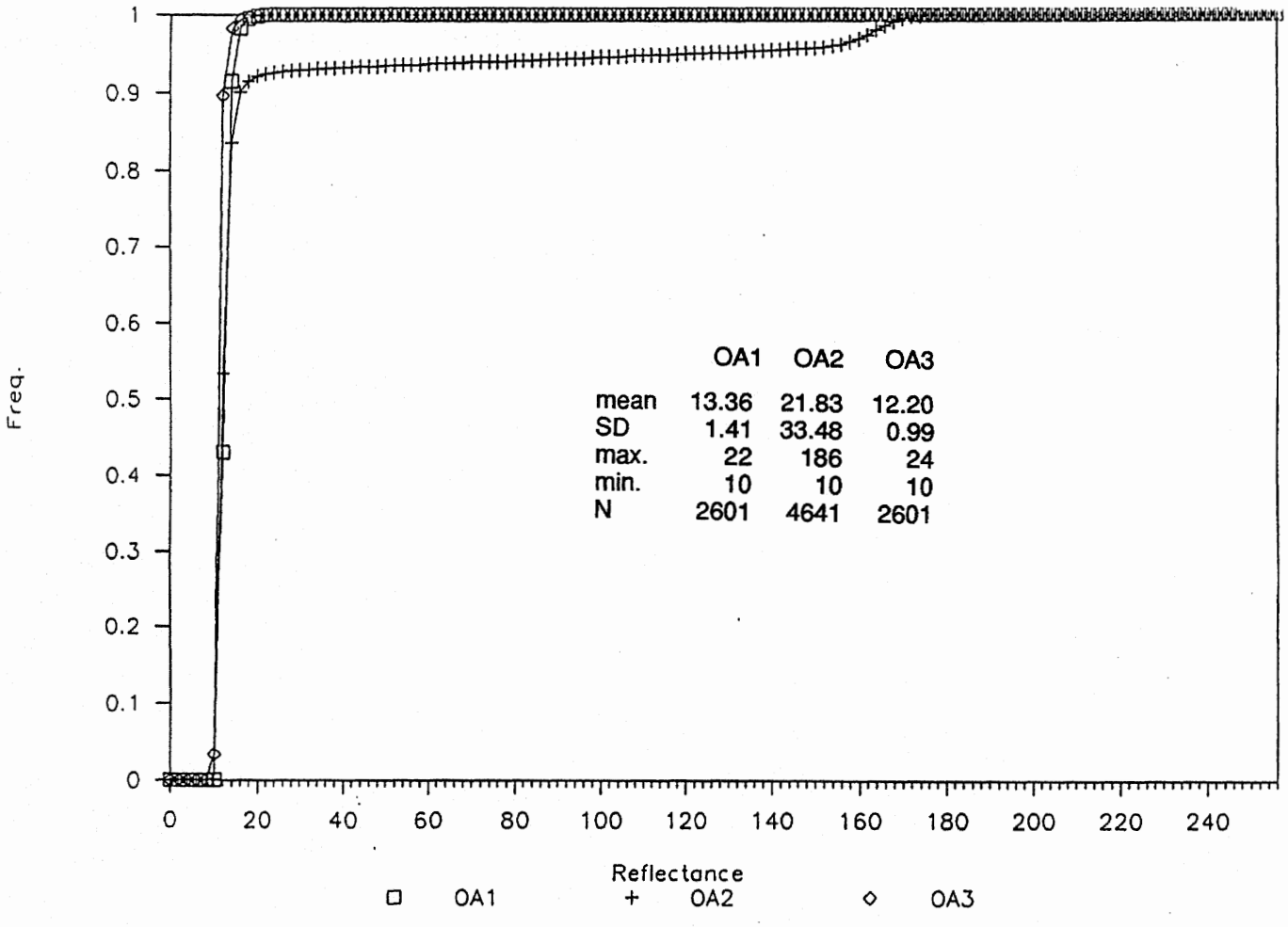

a. Three patches of asphalt pavement in east section.

Figure 3.5 Cumulative distributions of infrared pavement reflectances at Vicksburg, Mississippi airport.

Figure 3.5 (continued)

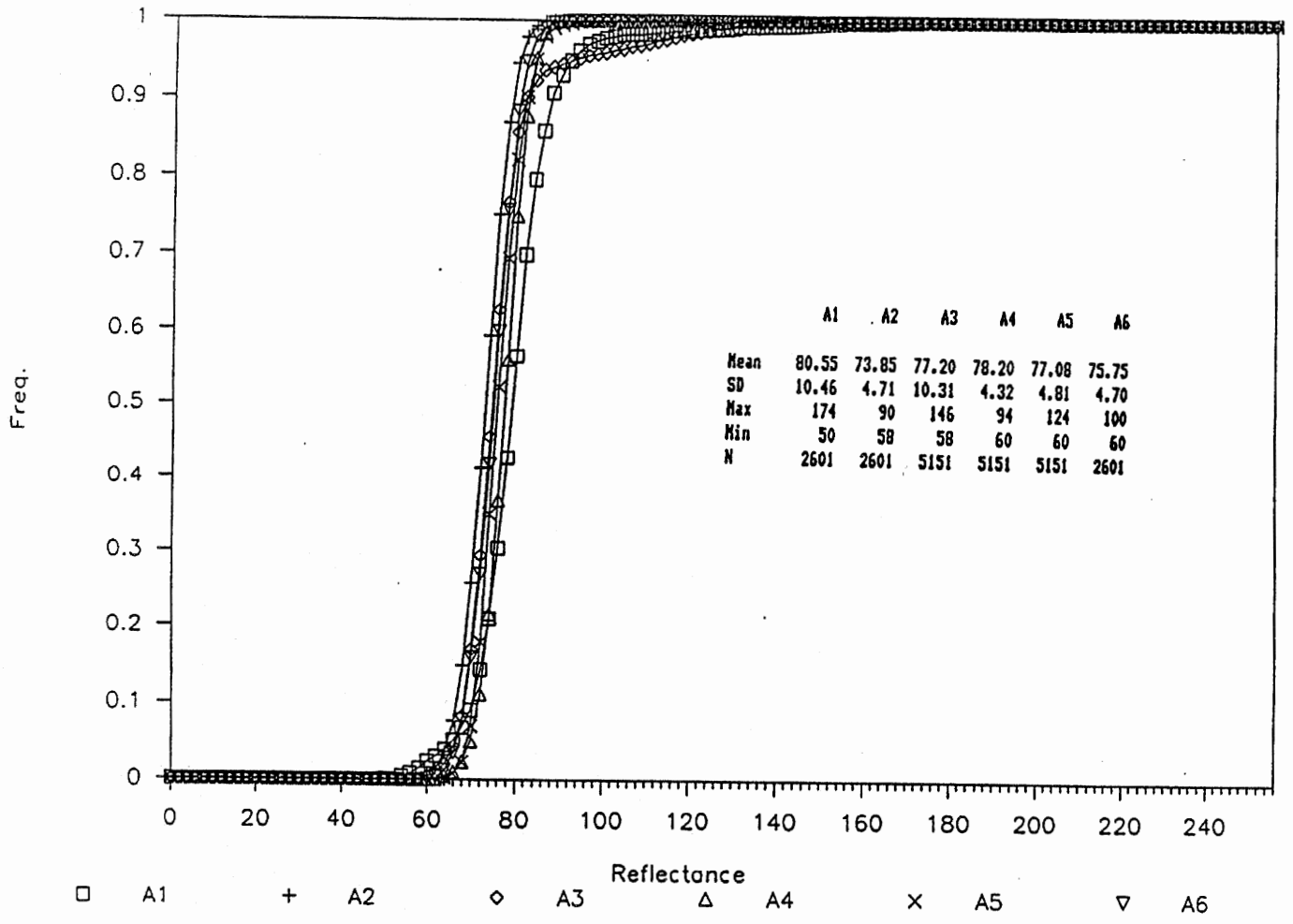

b. Six patches of asphalt pavement in north section.

Figure 3.5 (continued)

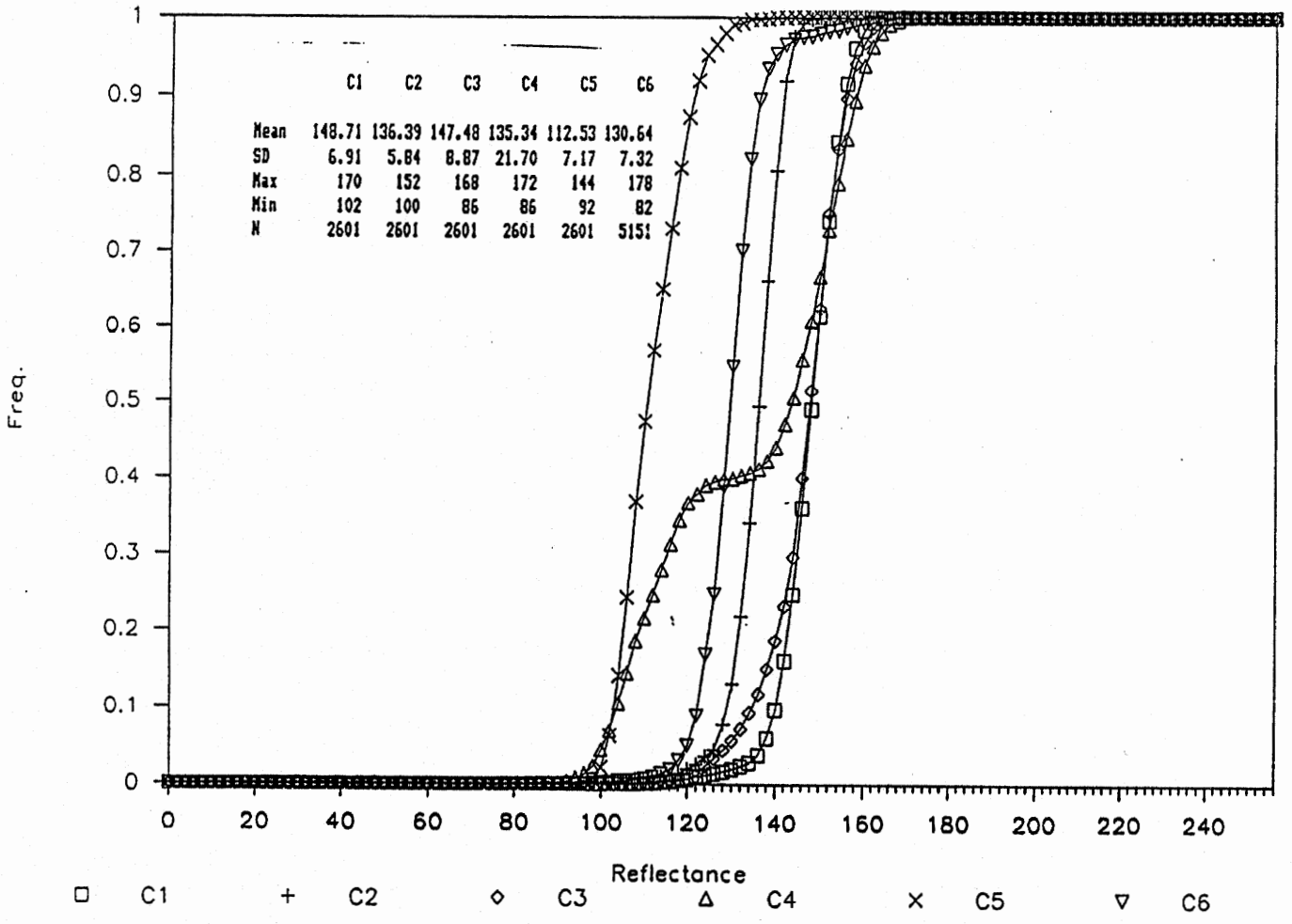

c. Six patches of concrete pavement.

different types of spectral measurements in support of the Spectral Studies Program. Detailed information is provided on the materials measured, descriptions of the instruments and methods used to collect and reduce the measurements, and hard-copy plots of the spectral reflectance measurements. Recorded visible/near infrared reflectances of various samples were measured for the 0.4-2.5 μm (visible, near infrared–VNIR–wavelength region) at a resolution of 0.01 μm, and the 2-14 μm (middle infrared–MIR) and 0.4-14 μm (combined VNIR/MIR) wavelength regions at a 0.15 μm resolution.

The samples in the database included construction materials, fabrics, metals, soils, paints and rubber, and were primarily directed to military applications. Reflectance values were measured and included absolute reflectance factor (%) as a function of wavelength, bidirectional reflectance and hemispherical reflectance.

We decided not to work with this data set, principally because there were not enough pertinent material types relevant to our study, since the materials were geared towards the military. We did see, however, that reflectance values for the color of paint varied by the number of coats of paint. For example, with two coats of green paint the absorption minima will be stronger due to the increased optical thickness of the paint (two coats instead of one). This reinforced our suspicions that it would be difficult to model R_{veh} with a unique distribution of vehicle reflectances.

3.4 SpectraFAX™ 440 Portable Field Spectroradiometer

We contacted Keith A. More (Manager, R&D Sales, Daedalus Enterprises, Inc., Ann Arbor, Michigan–an OSU Center for Mapping (CFM) corporate partner) to discuss the feasibility of obtaining ground signatures of vehicle and pavement reflectances. Daedalus specializes in developing multispectral scanning instruments to use in simulating satellite studies of the terrain.

Daedalus makes a portable spectroradiometer that could be used to gather information on typical vehicle and pavement reflectances. There are several modes of operation. The radiance mode will gather and store raw data. The reflectance mode will perform ratios with the calibration data. An averaging mode will store up to 10 unaveraged spectra with the next spectra being the average of 10 samples. The acquisition time is 3 seconds/spectra. Spectra are written as ASCII files. About 237 spectra can be stored on a 3.5-in. diskette. The instrument operates by aiming the head of the instrument at the object of interest from a distance of about 1 m. A trigger is squeezed and the reflectance spectrum for the selected range of wavelengths is recorded automatically.

We did not pursue this option, since it would have entailed quite a bit of field work. We would need to develop a scheme to sample a number of different cars, vans and trucks of various colors from overhead. We thought of sampling cars, vans and small trucks at a local car dealership. However, the larger semi-trailers would have to be sampled from bridges located over highways, or we would need to visit representative local trucking companies to obtain reflectance samples of their vehicles.

3.5 ODOT Panchromatic Images

Tim Pancher (Ohio Department of Transportation (ODOT) Bureau of Technical Services, Columbus, Ohio) provided us with data on pavement type and car and truck ADT's for highways in Franklin County. We used this information to identify two areas with different pavement types that would likely contain a number of vehicles. These areas include the I-270W and I-70 interchange and the I-70 and S.R. 315 interchange.

ODOT maintains a catalog of standard panchromatic aerial imagery (0.4-0.7 μm). The imagery is at a scale of 1" = 1000' (scale 1:12,000). We requested the aerial photography for our two selected areas from Ed Smith (ODOT, Aerial Engineering).

The photographs were scanned to provide a digital product that we could then use with an image processing program. We analyzed several highway sections where we thresholded the image so that the vehicles are shown as "black" (0) against a highway background ("white"–1). We then counted the vehicles to develop the total number of vehicles. The counting was compared to visual counts taken from the photography (our "ground truth") to develop data on how well we can automatically count and classify the vehicles from an image. The results from this analysis are described in the following sections.

We also examined the reflectances from several trailers and concrete pavement sections from the panchromatic images (Fig. 3.6a, b). Remember that these images were scanned to result in an array of relative reflectance values (256 levels) and that they are not true reflectances. Comparing Figure 3.6a and Figure 3.6b shows that the trailer reflectance observations overlap greatly with the concrete pavement observations. Based on this analysis of a panchromatic image, it would be difficult to detect a vehicle from a concrete pavement based only on reflectance values of the vehicle and highway. This would make the task of distinguishing trailers from the pavements troublesome. Techniques need to be developed to make the vehicles stand out from the surrounding pavement.

Had we known that the reflectance distributions of vehicles and pavements would have been so difficult to develop, we would not have developed the geometric model described in Appendix C that focuses entirely on the true reflectances of vehicles and pavements. Data on these types of reflectances was not available in the previous remote sensing literature, since the resolution of satellite sensors prohibited the detection of vehicles. Therefore, we view this finding of similar reflectances as somewhat significant. However, the relative reflectances of vehicles, shadows and pavements derived from our scanning process is still useful for simulating a satellite image of vehicles and pavements.

In summary, our efforts to determine unique vehicle and pavement reflectances resulted in the conclusion that vehicles and pavements have similar reflectance values. This is discouraging in the sense that it will be hard to distinguish vehicles as separate entities from the pavement based solely on their reflectance value. It also means that the mathematical modeling approach described in Appendix A will have limited use. Other image processing techniques will be necessary to make these vehicles stand out as

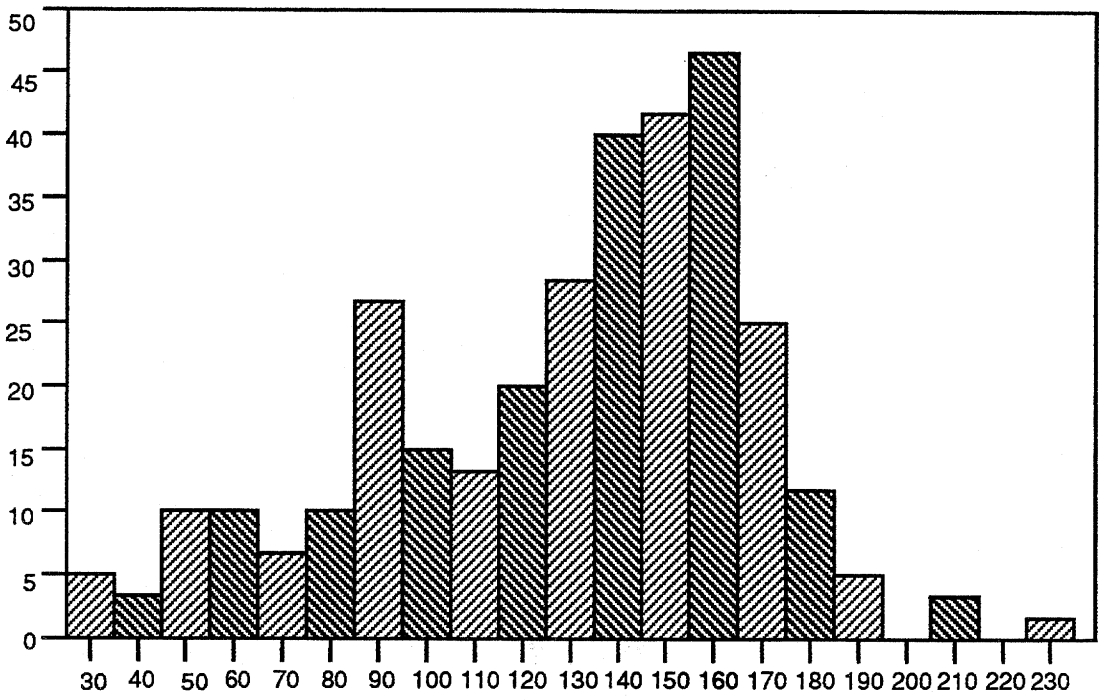

a. Trailers at loading dock.

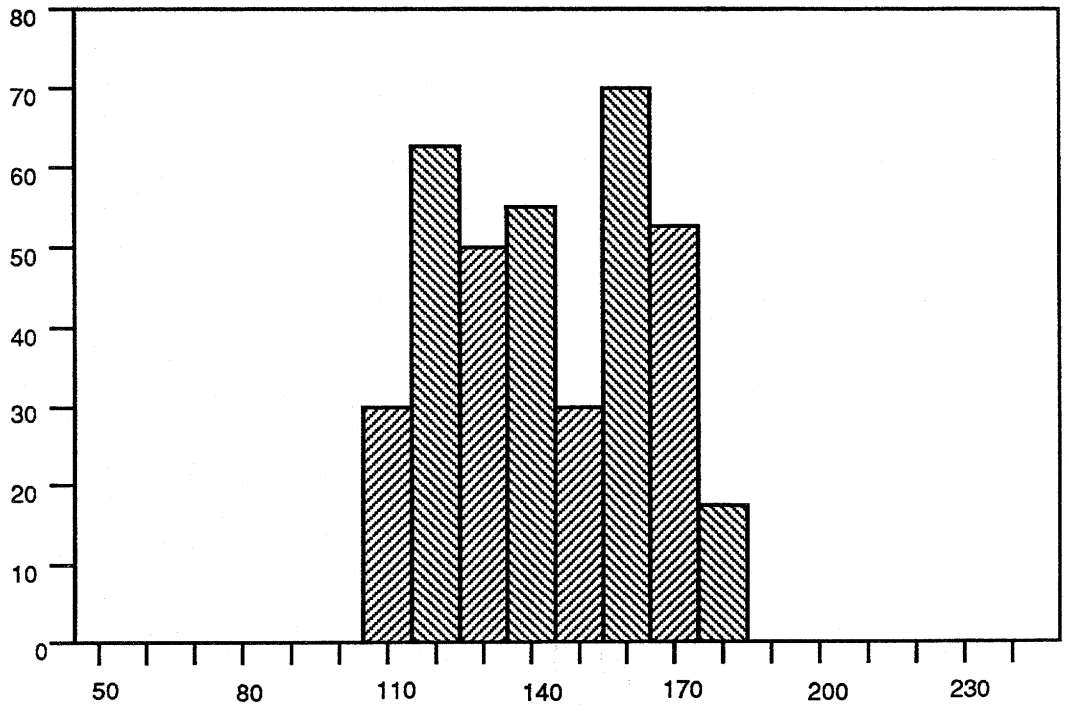

b. Highway pavement (no median, no vehicles).

Figure 3.6 Histograms of panchromatic reflectance values from scanned digital representation of aerial photo 514, simulated 1 m pixel resolution.

separate objects to be identified, counted and classified in a traffic situation. These were incorporated into our automatic image processing approach that will be described later.

3.6 Scanning of Aerial Photographs

Using the aerial photographs for the evaluation studies involved scanning the photographs to obtain digital representations of the scenes, selecting highway sections from the digital representations for analysis, using these highway sections in an image processing package to count and classify vehicles, and comparing the classifications to estimates of the "true" vehicle characteristics.

We scanned the aerial photographs at various scan resolution rates. Since the aerial photographs were at a 1:12,000 scale, scanning the photographs at a rate of D dots per inch (dpi) would simulate a resolution $PS(D)$ of:

$$\begin{aligned} PS(D) &= 1{,}000[\text{ft/in}]*(1/D)[\text{in/dot}]*0.3048[\text{m/ft}] \\ &= 304.8/D\ [\text{m/dot}] \end{aligned} \tag{3.1}$$

where, as in a satellite image, the resolution PS is given as the length along one side of a square area over which the scanner averages the reflectances in the panchromatic wavelengths (0.4-0.7 μm) for the area.

We scanned the four aerial photographs at rates D of 300, 144, and 72 dpi, which according to Eq. (3.1) simulated resolutions of 1.0 m, 2.1 m, and 4.2 m, respectively. To accomplish this, we used the HP ScanJet Plus scanner located at The Ohio State University's Center for Mapping. The output consisted of a matrix of integers between 0 and 255 (representing the 256 possible values on an 8-bit scale), where the numerical value in a cell was the average panchromatic reflectance (grey tone) of the pixel cell area of the photograph. In Figure 3.7, we show a digital representation of a highway segment, taken on I-70 in Franklin County, Ohio. The digital image was produced by scanning aerial photograph 514 as described above at a 300 dpi scan rate, i.e., a simulated resolution of 1.0 m. The hardcopy print is produced with standard image processing software by associating a different grey tone with each numerical value in the digital representation.

Based on comments we received at a project review at the Ohio Department of Transportation (ODOT), we later decided to scan at a resolution finer than 1 m. Specifically, we scanned at a rate of 500 dpi to simulate a 0.6 m resolution. Scanning at this rate required the use of the Optronics 5040 scanner at the OSU's Center for Mapping. We enlisted the cooperation of the Center for Mapping staff to scan selected highway sections of the four images. We do note, however, that we can now aggregate these matrices to simulate coarser resolutions without further rescanning.

As mentioned, the numerical value in each cell of the simulated digital representation was the average reflectance or grey tone in the area of the photograph corresponding to the cell. This value would simulate the contrast ratio (see Appendix A) that would be recorded by a digital panchromatic sensor of that area. The value would not be a perfect

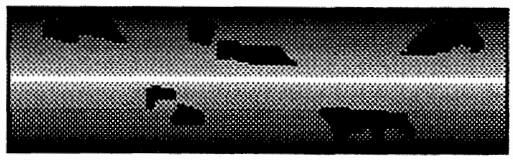

Figure 3.7 Digital representation of scanned aerial photograph of highway segment on I-70 in Franklin County, Ohio.

Figure 3.8 Binary representation of Figure 3.7 after thresholding at a level of 56.

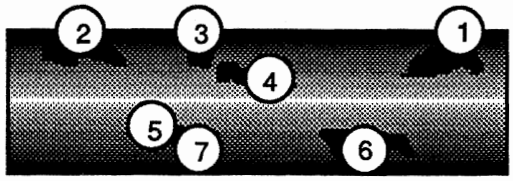

Figure 3.9 Binary representation of Figure 3.8 with identifiers attached to clumps.

estimate of the contrast ratio of the scene in that area, however, since the grey tone in the photograph would also be affected by the photographic development process. This source of error would not be present when sensing directly with a digital instrument. There would be some difference between the contrast ratio recorded from a digital sensor on a satellite platform and that recorded from an aircraft, due to the difference in altitudes of the platforms. We, therefore, do not believe that the numerical values obtained from scanning the aerial photographs would estimate the numerical values of the contrast ratios that would be obtained from a digital sensor. We do feel, however, that the relation between the numerical values in our scanned representation and those that would have been obtained by directly sensing the same scene with a digital sensor would be similar enough to perform the investigations reported in this section.

3.7 Image Processing of Highway Sections

To detect, count and classify vehicles we input the highway sections that were prepared as described above into an image processing package. We began by using OSU-MAP-for-the-PC, the same package used in our simulation programs described in Appendix B, but switched to the National Institute of Health's (NIH) Image package, since we found it to be more flexible for our needs. Using the NIH package required a great deal of subjectivity in counting and classifying the vehicles and required much operator interaction. Therefore, to test what we had learned with the interactive process using the NIH package, we developed a series of computer programs to automate the image processing tasks. The computer programs work in much the same fashion, however. Specifically, as described in Appendix B, the computer programs take a matrix of numbers as input and output a series of clumps (or clusters) with associated attributes and statistics.

The classification process using the NIH approach will be discussed first. The image (input matrix) is comprised of digital count values ranging from 0 to 255. To threshold an image is to convert the image to a 2-bit image, one that is comprised of only two grey levels – 0 and 1. The image was thresholded interactively using a command in Image. The threshold value was selected interactively by the operator to eliminate the patches of pavement that were not considered to be vehicles. This threshold value was a subjective evaluation, but the threshold procedure was consistent when analyzing each of the images. Specifically, the operator selected the largest value such that the highway median would just disappear. Because of changes of reflectance in the pavement across the image, the threshold value was not necessarily the same from one portion of highway to the next.

To form the clumps, the user first specifies a threshold level so that all cell entries above this level are converted to 1's and all values below this level are converted to 0's. As noted in Appendix B, it is straightforward to convert values below the level to 0's and values above the level to 1's. We call this step "eliminating the pavement," since we define the threshold level so that we anticipate converting to 1 almost all cell values that correspond to pixels (picture element–a grid cell) of only pavement. Because the reflectance values of the vehicles are distributed much like the reflectance values of the

pavement, we inevitably convert to 1 many cell values that correspond to vehicle pixels at this step. We discovered, however, that vehicle shadows were among the darkest elements in the images. Therefore, by converting to 0 all cell values below a low threshold value, the cells containing 0's were primarily associated with vehicle shadows.

In Figure 3.8, we see the results of thresholding the digital representation portrayed in Figure 3.7 at a level of 56. Specifically, Image converted all cell values greater than 56 to 1's and all values less than or equal to 56 to 0's. The Image package then plots all pixels with 0 values as black and does not plot anything for pixels with values of 1.

After obtaining a binary matrix (a matrix with cell values containing only 0's or 1's) in this way, the counting operation forms entities called clumps (or particles) of all contiguous pixels containing values of 0. The program also attaches identifiers and attributes to each clump. The identifiers are simply integers that number the clumps. The two attributes of most interest to us in this phase of the analysis were the number of pixels in the clump (area) and the perimeter of the clump.

In Figure 3.9 and Table 3.1, we see the results of the clumping process. The contiguous pixels of Figure 3.8 are grouped together into clumps and given the identifiers shown in Figure 3.9. The identified clumps are listed in Table 3.1, along with the number of pixels in the clump area and the perimeter of the clump.

Table 3.1. Identifiers, attributes, and classification of clumps in Figure 3.9.

Identifier	*Area (A)*	*Perimeter (P)*	*B = (P/A)*	*Classification*
1	28	26.14	0.93	other vehicle
2	111	50.21	0.45	truck
3	8	10.49	1.31	other vehicle
4	51	39.31	0.77	truck
5	4	7.66	1.92	other vehicle
6	75	44.73	0.60	truck
7	3	7.24	2.41	nonvehicle

Finally, we used a spreadsheet software package to produce histograms of the clump sizes. Figure 3.10 is the histogram of the number of pixels in the clumps identified in Figure 3.9 and Table 3.1.

To make this process operational, several issues would surface. For example, most of the commands used in Image can be used in more sophisticated software. The software runs faster, larger images can be held in memory, and macros can be written to automate the import of images, the analysis and the export of data, and to minimize the operator interaction with the image processing software. We envision that a network of highways would already be available for a city or rural highway system. Images received

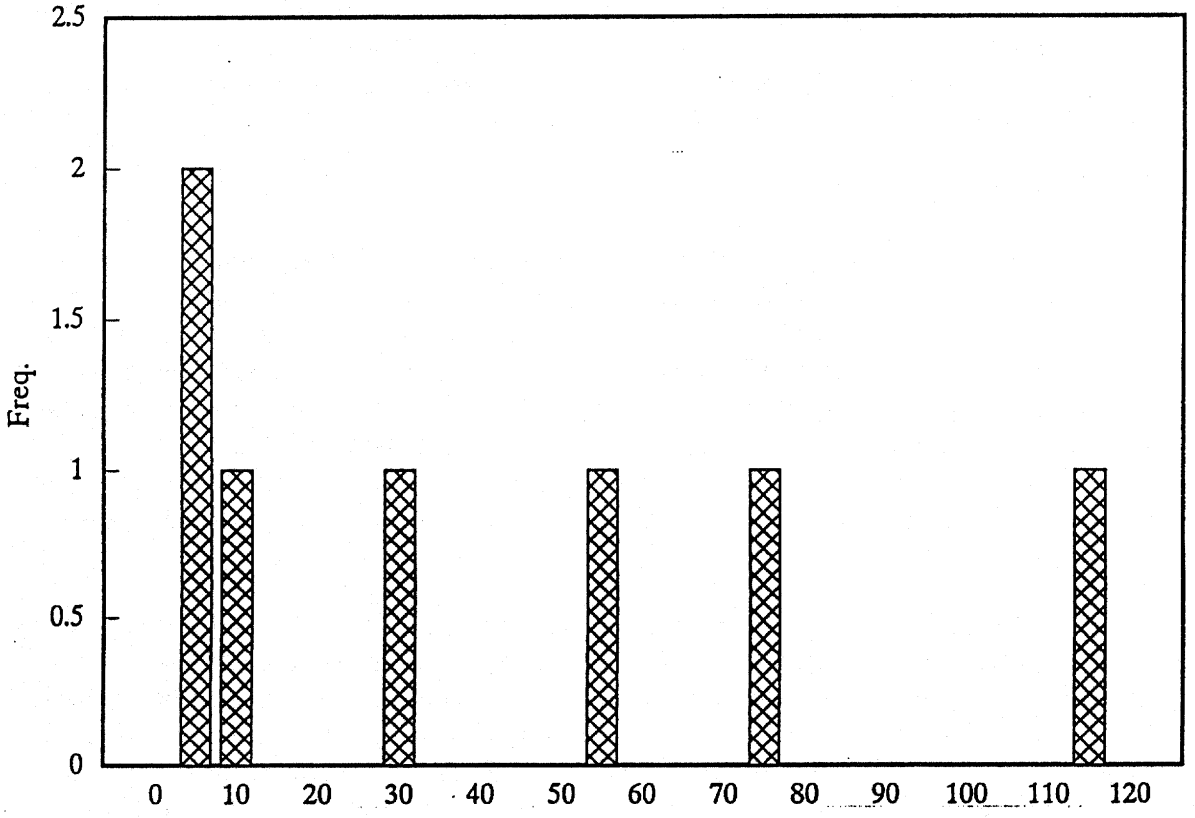

Figure 3.10 Histogram of areas (numbers of pixels) of clumps in Figure 3.9 and Table 3.1

from the satellite platform would be georeferenced with the highway network. A buffer zone around the highways would be an additional overlay in the system. Image areas within this buffer zone would be extracted from the satellite images. The thresholding operation would require some user intervention initially, but with time, given threshold values could be used as rules-of-thumb for a given area based on levels of contrast and brightness within an image. The counting process could be performed automatically by the program. The area and perimeter of each clump could be processed through a computer program to classify the clump into an individual class of vehicle. These were the processes that we incorporated as much as possible into our automatic image processing programs described later in this section.

3.8 Estimated Classification of Vehicles

The number of clumps could serve as an estimate of the total number of vehicles counted. Experience with the images showed that this process would often form clumps of elements not associated with vehicles, however. For example, shadows of signs, over-passes or trees would remain after thresholding to "eliminate the pavement." Also, some dark patches of pavement would form clumps. Therefore, we tried to use the clump attributes to classify each clump as being associated with a vehicle or with a "nonvehicle." We used the same attributes to classify the vehicles into what we called "trucks" (large vehicles) and "other vehicles" (smaller vehicles, which could be cars, vans, pick-ups and the like).

We used the number of pixels in the clump and the ratio of the clump's perimeter to its area to classify the clump as a truck, other vehicle or nonvehicle. (To be precise, we should say that we classified the clump "as being associated with" a truck, other vehicle, or nonvehicle, since the clump was usually produced by the shadow – perhaps with a few pixels actually produced by the object, such as the dark cab of a truck on a light pavement – of the element. We shall refer to the clump as "being" a truck, other vehicle, or nonvehicle, however, except where the distinction is needed for clarity.) We chose these attributes after noticing that the number of pixels in the clump offered a good first approximation of the nature of the clump and that many nonvehicle clumps were longer and thinner than vehicle clumps (this latter characteristic being represented by high perimeter to area ratios).

We call the number of pixels in the clump A (for area) and the perimeter to area ratio B. One could conceive of a study designed to find which values of A and B perform better than others. At this stage, however, we were only interested in exploring the possibilities of vehicle classifications and in producing a rough estimate of the performance of different resolutions. Therefore, we experimented only briefly before settling on A and B values used in our analysis. These levels can be found in the classification flow charts shown in Figures 3.11a-c. As seen there, the values of A and B change with the resolution used, since a shadow of a given metric area would cover fewer and fewer pixels as the size of the pixel increases, i.e., as the resolution becomes coarser.

As an illustration, consider again the clumps of Figure 3.9 and Table 3.1. These were produced from a 1.0 m simulated resolution. By applying the criteria illustrated in

the flow charts of Figure 3.11a (i.e., those that correspond to 1.0 m resolution) we obtained the classifications seen in Table 3.1. We call the classifications produced in this way the "estimated classification."

3.9 Comparison of Counted Vehicles to True Count

The final step was to compare the estimated classification to what we believed to be the true classification. We did this both formally, keeping track of statistics that summarize successful and unsuccessful classifications, or informally, qualitatively seeing how well the estimated classifications were performing.

In both cases we needed to determine what we believed to be the true classification for the given highway segment. We did this by having two individuals "manually" interpret the segment on the original aerial photograph under a magnifying lens, and having them come to an agreement on whether each vehicle observed was a truck or other vehicle. Note that this process would introduce error into our approximation of the true classification and, therefore, into any comparisons between the estimated classification and that approximated as the truth. One source of error would be the errors made by the individuals performing the manual classification – they could either misclassify a vehicle or not observe a vehicle that could be observed in the image. Another source of error would be that associated with the inability of the aerial photograph to capture the true image – e.g., vehicles in shadows would not be seen in the aerial photograph.

Once the true classification was approximated, we could then compare the vehicles identified in this "true data set" to the clumps produced in the estimated classification.

3.10 Discussion of Statistical Measures to Identify and Classify Vehicles

The traditional remote sensing measures of classification accuracy compare a classified pixel to an approximation of the true classification of the pixel. Our task was somewhat different in that we were not comparing the classification pixel by pixel, but rather comparing clumps and objects identified in a scene. Moreover, the number of objects in the simulated remote sensing product (the clumps output from the image processing stage) and in the truth (the number of vehicles identified from the aerial photograph) could be different. We, therefore, had to modify slightly the traditional measures to obtain meaningful statistics for our application.

After performing the steps described above, we could consider two lists for each highway segment analyzed, a list of clumps output from the image processing software and a list of vehicles from the analysis of the aerial photograph. Each clump in the "clump list" would have a location associated with it (by its x,y location in the image) and be classified as either a truck (t), other vehicle (o), or nonvehicle (n). Similarly, each vehicle in the "vehicle list" would have a location identified with it (by its location on the aerial photograph) and be classified as either a truck (t) or other vehicle (o). Note that there would be no nonvehicle classifications for the objects in the "vehicle list." We call

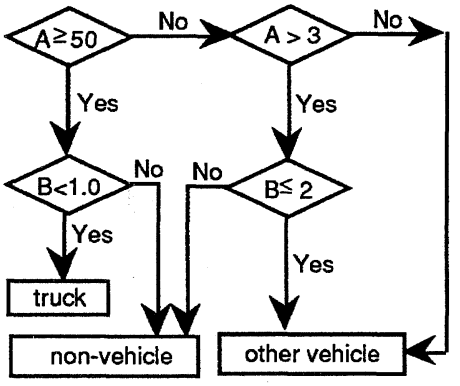

a. 1.0 m simulated resolution.

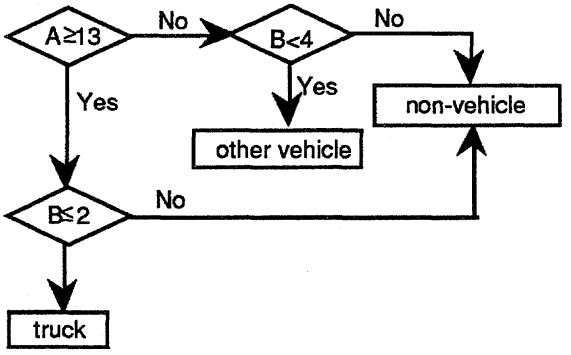

b. 2.1 m simulated resolution.

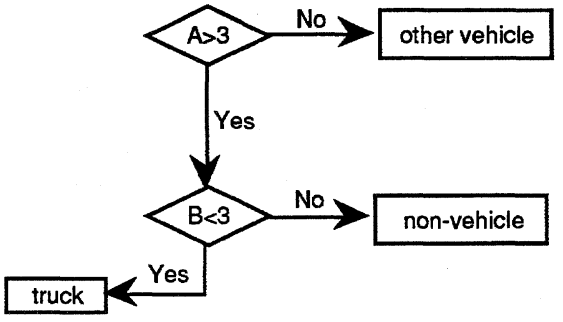

c. 4.2 m simulated resolution.

Figure 3.11. Classification logic based on number of pixels (A) and perimeter-to-area ratio (B) for different simulated resolutions.

the number of clumps in the clump list *NC*, and the number of clumps in the vehicle list *NV*.

First, consider the clump list. Since the objective is to identify and classify vehicles, the performance measure should reflect how well the classifications of the objects in the clump list match their true classifications. To define the appropriate terms, consider clump *i* in the clump list. It could be classified as either a truck (t), other vehicle (o), or nonvehicle (n). The area associated with the pixels of the clumps in the aerial photograph could be associated with the presence of a truck (t), other vehicle (o), or nonvehicle element (n). (We say that the area would be associated with a truck, for example, since the area might be imaging part of the vehicle itself, a shadow of the vehicle, or the sun's reflection off of the vehicle.) The nonvehicle designation of the area in the photograph is reserved for elements that could not be associated with a vehicle, e.g., patches of pavements or shadows of overpasses. We define an indicator variable I_{kl} (i) for element *i* of the clump list as follows.

$I_{kl}(i) = 1$, if the *i*th element in the clump list is classified as *k* in the estimated classification and the associated pixels in the aerial photograph truly correspond to classification *l*;
0, otherwise;
for $k = t, o, n$; and $l = t, o, n$. (3.2)

For example, if the *i*th clump was classified as a "truck" and the corresponding pixels in the aerial photograph were associated with an "other vehicle," then $I_{to}(i) = 1$, and $I_{tt}(i) = I_{tn}(i) = I_{ot}(i) = I_{oo}(i) = I_{on}(i) = I_{nt}(i) = I_{no}(i) = I_{nn}(i) = 0$. In this way, a correctly classified clump *i* would be indicated by $I_{kl}(i) = 1$, when *l* equals *k*, and a misclassified clump would be indicated by $I_{kl}(i) = 1$ for any *l* not equal to *k*.

We could then obtain an indicator for each clump *i* in the list and form the following sums from these indicator variables:

$$a_{kl} = \sum_{i=1}^{NC} I_{kl}(i), \text{ for } k = t, o, n, \text{ and } l = t, o, n. \quad (3.3)$$

The value of a_{kl} would give the number of clumps on the highway segment that were estimated to be of classification *k*, but were truly associated with classification *l* on the aerial photograph. The values of a_{tt} and a_{oo} would give the number of clumps that were correctly classified as trucks and other vehicles, respectively; the values of a_{to} and a_{tn} would give the number of clumps that were misclassified as trucks when they were truly other vehicles and nonvehicles, respectively; the values of a_{ot} and a_{on} would give the number of clumps that were misclassified as other vehicles when they were truly trucks and nonvehicles, respectively; and the values of a_{nt} and a_{no} would give the number of clumps that truly corresponded to trucks and other vehicles, respectively, but were classified as nonvehicles. Finally, the value of a_{nn} would give the number of clumps that were classified as nonvehicles that were truly nonvehicle elements, although this measure would be of less interest in our study. In summary, the a_{tt} and a_{oo} values give the number

of clumps that were correctly classified, and the a_{to}, a_{tn}, a_{ot} and a_{on} values would give the number of clumps that were misclassified as vehicles.

There could still be some vehicles that did not appear as clumps that would not be accounted for by the a_{kl} values. For example, the pixels associated with some of the vehicles might be eliminated when "eliminating the pavement" in the thresholding step of the image processing component. To account for the classification performance of the true vehicles, we considered the vehicles identified on the highway segment in the aerial photograph as forming a "vehicle list," consisting of *NV* elements (vehicles). We define an indicator variable $J_{kl}(i)$ for the ith element of the vehicle list as follows:

$J_{kl}(i) = 1$, if the *i*th vehicle in the vehicle list is truly of classification *k* and the corresponding clump in the clump list is estimated to be of classification *l*;
0, otherwise;
for k = t, o; and l = t, o, n. (3.4)

For example, if the *i*th vehicle in the vehicle list were truly an "other vehicle" in the aerial photograph and the corresponding clump were classified as a "nonvehicle," then $J_{on}(i) = 1$, and $J_{tt}(i) = J_{to}(i) = J_{tn}(i) = J_{ot}(i) = J_{oo}(i) = 0$. We note that the "n" classification could correspond to a clump being classified as a nonvehicle due to the attributes of the clump (see Fig. 3.11), or it could correspond to no clump having been formed in the image processing step that could be associated with the vehicle in the aerial photograph. We note also that since an element in the vehicle list would either be a truck (t) or other vehicle (o), there would be no "n" classification for the first subscript of the J indicator variable. Therefore, there would only be six categories when considering an element from the vehicle list, whereas, there would be nine when considering an element from the clump list. A vehicle *i* that was correctly classified in the image processing component would, therefore, be indicated by either $J_{tt}(i) = 1$ or $J_{oo}(i) = 1$ (i.e., $J_{kl}(i) = 1$, when *l* equals *k*), and a vehicle that was incorrectly classified in the image processing component would be indicated by $J_{kl}(i) = 1$ for any *l* not equal to *k*.

We could then obtain an indicator for each vehicle *i* in the vehicle list and form the following sums from these indicator variables:

$$b_{kl} = \sum_{i=1}^{NV} J_{kl}(i), \qquad \text{for } k = \text{t, o; and } l = \text{t, o, n.} \tag{3.5}$$

The value of b_{kl} would give the number of vehicles on the highway segment that were classified as *k* in the aerial photograph, but were estimated to be of classification *l* in the image processing step. The values of b_{tt} and b_{oo} would give the number of trucks and vehicles, respectively, that were correctly classified. Note that $b_{tt} = a_{tt}$ and $b_{oo} = a_{oo}$. The values of b_{to} and b_{tn} would give the number of trucks that were misclassified as other vehicles and nonvehicles (including not being identified), respectively. Note that $b_{to} = a_{ot}$ and $b_{tn} = a_{nt}$. The values of b_{ot} and b_{on} would give the number of other vehicles that were misclassified as trucks and nonvehicles (including not being identified), respectively. Note that $b_{ot} = a_{to}$ and $b_{on} = a_{no}$.

We summarize the a_{kl} data elements in the "Clump Classification Table" (Table 3.2a) and the b_{kl} data elements in the "Vehicle Classification Table" (Table 3.2b). We can then use these data elements to form performance measures. The summary statistics for the performance measures used in our study – fraction correct and errors of omission and commission – are described in Appendix D.

Table 3.2. Summary of classification data elements.

a. Clump classification table.

True classification of clump / Estimated classification of clump	**Truck**	**Other Vehicle**	**Non-Vehicle**
Truck	a_{tt}	a_{to}	a_{tn}
Other Vehicle	a_{ot}	a_{oo}	a_{on}
Non-Vehicle	a_{nt}	a_{no}	a_{nn}

b. Vehicle classification table.

Estimated classification of vehicle / True classification of vehicle	**Truck**	**Other Vehicle**	**Non-Vehicle**
Truck	b_{tt}	b_{to}	b_{tn}
Other Vehicle	b_{ot}	b_{oo}	b_{on}

3.11 Quantitative Results using the NIH Image Program

We analyzed seven highway segments in the aerial photographs at the four simulated resolutions (0.6 m, 1.0 m, 2.1 m, 4.2 m) resulting from the scan rates discussed above. All segments were on interstate routes in the west-central or central part of Franklin County, Ohio (see Fig. 3.12). Other characteristics of the segments can be found in Table 3.3. The scanned images at the 1.0 m resolution for these seven segments are shown in Appendix E. We chose a threshold value based on the analyst's iteratively thresholding the image until the highway median disappeared from the image. The classification criteria were those presented in Figure 3.11.

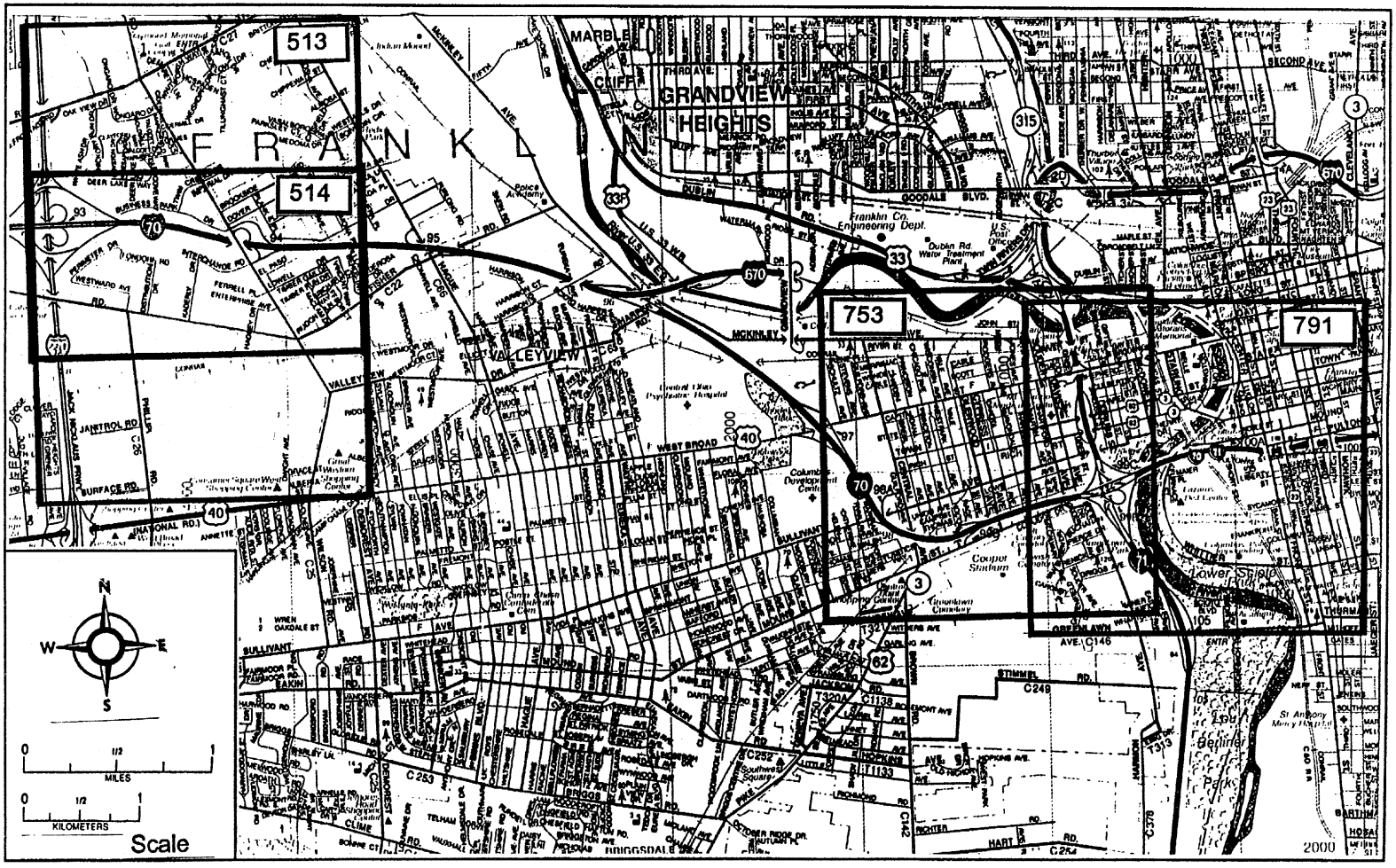

Figure 3.12 Locations of aerial photographs in Franklin County, Ohio, scanned for analysis.

Table 3.3. Characteristics of highway segments analyzed in the study.

Image No.: Orientation *(highway segment)*	*Facility & Location*	*Geometry*	*Length* *(km)*	*Pavement*
514: E-W	I-70, between I-270 & Hague Ave.	Tangent	0.7	Concrete
513: E-W	I-70, between I-270 & Hague Ave.	Tangent	4.1	Concrete
791: NW-SE	I-71, just south of I-70	Tangent	0.7	Concrete
791: E-W	I-70, just west of I-70	Tangent	0.6	Concrete, asphalt
753(1): NNW-SSE	I-70, between W. Broad & I-71	Horizontal curve	0.6	Asphalt, concrete
753(2): NW-SE	I-70, between W. Broad & I-71	Horizontal curve	0.6	Concrete, asphalt
753(3): EEN-WWS	I-70, between W. Broad & I-71	Horizontal curve	0.9	Asphalt, concrete

The nine summary performance statistics (see Appendix D) for the four resolutions can be found in the manual interpretation results of Table 3.4. We had some trouble determining the performance measures for some of the highway segments at the 4.2 m resolution, since we were comparing features manually in this study. If one were to digitize the locations of the vehicles in the aerial photographs, most of the difficulties encountered would disappear. A detailed statistical analysis of the manual interpretation results can be found in McCord *et al.* (1994).

In general, the Fraction Correct statistics improve as the resolution becomes finer. Considering the Fraction of Vehicles Correctly Identified (FVCI) (Table 3.4a.i), which indicates the ability to identify a vehicle of any kind that is present, the 2.1 m resolution performs better than the 4.2 m resolution on both of the segments where we have summary statistics for the two resolutions. Comparing the 1.0 m to the 2.1 m resolutions, the 1.0 m resolution performs better 7 out of 7 times. Comparing the 1.0 m to the 0.6 m resolutions, the 0.6 m resolution does not necessarily outperform the 1.0 m resolution. In fact, the 1.0 outperforms the 0.6 m resolution 4 *vs.* 2 times with one tie. The overall aggregate statistic is highest for the 1.0 m resolution.

Although the aggregate Fraction Correct statistic for the truck classifications – Fraction of Trucks Correctly Classified (FTCC) (Table 3.4b.i) – was worse at 2.1 m resolution than at 4.2 m resolution, this was due in part to not having statistics available at the 4.2 m resolution for those segments where the 2.1 m performance was poor. In fact, out of the five segments where we had statistics for the two resolutions, the 4.2 m resolution

Table 3.4 Statistical performance measures for vehicles, trucks and other vehicles.

3.4a. Fraction of vehicles correctly identified (FVCI).

i. Manual interpretation.

Resolution / Image #: Orientation (hwy segment)	0.6 m	1.0 m	2.1 m	4.2 m
514: E-W	32/44 = 0.727	41/44 = 0.932	38/44 = 0.864	25/44 = 0.568
513: E-W	38/38 = 1.000	33/38 = 0.868	27/38 = 0.711	22/38 = 0.579
791: NW-SE	43/50 = 0.860	50/50 = 1.000	46/50 = 0.920	N/A
791: E-W	40/41 = 0.976	35/41 = 0.854	29/41 = 0.707	N/A
753(1): NNW-SSE	46/49 = 0.939	48/49 = 0.980	31/49 = 0.633	N/A
753(2): NW-SE	32/32 = 1.000	32/32 = 1.000	31/32 = 0.969	23/32 = 0.719
753(3): EEN-WWS	51/55 = 0.927	52/55 = 0.945	46/55 = 0.836	N/A
Aggregate Statistic:	*282/309 = 0.913*	*291/309 = 0.942*	*248/309 = 0.803*	*48/76 = 0.632*

ii. Image processing.

Resolution / Image #: Orientation (hwy segment)		1.2 m	2.4 m	4.8 m
514: E-W		42/46 = 0.913	32/46 = 0.696	21/46 = 0.456
513: E-W		39/40 = 0.975	34/40 = 0.850	16/40 = 0.400
791: NW-SE		51/55 = 0.927	40/55 = 0.727	24/55 = 0.436
791: E-W		35/37 = 0.946	28/37 = 0.757	19/37 = 0.514
753(1): NNW-SSE		47/48 = 0.979	37/48 = 0.771	25/48 = 0.521
753(2): NW-SE		31/32 = 0.969	29/32 = 0.906	13/32 = 0.406
753(3): EEN-WWS		31/36 = 0.861	26/36 = 0.722	12/36 = 0.333
Aggregate Statistic:		*276/294 = 0.939*	*226/294 = 0.769*	*130/394 = 0.442*

Table 3.4b. Fraction of trucks correctly classified (FTCC).

i. Manual interpretation.

Resolution / Image #: Orientation (hwy segment)	0.6 m	1.0 m	2.1 m	4.2 m
514: E-W	5/9 = 0.556	9/9 = 1.000	9/9 = 1.000	9/9 = 1.000
513: E-W	8/8 = 1.000	6/8 = 0.750	6/8 = 0.750	6/8 = 0.750
791: NW-SE	6/8 = 0.750	5/8 = 0.625	5/8 = 0.625	N/A
791: E-W	2/2 = 1.000	1/2 = 0.500	1/2 = 0.500	1/2 = 0.500
753(1): NNW-SSE	7/7 = 1.000	7/7 = 1.000	4/7 = 0.571	5/7 = 0.714
753(2): NW-SE	3/3 = 1.000	3/3 = 1.000	3/3 = 1.000	3/3 = 1.000
753(3): EEN-WWS	8/9 = 0.889	9/9 = 1.000	6/9 = 0.667	N/A
Aggregate Statistic:	*39/46 = 0.848*	*40/46 = 0.870*	*34/46 = 0.739*	*24/29 = 0.828*

ii. Image processing.

Resolution / Image #: Orientation (hwy segment)		1.2 m	2.4 m	4.8 m
514: E-W		9/9 = 1.000	9/9 = 1.000	9/9 = 1.000
513: E-W		7/7 = 1.000	7/7 = 1.000	7/7 = 1.000
791: NW-SE		7/8 = 0.875	8/8 = 1.000	4/8 = 0.500
791: E-W		3/3 = 1.000	3/3 = 1.000	3/3 = 1.000
753(1): NNW-SSE		7/7 = 1.000	7/7 = 1.000	6/7 = 0.857
753(2): NW-SE		3/3 = 1.000	3/3 = 1.000	3/3 = 1.000
753(3): EEN-WWS		8/8 = 1.000	8/8 = 1.00	4/8 = 0.500
Aggregate Statistic:		*44/45 = 0.978*	*45/45 = 1.000*	*36/45 = 0.800*

Table 3.4c. Fraction of other vehicles correctly classified (FOCC).

i. Manual interpretation.

Resolution / Image #: Orientation (hwy segment)	0.6 m	1.0 m	2.1 m	4.2 m
514: E-W	23/35 = 0.657	32/35 = 0.914	29/35 = 0.829	16/35 = 0.457
513: E-W	30/30 = 1.000	24/30 = 0.800	19/30 = 0.633	15/30 = 0.500
791: NW-SE	36/42 = 0.857	42/42 = 1.000	38/42 = 0.905	N/A
791: E-W	37/39 = 0.949	34/39 = 0.872	28/39 = 0.718	26/39 = 0.667
753(1): NNW-SSE	39/42 = 0.929	40/42 = 0.952	26/42 = 0.619	18/42 = 0.429
753(2): NW-SE	29/29 = 1.000	29/29 = 1.000	28/29 = 0.965	19/29 = 0.655
753(3): EEN-WWS	43/46 = 0.935	43/46 = 0.935	39/46 = 0.848	N/A
Aggregate Statistic:	*237/263 = 0.901*	*244/263 = 0.928*	*207/263 = 0.787*	*94/175 = 0.537*

ii. Image processing.

Resolution / Image #: Orientation (hwy segment)		1.2 m	2.4 m	4.8 m
514: E-W		33/37 = 0.892	23/37 = 0.622	12/37 = 0.324
513: E-W		32/33 = 0.970	27/33 = 0.818	9/33 = 0.273
791: NW-SE		44/47 = 0.936	32/47 = 0.681	20/47 = 0.426
791: E-W		32/34 = 0.941	25/34 = 0.735	16/34 = 0.471
753(1): NNW-SSE		40/41 = 0.976	30/41 = 0.732	19/41 = 0.463
753(2): NW-SE		28/29 = 0.966	26/29 = 0.897	10/29 = 0.345
753(3): EEN-WWS		23/28 = 0.821	18/28 = 0.643	8/28 = 0.286
Aggregate Statistic:		*232/249 = 0.932*	*181/249 = 0.727*	*94/249 = 0.378*

Table 3.4d. Vehicle identification error of omission (VIEO).

i. Manual interpretation.

Resolution / Image #: Orientation (hwy segment)	0.6 m	1.0 m	2.1 m	4.2 m
514: E-W	12/44 = 0.273	3/44 = 0.068	6/44 = 0.136	19/44 = 0.432
513: E-W	0/38 = 0.000	5/38 = 0.132	11/38 = 0.289	16/38 = 0.421
791: NW-SE	7/50 = 0.140	0/50 = 0.000	4/50 = 0.080	N/A
791: E-W	1/41 = 0.024	6/41 = 0.146	12/41 = 0.293	N/A
753(1): NNW-SSE	3/49 = 0.061	1/49 = 0.020	18/49 = 0.367	N/A
753(2): NW-SE	0/32 = 0.000	0/32 = 0.000	1/32 = 0.031	9/32 = 0.281
753(3): EEN-WWS	4/55 = 0.073	3/55 = 0.055	9/55 = 0.164	N/A
Aggregate Statistic:	*27/309 = 0.087*	*18/309 = 0.058*	*61/309 = 0.197*	*44/114 = 0.386*

ii. Image processing.

Resolution / Image #: Orientation (hwy segment)		1.2 m	2.4 m	4.8 m
514: E-W		4/46 = 0.087	14/46 = 0.304	25/46 = 0.543
513: E-W		1/40 = 0.025	6/40 = 0.150	24/40 = 0.600
791: NW-SE		4/55 = 0.073	15/55 = 0.273	31/55 = 0.564
791: E-W		2/37 = 0.054	9/37 = 0.243	18/37 = 0.486
753(1): NNW-SSE		1/48 = 0.021	11/48 = 0.229	23/48 = 0.479
753(2): NW-SE		1/32 = 0.031	3/32 = 0.094	19/32 = 0.594
753(3): EEN-WWS		5/36 = 0.139	10/36 = 0.278	24/36 = 0.667
Aggregate Statistic:		*18/294 = 0.061*	*68/294 = 0.231*	*164/294 = 0.558*

Table 3.4e. Truck classification error of omission (TCEO).

i. Manual interpretation.

Resolution / Image #: Orientation (hwy segment)	0.6 m	1.0 m	2.1 m	4.2 m
514: E-W	4/9 = 0.444	0/9 = 0.000	0/9 = 0.000	0/9 = 0.000
513: E-W	0/8 = 0.000	2/8 = 0.250	2/8 = 0.250	2/8 = 0.250
791: NW-SE	2/8 = 0.250	3/8 = 0.375	3/8 = 0.375	N/A
791: E-W	0/2 = 0.000	1/2 = 0.500	1/2 = 0.500	1/2 = 0.500
753(1): NNW-SSE	0/7 = 0.000	0/7 = 0.000	3/7 = 0.429	2/7 = 0.286
753(2): NW-SE	0/3 = 0.000	0/3 = 0.000	0/3 = 0.000	0/3 = 0.000
753(3): EEN-WWS	1/9 = 0.111	0/9 = 0.000	3/9 = 0.333	N/A
Aggregate Statistic:	*7/46 = 0.152*	*6/46 = 0.130*	*12/46 = 0.261*	*5/29 = 0.172*

ii. Image processing.

Resolution / Image #: Orientation (hwy segment)		1.2 m	2.4 m	4.8 m
514: E-W		0/9 = 0.000	0/9 = 0.000	0/9 = 0.000
513: E-W		0/7 = 0.000	0/7 = 0.000	0/7 = 0.000
791: NW-SE		1/8 = 0.125	0/8 = 0.000	4/8 = 0.050
791: E-W		0/3 = 0.000	0/3 = 0.000	0/3 = 0.000
753(1): NNW-SSE		0/7 = 0.000	0/7 = 0.000	1/7 = 0.143
753(2): NW-SE		0/3 = 0.000	0/3 = 0.000	0/3 = 0.000
753(3): EEN-WWS		0/8 = 0.000	0/8 = 0.000	4/8 = 0.500
Aggregate Statistic:		*1/45 = 0.022*	*0/45 = 0.000*	*9/45 = 0.200*

Table 3.4f. Other vehicle classification error of omission (OCEO).

i. Manual interpretation.

Resolution / Image #: Orientation (hwy segment)	0.6 m	1.0 m	2.1 m	4.2 m
514: E-W	12/35 = 0.343	3/35 = 0.086	6/35 = 0.171	19/35 = 0.543
513: E-W	0.30 = 0.000	6/30 = 0.200	11/30 = 0.367	15/30 = 0.500
791: NW-SE	6/42 = 0.143	0/42 = 0.000	4/42 = 0.095	N/A
791: E-W	2/39 = 0.051	5/39 = 0.128	11/39 = 0.282	13/39 = 0.333
753(1): NNW-SSE	3/42 = 0.071	2/42 = 0.048	16/42 = 0.381	24/42 = 0.571
753(2): NW-SE	0/29 = 0.000	0/29 = 0.000	1/29 = 0.035	10/29 = 0.345
753(3): EEN-WWS	3/46 = 0.065	3/46 = 0.065	7/46 = 0.152	N/A
Aggregate Statistic:	*26/263 = 0.099*	*19/263 = 0.072*	*56/263 = 0.213*	*81/175 = 0.463*

ii. Image processing.

Resolution / Image #: Orientation (hwy segment)		1.2 m	2.4 m	4.8 m
514: E-W		4/37 = 0.108	14/37 = 0.378	25/37 = 0.676
513: E-W		1/33 = 0.030	6/33 = 0.182	24/33 = 0.727
791: NW-SE		3/47 = 0.064	15/47 = 0.319	27/47 = 0.574
791: E-W		2/34 = 0.059	9/34 = 0.265	18/34 = 0.529
753(1): NNW-SSE		1/41 = 0.024	11/41 = 0.268	22/41 = 0.537
753(2): NW-SE		1/29 = 0.034	3/29 = 0.103	19/29 = 0.655
753(3): EEN-WWS		5/28 = 0/179	10/28 = 0.357	20/28 = 0.714
Aggregate Statistic:		*17/249 = 0.068*	*68/249 = 0.273*	*155/249 = 0.622*

Table 3.4g. Vehicle identification error of commission (VIEC).

i. Manual interpretation.

Resolution / Image #: Orientation (hwy segment)	0.6 m	1.0 m	2.1 m	4.2 m
514: E-W	3/31 = 0.097	7/48 = 0.146	4/42 = 0.095	8/33 = 0.242
513: E-W	0/38 = 0.000	9/42 = 0.214	13/40 = 0.325	16/22 = 0.727
791: NW-SE	3/46 = 0.065	15/65 = 0.231	8/54 = 0.148	N/A
791: E-W	4/44 = 0.091	11/46 = 0.239	8/37 = 0.216	N/A
753(1): NNW-SSE	2/48 = 0.042	19/67 = 0.284	6/37 = 0.162	N/A
753(2): NW-SE	0/32 = 0.000	0/32 = 0.000	3/34 = 0.088	4/27 = 0.148
753(3): EEN-WWS	2/53 = 0.038	11/63 = 0.175	12/58 = 0.207	N/A
Aggregate Statistic:	*14/292 = 0.048*	*72/363 = 0.198*	*53/301 = 0.176*	*28/82 = 0.341*

ii. Image processing.

Resolution / Image #: Orientation (hwy segment)		1.2 m	2.4 m	4.8 m
514: E-W		3/46 = 0.065	3/46 = 0.065	1/46 = 0.022
513: E-W		1/40 = 0.025	1/40 = 0.025	1/40 = 0.025
791: NW-SE		4/55 = 0.073	0/55 = 0.000	2/55 = 0.000
791: E-W		5/37 = 0.135	0/37 = 0.000	1/37 = 0.027
753(1): NNW-SSE		3/48 = 0.062	0/48 = 0.000	1/48 = 0.021
753(2): NW-SE		1/32 = 0.000	0/29 = 0.000	0/29 = 0.000
753(3): EEN-WWS		1/36 = 0.028	1/36 = 0.028	2/36 = 0.056
Aggregate Statistic:		*18/294 = 0.061*	*5/294 = 0.017*	*8/294 = 0.027*

Table 3.4h. Truck classification error of commission (TCEC).

i. Manual interpretation.

Resolution / Image #: Orientation (hwy segment)	0.6 m	1.0 m	2.1 m	4.2 m
514: E-W	0/5 = 0.000	0/9 = 0.000	0/9 = 0.000	0/9 = 0.000
513: E-W	0/8 = 0.000	2/8 = 0.250	2/8 = 0.250	1/7 = 0.143
791: NW-SE	1/7 = 0.143	1/6 = 0.167	1/6 = 0.167	N/A
791: E-W	2/4 = 0.500	2/3 = 0.667	1/2 = 0.500	6/7 = 0.857
753(1): NNW-SSE	0/7 = 0.000	1/8 = 0.125	0/4 = 0.000	0/5 = 0.000
753(2): NW-SE	0/3 = 0.000	0/3 = 0.000	0/3 = 0.000	0/3 = 0.000
753(3): EEN-WWS	2/10 = 0.200	0/9 = 0.000	2/8 = 0.250	N/A
Aggregate Statistic:	*5/44 = 0.114*	*6/46 = 0.130*	*6/40 = 0.150*	*7/31 = 0.226*

ii. Image processing.

Resolution / Image #: Orientation (hwy segment)		1.2 m	2.4 m	4.8 m
514: E-W		0/9 = 0.000	0/9 = 0.000	1/9 = 0.000
513: E-W		0/7 = 0.000	0/7 = 0.000	0/7 = 0.000
791: NW-SE		0/8 = 0.000	0/8 = 0.000	0/8 = 0.000
791: E-W		0/3 = 0.000	0/3 = 0.000	1/3 = 0.333
753(1): NNW-SSE		0/7 = 0.000	0/7 = 0.000	0/7 = 0.000
753(2): NW-SE		0/3 = 0.000	0/3 = 0.000	0/3 = 0.000
753(3): EEN-WWS		0/8 = 0.000	0/8 = 0.000	0/8 = 0.000
Aggregate Statistic:		*0/45 = 0.000*	*0/45 = 0.000*	*2/45 = 0.044*

Table 3.4i. Other vehicle classification error of commission (OCEC).

i. Manual interpretation.

Resolution / Image #: Orientation (hwy segment)	0.6 m	1.0 m	2.1 m	4.2 m
514: E-W	7/26 = 0.269	7/39 = 0.179	4/33 = .121	8/24 = 0.333
513: E-W	0/3 = 0.000	10/34 = 0.294	13/32 = .406	16/31 = 0.516
791: NW-SE	3/39 = 0.077	17/59 = 0.288	10/48 = .208	N/A
791: E-W	3/40 = 0.075	9/43 = 0.209	7/35 = .200	13/39 = 0.333
753(1): NNW-SSE	2/41 = 0.049	19/59 = 0.322	7/33 = .212	5/23 = 0217
753(2): NW-SE	0/29 = 0.000	0/29 = 0.000	3/31 = .097	5/24 = 0.208
753(3): EEN-WWS	0/43 = 0.000	11/54 = 0.204	11/50 = .220	N/A
Aggregate Statistic:	*15/221 = 0.068*	*72/317 = 0.230*	*55/262 = 0.210*	*47/141 = 0.333*

ii. Image processing.

Resolution / Image #: Orientation (hwy segment)		1.2 m	2.4 m	4.8 m
514: E-W		3/37 = 0.081	3/37 = 0.081	0/37 = 0.000
513: E-W		1/33 = 0.030	1/33 = 0.030	1/33 = 0.030
791: NW-SE		4/47 = 0.085	0/47 = 0.000	2/47 = 0.043
791: E-W		5/34 = 0.147	0/34 = 0.000	0/34 = 0.000
753(1): NNW-SSE		3/41 = 0.073	0/41 = 0.000	1/41 = 0.024
753(2): NW-SE		0/29 = 0.000	0/29 = 0.000	0/29 = 0.000
753(3): EEN-WWS		1/28 = 0.036	1/28 = 0.036	2/28 = 0.071
Aggregate Statistic:		*17/249 = 0.068*	*5/249 = 0.020*	*6/249 = 0.024*

outperformed the 2.1 m resolution in only one case – 753(1):N-S – and the improvement was slight – 5/7 versus 4/7 correctly classified. Moreover, comparing the 1.0 m (best) and 2.1 m (worst) FTCC's, there appears to be no significant difference in performance. Specifically, in the seven segment-by-segment comparisons, the 1.0 m resolution outperforms the 2.1 m resolution only twice. (The other five comparisons show equal performance.) The 0.6 m resolution slightly outperformed the 1.0 m resolution 3/7 *vs.* 2/7 correctly classified with 2 ties. In terms of classifying trucks, the data in our analysis are not sufficient to say that the resolutions are not performing equally well. We would leave open the possibility that 4 m resolution might be sufficient to classify trucks.

The finer resolution seems to be important in classifying "other vehicles," however (see Table 3.4c.i). The 2.1 m resolution's Fraction of other Vehicles Correctly Classified (FOCC) is better than the 4.2 m resolution's FOCC in all five of the segments where we had statistics for both resolutions. Similarly, the 1.0 resolution outperforms the 2.1 m resolution in all seven of the segment-by-segment comparisons. The 1.0 m resolution also slightly outperforms the 0.6 m resolution 3 times out of 7 segments with 2 ties. We would tentatively conclude that the 1.0 m resolution offers an improvement over the coarser resolutions for classifying other vehicles.

We mentioned in Appendix A that a typical standard in remote sensing performance is an accuracy level of 85%. This measure is generally associated with the ability to correctly identify some element that is present in the image. Adapting this measure to our study, we could think of this as meaning a 0.85 probability of correctly identifying or classifying a vehicle that is present. However, we checked with engineers involved in counting operations, and they desire a 90% accuracy rate. Therefore, we adopted a conservative value of 90% accuracy, rather than 85%.

Summarizing the results of the Fraction Correct Analysis, we believe that the 1.0 m resolution performed better than the 2.1 m and 4.2 m resolutions in counting vehicles and correctly classifying "other vehicles." The 1.0 m resolution also performed better than the 90% accuracy standard in these two tasks, while the 2.1 m and 4.2 m resolutions performed worse than this standard. We determined that the 0.6 m resolution did not significantly improve our classification measures when compared to the 1.0 m resolution. For example, for the fraction of vehicles, trucks and other vehicles classified (i.e., FVCI, FTCC and FOCC, respectively), the totals and average ratios increased slightly (about 3%) for the 1.0 resolution when compared to the 0.6 m resolution. In terms of classifying vehicles as trucks, it appears that we did not have enough truck observations in our images to determine whether one resolution was significantly outperforming another or in determining how the resolutions compared to the 90% standard. We have already mentioned this lack of control on input data as a drawback of this type of analysis and a reason for attempting to build the mathematical model described in Appendix A.

The Errors of Omission statistics (Tables 3.4d-f.i) are the complements of the Fraction Correct statistics and exhibit the same characteristics, in terms of resolution, as those discussed above.

The errors of commission indicate how many excess vehicles are being counted or classified in the specific vehicle class. The statistic is scaled by the number of clumps in the clump list, since an excess vehicle could only be counted or classified if there was a clump present.

Referring to Table 3.4g-i.i, we first note that as the resolution becomes finer, more clumps tend to form. Investigating the original data shows that at finer resolutions some nonvehicle clumps form that might have been "smoothed out" into the background pavement at coarser resolutions.

The Vehicle Identification Error of Commission (VIEC) ratio (Table 3.4g.i) is better (smaller) at the 2.1 m resolution than at the 4.2 m resolution for the two segments where we have data for both resolutions. The segment-by-segment comparisons between the 1.0 and 2.1 m resolutions show that the 2.1 m resolution performs better in 5 out of 7 cases. The segment-by-segment comparisons between the 0.6 and 1.0 m resolutions show that the 0.6 m resolution performs better in 6 out of 7 cases with 1 tie. At the finer resolution a lower commission error is found.

The Truck Classification Error of Commission (TCEC) (Table 3.4h.i) shows identical performance between the 4.2 and 2.1 m resolutions in 3 of the 5 cases where we have data for both resolutions. Comparing the 2.1 m and 1.0 m resolutions, the two perform identically in 4 of 7 segments; in the other three segments, the 2.1 m performs better in 2 cases. Comparing the 1.0 m and 0.6 m resolutions, the two perform identically in 2 of 7 segments; in the other five segments, the 0.6 m resolution performs better in 2 cases and the 1.0 m resolution performs better in 1 case. These data do not allow us to conclude that any of the three resolutions is performing better than any other in terms of errors of commission – we would need more analysis before doing so.

The Other vehicle Classification Error of Commission (OCEC) (Table 3.4i.i) shows that the 2.1 m resolution outperformed the 4.2 m resolution in 5 of the 5 segments where we had data for both resolutions. Comparing the 2.1 m and 1.0 m resolution, the 2.1 m has a lower OCEC in 4 of the 7 cases. Comparing the 1.0 m and 0.6 m resolutions, the 0.6 m has a lower OCEC in 5 of the 7 cases with 1 tie. The 1.0 m and 2.1 m resolutions perform equally well in terms of errors of commission, whereas the 0.6 m resolution would show an improvement.

The errors of commission data, then, support the Fraction Correct data in saying the improved imaging offered by the 1 m resolution may not improve truck classification significantly, at least for the simple algorithms used here. It also appears that the 1.0 m resolution offers no improvement over the 2.1 m resolution in terms of errors of commission when counting total vehicles and classifying "other vehicles." These two resolutions both seem to perform better than the 4.2 m resolution in terms of errors of commission for these two tasks, however.

3.12 Qualitative Results using the NIH Image Program

In addition to allowing a quantification of the accuracy and errors associated with counting and classifying vehicles by remotely sensing them in the panchromatic wavelengths, our simulated empirical study also provided qualitative insights. These qualitative observations were made on the difficulties that might be involved when conducting this task in the way we have been considering and allowed us to speculate on ways to overcome these difficulties.

We noticed that the shadows of the signs near the highway were often identified as other vehicles with the classification criteria we were using (i.e., the area and perimeter-to-area ratio of the clump). If remote sensing of traffic characteristics were to become an operational process, we believe that these difficulties could be reduced significantly in several ways. Fine-tuning of the classification criteria or using filters that account for shapes might eliminate many of the errors of commission associated with shadows from signs. This consideration for developing additional criteria was accounted for in our automatic image processing algorithms discussed in the following section. It would also be possible to reduce the problem by coupling good geographic data on the static location of the signs with dynamic positions of the sun (from solar ephemeris) to estimate where the sign shadows would be located on the pavement when the satellite imaged the highway. Therefore, in our automatic image processing procedure, we require an input value of sun angle to determine the proper orientation of the vehicle shadows. Finally, if the satellite were equipped with two sensors imaging the highway a second or so apart, the stationary shadows could be separated from those that had moved in the one second interval and subtracted from the clump list to be analyzed.

Although we did not have enough data and information to analyze the effect of pavement type on the imaging performance, we did feel that the reflectance value of the pavement did make a difference. We did not feel comfortable comparing the imaging performance of different pavement shades in the original aerial photograph, since the photographic grey tone would be influenced by the development process. In one segment, however, the pavement grey tones were different enough in a local area to call our attention to this problem. Specifically, when thresholding the image so as to eliminate most of the darker pavement, we were eliminating some of the vehicles (including their shadows) on the lighter parts of the pavement. This resulted in increased errors of omission (decreased ability to identify and classify a vehicle that was present). Again, good geographic information on pavement type and variations should allow one to fine-tune the thresholding methods in such trouble spots. The literature was studied to determine automatic ways to determine an optimum threshold level and are discussed in the following section.

None of the segments analyzed in the quantitative study was in the downtown area. We, therefore, investigated an additional segment of I-70 in an area where the tall buildings of downtown Columbus were casting large shadows on the pavement. We noticed that we needed to amend our area and perimeter-to-area values to make sure that we were not classifying the large shadows as trucks. After a simple modification,

however, we noticed that the performance measures were similar to those recorded in Table 3.4 for those areas not in the shadows. Any vehicle that was in the building shadows when the photograph was taken, however, would not have been identified either in our estimated count and classification or in the aerial photograph (the estimate of the truth). Therefore, our errors of omission would be underestimated. Our experience did show, however, that we can amend our procedures so that large shadows are not incorrectly classified as trucks, and that we can do so without degrading the performance in areas not covered by the shadows. It should also be possible to update the estimates of vehicle counts (perhaps probabilistically), if the sizes of these shadows could be approximated.

We also imaged an arterial street to get a feel for possible differences from the expressways that we had investigated in more detail. The only additional difficulty that we noticed in the arterial segment was that associated with the shadows of trees on the pavement. We tended to classify the resulting clumps as other vehicles. This difficulty is similar to that encountered with the sign shadows, however, and we would expect that it could be handled in similar ways as those proposed there. This difficulty might be slightly more troublesome, however, since trees grow, and they sprout and lose leaves during the year. Therefore, the shadow characteristics would change. Moreover, we would expect that it would be much more likely to have good geographic information on expressway sign locations than on arterial tree locations.

Finally, our experience made us aware of the inevitable trade-off between errors of omission and commission. When thresholding at lower values in an attempt to eliminate more of the background pavement, more vehicle pixels are eliminated. The likelihood of committing the error of identifying a clump of dark pavement as a vehicle is reduced, but the likelihood of omitting a vehicle that is present is increased. We would anticipate this trade-off with finer resolution. Although we do not foresee a way to avoid this problem, it should be possible to get a handle on its effect so that better estimates could be produced from the imaging data.

3.13 Image Processing Techniques for Vehicle Detection and Identification

We realized that our results using the NIH Image software required a subjective evaluation and selection of the proper threshold. We wanted to obtain better accuracies of vehicle identification and classification through advanced image processing techniques. This would also allow us to make the techniques more automated and objective in scope. Also, many more highway segments could be analyzed using this consistent approach. We considered three major components in our development: image processing for edge detection and noise removal, representing the shape of the edges by several parameters, and developing constraints or heuristic rules designed for vehicle detection.

A sequence of image processing tasks was developed to process a satellite image into a final image showing candidate cars (see flowchart in Fig. 3.13). An example road segment showing the three resolutions analyzed with the image processing approach is shown in Figure 3.14.

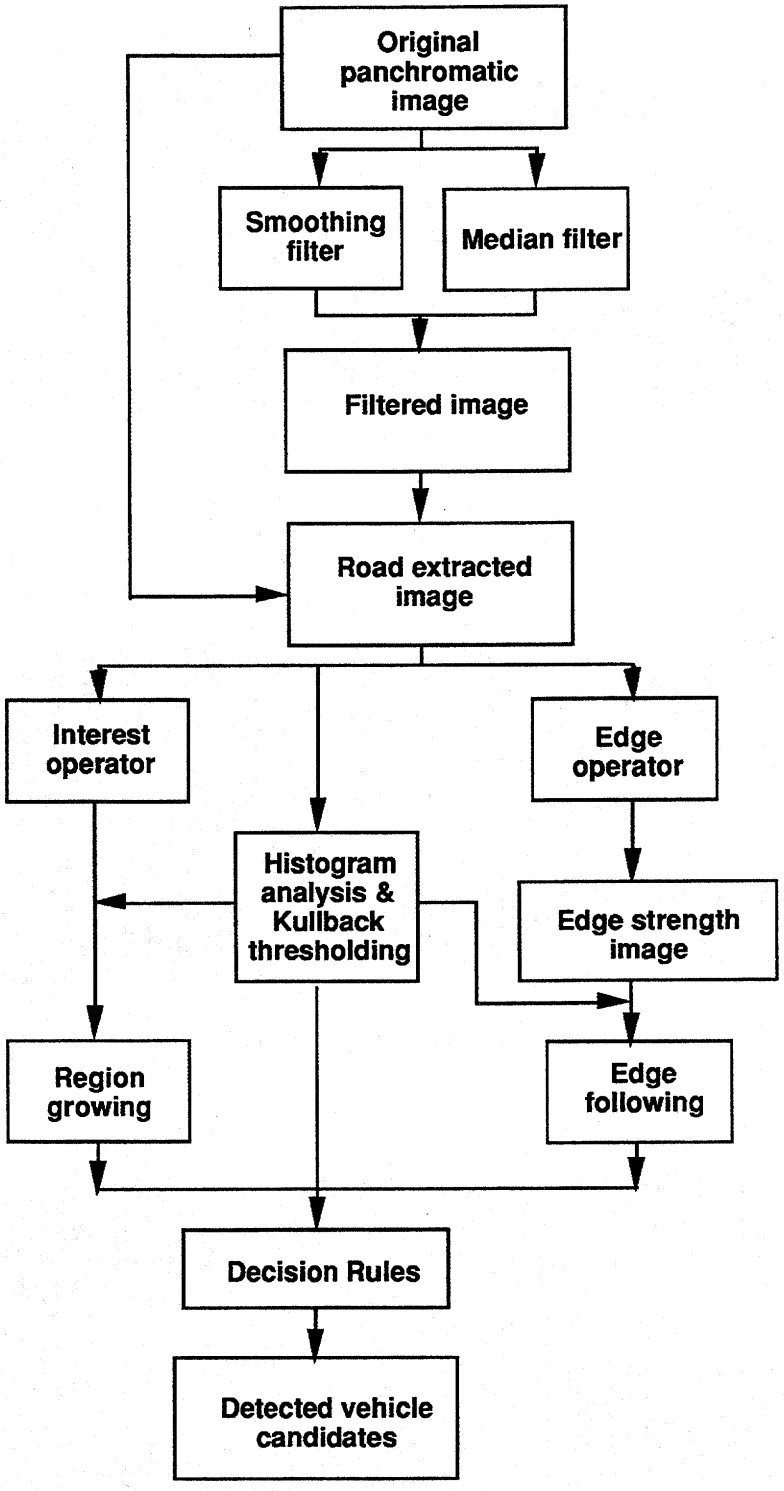

Figure 3.13 Image processing flowchart for detecting vehicles.

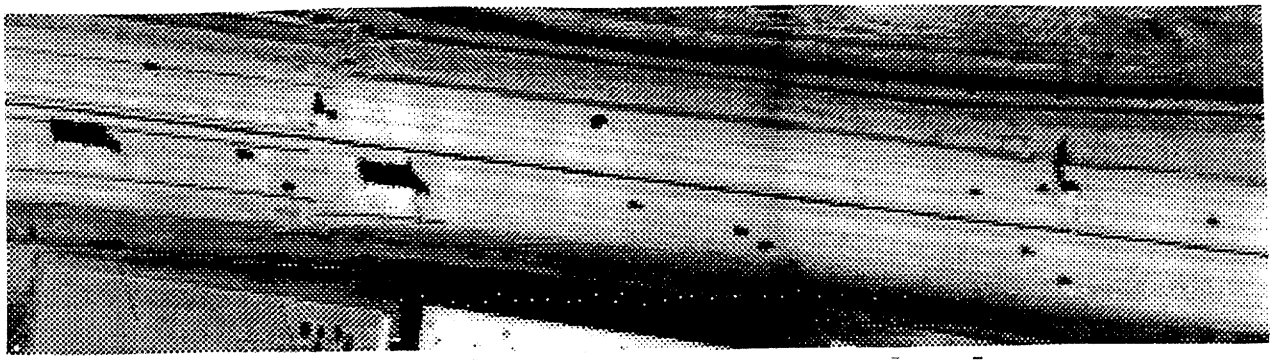

a. 1.2 m simulated resolution.

b. 2.4 m simulated resolution.

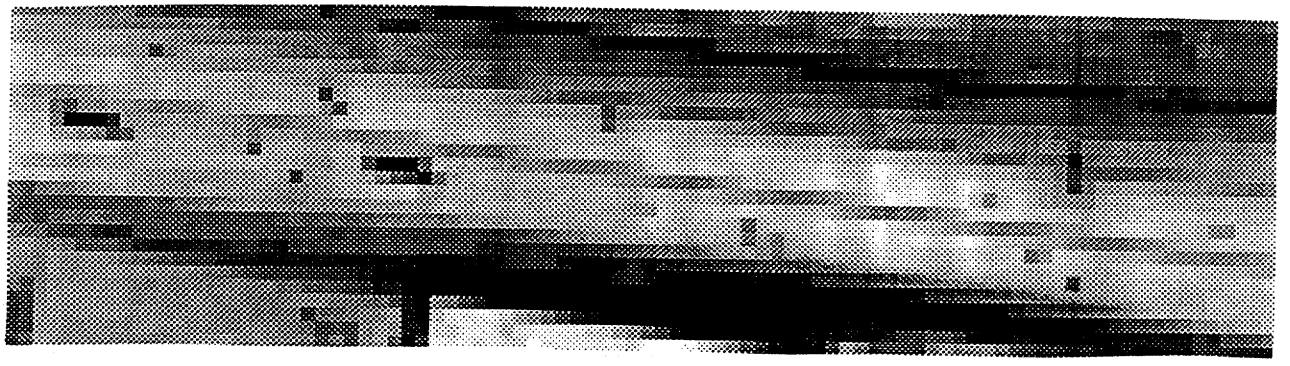

c. 4.8 m simulated resolution.

Figure 3.14 Highway segment 513:E-W shown at three resolutions.

To start the process, the original image is filtered using either a low pass filter (smoothing) or a median filter. The purpose of this step is to remove any noise in the image, but still preserve existing edges. Smoothing filters for noise reduction in the images were investigated. We found that the median filter provided the best noise reduction, while still preserving the edges in the original image. After noise removal, edge sharpening techniques were applied. Several edge operators were used: Kirsch, Prewitt, Laplacian, LoG and the Navatia operators (see Jensen, 1986 for details). We found that the Laplacian and LoG operators did not detect the edges as well as the Kirsch, Prewitt and Navatia operators, which can account for multiple edge directions (ranging from 8 to 12).

Two low pass filtering (smoothing) techniques were tested on our scanned panchromatic aerial images taken over Columbus. The size of the windows used in the low pass filters were a 3-by-3 and a 5-by-5 matrix, with a weight of 5 in the middle with the remaining filter values as 1's. The reason for the higher weight in the middle is to preserve the existing edges in the image.

The second low pass filter tested on the images was a median filter using a 3-by-3 window. Two types of median filter were designed – a box and a cross. The cross type of median filter is preferred in our case, because the filter maintains the step-edge effect found at the corner of the shadows cast by the vehicles.

Based on our panchromatic images, the use of filtering does not make a significant difference in the appearance of the images. This is probably due to the fact that our panchromatic images do not contain much noise. However, for the case of remotely sensed images acquired by satellites, the filtering techniques will most likely improve the images. Therefore, we kept this part of the image processing sequence of tasks for analyses of future images.

Next, using information from a transportation network file that may be contained in a GIS, the roadway network is registered with the satellite image. Knowledge of the spatial coordinates of the road location can be used to overlay on the satellite image. Two parallel lines, which are on either side of the highway, are developed knowing the width of a given type of highway. These lines defining the road network are then overlaid on the image file and the highway network is extracted from the image (Fig. 3.15). The resulting image shows the extracted road network. The roads with vehicles can be from either a filtered image or the original satellite image, depending on the quality of the satellite image data. Next, a buffer on either side of the road centerline can be created to eliminate the clumps representing the median strip (Fig. 3.15).

The road-extracted image is then processed two ways to produce information on the existence of vehicles on the extracted road segment. The first process, which corresponds to the left-side of Figure 3.13, uses only the gray scale values contained in the image. An interest operator, which was developed by Förstner (1986) and Förstner and Gülch (1987), is modified to locate the center of a small area that may be imaged against the background (pavement) of the image. The point detected by the interest

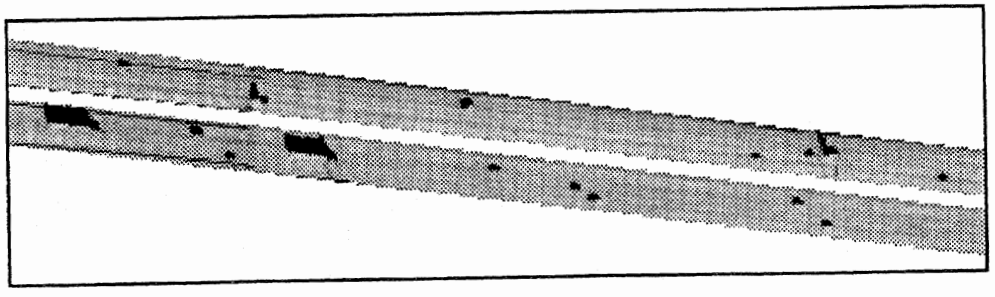

Figure 3.15 Extracted highway section 513:E-W with road medain removed.

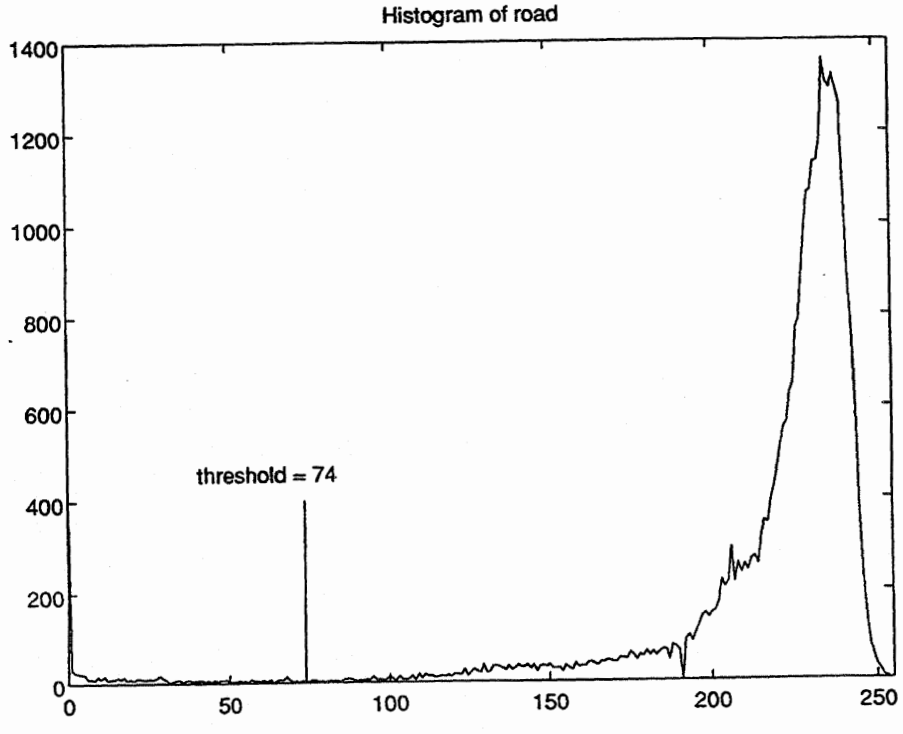

Figure 3.16 Histogram analysis of highway segment shown in Figure 3.15 with a threshold value of 74 selected.

operator is clustered with its neighborhood by a region growing algorithm. In this way global information is analyzed about the potential vehicle candidates.

Selection of the threshold value to separate the vehicles from the background pavement is critical. For our prior analyses, a subjective value was determined by the image analyst. The image processing technique does this in an automatic fashion. The histogram analysis and Kullback thresholding process is used to extract two histograms from an image gray level distribution (see Haralick and Shapiro, 1987). The assumption for this is that there are two distributions of gray tones – the pavement and the vehicle shadows. Thus, the two histograms correlate to the pavement pixels and the vehicle shadows, with the distributions assumed to be Gaussian. The technique that we used is a modification of the Kittler and Illingworth method. The main thrust of this technique is to minimize the Kullback information distance because we have a set of observations from a mixture of two Gaussian distributions (the pavement and the vehicle shadows). This modification will provide an automatic threshold of the image. The program then calculates the gray scale value that shows the optimum dividing line between the two distributions. For example, Figure 3.16 shows the histogram of the highway segment shown in Figure 3.15 with its corresponding threshold value. Again, this is a global process to assist in analyzing the distribution of gray scale values of the image to identify potential vehicle candidates.

This process results in images showing clumps that correspond to vehicle locations. Decision rules were developed to classify potential vehicle "clumps" into vehicle types. A flowchart of these decision rules and the input parameters necessary for calculation are shown in Figure 3.17. The decision rules include the vehicle's shadow area, shadow perimeter, shadow area and perimeter ratio, shadow major axis length, shadow major axis and minor axis ratio, and shadow orientation. These parameters are calculated to sort the vehicle clumps into various classes. The area and perimeter values are used to correct (or discard) any long strips of median pavement that may have been misclassified into the vehicle list.

On the right-side of Figure 3.13, concurrent with the process on the left-side, the original (or filtered) image is subjected to an edge operator. This process results in an edge strength image that shows the strength of the mapped edges. Thus, the stronger the edge, the more likely it is to be associated with a vehicle. The edges are then connected with the edge following algorithm to result in an image of detected vehicle candidates. The edge strength provides local information that the interest operator process cannot produce. Figure 3.18 shows example results from the thresholding and edge enhancement processes of the road segment in Figure 3.15.

In applying a step edge operator, such as the Prewitt or Kirsch, the key factor is to decide on a threshold number. To aid in this process, a histogram of scores (or strengths) of the edges defined by the edge operator is generated and analyzed on a global level for the image. A number of *edge images* can be generated for different threshold numbers. Based on an analysis of the histogram, a threshold number that corresponds to 3-4% of the edge scores is selected. However, if we find that the edges detected by the selected

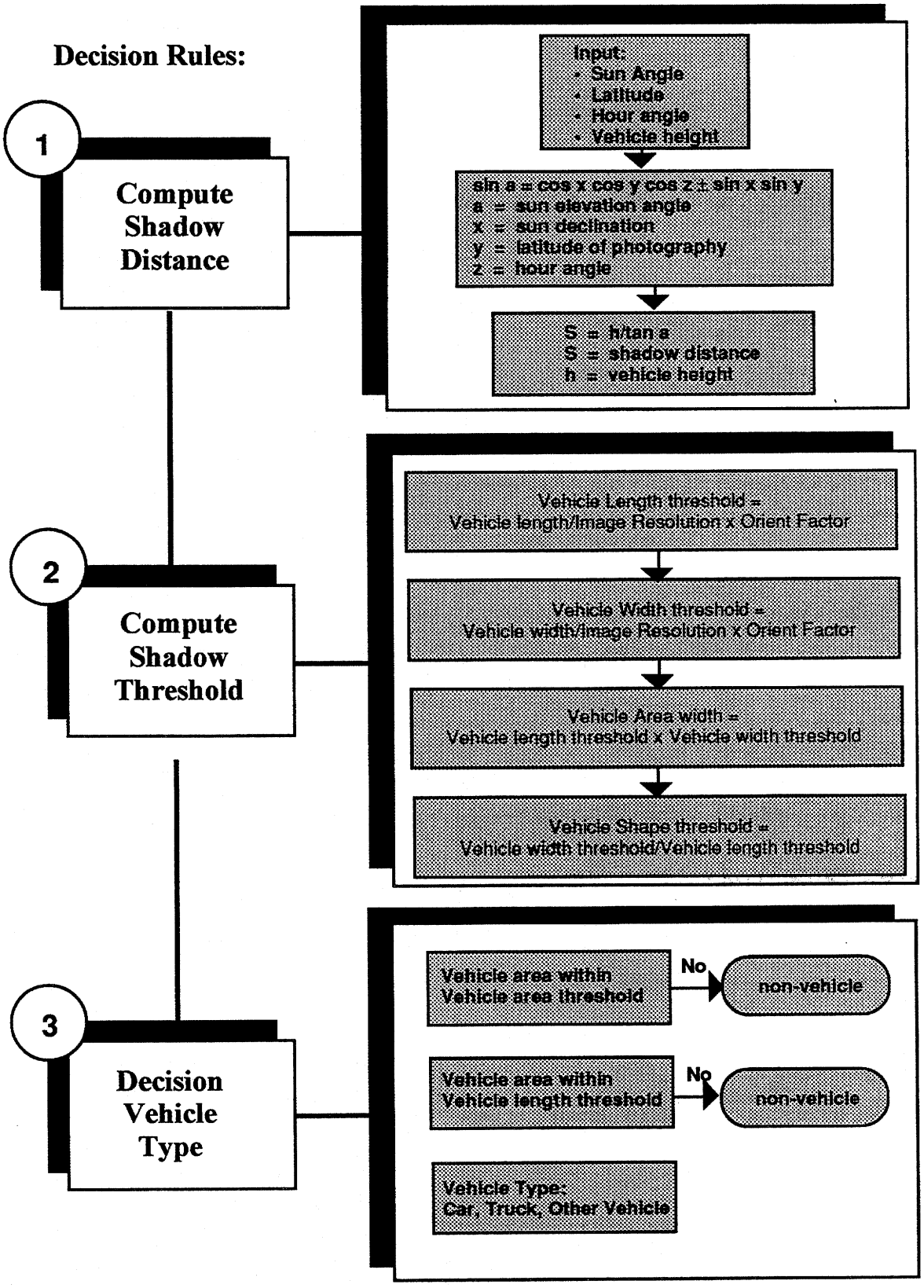

Figure 3.17 Flowchart of the decision rules for classification of vehicles.

Figure 3.17 (continued)

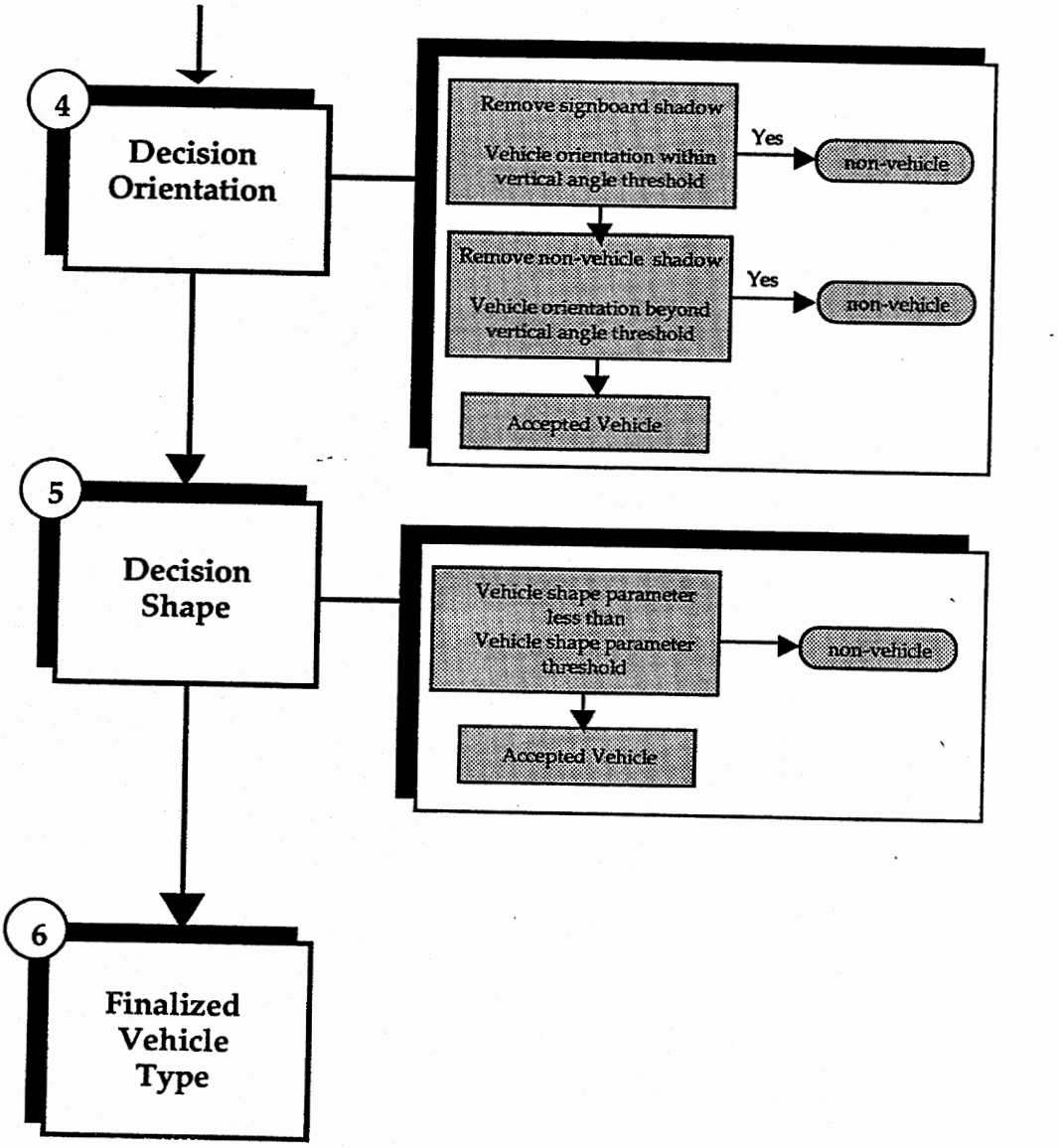

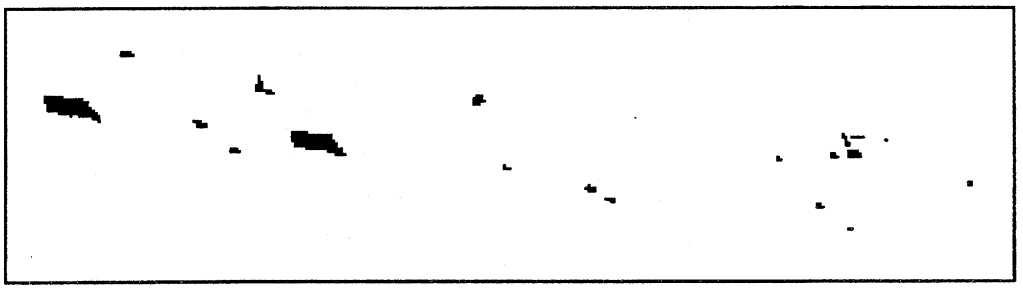

a. Results of thresholding.

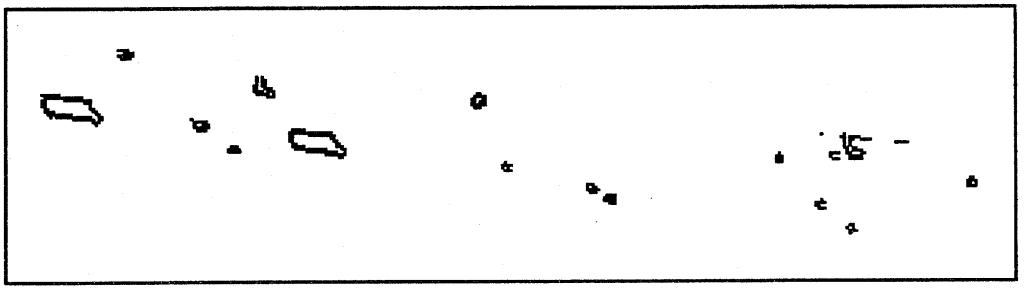

b. Edge enhancement of vehicles.

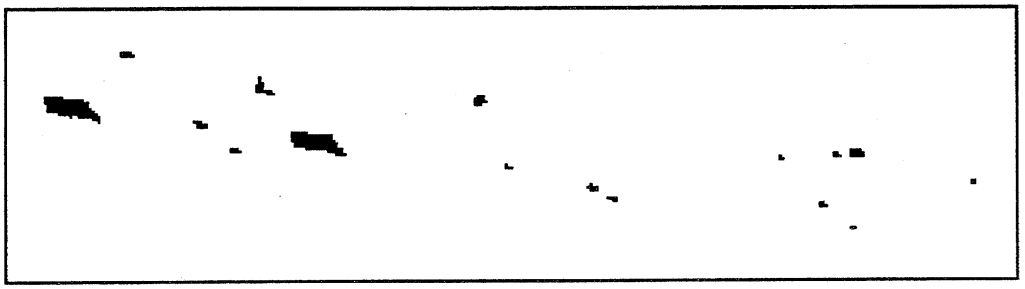

c. Final display of vehicles.

Figure 3.18 Thresholding and edge enhancement results of highway segment 513:E-W with final display of vehicles

threshold number is not enough to generate edges, then the program automatically reduces the threshold number to generate more edges at the local level.

In summary, three types of information are used to make the final decision on detected vehicle candidates – the region growing image, the results from the histogram analysis and Kullback thresholding step, and the edge following image.

3.14 Quantitative Results using the Image Processing Approach

We tested the automated image processing approach on the seven highway segments. The 0.6 m resolution images that were scanned on the Optronics 5040 were resampled to result in resolutions of 1.2, 2.4 and 4.8 m. The results are shown in Tables 3.4a-i under ii – image processing. Overall, the image processing method is performing better than our manual method, and we are encouraged by these results.

For example, in the fraction correct statistics (Table 3.4a-c.ii), the correctly identified cars (FVCI) were 93.9% overall for the 1 m resolution, which is similar to the results found with the manual approach (0.942). However, most accuracies for the image processing approach were consistently above 0.90, except for highway segment 753(3). In this case we believe the accuracy dropped to 0.86 because of the varying shades of the pavement that caused confusion with the classifier.

At the 2.4 m resolution the accuracy dropped to 0.769. We had hoped that a 2-m resolution would be suitable for identifying a car-sized vehicle, but our tests show that we cannot achieve the desired accuracy. At the 4.8 m resolution, the overall accuracy drops to 0.442.

We are able to accurately map the trucks at the 1.2 and 2.4 m resolutions (see Table 3.4b.ii). However, at the 4.8 m resolution, we could only map all of the trucks 4 out of 7 times. In two cases, we were able to map 50% of the trucks and for the remaining segment we were able to achieve an accuracy of 0.857. For this case, if we only had to detect a truck-size vehicle, we could use the 2.4 m resolution.

The other vehicles category (FOCC) was mapped to a 93.2% accuracy (Table 3.4c.ii) at the 1.2 m accuracy. The accuracy for the 2.4 and 4.8 m resolutions drops to 0.727 and 0.378, respectively. As with the vehicle identification category, a 1-m resolution is needed to detect and identify other vehicles.

The errors of omission are similar for the vehicles and other vehicles categories using the image processing method when compared to the manual method (Table 3.4d,f.ii). The errors of omission for the truck category (Table 3.4e.ii) were lower using the image processing approach.

The errors of commission were much lower for the image processing method when compared to the manual approach (Tables 3.4g-i.ii). At the 1.2-m resolution the overall commission error was 0.061 when compared to 0.198 for the vehicle identification category. This also was the case for the other vehicle category (0.068 *vs.* 0.230). For

the truck category, there were no committed errors for the 1.2 and 2.4 m resolutions. At the 4.8 m resolution the error of commission was lower for the image processing method than the manual approach (0.044 *vs.* 0.226).

3.15 Additional Testing on a Congested Highway Segment

We scanned a highway segment at resolutions of approximately 1, 2 and 4 m. This highway segment differed from previous segments by being heavily congested and, therefore, it would be more difficult to obtain good performance from our image processing utilities. Our image processing algorithm was run to determine how many vehicles could be successfully detected. The performance is poorer than that on less congested highways, but we were encouraged with the reasonable results achieved. Table 3.5 shows the results of our analysis.

Table 3.5. Results of image processing procedure for the congested highway segment on S.R. 315-S near Columbus, Ohio, at the 1-m resolution.

Vehicle type	*Total number of vehicles*	*Vehicles detected (counts - %)*	*Omission error (counts - %)*	*Commission error (counts - %)*
Trucks	4	4 (1.0)	0 (0.0)	1 (0.25)
Other vehicles	145	123 (0.85)	22 (0.15)	0 (0.0)
Total	149	127 (0.85)	22 (0.15)	1 (0.01)

There were 149 vehicles on this stretch of highway (Fig. 3.19). Of these 149 vehicles, there were 4 trucks, the remaining 145 vehicles were cars. The highway segment is of S.R. 315-S located just north of Columbus, Ohio. Traffic congestion can be observed on the left side (west) of S.R. 315. For this example case, there are also overlapping vehicle shadows and some vehicle separations of less than 2 m.

We find that all four trucks were detected by the image processing algorithm at the 1-m resolution (Table 3.5). However, we do count one vehicle as a truck, when in reality it is not (commission error of 1). The interest operator detected 85% of the remaining vehicles, omitting several vehicles (22), but there were no commission errors.

At the 2-m resolution all four trucks were detected by the interest operator (Table 3.6). Again, we do count one vehicle as a truck, when in reality it is not (commission error of 1). Because of the extremely tight car spacing, there are not enough pixels in between the vehicles to cause an adequate separation distance to detect all vehicles. Thus several vehicles are omitted and the accuracy decreases to 32% for vehicles.

Figure 3.19 Highway segment S.R.-315-S scanned at a 1 m resolution
located just north of Columbus, Ohio

Table 3.6. Results of image processing procedure for the congested highway segment on S.R. 315-S near Columbus, Ohio, at the 2-m resolution.

Vehicle type	*Total number of vehicles*	*Vehicles detected (counts - %)*	*Omission error (counts - %)*	*Commission error(counts - %)*
Trucks	4	4 (1.0)	0 (0.0)	1 (0.25)
Other vehicles	145	47 (0.32)	98 (0.68)	0 (0.0)
Total	149	51 (0.34)	22 (0.66)	1 (0.01)

At the 4-m resolution only one truck was detected by the interest operator (Table 3.7). Three of the trucks were omitted and overall, the accuracy decreases to 7% for vehicles.

Table 3.7. Results of image processing procedure for the congested highway segment on S.R. 315-S near Columbus, Ohio, at the 4-m resolution.

Vehicle type	*Total number of vehicles*	*Vehicles detected (counts - %)*	*Omission error (counts - %)*	*Commission error (counts - %)*
Trucks	4	1 (0.25)	3 (0.75)	0 (0.0)
Other vehicles	145	10 (0.07)	135 (0.93)	0 (0.0)
Total	149	11 (0.07)	138 (0.93)	0 (0.0)

Thus, in these congested traffic conditions, the 4-m resolution was not adequate for detecting vehicles of any size. The 2-m resolution appeared adequate for trucks, but not for the remaining vehicles. At the 1-m resolution, the overall accuracy was 85%.

In summary, the image processing method demonstrated that one can automatically count and classify vehicles at reasonable levels of accuracy. The method incorporates image processing methods for enhancing the edges of vehicles. The edge-enhanced map is then used in conjunction with decision rules to test whether a particular object is a car, truck or other vehicle. Accuracies above 90% are achievable for the highway segments tested in this study. Based on these tests, we recommend that the resolution from a satellite platform be 1 m to count and classify vehicles.

Section 4. Orbital Coverage

4.1 Introduction

Satellite orbits are governed and constrained by physical relations. A satellite can orbit above the equator in such a way that it orbits in unison with the rotation of the earth and is always stationed above the same point on the earth. Satellites in these "geostationary orbits" have the advantage of continually covering (subject to the imaging limitations from darkness or cloud cover) an area of interest. To remain in unison with the earth's rotation, a geostationary satellite must not only orbit in a plane containing the equator, it must do so at very high altitudes. For example, GOES/M'SAT is a geostationary satellite that orbits at an altitude of over 35,000 km (Pease, 1991). At such high altitudes, it is currently impossible to obtain the 1 m resolution needed to count and classify vehicles with the precision and methods we have been investigating. Orbiting above the equator also means that higher latitudes would be viewed at oblique angles, leading to poorer quality of data, and there may be limited spatial coverage. Therefore, we limited our analysis to satellites that orbit at a given inclination angle to the equator.

Like a geostationary satellite, the orbital plane of a non-geostationary satellite contains the center of the earth. Unlike in the case of a geostationary satellite, however, the orbital plane is different than that containing the equator, and the net result is that the satellite will be located over different points on the earth's surface at different times. Geosynchronous satellites are designed to repeat these locations with each orbit (Elachi, 1987). Because of their high altitudes, limited spatial coverage, and the poor data quality that would result from the oblique, off-nadir views that would be required, we did not consider geosynchronous orbits either. Satellites that are neither geostationary nor geosynchronous have much more extensive spatial coverage of nadir views. This coverage is often represented by mapping out the satellite's ground tracks, where the ground tracks are the projection of the satellite orbit on the earth's surface and can be thought of as the intersection of the earth's surface with a line passing through the satellite and the center of the earth. For example, Figure 4.1 depicts the "ground tracks" of a satellite that repeats its coverage patterns with respect to the earth every eight days, makes 14.875 orbits per day, and crosses the equator at an inclination angle of 97.81°.

The ground tracks shown in Figure 4.1 represent all the locations that the satellite would cover in its orbital cycle of eight days. The width of coverage (swath width) along a ground track that would be possible for the resolutions that would be required to count and classify vehicles would be approximately 15 km (see below), and it becomes apparent that there would be large areas that are never imaged by the sensor. All areas could be imaged, but at the expense of poorer temporal coverage. For example, the satellite corresponding to the ground tracks of Figure 4.1 would repeat its set of ground tracks approximately every eight days. One can calculate that to cover the entire earth with the same swath width would increase the length of the repeat period to 179 days. That is, if these were the only two options, the choice would be between covering the

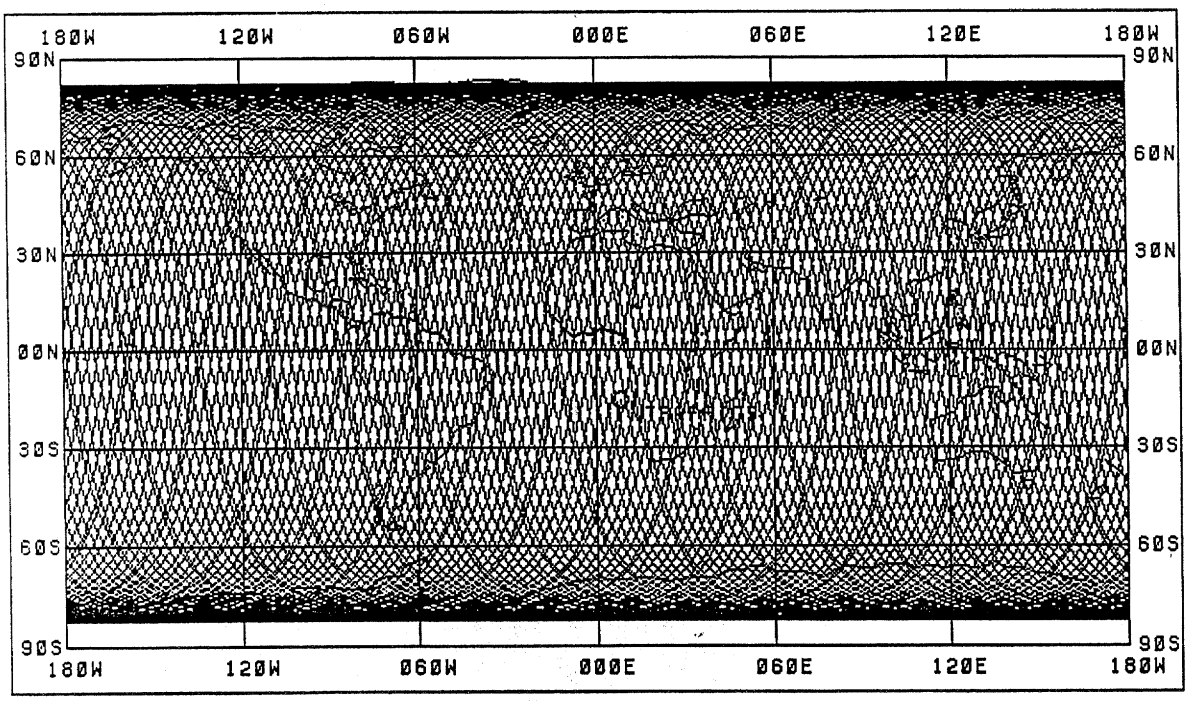

Figure 4.1 Ground tracks for an 8-day repeat period satellite with inclination angle *i* of 97.81°

highway segments within the 15-km band around the ground tracks of Figure 4.1 every eight days or covering all highway segments once every 179 days.

In short, spatial-temporal coverage becomes an issue of interest for an orbiting satellite. In this section, we investigate the coverage of an orbiting satellite for imaging U.S. highways. The approach is to approximate the area of the continental U.S. covered by the ground tracks per unit time – we use a day. In this feasibility study we consider that highways are equally distributed per unit area. That is, we assume that if a satellite can cover *x*% of the area of the continental U.S. per day, it would image *x*% of its highways. Although this assumption would not hold when comparing specific areas – e.g., there would be fewer highway miles per unit area in Nevada than in New Jersey – the approach should approximately hold for aggregate U.S. coverage.

We investigate the coverage issues by developing an analytical system based on orbital relations. We were surprised that we could not find literature offering the type of analysis presented here. Moreover, orbit design software did not allow the type of coverage investigation in which we were interested.

We find that a 1-m resolution satellite would cover approximately 1% of the highways in the continental United States per day. If the resolution could be increased to 2 m and still maintain acceptable accuracy, the coverage would increase by a factor of more than two. Other than the spatial resolution, the critical parameter appears to be the data transmission rate for such a satellite sensor.

4.2 Coverage Parameters

Satellite orbits that are used to image the Earth are generally circular or elliptical, with the earth located at one of the focal points (Elachi, 1987). Circular orbits are the most common for nonmilitary purposes, such as observing and monitoring earth resources. Moreover, they lead to easier imaging, since satellites in circular orbits maintain approximately the same altitude above the earth at all times (Elachi, 1987). (The oblate shape of the earth would make the altitude vary at different latitudes by a few kilometers, even for circular orbits.) Therefore, we considered circular orbits in our analysis.

In a circular orbit, the satellite can be considered to orbit at a constant radius from the earth's center. The circle and center of the earth are contained in the same orbital plane. While the satellite traces the circle, the earth is rotating beneath, leading to coverage such as that depicted in Figure 4.1. The pattern, location, and swath width of the ground tracks, and, therefore, the characteristics of the coverage, will depend on the angle of the orbital plane and on parameters that can be considered independently of the orbital plane. In this subsection, we present these parameters and relationships among them that allow us to develop a system of constraints on the coverage measure presented in Section 4.3.

In our analysis we considered that the highway kilometers imaged per day would be proportional to the area per day covered by satellite ground tracks. The area covered by ground tracks would be equal to the width of the ground tracks times the length of the tracks. The width and length depend on several parameters and the relations among them.

Swath Width: The swath width *SW* of the image on the ground can be found by multiplying the number of pixels that are contained on a scan line of the sensor *PPAL* (pixels per array line) by the width that the pixel images on the ground. Since we are using square pixels, the width of the pixel is given by its resolution *RES*. The *SW* is usually given in kilometers and *RES* is usually given in meters. Therefore, a conversion is necessary, and we have:

$$SW = RES * PPAL * 10^{-3} \text{ [km]}, \tag{4.1}$$

where, as mentioned above, *SW* is the swath width in kilometers, *RES* is the resolution of the square pixel in meters, and *PPAL* is the number of pixels per array line on the scanner.

For a given resolution, the swath width varies only with the number of pixels per array line. Coverage would increase in *PPAL*, and one would, therefore, want to maximize the value of this parameter. PPAL's of 15,000 are feasible (Al-Obaida, 1993), leading to a swath width of 15 km for 1 m resolution. To consider the impact of technological advances, we considered the maximum number of pixels per array scan line as a parameter. Letting $PPAL_{max}$ denote this parameter yields the following constraint:

$$PPAL \leq PPAL_{max}. \tag{4.2}$$

Altitude, Orbits per Day, and Velocity: In Appendix F, we determine the relationship between the number of orbits *n* that the satellite would make per day and the altitude *H* of the satellite above the earth's surface that would lead to the gravitational force required to produce the centripetal acceleration allowing these *n* orbits per day. Specifically, we have:

$$n = 8{,}681{,}665.8/(H + 6371)^{1.5} \text{ [orbits/day]}, \tag{4.3}$$

where, *H* is the altitude of the satellite above the earth's surface in kilometers and *n* is the number of orbits that the satellite makes per day.

Limits on *H* will limit the number of orbits per day. The atmospheric drag on satellites orbiting at altitudes less than 200 km (Elachi, 1987) will be such that the satellite could not maintain the velocity required to stay in the orbit, and the gravitational force of the earth will cause the satellite to fall out of its orbit to the earth. Therefore, to maintain a given orbital altitude for inclination angles suitable for imaging the earth, we are limited to satellite altitudes greater than 200 km. Thus we are constrained by:

$$H \geq 200 \text{ [km]}, \tag{4.4}$$

which combined with Equation (4.3), implies:

$$n \leq 15.6 \text{ [orbits/day]}. \tag{4.5}$$

The primary parameter of interest for the imaging system is the focal length *FL* of the sensor. In Appendix F, we show that the focal length *FL* required to image at resolution *RES* meters when the sensor is at altitude *H* kilometers above the earth's surface is:

$$FL = H * PWPD * 10^{-3} / RES \text{ [m]}, \tag{4.6}$$

where *FL* is the focal length in meters, *PWPD* is the physical width of the pixel on the detector in micrometers (=10^{-6} m), and, as above, *RES* is the pixel resolution in meters. From Equation (4.6) the required focal length can be seen to decrease as the size of the pixel on the detector *PWPD* decreases. Currently, PWPD's between 7 and 15 μm are feasible (D.L. Light, pers. comm., 1993; C. Ullathorne, pers. comm., 1994), and we used PWPD = 10 in our analysis. The required focal length increases as the resolution decreases and as the altitude increases. To image at 0.5 m resolution at an altitude of 400 km would require a focal length of FL = 400 * 10 * 10^{-3} / 0.5 = 8 m, which is feasible (J. Johnson, pers. comm., 1994; C. Ullathorne, pers. comm., 1994; K. More, pers. comm., 1994).

Substituting PWPD = 10 in Equation (4.6) and solving for *H* yields H = FL*RES*10^2 [km]. Limits on the maximum focal length will limit the maximum altitude at which the satellite can orbit and obtain the desired resolution. Letting FL_{max} denote the maximum focal length achievable, we have the following constraints on the altitude:

$$H \leq FL_{max} * RES * 10^2 \text{ [km]}. \tag{4.7}$$

Combining this with Equation (4.3) yields:

$$n \geq 8{,}681{,}665.8 / (FL_{max} * RES * 10^2 + 6371)^{1.5}. \quad (4.8)$$

We see below that making fewer orbits per day may actually increase coverage because of the impact, through data transmission constraints, on *PPAL* and because of the impacts on the length of the ground track per orbit. Therefore, the inequality of (4.8) may lead to a binding constraint on coverage.

Data Transmission and Compression: Given the number of pixels being imaged and the amount of information that needs to be transmitted per pixel, the number of orbits per day will influence the amount of data transmitted. Limitations on the data transmission rate could, therefore, affect the relationship between the number of orbits per day that can be obtained and the number of pixels that are being imaged.

A satellite making *n* orbits per day (= 86,400 seconds) would cover n*2*p*R kilometers of the earth's surface in the day, where *R* is the (mean) radius of the earth. Taking 6371 [km] for *R* (Light, 1992a), one could derive the "satellite velocity on the ground" (Light, 1992a) – i.e., how fast the satellite progresses with respect to the surface of the earth – as:

$$V_{sg} = 0.4633 * n \text{ [km/sec]}. \quad (4.9)$$

If the number of pixels per scan array line is *PPAL* and the resolution of a square pixel on the ground is *RES*, the instrument would image *PPAL* pixels every time the satellite progresses a distance *RES* on the ground. That is, it would image $PPAL*V_{sg}/(0.001*RES) = 463.3*n*PPAL/RES$ pixels per second.

Storing data onboard the satellite should be avoided where possible, because of the unreliability of the tape recorders. Therefore, the data has to be transmitted at the rate that it is collected. If the sensor images *NBP* bands per pixel, there are *NBB* bits of information per band, and the data can be compressed by a factor *COMP* before transmission, the data transmission rate *DTR* required to keep up with a satellite making *n* orbits per day with *PPAL* pixels per array line would be: DTR = (463.3*n*PPAL*NBP*NBB)/(RES*COMP) [bits/sec]. Data transmission rates are usually provided in mega-bits per second (1 [Mbit/sec] = 10^6 [bits/sec]). Therefore, the data transmission rate becomes:

$$DTR = (4.633*n*PPAL*NBP*NBB*10^{-4}) / (RES*COMP) \text{ [Mbits/sec]}. \quad (4.10)$$

The panchromatic imaging system we have been investigating would image 1 band per pixel (NBP=1) with 8 bits per band (NBB=8). Therefore, the data transmission rate would be:

$$DTR = (3.706*n*PPAL*10^{-3})/(RES*COMP) \text{ [Mbits/sec]}. \quad (4.11)$$

Rearranging (4.11) to find the relation between *n* and *PPAL* yields:

$$PPAL = (2.698*RES*DTR*COMP*10^2)/n. \quad (4.12)$$

Given a limit on the data transmission rate *DTR* and ability to compress data *COMP*, Equation (4.12) shows, as expected, that as the number of orbits per day increases, the number of pixels that a sensor can image per scan array line must decrease for a fixed resolution, and vice-versa. Considering the effects of data transmission and compression together and letting $(DTR*COMP)_{max}$ denote the maximum rate at which "useful" data can be transmitted, Equation (4.12) yields the following constraint:

$$PPAL \leq 2.698 * (DTR * COMP)_{max} * RES * 10^2 / n. \quad (4.13)$$

Note that when data transmission constraint (4.13) is binding, the influence of resolution on the *PPAL* is linear – i.e., a doubling of the resolution would allow a doubling of the number of pixels per array line that could be transmitted. The effect on coverage would be quadratic, however, since increasing the resolution by a factor of x would increase *PPAL* by a factor of x, but the increased resolution would lead to the width on the ground covered by the pixel being increased by a factor of x (see Eq. (4.1)), thereby leading to an increase of coverage per unit time of x^2.

Inclination Angle: The satellite orbital plane must contain the center of the earth, but the angle that the plane makes with the equator is a parameter of the problem. The orientation of the orbit is specified in relation to the earth's equatorial plane and the vernal equinox (Elachi, 1987). The angle between the orbital plane and the equatorial plane is the inclination angle and denoted *i*, is typically greater than 90°, and corresponds to the greatest latitudes north and south of the equator that the satellite will cover. Specifically, for inclination angle *i*, $i \geq 90°$, the satellite will orbit between north and south latitudes of 180°-i.

Figure 4.2a shows the ground tracks that would be covered in one day by the satellite used to generate the complete (8-day) tracks in Figure 4.1. Figure 4.2b shows the ground tracks that would be covered in one day by a satellite orbiting with the same parameters, but with an inclination angle of 120°. Comparing the ground tracks of Figures 4.2a and 4.2b, one can see that, since less time is spent at the higher latitudes in Figure 4.2b, a greater proportion of the coverage is over the continental United States.

To increase coverage, then, we would want to make the inclination angle *i* as small as possible while ensuring that the satellite covers the highest latitudes of interest. Our interest was in imaging highways in the continental U.S. We considered the northern border of the continental U.S. to correspond to 50°N, leading to the following constraint:

$$90° \leq i \leq 130°. \quad (4.14)$$

A potential difficulty associated with an inclination angle of 130° is that it does not allow for the satellite to be sun-synchronous, i.e., to always cover a specific locationon the earth at the same local time (Elachi, 1987). The inclination angle of a sun-synchronous orbit must be between 96.3° and 100.2°.

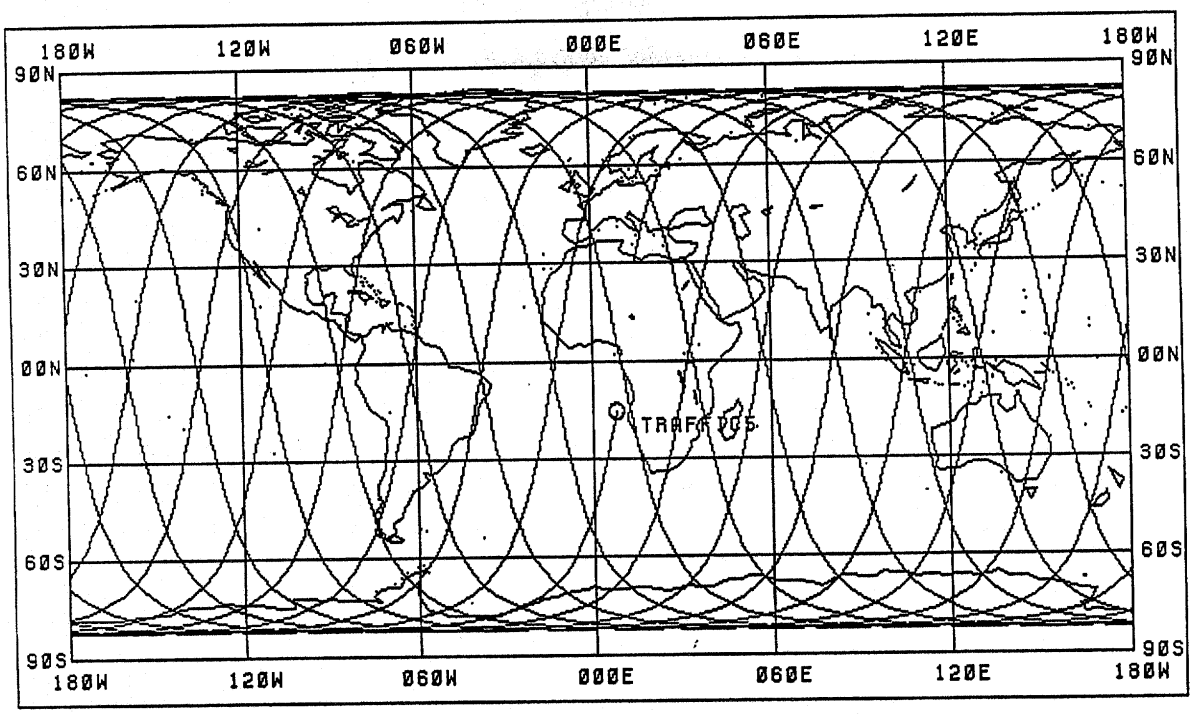

a. One-day ground tracks for the satellite corresponding to Figure 4.1 with inclination angle of 97.81°

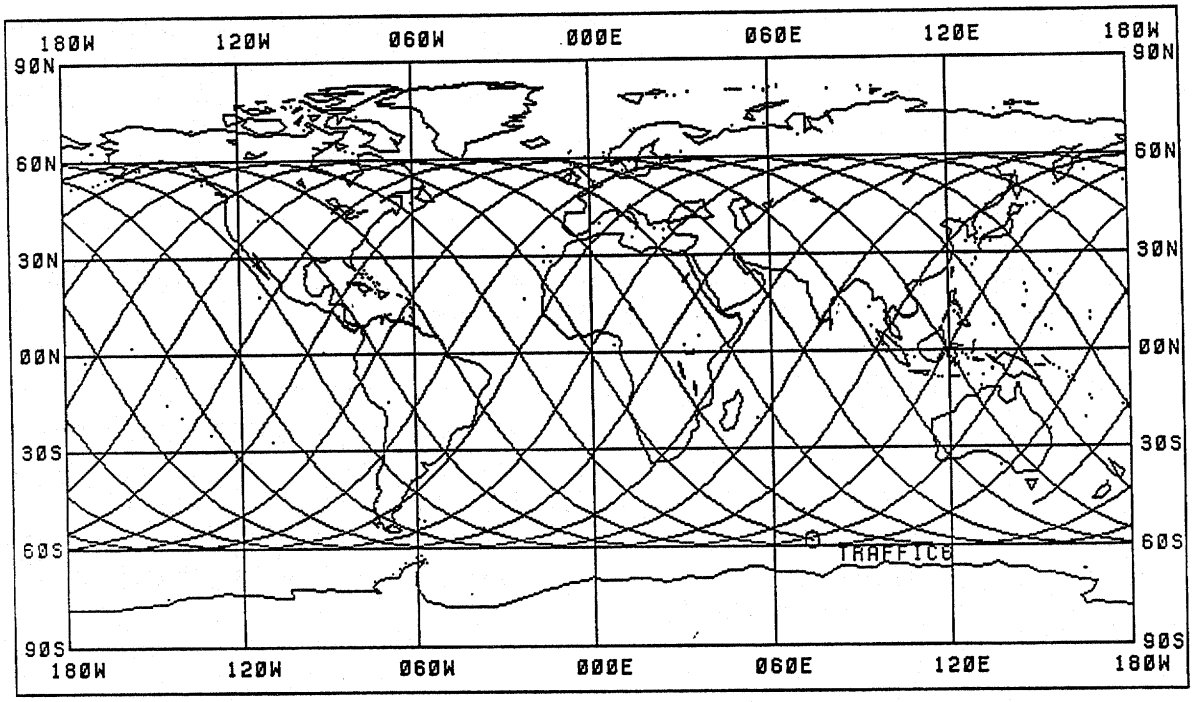

b. One-day ground tracks for the satellite corresponding to Figure 4.1 and 4.2a, but with inclination angle *i* of 120°

Figure 4.2 One-day ground tracks for the satellite corresponding to Figure 4.1

Although there is no reason that the satellite has to return to locations at the same local time, sun-synchronous orbits often make interpretation of traditional remote sensing images involved with the monitoring of natural resources easier because of similar lighting conditions. Returning at the same local time may also be of some value in the panchromatic sensing systems we have been considering by possibly allowing easier detection of fixed, nonvehicle objects (e.g., shadows from signs or overpasses, pavement patches) that depend on the orientation of the sun. This could conceivably reduce the errors of commission. We believe that an imaging processing system similar to that discussed in Section 3 could be developed to distinguish nonvehicle objects fairly accurately, however, and that the increased coverage obtained by orbits that are not sun-synchronous would compensate for any decrease in sensing accuracy. Still, we investigated coverage for sun-synchronous orbits, as well as for orbits with an inclination angle of 130°.

4.3 Coverage Measure

As mentioned above, we found nothing in the literature on how to measure satellite coverage of a dynamic system such as traffic data. What we found (Al-Obaida, 1993; Light, 1990, 1992a, 1992b; CNES, 1987; Colvocoresses, 1979) deals with complete spatial coverage between certain latitudes. Traffic parameters are continually changing, however, and it may be preferable to cover certain areas more frequently at the expense of not covering some areas at all. Therefore, we developed our own measure of coverage. This measure, presented below, is based on the daily percentage of the continental U.S. covered by ground tracks, PCD_{US}:

$$PCD_{US} = [A^{sat}{}_{US}/A_{US}] * 100\%, \tag{4.15}$$

where $A^{sat}{}_{US}$ is the area of the continental United States covered by the satellite ground tracks and A_{US} is the area of the continental United States.

We approximated PCD_{US} by assuming that the continental U.S. is contained between north latitudes 25° and 50° with eastern and western boundaries along a meridian. Since the ground tracks of orbits are regularly spaced, the percentage of this regular area – i.e., an area whose borders are two latitudes and two longitudes, a quadrilateral in a plane projection – representing the continental U.S. covered daily by the satellite ground tracks would be the percentage of the earth between 25°N and 50°N latitudes covered daily by the satellite ground tracks. That is:

$$\begin{aligned} PCD_{US} &= [A^{sat}{}_{US} / A_{US}] * 100\% \\ &= \{A^{sat}{}_{[25N,50N]} / A_{[25N,50N]}\} * 100\%, \end{aligned} \tag{4.16}$$

where $A^{sat}{}_{[25N,50N]}$ and $A_{[25N,50N]}$, respectively, are the area between latitudes 25° and 50° north covered by the satellite ground tracks per day, and the area of the earth between latitudes 25° and 50° north.

The area of the earth between any two latitudes LAT_1 and LAT_2, $LAT_1 < LAT_2$ with both LAT_1 and LAT_2 either north or south of the equator, can be found (Eshbach, 1947) to be:

$$A_{[LAT1,LAT2]} = 2*p*R^2*[\sin(LAT_2) - \sin(LAT_1)], \tag{4.17}$$

where R is the mean radius of the earth. Taking R = 6371 km, $LAT_1 = 25°$ and $LAT_2 = 50°$, we approximate the area of the continental U.S. as:

$$A_{US} = A_{[25N,50N]} = 8.758*10^7 \text{ [km}^2\text{]}. \tag{4.18}$$

On a given orbit a satellite would cross the zone between LAT_1 and LAT_2 two times. For example in Figure 4.1 we see a set of (descending) ground tracks going primarily from northeast to southwest and a second set of (ascending) ground tracks going primarily from southeast to northwest. There is one descending and one ascending track per orbit, and, therefore, each would cross the zone between LAT_1 and LAT_2, as long as the inclination angle i is such that 180°-i is greater than both LAT_1 and LAT_2. Therefore, the area between LAT_1 and LAT_2 covered per orbit would be two times the swath width of the ground track times the length of the orbit between LAT_1 and LAT_2. Since the swath width is the number of pixels in a scan line *PPAL* times the resolution of the pixel on the ground *RES*, this area per orbit, $A^{sat}_{[LAT1,LAT2]}$, given in km^2, would be $2*PPAL*RES*L_{[LAT1,LAT2]}*10^{-3}$, where $L_{[Lat1,Lat2]}$ is the length of one of the ground tracks between LAT_1 and LAT_2 in km, and *RES* is given in m. Since there are n orbits per day:

$$A^{sat}_{[LAT1,LAT2]} = 2 * n * PPAL * RES * L_{[LAT1,LAT2]} * 10^{-3} \tag{4.19}$$

The length of the ground tracks between LAT_1 and LAT_2 would depend on the inclination angle i. As i increases, the length of the track between LAT_1 and LAT_2 would increase, as depicted in Figure 4.2. Given i, however, it is still not straightforward to determine the length of the satellite ground track between LAT_1 and LAT_2 because the earth is rotating beneath the orbit of the satellite. The trace and, therefore, length of the ground track will depend on the distance that the earth has rotated during the time that the satellite has traveled between LAT_1 and LAT_2. This will depend on the speed of the satellite. As we discussed above, the satellite speed is directly related to its elevation, which uniquely determines the number of orbits per day n that the satellite makes. Therefore, the length of the ground track between LAT_1 and LAT_2 depends on the inclination angle i and the number of orbits n that the satellite makes per day. We denote this:

$$L_{[Lat1,Lat2]} = L(LAT_1,LAT_2; i,n) \tag{4.20}$$

In Appendix G, we present the algorithmic approach we used to evaluate this ground track length.

To approximate the percentage of the continental U.S. that would be covered by the satellite ground tracks for a given inclination angle i, number of orbits per day n, number of pixels in a scan line $PPAL$, and resolution RES, we would: i) determine $L_{[25N,50N]}$ from the algorithm given in Appendix G using i and n; ii) determine $A^{sat}_{[25N,50N]}$ using Equation (4.19), n, $PPAL$, RES, and $L_{[25N,50N]}$; and iii) divide $A^{sat}_{[25N,50N]}$ by $8.758*10^7$ and multiply by 100%.

This would yield PCD_{US}, the percentage of the continental U.S. covered by satellite ground tracks per day. To approximate the percentage of the number of highways that could be imaged per day, we would have to factor this down to account for times that we could not obtain images of the surface. There would primarily be two reasons that the satellite could not image the ground. It would not be able to image when it is nighttime and when it is cloudy. Letting f_n be the fraction of ground tracks that pass over the continental U.S. during the night, and f_c be the fraction of ground tracks that pass over the continental U.S. during the day when it is cloudy, we can find the aggregate fraction of "nonproductive ground tracks" f_{npgt} as:

$$f_{npgt} = f_n + f_c \tag{4.21}$$

The fraction of productive passes, then, would be $1\text{-}f_{npgt}$ and the approximate percentage of highways in the continental U.S. imaged per day, PID_{US}, would be:

$$\begin{aligned} PID_{US} &= (1 - f_{npgt}) * PCD_{US} \\ &= (1 - f_{npgt}) \{A^{sat}_{[25N,50N]} / (8.758 * 10^7)\} * 100\% \\ &= (1-f_{npgt}) \{2*n*PPAL*RES*L_{[25N,50N]}*10^{-3} / (8.758*10^7)\}*100\% \end{aligned} \tag{4.22}$$

4.4 Numerical Results

Different values of orbital parameters would lead to different measures of coverage. We investigated the maximum coverages that could be obtained as a function of the various parameters presented above. We also investigated coverage measures that would be produced for orbits with additional constraints.

4.4.1 Maximum Coverage

To determine the maximum feasible coverage we would choose the orbital decision variables that would maximize PID_{US} in Equation (4.22), subject to the constraints presented in Section 4.2. Specifically, we would need to solve the following nonlinear program:

$$\begin{aligned} \text{Maximize:} \quad & PID_{US} = (1\text{-}f_{npgt}) * \{2*n*PPAL*RES*L(25,50; i,n) \\ n,PPAL,i \quad & \qquad *10^{-3}/8.758*10^7)\} * 100\% \end{aligned}$$

subject to:

$$\begin{aligned} & PPAL \leq PPAL_{max} \\ & PPAL \leq 2.698*(DTR*COMP)_{max}*RES*10^2/n \\ & n \quad \leq 15.6 \\ & n \quad \geq 8{,}651{,}665.8/(FL_{max}*RES*10^2+6371)^{1.5} \\ & i \quad \geq 90° \\ & i \quad \leq 130° \\ & PPAL \geq 0 \\ & n \quad \geq 0, \end{aligned} \tag{P1}$$

where all variables are defined as before.

The aggregate fraction of nonproductive ground tracks f_{npgt} would be an exogenously determined constant; i.e., it would not depend on the values of the decision variables, and it could be factored in after solving the problem. Likewise, the resolution *RES* would be determined exogenously to the problem. Using the approach of Section 3, a 1 m resolution would be needed to count and classify vehicles with 90% accuracy. We, therefore, consider RES = 1 m as the base value of the parameter in the results. To allow for future developments or different requirements, however, we consider it an exogenously determined parameter to the problem. We saw above that maximum coverage would occur at i = 130°. To investigate the effect of the inclination angle on the solution, however, we considered *i* as an exogenously set parameter. The maximum number of pixels that could fit on a scan line of the detector $PPAL_{max}$, the maximum rate at which useful data could be transmitted $(DTR*COMP)_{max}$, and the maximum focal length that could be used FL_{max} would be determined exogenously from technological constraints. We investigated their influence on coverage performance by solving the problem for various values and interpolating curves based on the results.

With these considerations, the solution to Program (P1) could be found by defining:

$$\begin{aligned} PID_{US'} &= 8.758*PID_{US}*10^7/\{2(1-f_{npgt})*RES*10^{-3}*100\% \\ &= n * PPAL * L(25,50; i,n); \end{aligned} \tag{4.23}$$

fixing f_{npgt}, *RES*, *i*, $PPAL_{max}$, $(DTR*COMP)_{max}$, and FL_{max} at exogenously determined values; and solving the following nonlinear program for these values:

Maximize: $PID_{US'} = n * PPAL * L(25,50; i,n)$
n, PPAL

subject to:

$$\begin{aligned} & PPAL \leq PPAL_{max} \\ & PPAL \leq 2.698*(DTR*COMP)_{max}*RES*10^2/n \\ & n \quad \leq 15.6 \\ & n \quad \geq 8{,}651{,}665.8/(FL_{max}*RES*10^2+6371)^{1.5} \\ & PPAL \geq 0 \\ & n \quad \geq 0. \end{aligned} \tag{P2}$$

The coverage performance measure PID_{US} would be found by solving Program (P2) for $PID_{US'}$ and rearranging and solving Equation (4.23) for PID_{US}, given this value of $PID_{US'}$.

We solved Program (P2) 576 times, once for each combination of the input parameter values shown in Table 4.1. (We describe how to solve Program (P2) for $PID_{US'}$ in Appendix H and present a listing of the program in Appendix I.) We used RES = 0.5 m, 1.0 m, 2.0 m and 4.0 m to represent (approximately) the resolutions investigated in Section 3. The base case value was set at RES = 1.0 m, based on our results there. We used inclination angle i = 130° to allow for maximum coverage per day in the continental U.S., as described above. We used i = 100° to approximate a maximum inclination angle value. The ability to point the sensor would allow coverage of the poles at latitudes of 80° (= 180°-100°) north and south. We used i = 115° as an intermediate value between the two extremes. We chose the lowest values of the other input parameters in Table 4.1 – namely, $(DTR*COMP)_{max}$ = 400, $PPAL_{max}$ = 15 and FL_{max} = 6 – to represent current designs (Light, pers. comm., 1993; J. Johnson, pers. comm., 1994; Itek, 1981; K. More, pers. comm., 1994; Ullathorne, pers. comm., 1994). We chose the largest values of the input parameters in Table 4.1 – namely, $(DTR*COMP)_{max}$ = 1600, $PPAL_{max}$ = 30 and FL_{max} = 14 – as values that might stretch present technologies, but that could probably be obtained in the near future. The other values were chosen as intermediate values. The base case values were chosen to reflect what could probably be used today, but are not currently in place on a satellite (Light, pers. comm., 1993; J. Johnson, pers. comm., 1994; Itek, 1981; K. More, pers. comm., 1994; Ullathorne, pers. comm., 1994).

We used f_n = 0.5, assuming that on average 50% of the satellite passes would fly over the continental United States during nighttime hours, and f_c = 0.23, based on a crude analysis of aggregate cloud cover statistics for the continental United States (Solar Energy Research Institute, 1981) and recalling that f_c represents the fraction of total (day and night) coverage that could not be obtained due to cloud cover in daytime hours. This resulted in a value of 0.73 for f_{npgt}, and thus a factor of $(1-f_{npgt})$ = 0.27 for use in determining PID_{US}.

The base case result is PID_{US} = 0.9%. That is, based on these results, a satellite could image approximately 0.9% of the U.S. highways per day. The output for the 576 combinations and the cases described in Appendix H to which the combinations correspond are presented in Appendix J. (For programming reasons, the coverage measures in Appendix J are in terms of $PID_{US}*(1-f_n)$, i.e., the daily coverage measure times the fraction of ground tracks that pass over the continental U.S. during the day. The PID_{US} value is found by multiplying by $(1-f_{npgt})/(1-f_n)$, which we considered to be 0.54 in this study.)

We show the effect of the input parameters with the values of the other input parameters set at their lowest (those designed today), base (those that could be designed today), and highest (those that could probably be designed in the near future) values in Figures 4.3-4.6.

Table 4.1 Values of input parameters and base case values to determine maximum daily satellite coverage in the continental U.S., PID_{US}.

Parameter description notation (units)	*Input values*	*Base case value*
Pixel resolution on ground, RES (m)	0.5, 1.0, 2.0, 4.0	1.0
Inclination angle of satellite orbit at equator, i (°)	100, 115, 130	130
Maximum product of data transmission rate and compression factor, $(DTR*COMP)_{max}$ (Mbits/sec)	400, 800, 1200, 1600	800
Maximum number of pixels that could be held per array line of the sensor, $PPAL_{max}$ (10^3)	15, 20, 25, 30	20
Maximum sensor focal length that could be deployed, FL_{max} (m)	6*, (8*), 10, 14	10
Daily coverage of continental United States, PID_{US} (%)	see App. I and Figures 4.3-4.6	0.9

*A 6-m focal length will not allow 0.5 m resolution for altitudes considered here (above 400 km). An 8-m focal length was used in its place for the 0.5 m resolution only.

By examining all the figures one can see the importance of the resolution. When increasing the resolution from 1 m to 2 m, the daily coverage always increases at least by a factor of two, and often (depending on the values of the other input parameters) by a factor of more than two. When the other parameters are set at their base case values, increasing the resolution from 1 m to 2 m would increase the daily coverage by a factor of almost three (from 0.9% to 2.5%). Similarly, if the resolution could be increased from 1 m to 4 m the daily coverage would always increase at least by a factor of four, and often by a factor of more than four. When the other parameters are set at their base case values, increasing the resolution from 1 m to 4 m would increase the daily coverage by a factor of almost six (from 0.9% to 5.0%).

The influence of the inclination angle is shown in Figure 4.3. The effect of i on daily coverage increases as the inclination angle increases. That is, the effect when increasing the inclination angle from 115° to 130° is greater than when increasing it from 100° to 115° for all combinations of the other input variables shown there.

Finally, Figures 4.4b, 4.5b, and 4.6b indicate that the value of $(DTR*COMP)_{max}$ has more of an impact on daily coverage than $PPAL_{max}$ or FL_{max} when the other variables are at their base values. Specifically, daily coverage increases approximately linearly (see Fig. 4.4b) with $(DTR*COMP)_{max}$, either when this parameter increases or decreases from its base value ($(DTR*COMP)_{max} = 800$) at the base 1 m resolution, whereas daily coverage remains constant when $PPAL_{max}$ (Figure 4.5b) and FL_{max} (Fig. 4.6b) increase or decrease from their base values at the base 1 m resolution.

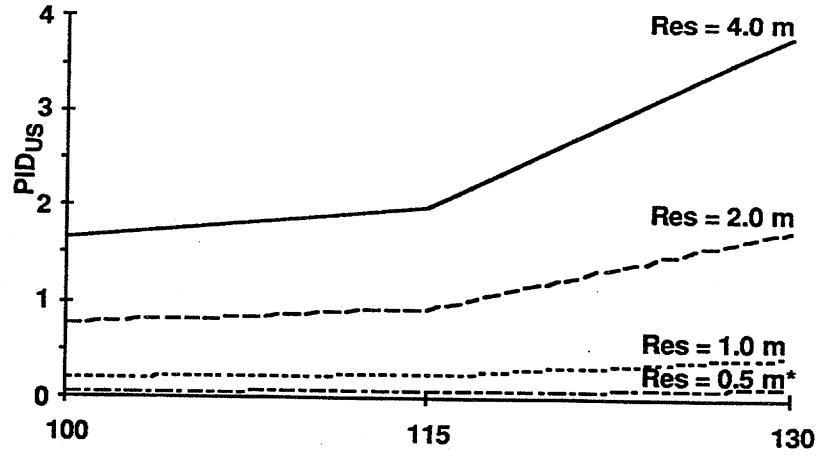

a. $(DTR*COMP)_{max}$ = 400 Mbps, $PPAL_{max}$ = 15000, FL_{max} = 6 m.
($*FL_{max}$ = 8 m for 0.5 m resolution)

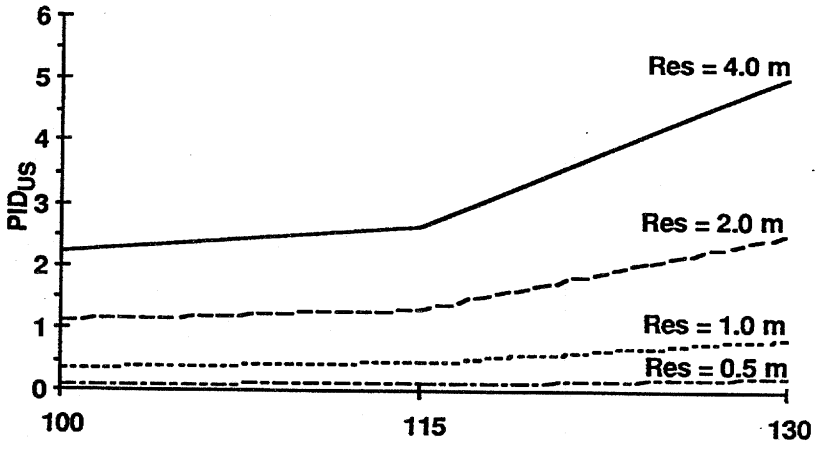

b. $(DTR*COMP)_{max}$ = 800 Mbps, $PPAL_{max}$ = 20000, FL_{max} = 10 m.

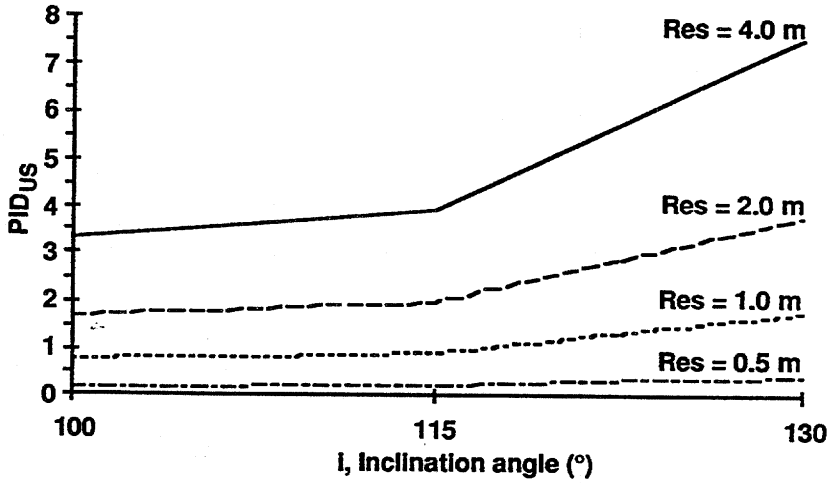

c. $(DTR*COMP)_{max}$ = 1600 Mbps, $PPAL_{max}$ = 30000, FL_{max} = 14 m.

Figure 4.3 Effect of inclination *i* on daily satellite coverage of the continental United States PID_{US} by resolution.

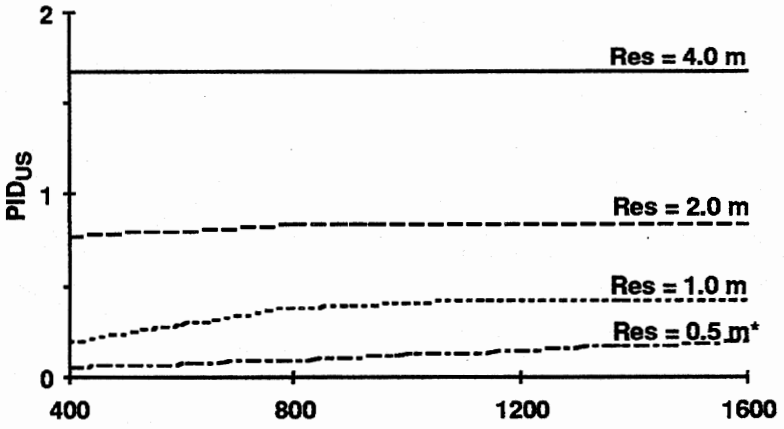

a. i = 100°, $PPAL_{max}$ = 15000, FL_{max} = 6 m.
*(FL_{max} = 8 m for 0.5 m resolution)

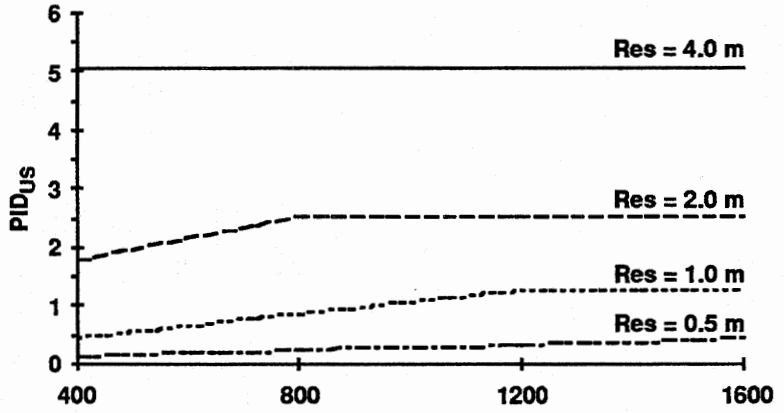

b. i = 130°, $PPAL_{max}$ = 20000, FL_{max} = 10 m.

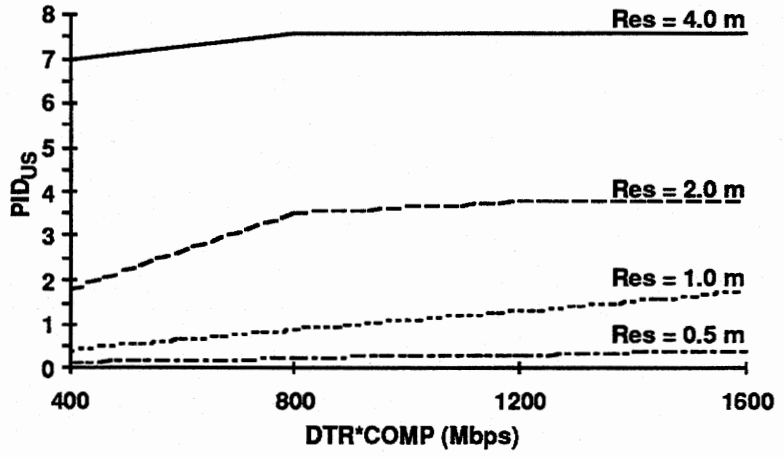

c. i = 130°, $PPAL_{max}$ = 30000, FL_{max} = 14 m.

Figure 4.4 Effect of maximum data transmission and compression $DTR*COMP_{max}$ on daily satellite coverage of the continental United States PID_{US} by resolution.

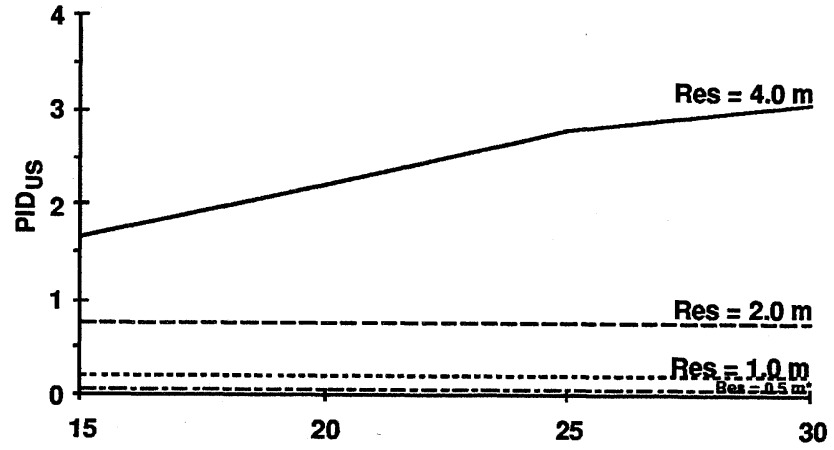

a. i = 100°, $(DTR*COMP)_{max} = 400$, $FL_{max} = 6$ m.
*($FL_{max} = 8$ m for 0.5 m resolution)

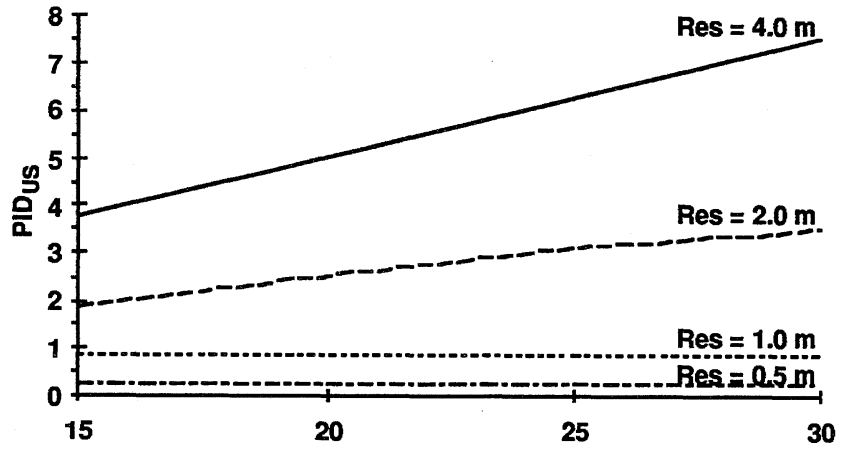

b. i = 130°, $(DTR*COMP)_{max} = 800$, $FL_{max} = 10$ m.

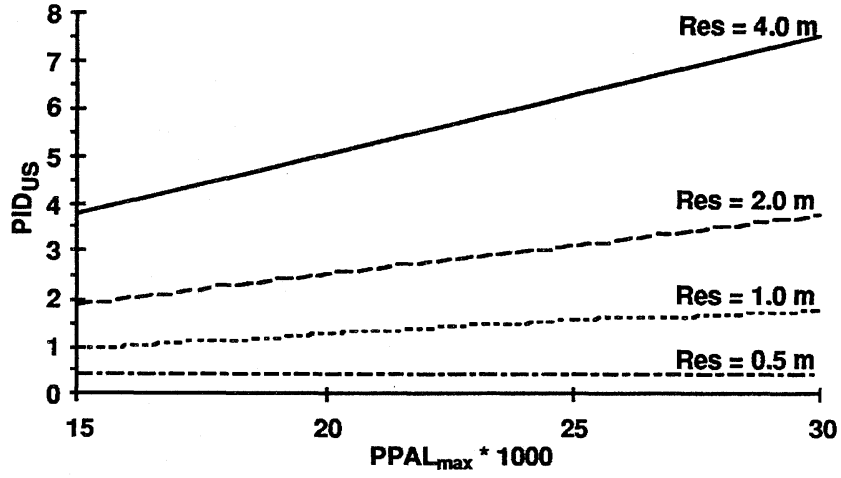

c. i = 130°, DTR*COMP = 1600 Mbps, $FL_{max} = 14$ m.

Figure 4.5 Effect of the maximum number of pixels per array line $PPAL_{max}$ on daily satellite coverage of the continental United States PID_{US} by resolution.

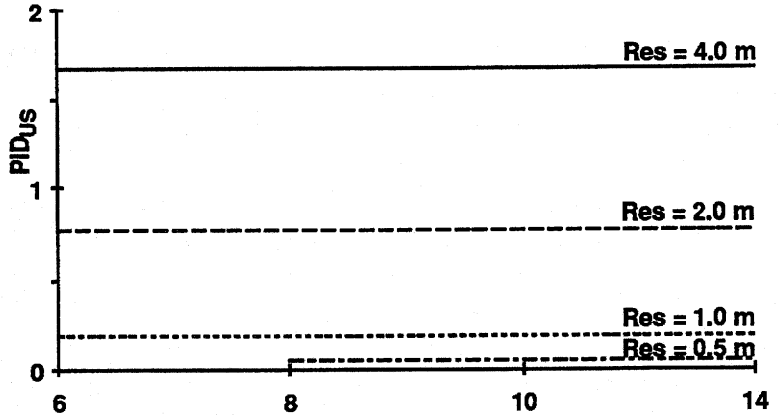

a. i = 100°, PPAL = 15000, DTR*COMP = 400 Mbps.
*(FL_{max} = 8 m for 0.5 m resolution)

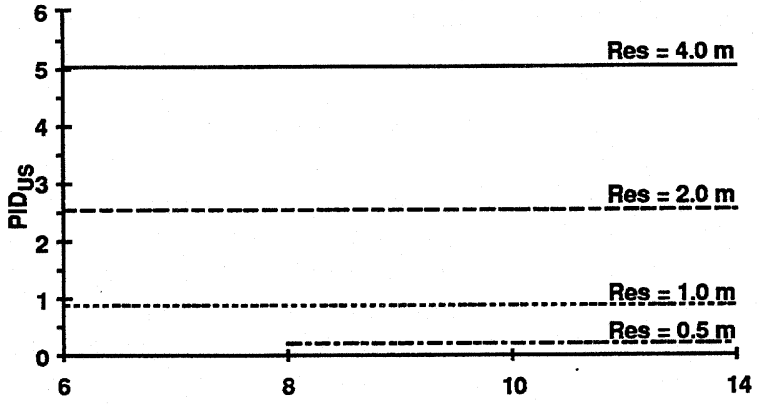

b. i = 130°, PPAL = 20000, DTR*COMP = 800Mbps.

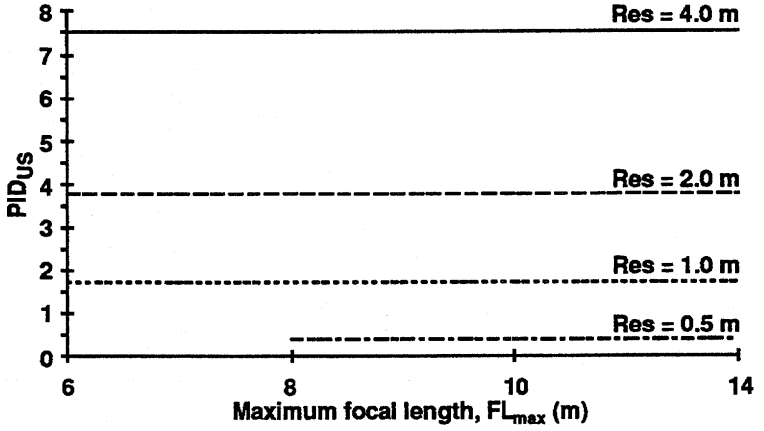

c. i = 130°, PPAL = 30000, DTR*COMP = 1600 Mbps.

Figure 4.6 Effect of maximum possible focal length constraint FL_{max} on daily satellite coverage of the continental United States PID_{US} by resolution.

4.4.2 Coverage for Systems with Additional Constraints

The results presented above are in terms of maximum daily coverage when the satellite is restricted only by the constraints of Section 4.2. We discussed that a sun-synchronous orbit would allow the satellite to return to the same spots on the earth at the same local times. This might make it easier to distinguish moving vehicles from fixed objects on the highway – e.g., sign shadows. The inclination angle i is restricted to be between about 97° and 100° for a sun-synchronous orbit, and the inclination angle and the altitude of the satellite H must respect certain relations to ensure that the satellite orbits at a speed and angle that allow the synchronized orbits (King-Hele, 1964). Based on the results of our numerical analysis, we saw that at i = 100°, RES = 1 m, and the other input parameters set at their base case values, the maximum coverage was obtained by having the satellite orbit at altitudes as high as possible (see App. H and J). We, therefore, calculated that the maximum daily PID_{US} for a sun-synchronous orbit with other parameters set at the base case values would be 0.4%. That is, requiring a sun-synchronous orbit would decrease the daily coverage by 0.5% per day (from 0.9% to 0.4%).

We also determined the coverage that would be provided by a planned 1 m resolution satellite. Eyeglass™ (C. Ullathorne, pers. comm., 1994) is a commercial satellite that will be in a sun-synchronous orbit and is planned for launch in 1997. In addition to its 1 m resolution (RES = 1), Eyeglass™ is designed to have an inclination angle i of 98.173°, 15,000 pixels per scan line (PPAL = 15), a focal length FL of 5.6 m, and orbit at an altitude H of 700 km (which leads to n = 14.6 orbits per day). With these parameters, we calculated that Eyeglass™ would cover 0.4% of the continental United States per day. That is, compared to our base case analysis, Eyeglass™ would have 0.5% less coverage over the continental United States.

Section 5. Costs of a Satellite System

Costs of a satellite system are described in this section. These costs are estimates and given for illustrative purposes. Technical issues are discussed that will impact the costs of a designed satellite system. Detailed costs would need to be developed once a final satellite sensor design is decided.

5.1 Typical Satellite Costs

We researched the literature to obtain costs of comparable satellite systems (see Table 5.1). These costs range from a high of $660 million for the Canadian Radarsat satellite to a low of $81 million for Mapsat. The most recent successful launch of an earth resources satellite was the French SPOT system in September, 1993 for $250 million.

Table 5.1 Typical costs of comparable satellite systems in 1992 dollars (from KPMG Peat Marwick and NASA, 1992).

Satellite	*Cost of system ($ million)*	*Launch or proposed launch date*
Landsat-4	250	1982
Landsat-5	250	1985
Landsat-6	256.6	1993
SPOT-3	250	1993
SPOT-4	510	1998
Mapsat	81	conceptual design
JERS-1	330	1992
ADEOS	553	1995
Radarsat	660	1995

The system with properties most similar to those we studied would be the Mapsat satellite. The Mapsat satellite was a proposed satellite system for acquiring 2.5-m stereo panchromatic (0.51-0.73 μm) imagery for a 60 by 60 km area. The estimated cost for this system was $81 million. The $81 million includes $75 million for the satellite and $6 million for ground tracking, telemetry, and control of the satellite.

KPMG Peat Marwick and NASA (1992) provided details about the MAPSAT costs. A $15 million cost during the first year of operation is necessary for the initial launch of the satellite. Operation of the satellite would require an additional $5 million per year ($4 million for the ground operations and $1 million for producing image data products).

5.2 Purchasing Data from a Commercial Company

We checked with a proposed commercial company, Eyeglass International, to determine the costs of acquiring imagery from a private company. This company will provide 1-m panchromatic image data in 1997. The images from Eyeglass™ for a 15 by 15 km area will cost $2,000 per image. Their system will provide for a revisit period of two days. There will be two ground stations with direct downlink capability that will acquire imagery over the conterminous United States, providing for about 180 images per day. If cloud cover were not a problem and if we obtained all images taken over the United States, this would amount to $36,000 per day or $4.32 million per year. For this large purchase, we would qualify for "bronze level" status – a preferred customer. This permits us a discount on imagery because of the large volume of imagery purchased. Once $2.5 million is purchased, then a 25% discount is applied. This would reduce the price for a year's worth of Eyeglass™ data to $3.24 million. Based on our approximation of the continental U.S. area in Section 4, these 180 images of a 15 x 15 km area (225 km^2) would cover approximately 0.05% (= $(180*225)/8.75*10^7$) of the U.S. highways (not accounting for cloud coverage per day).

Purchasing imagery from a commercial company would be a less expensive alternative when compared to building, launching, and operating a dedicated satellite system. However, satellite launch costs are decreasing. Recently, when talking with a company that launches small satellites for specific purposes, a cost of $75 to $80 million would be possible (W.D. Thompson, pers. comm., 1995). This includes $25 million for the bus, $35 to $40 million for the payload and $15 million for the launch.

However, there is a disadvantage to the Eyeglass™ data. The data will be acquired at the same local time each day, since Eyeglass™ is in a sun-synchronous orbit. For the satellite design described in this study, we recommend a non-sun-synchronous orbit so that imagery can be acquired at different local times throughout the day.

5.3 Technical Design Considerations

We also checked with a camera manufacturer in an attempt to determine the relationship between costs and focal length, pixels per array line, and data transmission rate for a given sensor. Unfortunately, such relationships do not seem available presently. It is difficult to derive costs for a specific component of a sensor package, as the cost depends on the total integrated design of a sensor system. Therefore, modeling as a function of individual components would require a concentrated research effort.

A bus (launch vehicle) would need to be supplied for the sensor package. Launch services and buses can be readily obtained. The more difficult cost to be determined, however, is for the sensor package to place on the launch vehicle.

In general, the satellite is a very stable platform for a linear array sensor, such as that proposed to acquire 1-m panchromatic imagery. Space-qualified linear arrays are now being designed using TDI (time delay integration). The integration time can be increased for an individual scan line, depending on image motion and the scan rate

desired. Integration time is the amount of time that the sensor has to "stare" at the ground to receive and record the signal for a given scanline. By using TDI technology, we can get a better signal to noise ratio (S:N). If pixels are placed close enough together and the scan rate is synchronized appropriately, high resolution pixels can be acquired for large spatial areas. For example, Eastman Kodak is making a 9,000 by 64 TDI array (C. Mondello, pers. comm., 1994).

In conclusion, final costs for a satellite sensor to acquire high resolution imagery would need to be developed by a commercial manufacturer. However, in this study we have developed the preliminary design specifications for an ideal sensor that would be required to acquire high resolution imagery from a satellite platform to classify and count vehicles from space. Based on the figures in Table 5.1, it appears that to launch and operate a 1-m satellite system would cost on the order of $100 million. Purchasing data from a scheduled mission such as Eyeglass™ would cost on the order of $3 million per year.

Section 6. Evaluation of Other Potential Remote Sensors

6.1 Introduction

Our study has focused principally on using high resolution panchromatic imagery for classifying and counting vehicles. This was principally done such high spatial resolution imagery will be commercially available within the next few years. From our tests with simulated satellite data we found that the data would have to be approximately 1 m for remote sensing imagery taken in the visible part of the electromagnetic spectrum (i.e., panchromatic imagery). However, we realize that cloudy conditions will prevent image acquisition. Therefore, we evaluated other types of remote sensing data that are available from satellites now or in the near future to assess the feasibility of these techniques.

6.2 Radar Sensors

Radar (*ra*dio *d*etection *a*nd *r*anging) systems operate in the microwave band of the electromagnetic spectrum at wavelengths from about 0.1 cm to 1 m. Passive and active sensors have been designed for this wavelength region. Passive microwave radiometers record the natural microwave radiation that is emitted by the earth. Radar is an active system and generates short pulses or bursts of microwave radiation of known frequency and wavelength and records the reflection from the earth's surface. Table 6.1 shows the wavelengths or bands of the microwave spectrum that are commonly used in imaging radars. Because radar provides its own energy and does not rely on the sun, the radar can operate day or night. Also, the long wavelength band radars (e.g., L- and P-bands) can penetrate clouds and precipitation and thus can operate during inclement weather conditions. The angle and look direction of the microwave signal can also be controlled to enhance features of interest.

Table 6.1 Band designations and radar wavelengths (from Avery and Berlin, 1992).

Band designation	*Wavelength range (cm)*
K_a	0.8 - 1.1
K	1.1 - 1.7
K_u	1.7 - 2.4
X	2.4 - 3.8
C	3.8 - 7.5
S	7.5 - 15.0
L	15.0 - 30.0
P	30.0 - 100.0

The tones seen on a radar image are a measure of the microwave echo strength. They are a function of the feature (dielectric properties), and ground and radar system properties. Normally, features that are good reflectors of the radar signal are shown in

light tones, whereas features that are poor reflectors are shown in dark tones; likewise features that are moderate reflectors are shown in medium tones. Features with no measurable echo are shown in black.

Synthetic aperture radar (SAR) was developed to achieve fine resolution at typical satellite altitudes. The radar signal is directed to the side of the spacecraft at some look angle and look direction. There have been two NASA spacecraft that have operated successful SARs. Seasat was operated in 1978 and was designed to observe the ocean waves, sea ice and coastlines. Seasat used a 23-cm (L-band) radar and achieved a ground resolution of 25 m for a 100 km swath width. The Space Shuttle has operated three radar missions – SIR-A (November 1981), SIR-B (October 1984) and most recently SIR-C (April 1994). SIR-A used a 23.5-cm (L-band) radar and achieved a ground resolution of 40 m for a 50-km swath width. SIR-B used a 23-cm (L-band) radar and achieved a ground resolution of 25 x 17 m (at 60° depression angle) or 25 x 58 m (at a 15° depression angle) for a 40 to 50 km swath width. SIR-C used 24-cm (L-band) and 5.6-cm (C-band) radars and achieved a ground resolution of either 25 or 40 m for a 40 to 90 km swath width. It is apparent that these radar systems do not have the fine spatial resolution that is required to detect vehicles.

Existing systems include the ERS-1 (Eurimage – European consortium), which has a 30 m resolution SAR and the JERS-1 (Japanese government), which has a 18 m resolution SAR. Radarsat is expected to be launched by the Canadian government in mid-1995. The best resolution that this SAR can attain is 8 to 10 m. The standard mode of operation for Radarsat is typically 25 m. Again, all these resolutions would be too coarse to count and classify vehicles.

We talked to experts in the radar field to determine if radar could potentially be used to count and classify vehicles. The answer is *yes*. This has been done in the classified sector, principally to detect military targets. The military use radar systems primarily depend on a high geometric resolution. However, in a practical mode, the answer would be *no*. The problem is trying to detect the cars from a background with only a single look image. We can eliminate one problem of determining where the background is by integrating our road network from a GIS to overlay on the radar image. This then tells us where the background is, and the road would typically be smooth (or dark). Next, we would need to determine what is different on that background, which would be the moving vehicle. We would probably see the glint off of a vehicle, but to truly determine if the glint is indeed a vehicle, we would need a strong radar cross-sectional area. At this time the best SAR resolution is 8 m. There may not be enough cross-sectional area of a potential target with the SAR to correlate the signal with a vehicle. Another problem is speckle or noise, as radar data normally contains a lot of speckle. It will be difficult to determine the targets (vehicles) from the speckle. Also, counting and classifying many cars is different than looking for one stationary military target.

6.3 Thermal Sensors

Thermal imagery has also been suggested as an alternative. The principal means of detecting a vehicle would be to map the warmer temperatures (recorded as the light

tones) that would be associated with the vehicle's engine with the assumption that the highway segments would be cooler. Again, we would need fine spatial resolution to do this.

The present satellite system that contains thermal data is the Landsat Thematic Mapper (TM) sensor. TM has one thermal band – TM band 6 – that records in the wavelengths of 10.4 to 12.5 μm. However, the spatial resolution is 120 m and, thus, detecting vehicles and even locating the highway would not be possible.

A future sensor to be launched on the EOS platform in mid-1998 is the Advanced Spaceborne Thermal Emission and Reflection Radiometer (ASTER). Although five bands of thermal data between 9 to 12 μm will be acquired at a better spatial resolution (90 m) than the TM sensor, the resolution will still be too coarse for locating the highway or detecting vehicles.

6.4 Digital Cameras in a Tethered Balloon

We also investigated the resolutions available when using a tethered balloon to image a highway segment. We investigated available digital video cameras. Two cameras used at the Center for Mapping include one with a variable focal length from 1.4 to 5 mm and a second camera with a fixed focal length of 8 mm. For the second camera, we have an additional technical specification that a pixel has a width of 11 μm and a height of 13 μm on the CCD (charge coupled device). Typical image array sizes for a video frame would be 480 pixels wide by 640 rows.

Tables 6.2 and 6.3 shows varying altitudes ranging from 25 to 500 m with the corresponding spatial resolution (m) and area covered on the ground (km^2) from the resulting image.

From Table 6.2 the best spatial resolution would be with the 5-mm focal length at an altitude of 25 m. At this altitude, the resolution would be 13 cm for an area of 0.01 km^2. When moving the balloon to a higher altitude of 500 m, then the resolution of the image decreases to 2.65 m, but the image will contain a larger spatial area (2.15 km^2). The 8-mm camera (Table 6.3) will give a finer resolution, ranging from a 3 by 4 cm pixel at a 25-m altitude to a 69 by 81 cm pixel at an altitude of 500 m. The spatial area covered with a digital image would increase from 0.0004 km^2 at a 25-m altitude to 0.1716 km^2 at the 500-m altitude. Therefore, such an approach would rarely be able to count and classify vehicles. The system would be useful for looking at specific areas. Compared to a satellite-mounted sensor, however, the spatial coverage would be extremely limited.

Table 6.2. Analysis of spatial resolution (m) and area covered (km^2) from a tethered balloon using a digital video camera with a varying focal length (1.4 to 5.0 mm).

Altitude (m)	*1.4 mm*	*2.8 mm*	*3.0 mm Resolution (m)*	*4.0 mm*	*5.0 mm*
25	0.47	0.24	0.22	0.17	0.13
50	0.94	0.47	0.44	0.33	0.26
75	1.42	0.71	0.66	0.50	0.40
100	1.89	0.94	0.88	0.66	0.53
125	2.36	1.18	1.10	0.83	0.66
150	2.83	1.42	1.32	0.99	0.79
175	3.31	1.65	1.54	1.16	0.93
200	3.78	1.89	1.76	1.32	1.06
225	4.25	2.13	1.98	1.49	1.19
250	4.72	2.36	2.20	1.65	1.32
275	5.20	2.60	2.43	1.82	1.46
300	5.67	2.83	2.65	1.98	1.59
325	6.14	3.07	2.87	2.15	1.72
350	6.61	3.31	3.09	2.32	1.85
375	7.09	3.54	3.31	2.48	1.98
400	7.56	3.78	3.53	2.65	2.12
425	8.03	4.02	3.75	2.81	2.25
450	8.50	4.25	3.97	2.98	2.38
475	8.98	4.49	4.19	3.14	2.51
500	9.45	4.72	4.41	3.31	2.65

Altitude (m)	*1.4 mm*	*2.8 mm*	*3.0 mm Area (km^2)*	*4.0 mm*	*5.0 mm*
25	0.07	0.02	0.01	0.01	0.01
50	0.27	0.07	0.06	0.03	0.02
75	0.62	0.15	0.13	0.08	0.05
100	1.10	0.27	0.24	0.13	0.09
125	1.71	0.43	0.37	0.21	0.13
150	2.47	0.62	0.54	0.30	0.19
175	3.36	0.84	0.73	0.41	0.26
200	4.39	1.10	0.96	0.54	0.34
225	5.55	1.39	1.21	0.68	0.44
250	6.86	1.71	1.49	0.84	0.54
275	8.30	2.07	1.81	1.02	0.65
300	9.87	2.47	2.15	1.21	0.77
325	11.59	2.90	2.52	1.42	0.91
350	13.44	3.36	2.93	1.65	1.05
375	15.43	3.86	3.36	1.89	1.21
400	17.56	4.39	3.82	2.15	1.38
425	19.82	4.95	4.32	2.43	1.55
450	22.22	5.55	4.84	2.72	1.74
475	24.76	6.19	5.39	3.03	1.94
500	27.43	6.86	5.97	3.36	2.15

Table 6.3. Analysis of spatial resolution (m) and area covered (km^2) from a tethered balloon using a digital video camera with 8 mm focal length.

Altitude (m)	*Resolution (width)*	*Resolution (height)*	*Area covered (km^2)*
25	0.03	0.04	0.0004
50	0.07	0.08	0.0017
75	0.10	0.12	0.0039
100	0.14	0.16	0.0069
125	0.17	0.20	0.0107
150	0.21	0.24	0.0154
175	0.24	0.28	0.0210
200	0.28	0.32	0.0275
225	0.31	0.37	0.0348
250	0.34	0.41	0.0429
275	0.38	0.45	0.0519
300	0.41	0.49	0.0618
325	0.45	0.53	0.0725
350	0.48	0.57	0.0841
375	0.52	0.61	0.0965
400	0.55	0.65	0.1098
425	0.58	0.69	0.1240
450	0.62	0.73	0.1390
475	0.65	0.77	0.1549
500	0.69	0.81	0.1716

6.5 Future Commercial Satellites

Even though the U.S. Landsat-6 satellite failed shortly after launch in September 1993, there have been a number of privately funded firms and government initiatives to collect and market satellite data. For example, Eosat has added the Russian Soyuz data to their commercial product line. These data are available at a 3 m spatial resolution for the visible bands. However, this product is available only in a photographic form and not in a digital mode. Moreover, according to our analysis the 3-m resolution would not be sufficient to classify small vehicles.

Eosat also markets the Indian government satellite IRS-1B data in both digital and photographic formats. Two Linear Imaging Self Scanners (LISS-I and LISS-II) collect data in four spectral bands, all of which are nearly identical to the Landsat TM's visible and near infrared bands (TM bands 1 through 4). LISS-I has a 36 m resolution, whereas LISS-II has a resolution of 72 m. IRS-1C is due to be launched in the summer 1995 and will have additional spectral coverage in the shortwave infrared region, stereo viewing capability, a Wide Field Sensor, and a 10-m panchromatic band.

In addition, Eosat markets JERS-1, the Japanese Earth Resources Satellite-1, multispectral and radar data. The products include data from the Optical Sensor (OPS),

which collects data in four visible and near infrared bands at a 18.3 x 24.2 m resolution, and a Synthetic Aperture Radar (SAR), which acquires data at a resolution of 18 m and is capable of penetrating clouds. OPS is also capable of stereoscopic observation by forward (15.4°) and nadir look angles in the near infrared band 4.

The U.S. government has started opening selected Central Intelligence Agency (CIA) image archives to the commercial marketplace. Initially, these images will probably be available in hard copy photographic form.

GDE Systems, Inc., Litton's Itek Optical Systems Division and Orbital Sciences Corporation was issued a fully operating license from the U.S. Department of Commerce for a newly-formed company called Eyeglass International. They are proposing high resolution satellite imagery at a 1-m resolution (panchromatic – 0.5-0.9 μm) available in early 1997. The satellite will be in a sun-synchronous orbit at 700 km and will provide images at a 15 km swath width. A revisit period of 2 days is possible by using a ±45° in- and cross-track capability. The pointing capability also allows for stereo coverage, both fore and aft. The stereo images are designed for a B:H (base to height) ratio of 1.0 with the time between images being approximately two minutes (100 sec). This will make it difficult to determine vehicle speeds between two images when they are separated by this long time interval. Eyeglass™ will be launched and operational by 1997.

Space Imaging was formed in 1994 as a satellite imaging venture. Lockheed Missiles and Space Company, a Sunnyvale Lockheed subsidiary, recently received a U.S. government license to produce 1 m data. They plan to develop, launch and operate a high-resolution system that will include an optical sensor that operates like a digital camera. Black and white images with a resolution of 1 m and multispectral images with a resolution of 4 m are planned with data available in 1997.

Worldview Imaging (San Francisco, California) was the first company to receive a license from the U.S. Department of Commerce to build and operate a high resolution commercial remote sensing system. Ball Corporation's Aerospace and Communications Group (Broomfield, Colorado) received a commercial remote sensing license in the summer 1994. Just recently, Ball Aerospace merged with WorldView Imaging Corporation to form a new company called EarthWatch. A commercial remote sensing satellite – EarlyBird – with a spatial resolution of 3 m (panchromatic black and white images) will be launched in early 1996. A multispectral sensor at 15 m resolution will also be included. In mid-1997 they will launch QuickBird with a 1-m panchromatic sensor and a 4-m multispectral sensor.

In summary, fine resolution data will be available from the commercial market-place in the very near future. Some of these satellite systems will provide products at the 1-m resolution, which is within our required design to count and classify vehicles from a satellite platform. However, one drawback is that these future satellite systems will be from sun-synchronous orbits. Such orbits will not allow U.S. highways to be imaged at various times throughout the day. These systems will only provide one view at the same time of day for any given location.

Section 7. Future Efforts

The previous sections have discussed the work that was performed over the past two years. Throughout our study we have found several interesting problems that would warrant additional work. This section outlines future research topics.

7.1 Additional Vehicle Detection Tests

In our analysis of the ODOT panchromatic imagery, we determined that the shadows of the vehicles rather than the vehicles themselves were being detected from the pavement. Although we were able to count and classify vehicles with fairly good accuracy based on their shadows, the shadows can be highly variable depending on the orientation of the highway, the time of day, and the time of year. We also determined that additional factors of traffic and pavement conditions can influence how well we would be able to count and classify vehicles. Additional tests should be directed to examining the following conditions: varying shadow lengths from the vehicles, overlapping shadows from several vehicles, different orientations of the highway with respect to the sun, different types of pavement, oily patches on the pavement, and rush-hour conditions of traffic flow. It should be possible to develop rules to control for some of these factors.

7.2 Coordinated Aircraft Imagery with Ground Counts Test

Since the 1-m satellite data is not immediately available, the techniques developed during our study could be applied directly to aircraft data at the present time. We propose to acquire digital image data from an aircraft platform over a test site at a fine spatial resolution to simulate high resolution satellite data. This could be a cooperative effort with the Ohio Department of Transportation (ODOT). ODOT is willing to fly the aircraft to acquire the imagery and to gather ground counts. The image data can be processed and merged into a GIS containing the highway network in the test site area. Data concurrently collected from traditional ground-based methods can then be processed and merged as a second data set into the GIS. The data sets can be combined to estimate traffic parameters (e.g., VMT, percent trucks, densities during specific time periods, velocities) under various scenarios (e.g., having fewer sources of ground-based count information). The results can be compared against those obtained when combining all of the ground-based information and the aircraft information, which is considered to be an accurate estimate of ground truth.

7.3 Calculating Vehicle Speeds

We did not have the resources in this project to calculate vehicle speeds from two images. To determine vehicle speeds from a set of two images, one needs to solve a correspondence problem (matching problem). A vehicle detected on one image needs to correspond with the same vehicle on a second image so that a change in speed can be calculated. There are two major methods used to solve the correspondence problem—area-based matching and feature-based matching. These two methods take into account the geometric relationship between two or more images and assume that the objects to be

matched are stationary, rather than dynamic. This procedure is followed when creating digital elevation models (DEMs), as one assumes that the landscape (elevation of the land surface) does not change from one image to the next. Thus the two matching methods cannot provide the information for computing the speed of moving vehicles because the vehicles are changing in x,y,z location while the image is being acquired. Any required matching method should contain the geometric and topological relationships between two or more images taken within a short period of time. Because of this constraint, a suggested matching method is relational matching, which matches the geometric and topological relations between the features existing in two or more images.

The relational matching method compares two relational descriptions between the two images and finds the best match between two data descriptions and their relationships. To find the best match, there should be measures of similarity. These measures include an evaluation function using an efficient search method.

The basic elements of data descriptions are called primitives. These elements were used in our image processing routines to describe the various types of vehicles. For example, the primitives defined included the size of shadow, semi-major and semi-minor axis of the shadow, shape parameter of the clump, gray level distribution, and the shadow orientation. Thus the data descriptions are merely the list of primitives, which are the feature-based descriptions. The geometric relationship of each primitive is the locational relation, which is termed the structural description.

The evaluation function (cost function) shows the best match between the list of primitives with their relations. The objective of the evaluation function is to move through the search method to reach the best match. The best match is obtained when the evaluation function is minimized. The search space will be large in size, so the evaluation function and search method should be interactive to reduce the amount of search space while still optimizing the evaluation function. There are many search methods that could be used in such a study and include tree search, simulated annealing and relaxation labeling.

The search space of the correspondence problem in relational matching can be represented as a tree. The search begins at the root level (the top of the tree), which represents the initial problem state. At each level the primitives are tested and then assigned to satisfy the predefined relations until the bottom leaf level is reached. At the end of the process there will be only one path in the tree that will best match and optimize the evaluation (cost) function. The simulated annealing process simulates the physical process of annealing. The annealing process can be compared to a physical system where the temperature is slowly lowered until the system is reduced to its lowest energy state. In this analogy the "energy" is the value of the evaluation function, which is minimized by a stochastic optimization technique. A drawback is that the simulated annealing method requires a large amount of computation time. The relaxation labeling method is an iterative process that finds the best match using the constraints, such as the relations between the primitives. The relaxation labeling is not guaranteed to converge to a single solution, however, this could be implemented in parallel processing to overcome this.

Once the correspondence problem between two images is solved, the vehicle speed can be computed by a simple calculation. Since any digital image will be co-registered with a map coordinate system, the distance that a vehicle moves from one image to the next can be easily measured. The vehicle speed will be a ratio of the distance and time traveled between the two images.

The important part of computing vehicle speeds is to solve the correspondence problem between two images, since the vehicles are changing from one image to the next image. As long as the matching between two images is well established, the computation of vehicle speeds is a simple numerical calculation.

Section 7.4 Demonstration Project to Prepare for Eyeglass™ Data

The work proposed here would be a further extension of the work described in Section 7.2. The objective is to develop the infrastructure required to conduct a satellite demonstration project based in Ohio. We would demonstrate the use of satellite imagery to count and classify vehicles for traffic data collection. Specifically, we aim to process aerial photographs at a resolution simulating 1-m satellite panchromatic imagery, use this processed imagery to count and classify vehicles on selected highway segments, georeference the counts and classifications into a geographic information system (GIS) database, georeference concurrent traffic ground counts to the same GIS database, and compare the aerial-based and ground-based vehicle counts and classifications. In a satellite-based demonstration project in 1997, all of these tasks would be conducted automatically. However, in this preliminary study, we plan to conduct the tasks with limited automation to understand the technical components. In this way we can be in a better position to prioritize the tasks required to eventually achieve the required level of automation for a large-scale satellite-based project.

In conjunction with ODOT's Bureau's of Aerial Engineering and Technical Services, we could define a set of highways in a limited geographic area near Columbus. The Bureau of Aerial Engineering could obtain aerial panchromatic imagery of the highways. The Bureau of Technical Services could obtain ground-based traffic counts and vehicle classification data on the highways concurrently with the aerial imagery. We will scan the aerial imagery to simulate 1-m data and use the image processing programs developed in this project to count and classify vehicles into at least three categories based on our developed decision rules. We will input the classifications obtained from the aerial imagery and from the Technical Services ground counts into the same geographically-referenced database. We will then compare the data in several ways. We will need to develop a means to compare the traffic density information estimated from the aerial imagery to the traffic volume data estimated from the ground counts. We then would compare the vehicle counts and classifications on the highway segments. We also anticipate comparing differences among highway segments in traffic densities obtained from the aerial imagery to differences among the same highway segments in traffic volumes obtained from the ground counts. The results from this effort would be essential to understanding the required technical components necessary for a larger demonstration.

The major benefit of this project would be to have simulated on a small-scale the process that would be used for a large-scale project. Our work would uncover the areas where development efforts would need to be concentrated on in the future to prepare for the satellite demonstration project in 1997. Developing suitable statistics to make meaningful comparisons, automating the aerial image-based classification routines, automatically referencing the aerial image-based classifications to the GIS database, and automatically referencing the ground counts to the GIS database will all need different levels of development effort.

Section 8. Conclusions

Recent legislation requires the collection of more and better quality traffic data. At the same time, the end of the Cold War has loosened restrictions on civilian use of fine resolution satellite data. The coincidence of these two trends motivates an interest in using satellites as an *off-the-road* traffic data sensor to complement traditional sources of data.

We were tasked to investigate the feasibility of using satellite remote sensing data to collect traffic data. We determined that the resolutions required to count and classify vehicles would not allow the use of geo-stationary or geosynchronous orbits, since satellites in these orbits must be at extremely high altitudes (around 35,900 km). Thus, it would be necessary to place an orbiting remote sensing satellite into a near-polar, circular orbit at altitudes ranging from 400 to 1,000 km that would take about 90 to 100 minutes to circle the earth. The resulting coverage from an orbiting satellite would imply that satellite data would augment, rather than replace traffic data collection. We investigated the resolution, the orbital parameters, and the commercial feasibility of a satellite system that could count and classify vehicles.

To determine the necessary spatial resolution, tests were performed with simulated satellite data at various resolutions (1.2 m, 2.4 m, and 4.8 m) of panchromatic imagery (0.5-0.9 μm) over selected highway segments in Franklin County, Ohio. From our analyses, we determined that a 1-m resolution would be necessary to count and classify vehicles (cars and trucks) with greater than a 90% accuracy.

The next technical issue that was addressed included the coverage that could be obtained from an orbiting satellite with a 1-m sensor onboard. This coverage would be a function of the sensor and orbital design parameters. Mathematical formulations were developed to represent the interrelations among these parameters and to allow easy evaluation of various satellite designs for circular orbits. We formulated a *percent continental U.S. covered per day* performance measure and related this measure to the orbital and sensor parameters. Based on present and anticipated limits on sensor parameters and on physical relations among the parameters, we developed a nonlinear program to determine the maximum coverage based on sensor parameters.

We recommend an inclination angle of 130° to achieve the maximum coverage per day over the continental U.S. A swath width of 15 km (using a pixel array of 15,000) was used for the satellite altitudes under consideration to achieve the 1-m resolution. With this satellite design, our mathematical program results showed that, after factoring down for unavailability of images during night and cloud cover, we can cover approximately 1% of the highways in the U.S. per day. The primary limiting constraint that we have at present is the data transmission rate. Given that satellites would cover spatial traffic parameters at an *instant of time*, whereas existing traffic data collection systems capture temporal parameters at a *point in space*, the effects of such daily satellite coverage on estimates of traffic parameters when combining the two systems is still an unanswered question.

The last technical issue is the commercial feasibility of such a satellite design. Comparing to planned satellite missions with similar specifications, it appears that launching and operating a required system would cost on the order of $75-100 million. Several commercial companies are designing satellites that will achieve 1-m resolution in the very near future. One system, Eyeglass™, will be launched and operational by 1997. The only drawback to this system is that Eyeglass™ is in a sun-synchronous orbit. However, with its design of fore-and-aft and side-to-side image coverage using angles up to ±45°, it will be possible to achieve additional times of satellite coverage. We determined that acquiring enough Eyeglass™ data to cover approximately 0.05% of the U.S. highways per day (if possible) would cost on the order of $3 million per year.

Before satellite data could be used routinely to count and classify traffic data on an operational basis, the infrastructure required to process and use the satellite data must also be considered. With preliminary testing of Eyeglass™-type sensor data as proposed in Section 7, several of these technical issues should become clearer. Also, unanticipated problems that may be encountered with the image data flow and processing could be worked out before actual demonstration and use of Eyeglass™ data in future traffic data collection studies.

The planned future commercial remote sensing missions were not designed, or even conceived, with traffic data collection in mind. Moreover, determining how to integrate the spatial data collected from a satellite with the temporal data collected from ground counts and developing the infrastructure to collect, process and transmit the information are issues that need to be addressed before satellite data could be used on an operational basis. Therefore, we believe that at this time it is premature to attempt to use high resolution remote sensing data from commercial missions on an operational basis.

These missions do, however, offer a fortuitous opportunity to conduct operational tests and address the development issues in a realistic setting. Our simulation results indicate that a 1-m resolution (panchromatic data) is required to distinguish trucks from passenger cars. The decisions to launch 1-m panchromatic sensors, which were made independently of our results, will allow the civilian world to work with 1-m data for the first time. Also, researchers can test prior simulation results with actual satellite 1-m data. At the same time, planning for operational tests in limited areas in which the data are collected, processed, and delivered to selected users would hasten the design of the necessary supporting infrastructure. Conducting operational tests first with the Eyeglass™ data and later with the EarthWatch and Space Imaging data would indicate the weak links in the preliminary design of such an operational system.

Given the lead time required to plan and implement operational tests and the added value of testing concepts *in the field* by testing them *in the laboratory,* we recommend that the next step in determining the feasibility of using satellite data for traffic data collection should be to take advantage of Eyeglass™, EarthWatch and Space Imaging data, and any other near-term satellite missions. In this way we can test and demonstrate concepts and identify the relative magnitude of problems that would need to be resolved before satellite data could be used in a routine manner to collect highway traffic data.

References Cited

Al-Obaida, A.I., 1993. "Design and simulation of a real-time mapping satellite for the Kingdom of Saudi Arabia," unpublished PhD dissertation, The Ohio State University, Columbus, Ohio.

Anderson, J.R., E.E. Hardy, J.T. Roach and R.E. Wimer, 1976. A land use and land cover classification system for use with remote sensor data, U.S. Geological Survey Professional Paper 964.

Ashwood, J.E. and P.F. Inglis, 1975. Time-lapse aerial photography: application to traffic surveys, *Traffic Engineering Control*, 16(1):19-21.

Ashworth, R., 1976. A videotape-recording system for traffic data collection and analysis, *Traffic Engineering Control*, 17(11):468-470.

Avery, T.E. and G.L. Berlin, 1992. *Fundamentals of Remote Sensing and Airphoto Interpretation*, Macmillan Publishing Company, New York.

Bullock, D., J. Garrett, Jr. and C. Hendrickson, 1993. A neural network for image-based vehicle detection, Transportation Research-C, 1(3):235-247.

CNES, 1987. SPOT User's Handbook, Vol. 1: Reference Manual, SPOT Image Corporation, Reston, Virginia.

Colvocoresses, A.P., 1979. "Proposed parameters for Mapsat," *Photogrammetric Engineering and Remote Sensing*, 45(4):501-506.

Colwell, M., 1966. "Uses and limitations of multispectral remote sensing," Proceedings of the Fourth International Symposium on Remote Sensing of Environment, Environmental Research Institute of Michigan, University of Michigan, Ann Arbor, Michigan, pp. 71-100.

Elachi, C., 1987. *Introduction to the Physics and Techniques of Remote Sensing*, John Wiley and Sons, Inc., New York, 413 p.

FHWA, 1992. "Traffic Monitoring Guide," US DOT, Office of Highway Information Management, FHWA-PL-92-017, October.

FHWA, 1987. "Highway Performance Monitoring System – Field Manual for the Continuing Analytical and Statistical Data Base," US DOT, December.

Förstner, W., 1986. A feature based correspondence algorithm for image matching, International Archives of Photogrammetry and Remote Sensing, Rovaniemi, 26(3/3):150-166.

Förstner, W. and E. Gülch, 1987. A fast operator for detection and precise location of distinct points, corners and centres of circular features, ISPRS Intercommission Workshop, Interlaken, June, pp. 281-305.

Garner, J.B. and L.J. Mountain, 1978. Traffic data collection – an alternative method?, *Traffic Engineering Control*, 19(10):451-454.

Haralick, R.M. and Shapiro, L.G., 1987. *Computer and Robot Vision,* Addison-Wesley Publishing Company, New York, pp. 23-28.

Hockaday, S., 1991. Evaluation of image processing technology for application in highway operations, Technical Report TR 91-2, California Polytechnic State University, San Luis Obispo, California.

Hockaday, S., A. Chatziioanou, R. Nodder and S. Kuhtenschmidt, 1992. Evaluation and comparison of video image processing systems for traffic detection, Transportation Research Board Preprint #920744.

Itek, 1981. Conceptual design of an automated mapping satellite system (MAPSAT), Final Technical Report, 3 February, Itek 81-8449A-2.

Jensen, J.R., 1986. *Introductory Digital Image Processing - A Remote Sensing Perspective*, Prentice-Hall, Englewood Cliffs, New Jersey.

King, D.J., 1990. Connecticut's photolog laser videodisc viewing system, The Council of State Governments RM-792.

King-Hele, 1964. Theory of Satellite Orbits in an Atmosphere, William Clowes and Sons, Limited, London, England, 165 p.

KPMG Peat Marwick and NASA, 1992. *MAPSAT market review*. The Ohio State University, Center for Mapping, Columbus, Ohio.

Light, D.L., 1990. "Characteristics of remote sensors for mapping and earth science applications," *Photogrammetric Engineering and Remote Sensing*, 56(12):1613-1623.

Light, D.L., 1992a. "An international opportunity for an orbital imaging system," ISPRS #828, XVII Congress, International Society for Photogrammetry and Remote Sensing, Washington, DC, 2-14 August.

Light, D.L., 1992b. "The orbital imaging system and its potential for digital terrain models of the Earth," Proceedings of Satellite Symposia, Munich, Germany, 30 March-4 April.

McCord, M.R., C.J. Merry, X.D. Sun and F. Jafar, 1994. "Resolution effects on vehicle counts and classification with simulated satellite imagery," Transportation

Research Forum Annual Meetings, 3-5 November, Daytona Beach, Florida, pp. 195-211.

Moffitt, F.H. and E.M. Mikhail, 1980. *Photogrammetry*, Harper and Row Publishers, Inc., New York.

Pease, C.B., 1991. *Satellite Imaging Instruments, Principles, Technologies, and Operational Systems*, Ellis Horwood Limited, New York.

Peat Marwick, Mitchell and Co., 1984. "Development of a Statewide Traffic Counting Program Based on the Highway Performance Monitoring System," Contract #DTFH61-82-6-0009, March.

Polus, A., M. Levneh and S. Borovsky, 1978. Traffic Engineering Control, 19(3):123-125.

Robinson, A., R. Sale, J. Morisson and P. Muehrcke, 1984. *Elements of Cartography*, John Wiley and Sons, Inc., New York, 544 p.

Snyder, J.P., 1981. "Map projections for satellite tracking," *Photogrammetric Engineering and Remote Sensing*, 47(2):205-213.

Solar Energy Research Institute, 1981. Solar radiation energy resource atlas of the United States, Solar Energy Research Institute, Golden, Colorado, SERI/SP-642-1037, October.

Whited, J. and B. McCall., 1991. Video imagery systems for highway applications, FHWA-SA-91-041.

Notation

The following symbols are used in this report:

Section 2:

AADT	average annual daily traffic
ADT	average daily traffic
DF	daily variation factor
DHV	design hourly volumes
K	the proportion of AADT occurring during the 30th highest peak hour of the year for rural roads or 15th highest peak hour for urban areas (K factor)
MF	monthly variation factor
VMT	vehicle miles traveled

Section 3:

a_{tt}	number of clumps that were correctly classified as trucks
a_{oo}	number of clumps that were correctly classified as other vehicles
a_{nn}	number of clumps that were classified as nonvehicles that were truly nonvehicle elements
a_{to}	number of clumps that were misclassified as trucks when they were truly other vehicles
a_{tn}	number of clumps that were misclassified as trucks when they were truly nonvehicle elements
a_{ot}	number of clumps that were misclassified as other vehicles when they were truly trucks
a_{on}	number of clumps that were misclassified as other vehicles when they were truly nonvehicle elements
a_{nt}	number of clumps that truly corresponded to nonvehicle elements, but were classified as trucks
a_{no}	number of clumps that truly corresponded to other vehicles, but were classified as nonvehicles
b_{tt}	number of vehicles that were correctly classified as trucks
b_{to}	number of vehicles that were misclassified as trucks when they were truly other vehicles
b_{tn}	number of vehicles that were misclassified as trucks when they were truly nonvehicles
b_{ot}	number of vehicles that were misclassified as other vehicles when they were truly trucks
b_{oo}	number of vehicles that were correctly classified as other vehicles
b_{on}	number of vehicles that were misclassified as other vehicles when they were truly nonvehicles
A	area
B	perimeter to area ratio

D	dots per inch (dpi)
$PS(D)$	scanned pixel resolution
R_{pvt}	reflectance from pavement
R_{veh}	reflectance from vehicle

Section 4:

A^{sat}_{US}	area of the continental United States covered by the satellite
A_{US}	area of the continental United States
$A^{sat}_{[25N,50N]}$	area between latitudes 25° and 50° north covered by the satellite
$A_{[25N,50N]}$	area of the earth between latitudes 25° and 50° north
$A_{[LAT1,LAT2]}$	area of the earth between two latitudes, designed as LAT1 and LAT2
$COMP$	data compression rate before transmission
DTR	data transmission rate in megabits per second
$(DTR*COMP)_{max}$	maximum product of data transmission rate and compression factor in megabits per second
FL	focal length in meters
FL_{max}	maximum focal length in meters
f_n	fraction of ground tracks that pass over the continental U.S. during the nighttime
f_c	fraction of ground tracks that pass over the continental U.S. during the daytime when it is cloudy
f_{npgt}	fraction of nonproductive ground tracks
H	altitude of satellite in kilometers
i	inclination angle of satellite orbit
$L_{LAT1,LAT2}$	length of a ground truck between LAT_1 and LAT_2
n	orbits per day
NBB	number of bits of information per band
NBP	number of bands per pixel
PCD_{US}	percentage of the continental U.S. covered by the satellite per day
PID_{US}	percentage of highways in the continental U.S. imaged per day
$PPAL$	number of pixels per array line
$PWPD$	physical width of the pixel on the detector in micrometers
R	the (mean) radius of the earth in kilometers
RES	resolution of the square pixel in meters
SW	swath width in kilometers
V_{sg}	satellite velocity on the ground in kilometers per second

Appendix A:

a	vehicle width
A_i	area of element i in the pixel
A_{pix}	area of the pixel
A_{pvt}	area of the pavement
A_{veh}	area of the vehicle
b	vehicle length
CR_{pix}	contrast ratio of a pixel
θ	orientation angle

PS	pixel size
R_i	panchromatic spectral reflectance of element i in the pixel
R_{veh}	reflectance of the vehicle
R_{pvt}	reflectance of the pavement

Appendix D:

FOCC	Fraction of Other Vehicles Correctly Identified
FTCC	Fraction of Trucks Correctly Classified
FVCI	Fraction of Vehicles Correctly Identified
OCEC	Other vehicle Error of Commission
OCEO	Other vehicle Classification Error of Omission
TCEC	Truck Classificaiton Error of Commission
TCEO	Truck Classification Error of Omission
VIEC	Vehicle Identification Error of Commission
VIEO	Vehicle Identification Error of Omission

Appendix F:

DA	detector aperture
F_c	centripetal force
F_g	gravitational force exerted by the earth
GM	gravitational constant
m	mass of satellite
R+H	radius of the earth plus the satellite height above the earth
v	linear velocity

Appendix H:

GC	great circle arc length between two points

APPENDIX A

Mathematical Modeling of Imaging Performance

Appendix A. Mathematical Modeling of Imaging Performance

A.1 Contrast Ratio Model

The ability to sense an object using a remote sensing instrument is related to the degree to which the object contrasts with its background. In our case, the vehicle to be imaged would have to contrast sufficiently with the surrounding pavement. Considering a digital product, the contrast would be obtained by the pixels in which the vehicle is located having sufficiently different contrast ratios from those in which the vehicle is not located. In our case, the pixel contrast ratio is a numerical encoding of the panchromatic reflectance of the pixel and is determined by the weighted (by area) average of the panchromatic spectral reflectances of the objects in the pixel. Specifically, the contrast ratio of a pixel CR_{pix} could be modeled as:

$$CR_{pix} = \sum_{i=1}^{I} (R_i * A_i)/A_{pix} \qquad (A.1)$$

where R_i is the panchromatic spectral reflectance of element i in the pixel, A_i is the area of element i in the pixel, the sum is over all elements contained in the pixel, and A_{pix} is the area of the pixel (i.e., $A_{pix} = \sum_{i=1}^{I} A_i$).

For our analysis, we considered there to be at most two elements in the pixel (I=2), a vehicle element and a pavement element. We could, therefore, write Eq. (A.1) as:

$$CR_{pix} = [(R_{veh}*A_{veh})+(R_{pvt}*A_{pvt})]/A_{pix} \qquad (A.2)$$

or:

$$CR_{pix} = R_{veh}*(A_{veh}/A_{pix}) + R_{pvt}(1-A_{veh}/A_{pix}) \qquad (A.3)$$

where the subscripts veh, pvt, and pix, stand for the vehicle element, the pavement element, and the pixel, respectively.

In assuming that there would be no elements in the pixel other than vehicle and pavement elements, we were assuming that there would be no off-highway elements in the pixels of interest, i.e., the pixels containing a vehicle element. We believed that this would be an acceptable assumption for a first approximation model. We believe that the pixel size would eventually be small enough that, in all but very rare cases of vehicle positioning, any pixel containing a large enough vehicle area to be of interest would be far enough from the pavement edge that there could not be any significant area of off-highway element in the pixel. Any error due to the approximation would be reduced even more when considering highways with shoulders of the same material as the highway pavement.

Our "two-element approximation" also assumed that there would be no shadow effects in the pixel. We had intended to consider these as secondary effects after obtaining preliminary results. As we determined later, however, the shadows appear to be the principal means of vehicle detection, rather than a complication of it.

A.2 Geometric Model

The objective of the model is to investigate the properties of an array simulating remotely sensed contrast ratios corresponding to vehicles on pavements through the use of Eqs. (A.2) or (A.3). To accomplish this we anticipated simulating the superposition of vehicles with known geometry and location on a grid of pixels of specified dimensions to determine A_{veh}/A_{pix} for each pixel, inputting R_{veh} and R_{pvt} values to each pixel, and determining CR_{pix} according to Eq. (A.3). Although our results of Section 3 show that the R_{veh} and R_{pvt} values are such that this model would not work, the geometric part of the model that involved determining A_{veh}/A_{pix} led to interesting conclusions.

To determine A_{veh} and A_{pix} we superimposed a rectangular vehicle on a grid of square pixels. As illustrated in Figure A.1, the rectangular vehicle had width of a meters and length of b meters. The parameters a and b would distinguish the type of vehicle, e.g., a car or a truck. Some different classes of vehicles in FHWA's 13-category vehicle classification scheme (see Table 2.2, Sect. 2.1.5) have very similar width and length, but differ by number of axles. Therefore, we realized that vehicle type could not be completely distinguished by the a and b parameters. In this investigation we were interested in the remote sensing of general vehicle groups, however, so that the process would lend itself to large-scale, operational use, as opposed to a detailed investigation of precise vehicle classes.

We considered square pixels of length PS (pixel size), as is also illustrated in Figure A.1. A square pixel with length PS meters is said to have PS m resolution. Pixels do not have to be square, but they usually are with recent satellite sensors. Indeed, since the objects of interest, the vehicles, are rectangular, a rectangular pixel size might be of interest. We felt that this would be, at most, a secondary consideration, however. Moreover, without going into any detailed study, we also felt that, since the highways to be monitored would not have any dominant orientation, any improved performance that might be obtained by correlating the axes of a rectangular pixel grid with a given highway orientation would lead to decreased performance on those highways 90° from this orientation. The pixel resolution PS was a design parameter, and we were interested in studying its effect.

Referring again to Figure A.1, we called θ the orientation between the longitudinal vehicle axis (which would correspond to the centerline axis of the highway) and an axis taken along an axis of the pixel grid. The symmetry of the square pixels implied that either axis of the pixel grid could be chosen. This orientation parameter θ might be considered an unknown (to an observer or a software algorithm that would eventually be used to interpret the remotely sensed image) random variable over which the results might have to be integrated to make for meaningful interpretation. Or, it could be considered a known parameter upon which the results might have to be conditioned to lead to better interpretation. The orientation of the pixel grid would be known accurately to some external coordinate or reference system. We also believe that the centerline orientation of highways important enough to be monitored could be known accurately to the same external reference system. We, therefore, propose that θ would be a known parameter. In either case, as described below, the results obtained from our geometric analysis indicate that the orientation angle can influence the characteristics of the remotely sensed image (see Section A.3).

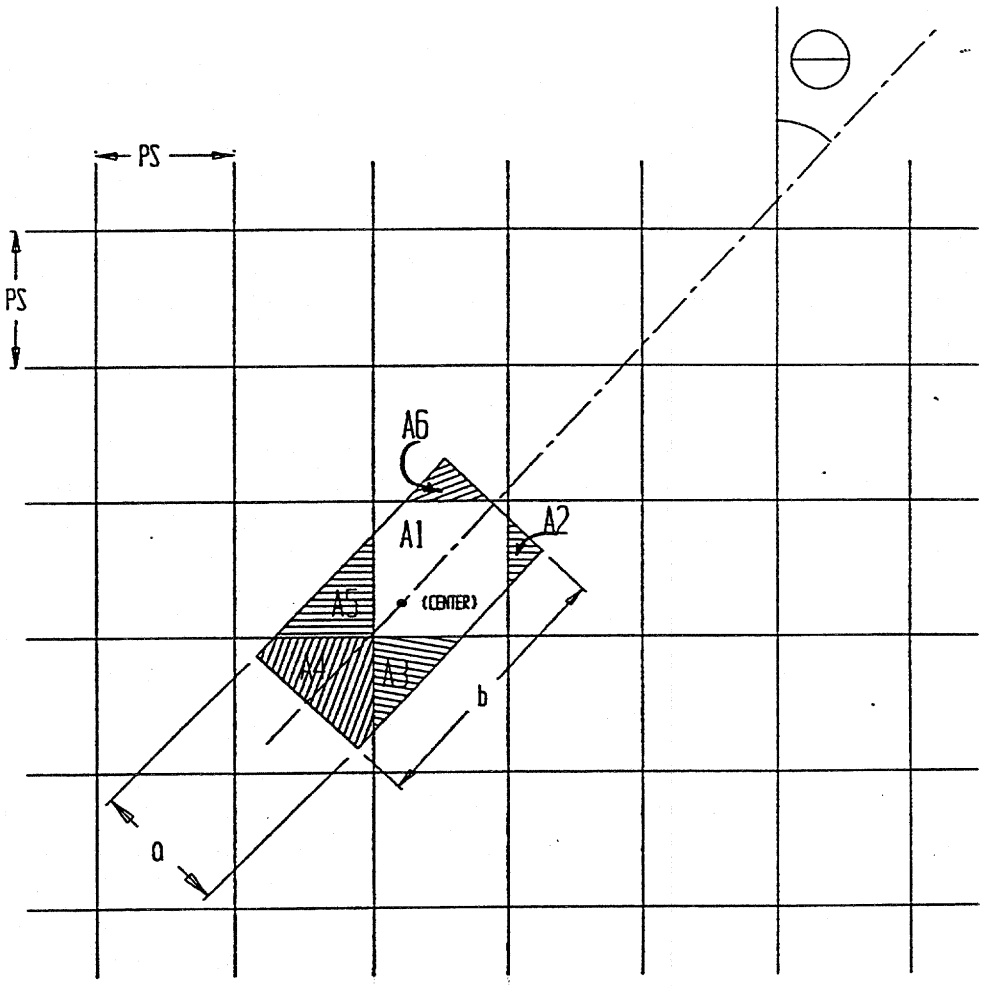

Figure A.1 Modeled geometry of a vehicle in a pixel grid

Given the parameters *a, b, PS,* and θ, representing, respectively, vehicle width, vehicle length, pixel resolution, and orientation angle, locating the center of the vehicle in the pixel grid uniquely determined the geometry of the problem. By "the geometry of the problem" we mean the constant pixel area A_{pix} and the vehicle pixel area A_{veh} and, therefore, the ratio A_{veh}/A_{pix} in each pixel of the array of pixels (see Fig. A.1). Due to the symmetry of the problem we only needed to consider centers in one of the four "quadrants" of the pixel, where the four quadrants (see Fig. A.2) are mutually exclusive and collectively exhaustive regions of the pixel consisting of sets of points (x,y). They can be defined by considering one corner of the pixel to have coordinates (0,0) in a coordinate system with axes parallel to the sides of the pixel and calling:

Quadrant 1 = {(x,y) such that $0 \le x \le PS/2$, $0 \le y \le PS/2$};
Quadrant 2 = {(x,y) such that $PS/2 \le x \le PS$, $0 \le y \le PS/2$};
Quadrant 3 = {(x,y) such that $0 \le x \le PS/2$, $PS/2 \le y \le PS$};
Quadrant 4 = {(x,y) such that $PS/2 \le x \le PS$, $PS/2 \le y \le PS$}.

That is, given a set of parameters [*(a,b),PS*, θ] and the location of the center of the vehicle in some quadrant, the geometry portrayed in Figure A.1 could be obtained with the center of the vehicle at unique points with unique rotation angles in each of the other quadrants. We, therefore, analyzed the geometry by varying the center of the vehicle *(a, b)* systematically throughout one quadrant and the rotation angle θ systematically from 0 to 2π for each location of the center. We wrote a computer program to perform the mathematical computations. A listing of this program and a description of its logic can be found in Appendix C.

A.3 Geometric Study

In remote sensing studies, one is often interested in obtaining at least one pixel that is dominated by the object sought so that it would appear sufficiently distinct from its background. In our case, this would imply that the A_{veh}/A_{pix} ratio would be "large enough" in at least one pixel. How large this ratio would need to be could not be determined without further study (the types envisioned are described in Section A.4 below), but we could investigate the distribution of the maximum A_{veh}/A_{pix} ratio that would occur for a vehicle class and pixel resolution.

Our approach was to specify [*(a,b), PS*, θ] and fix the center of the vehicle at some point (x,y) in a quadrant of the pixel. For this specification, we then used the computer program of Appendix C to determine A_{veh} for each of the pixels in which part of the vehicle would lie, found the maximum A_{veh} thus determined, and divided this by the pixel area, PS^2. We then repeated these steps for the same [*(a,b), PS*, θ], but for a different center location (x,y) in the quadrant. We did this for 360 center locations equally distributed throughout one quadrant of the pixel, recording one (the maximum) A_{veh}/A_{pix} ratio each time. We then changed the rotation angle θ and repeated the same procedure for the same 360 center locations. We did this for 20 rotation angles, specifically, for all rotation angles from $\pi/20$ to π, incrementing by $\pi/20$ radians each time. We then could form distributions of the maximum A_{veh}/A_{pix} ratios as a function of the vehicle class *(a,b)*, the pixel resolution *PS*, and, if desired, the rotation angle θ. We could then form different distributions for different vehicle classes and pixel resolutions.

As mentioned in Section A.2, if we were to consider the rotation angle unknown, we should aggregate the results over all values of θ, as well as all center locations (over which we would have no control and for which we would have no knowledge). In Figures A.3a and b, we present the maximum A_{veh}/A_{pix} cumulative distributions for 1 m, 2.5 m, 5 m, and 10 m resolutions for the case in which we would have no knowledge of θ.

In Figure A.3a, we present the distributions for vehicles with a = 1.5 m and b = 5 m, values representative of cars. In Figure A.3b, we present the distributions for vehicles with a = 2.5 m and b = 15 m, values representative of large trucks. Considering the criterion of "having at least one pixel dominated by the object of interest," it would appear that 1 m would be sufficient resolution to detect both cars and trucks. Specifically, the 1 m resolution cumulative distribution curve in Figure A.3a shows that there would be less than 0.10 probability of a car covering 96% or less of the maximally covered pixel, and almost no probability of a car covering less than 80% of the maximally covered pixel. For trucks, Figure A.3b shows that there would be virtually no probability of a truck covering less than 99% of the maximally covered pixel at this resolution.

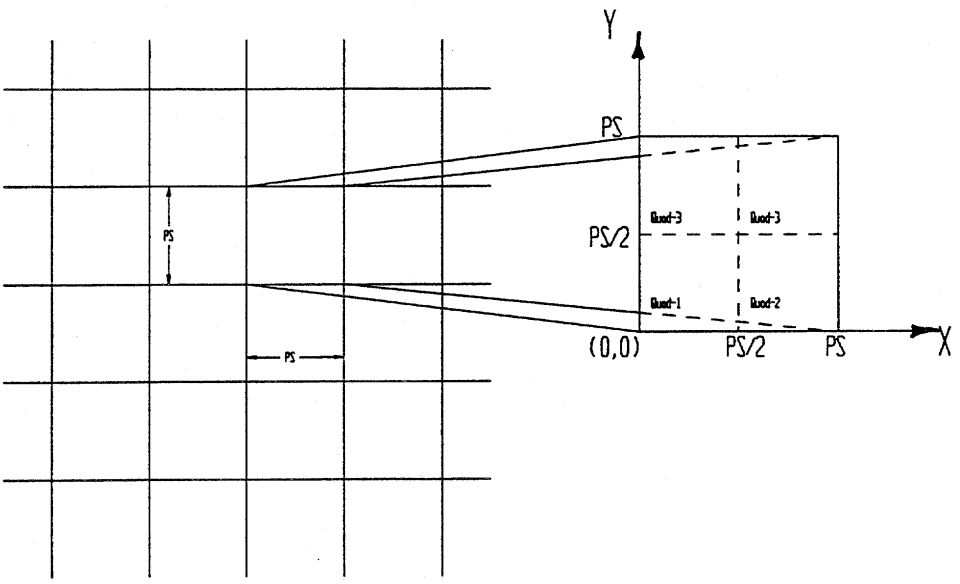

Figure A.2 Illustration of "pixel quadrants"

There seems to be an important decrease in car imaging potential when decreasing the spatial resolution from 1 m. Figure A.3a shows that, while there would be no chance of a car covering less than 50% of the maximally covered pixel at the 1 m resolution, there would be between a 0.35 and 0.40 probability of a car covering less than 50% of the pixel at the 2.5 m resolution, and that there would be no chance of a car covering 50% or more of a pixel at 5 m or 10 m resolution.

Changing the resolution from 1 m to 2.5 m does not seem to affect truck imaging as much. Figure A.3b shows that the probability remains at approximately 0.0 of the truck covering less than 50% of the maximally covered pixel. The slope of the cumulative curve, which gives the probability density, indicates a high probability that the vehicle would cover between 85% and 90% of the maximally covered pixel. The probability of a truck covering at least 50% of a pixel would decrease dramatically to between 0.5 and 0.6 at 5 m resolution and to 0.0 at 10 m resolution.

These results led us to believe that, based on geometric considerations, it might be possible to image cars at somewhere around 2.5 m resolution and that it would definitely be possible to image trucks at this resolution. Therefore, we investigated the maximal A_{veh}/A_{pix} ratios at resolutions around 2.5 m. In Figures A.3c, d we present the results for 2.0 m, 2.5 m, and 3.0 m resolutions. From Figure A.3c, we see that a car would definitely (i.e., with probability of 1.0) cover approximately 36%, 30%, and 25% or more of the maximally covered pixel for the 2.0 m, 2.5 m, and 3.0 m resolutions, respectively, and cover at least 50% of the maximally covered pixel with probabilities of approximately 0.9, 0.6, and 0.1 for these resolutions. Figure

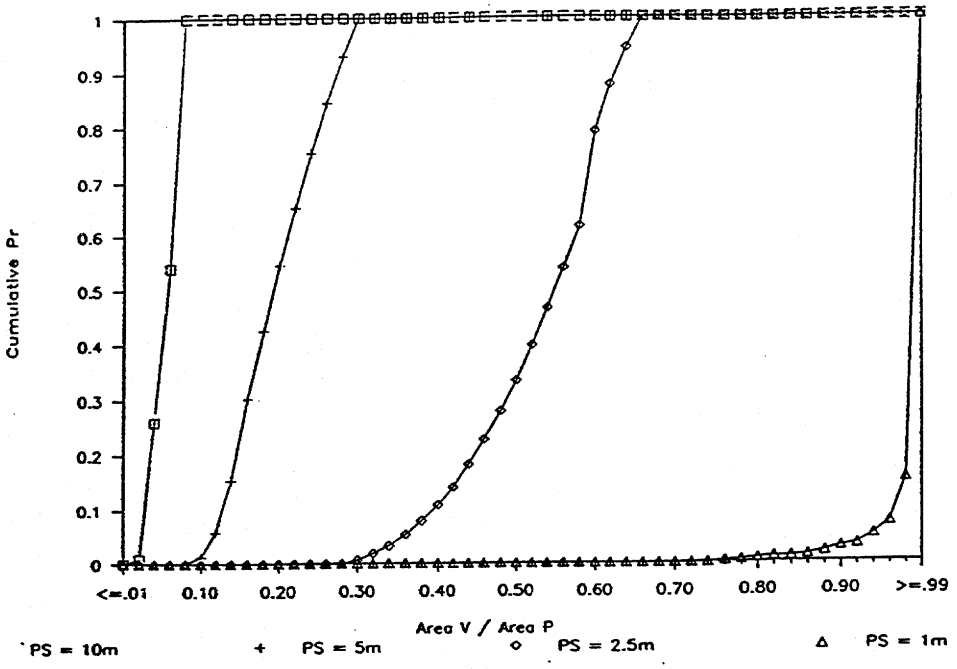

a. Vehicle type representative of passenger car: a = 1.5 m; b = 5.0 m; Pixel resolutions = 10 m, 5 m, 2.5 m, and 1 m.

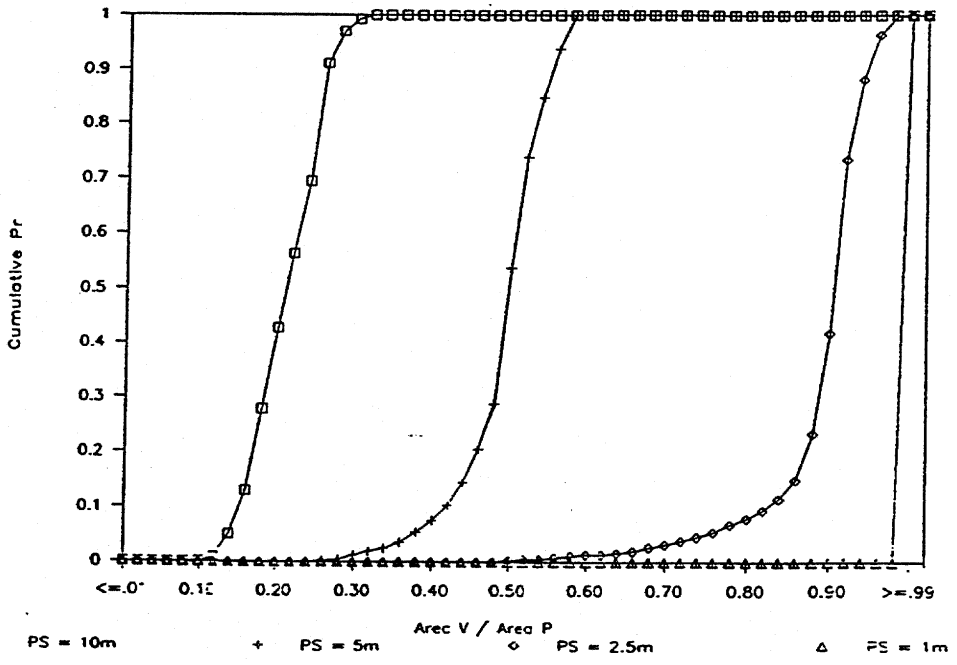

b. Vehicle type representative of large truck: a = 2.5 m; b = 15.0 m; Pixel resolutions = 10 m, 5 m, 2.5 m, and 1 m.

Figure A.3 Cumulative distributions of maximum A_{veh}/A_{pix}.

Figure A.3 continued

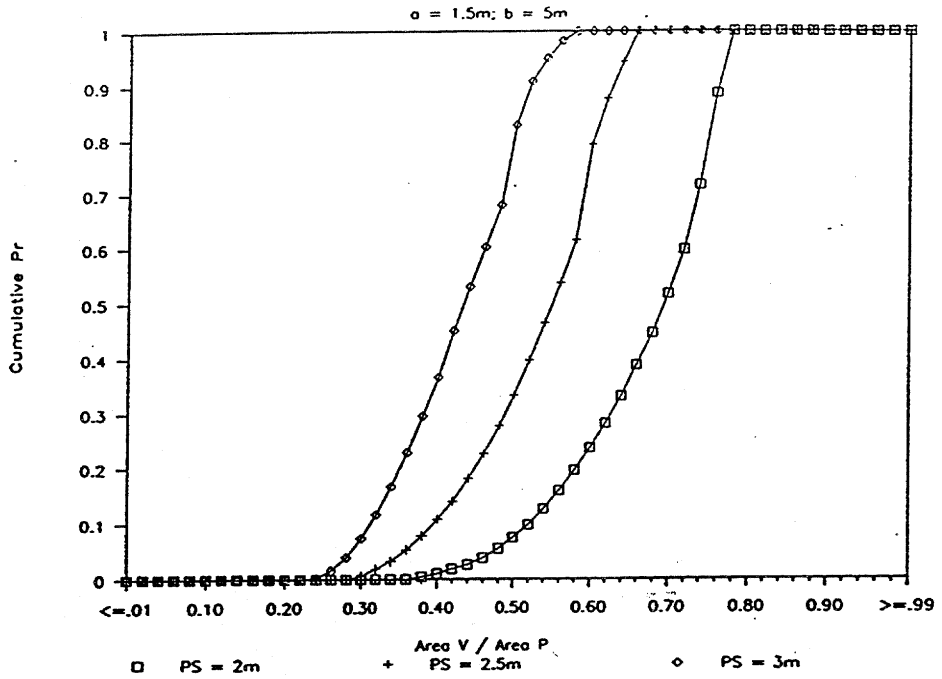

c. Vehicle type representative of passenger car: a = 1.5 m; b = 5.0 m; Pixel resolutions = 3 m, 2.5 m, and 2.0 m.

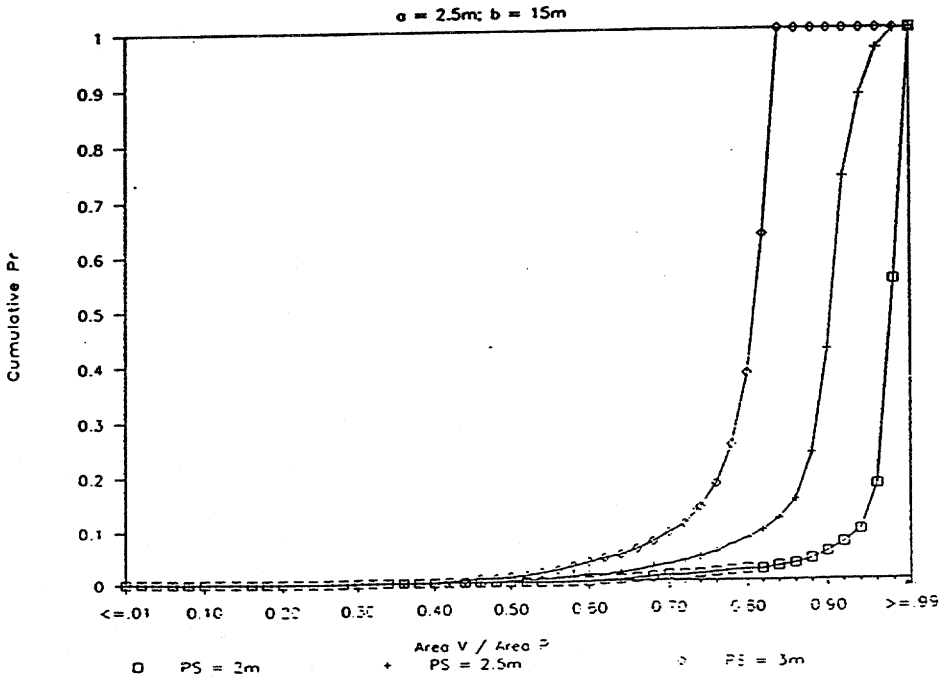

d. Vehicle type representative of large truck: a = 2.5 m; b = 15.0 m; Pixel resolutions = 3.0 m, 2.5 m, and 2.0 m.

A.3d shows that a truck would definitely cover approximately 65%, 55%, and 45% of the maximally covered pixel at the 2.0 m, 2.5 m, and 3.0 m resolutions, and almost certainly cover at least 50% of the maximally covered pixel for all of these resolutions.

As mentioned above, the percentage of the pixel that would need to be covered by the vehicle for the vehicle to dominate the pixel could not be precisely determined without knowing the relative reflectances of the vehicle and pavement. As a first approximation, however, we might consider that the vehicle should cover at least 50% of some (i.e., the maximally covered) pixel. Remote sensing studies have typically used an 85% accuracy rate (Anderson and others, 1976) as a standard for accuracy. In our case, we interpret this as meaning that the vehicle should cover at least 50% of some pixel with at least 0.85 probability. The preceding discussion and the cumulative distributions of Fig. A.3 show that we would need between 1 m and 2 m resolution to meet this standard when imaging cars and between 3 m and 5 m resolution to meet this standard when imaging trucks.

The above results are obtained by aggregating over the rotation angle Θ, representing the case where θ would be unknown to the human or computer interpreter. As we mentioned above, we believe that if θ were a parameter that influenced the interpretation, efforts would probably be made to make it known to the interpreter. We, therefore, investigated the results stratified by rotation angle θ.

In Figure A.4 we present maximum A_{veh}/A_{pix} cumulative distributions, aggregated across different locations of the vehicle's center, as described above, but at fixed values of θ for 1 m, 3 m, and 5 m resolutions. Note that at 1 m resolution (Fig. A.4a), $\theta = 0$ produces a very different result for cars than do the other values of θ. We verified this result with a scale model and in Figure A.5 examined in more detail the rotation angles around $\theta = 0$. We obtained different results for $\theta < \pi/15$ radians and, therefore, within $\pm \pi/15$ radians of 0, $\pi/2$, π, and $3\pi/2$ radians. There is no influence of θ on the A_{veh}/A_{pix} distributions for trucks at 1 m resolution (Fig. A.4b); as seen earlier in Figure A.3b, the truck always covers the entire pixel at 1 m resolution.

Figure A.4c shows that the car A_{veh}/A_{pix} distributions depend on all of the values of θ investigated at the 3 m resolution. The dependence of the truck's A_{veh}/A_{pix} distributions on the θ values at the 3 m resolution (Fig. A.4d) resemble those of the car's dependence at the 1 m resolution.

The 5 m resolution is so coarse with respect to the car's dimensions that the angle has little effect on the distribution (Fig. A.4e). On the other hand, the truck is large enough that the angle still makes a difference in the A_{veh}/A_{pix} distributions (Fig. A.4f). Figure A.5 shows additional cumulative distributions for A_{veh}/A_{pix} ratios for a car vehicle type at different rotation angles for a 1 m resolution. These results further verify that the rotation angle does make a difference in our calculations.

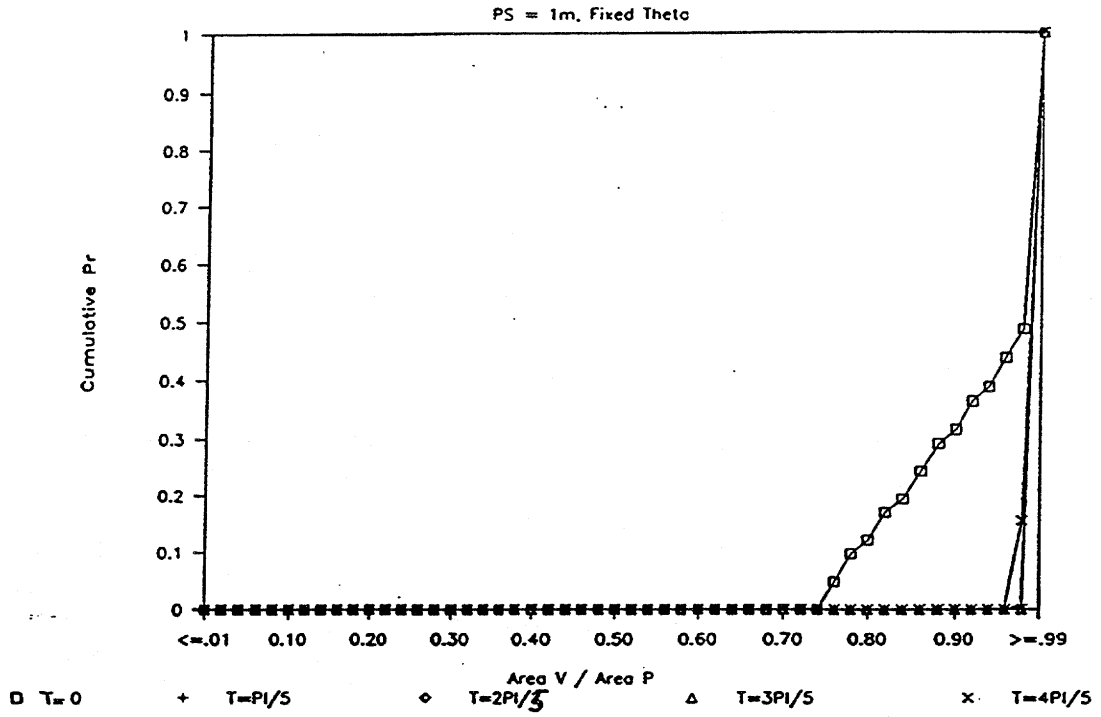

a. Vehicle type representative of passenger car: a = 1.5 m; b = 5.0 m; Pixel resolutions = 1.0 m.

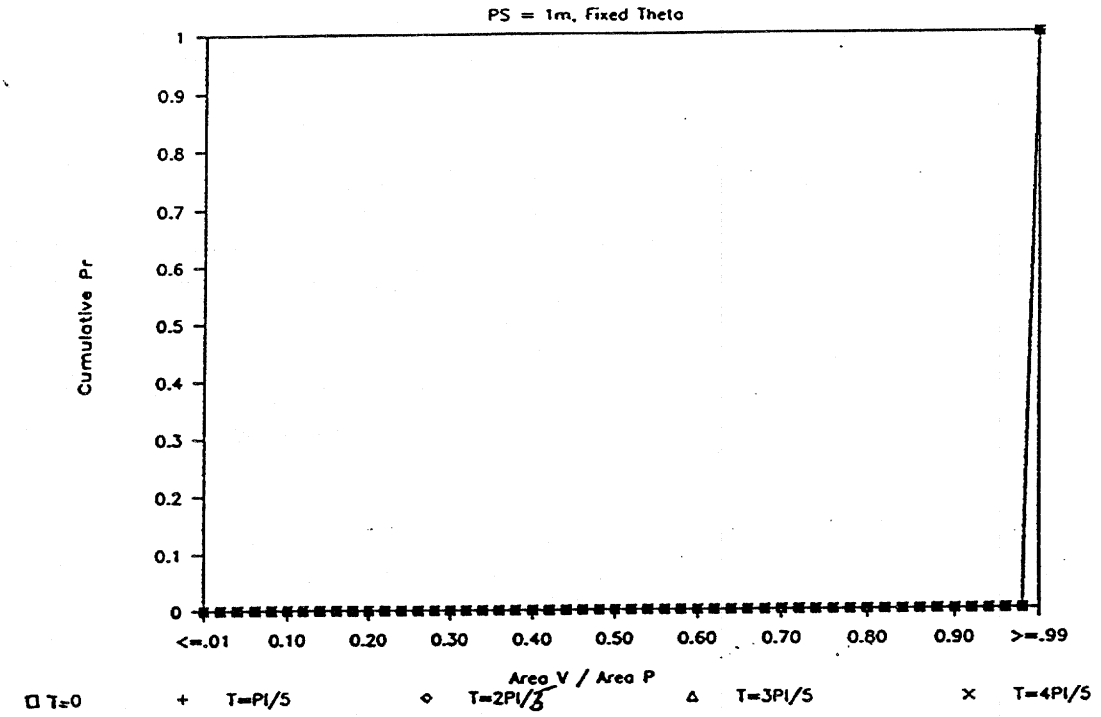

b. Vehicle type representative of large truck: a = 2.5 m; b = 15.0 m; Pixel resolutions = 1.0 m.

Figure A.4 Cumulative distributions of maximum A_{veh}/A_{pix} ratios for two vehicle types and three pixel resolutions for rotation angles of $T(\theta) = 0, \pi/5, 2\pi/5, 3\pi/5$ and $4\pi/5$.

Figure A.4 continued

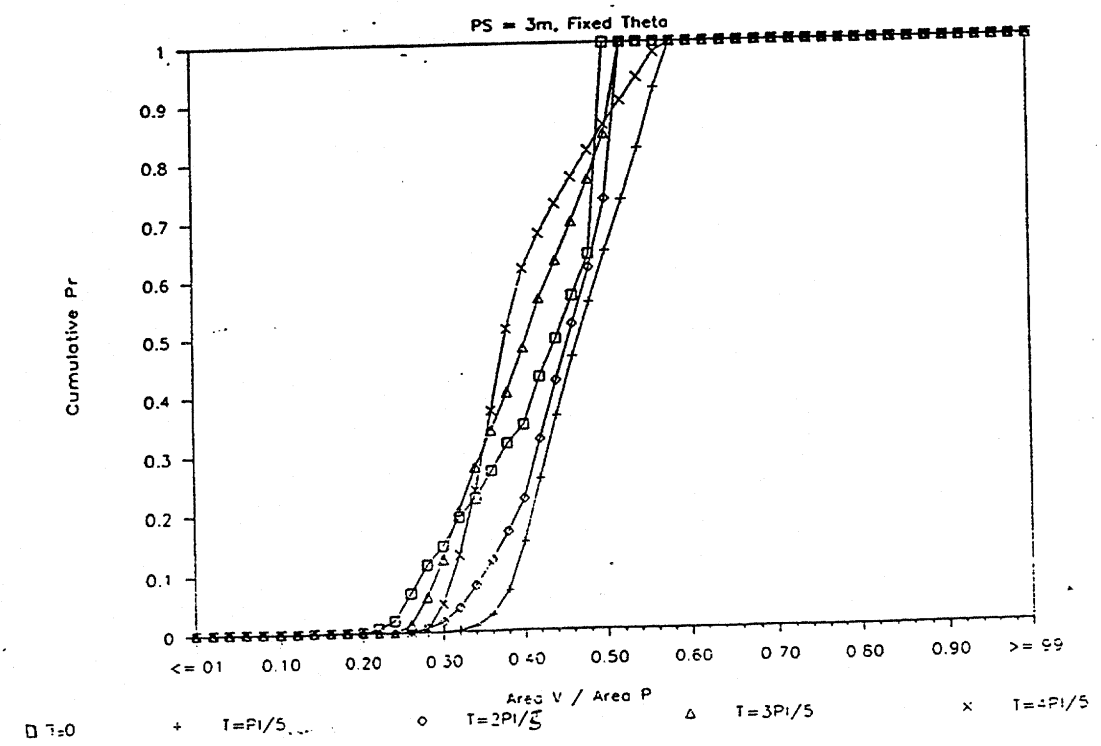

c. Vehicle type representative of passenger car: a = 1.5 m; b = 5.0 m; Pixel resolutions = 3.0 m.

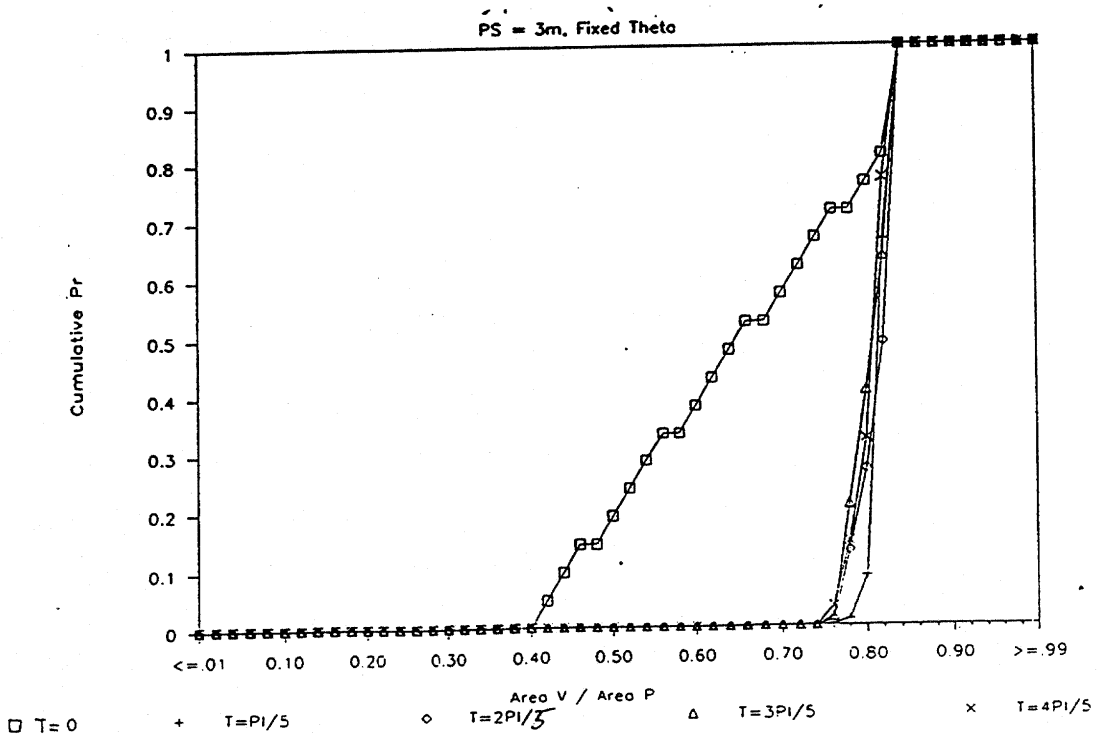

d. Vehicle type representative of large truck: a = 2.5 m; b = 15.0 m; Pixel resolutions = 3.0 m.

Figure A.4 continued

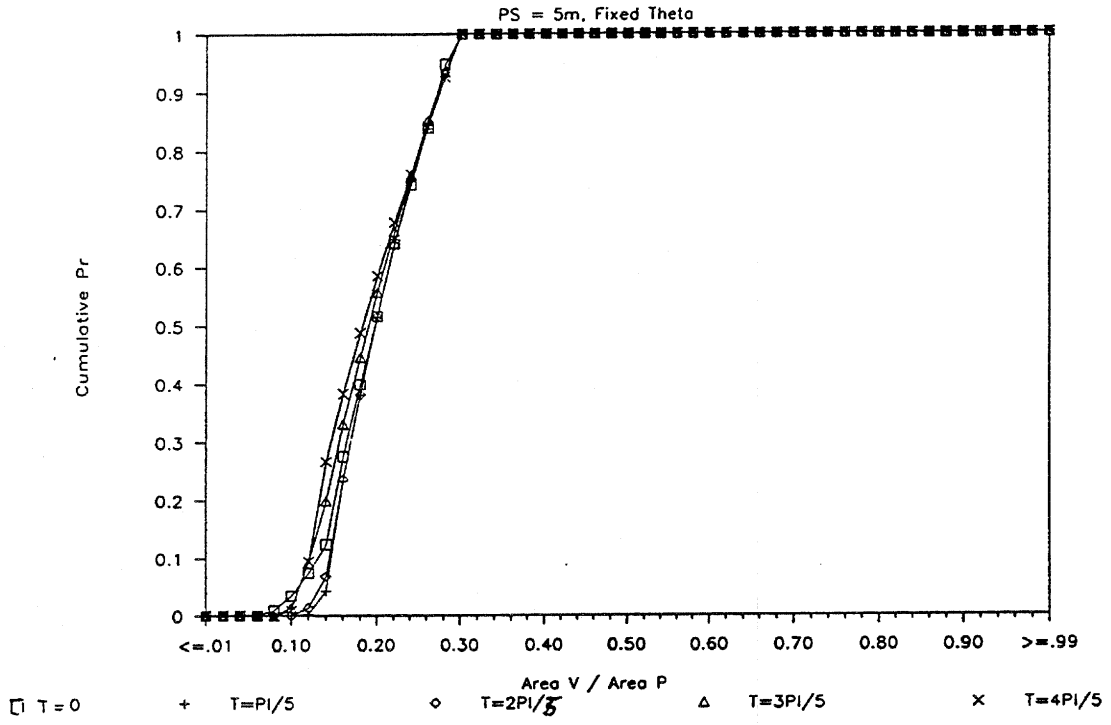

e. Vehicle type representative of passenger car: a = 1.5 m; b = 5.0 m; Pixel resolutions = 5.0 m

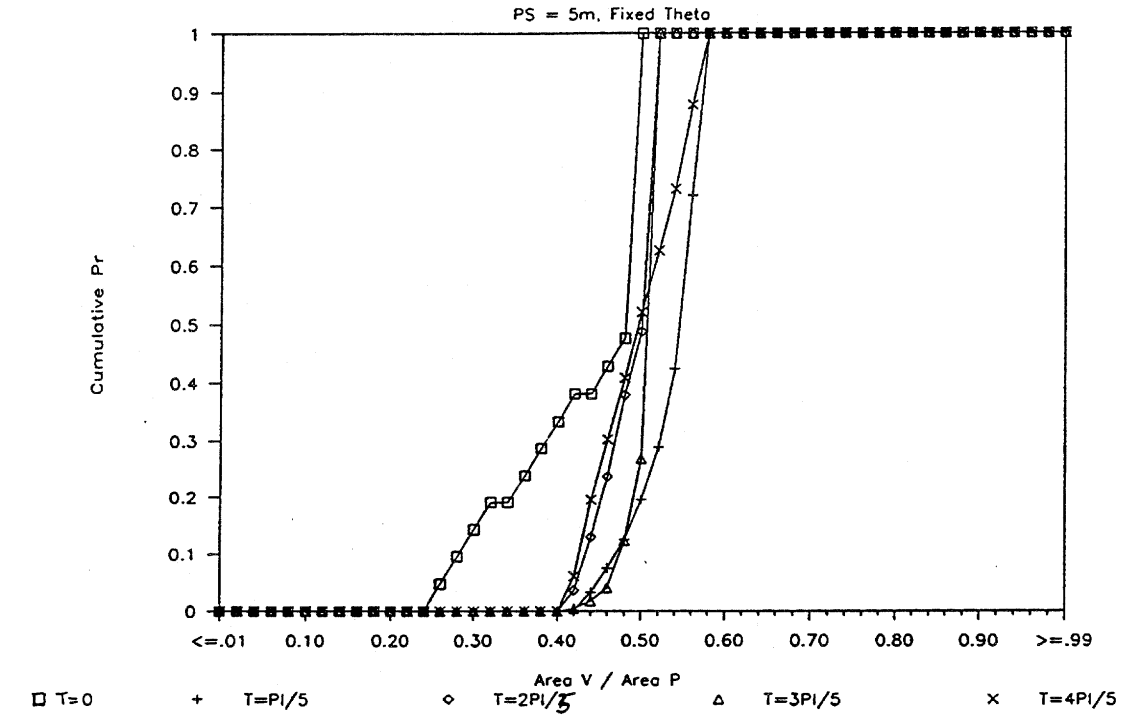

f. Vehicle type representative of large truck: a = 2.5 m; b = 15.0 m; Pixel resolutions = 5.0 m

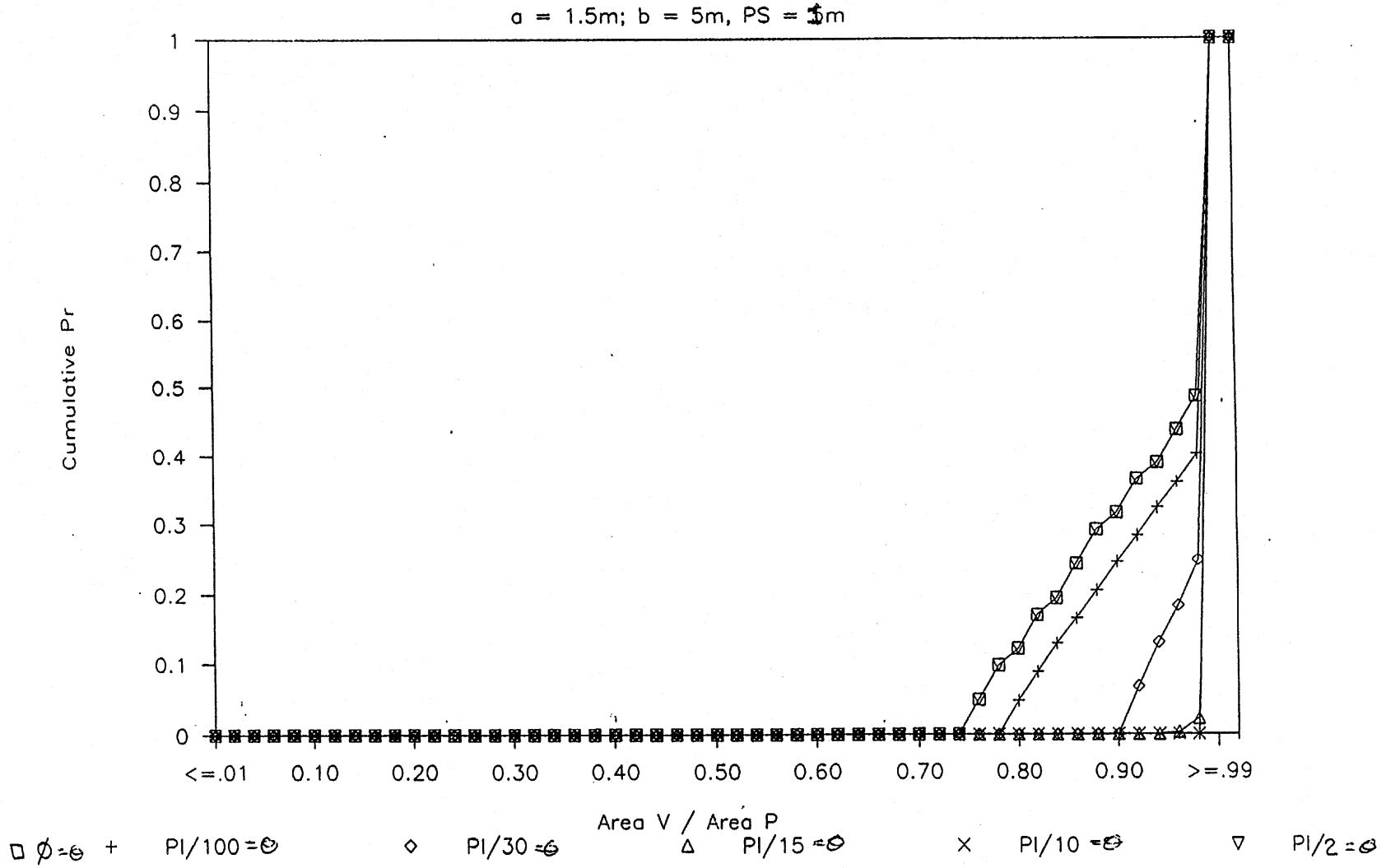

Figure A.5 Cumulative distribution of maximum A_{veh}/A_{pix} ratios for a vehicle type representative of a car (a=1.5 m, b=5.0 m) at 1.0 m pixel resolution for rotation angles T(θ)=0, π/100, π/30, π/15, π/10, and π/2.

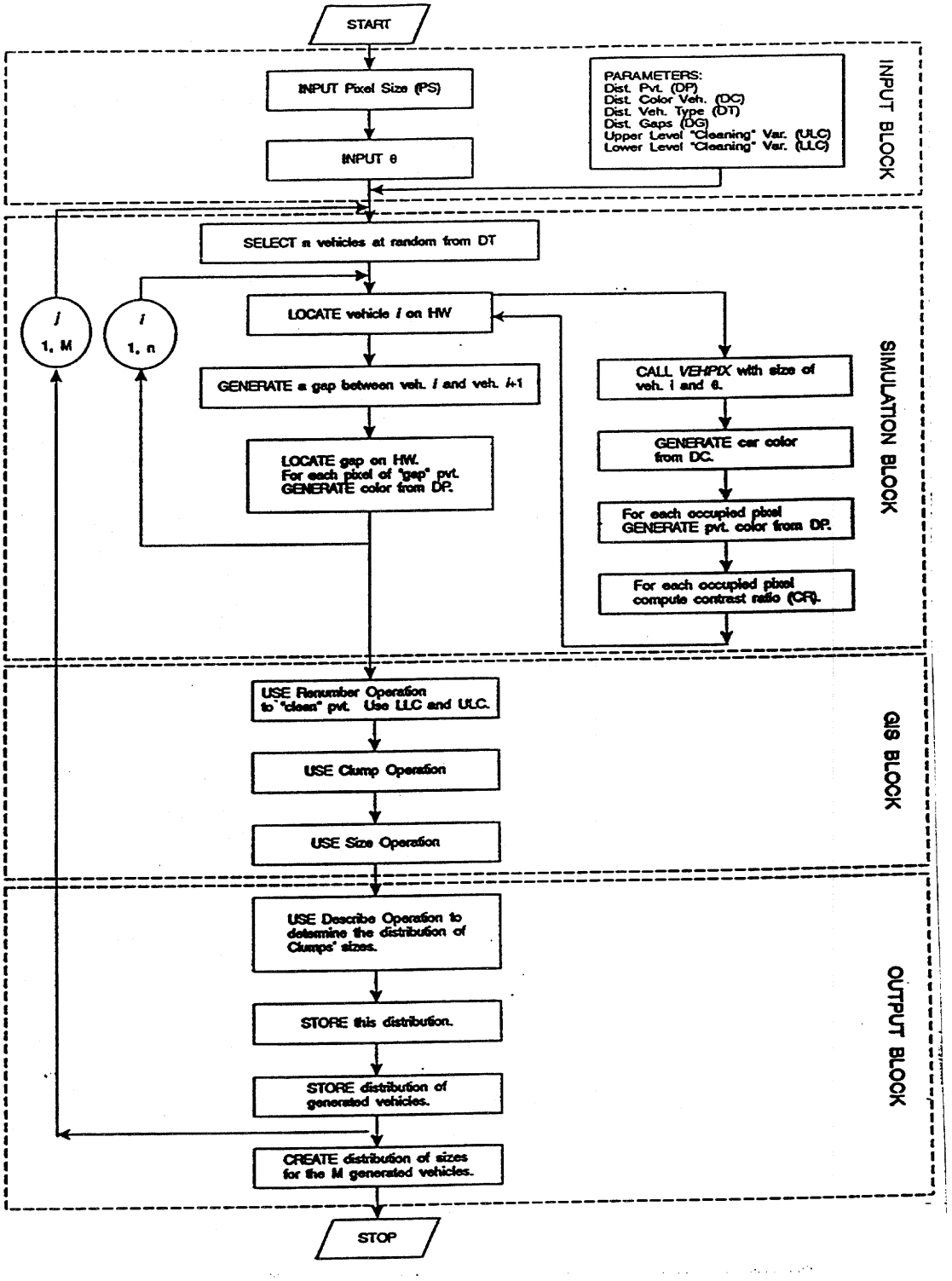

Figure A.6 Flowchart for logic of simulation model based upon mathematical model of imaging performance.

In conclusion, we recommend that if the criterion were one of having at least one pixel sufficiently covered by the vehicle, then we would not need to condition the analysis on the rotation angle θ only if we were simply interested in detecting trucks with 1 m or finer pixel resolution. We would probably have to be sensitive to the rotation angle when detecting cars, however, or when using coarser resolutions for trucks.

A. 4 Simulation Model

The geometric modeling led to the conclusion that we would need between 1 m and 2 m resolution to image cars and between 3 m and 5 m resolution to image trucks, if the criterion were one of the vehicle covering at least 50% of some pixel with probability 0.85. These results served as a first estimate of resolutions of interest for the studies in Section 3. The geometric modeling also showed that if the angle between the pixel axes and the longitudinal axis of the vehicle is close to an integer multiple of $\pi/2$, then the coverage of the maximum pixel will be different from the coverage obtained at other angles.

We had anticipated coupling the geometric models that we developed with image processing and Monte Carlo simulation components to perform large scale simulation of the characteristics of vehicle imaging at different resolutions in the panchromatic region. Two inputs to these anticipated simulations were distributions of vehicle reflectances R_{veh} and pavement reflectances R_{pvt}. In parallel to our development of the simulation, we were trying to obtain empirical estimates of these values (see Sect. 3). This investigation showed that the distributions of these values seem to overlap so much that this approach to vehicle detection would not work. Therefore, we only ran the simulation model with fabricated values for vehicle reflectances R_{veh} and pavement reflectances R_{pvt}, and we shall not report on these results.

We briefly describe our approach to generating the digital representation, however, since it appears that the characteristics of the vehicle shadows and perhaps of the vehicle edges (see Sect. 3) may make it possible to detect and classify vehicles using images in the panchromatic region. Also, it may be possible to alter this aspect of the simulation model to handle these characteristics. The image processing component of the model is also of interest, since it was used in our empirical investigation of Section 3.

Our computer simulation consisted of: i) generating a digital representation to simulate the image that would be obtained by remotely sensing vehicles on a highway with a panchromatic sensor; ii) processing the digital representation through an image processing software package to reduce the dimensionality of the representation; and iii) summarizing the results according to developed criteria.

To simulate the digital representation, we generated rectangular vehicles of various widths a and lengths b with given spacings between pairs of vehicles along a lane of highway. We then overlaid a grid of pixels of resolution PS rotated at angle θ from the longitudinal direction of the highway, and determined the geometry as explained in Section A.2 above. Next, we generated R_{pvt} values from a distribution (fabricated) of pavement reflectances for each pixel containing some pavement area and R_{veh} values from a distribution (fabricated) of vehicle

In conclusion, we recommend that if the criterion were one of having at least one pixel sufficiently covered by the vehicle, then we would not need to condition the analysis on the rotation angle θ only if we were simply interested in detecting trucks with 1 m or finer pixel resolution. We would probably have to be sensitive to the rotation angle when detecting cars, however, or when using coarser resolutions for trucks.

A. 4 Simulation Model

The geometric modeling led to the conclusion that we would need between 1 m and 2 m resolution to image cars and between 3 m and 5 m resolution to image trucks, if the criterion were one of the vehicle covering at least 50% of some pixel with probability 0.85. These results served as a first estimate of resolutions of interest for the studies in Section 3. The geometric modeling also showed that if the angle between the pixel axes and the longitudinal axis of the vehicle is close to an integer multiple of $\pi/2$, then the coverage of the maximum pixel will be different from the coverage obtained at other angles.

We had anticipated coupling the geometric models that we developed with image processing and Monte Carlo simulation components to perform large scale simulation of the characteristics of vehicle imaging at different resolutions in the panchromatic region. Two inputs to these anticipated simulations were distributions of vehicle reflectances R_{veh} and pavement reflectances R_{pvt}. In parallel to our development of the simulation, we were trying to obtain empirical estimates of these values (see Sect. 3). This investigation showed that the distributions of these values seem to overlap so much that this approach to vehicle detection would not work. Therefore, we only ran the simulation model with fabricated values for vehicle reflectances R_{veh} and pavement reflectances R_{pvt}, and we shall not report on these results.

We briefly describe our approach to generating the digital representation, however, since it appears that the characteristics of the vehicle shadows and perhaps of the vehicle edges (see Sect. 3) may make it possible to detect and classify vehicles using images in the panchromatic region. Also, it may be possible to alter this aspect of the simulation model to handle these characteristics. The image processing component of the model is also of interest, since it was used in our empirical investigation of Section 3.

Our computer simulation consisted of: i) generating a digital representation to simulate the image that would be obtained by remotely sensing vehicles on a highway with a panchromatic sensor; ii) processing the digital representation through an image processing software package to reduce the dimensionality of the representation; and iii) summarizing the results according to developed criteria.

To simulate the digital representation, we generated rectangular vehicles of various widths a and lengths b with given spacings between pairs of vehicles along a lane of highway. We then overlaid a grid of pixels of resolution PS rotated at angle θ from the longitudinal direction of the highway, and determined the geometry as explained in Section A.2 above. Next, we generated R_{pvt} values from a distribution (fabricated) of pavement reflectances for each pixel containing some pavement area and R_{veh} values from a distribution (fabricated) of vehicle

reflectances for each vehicle. Last, the R_{pvt} and R_{veh} values were used with the modeled geometry and Eq. (A.3) to determine a single numerical value of the contrast ratio CR for each pixel.

The inputs to the simulation were user-specified, fixed values of PS and θ, distributions of R_{veh} and R_{pvt}, a distribution of the types of vehicles (i.e., probabilities of a random vehicle having width and length parameters a and b from among a set of (a,b) pairs), and a distribution of gaps or spacings between successive vehicles on the highway. The output of this component was a matrix of numbers representing the contrast ratios in each pixel of the grid. The logic for this component of the model can be found in Figure A.6, and is shown in the Input Block and Simulation Block.

We used OSU-MAP-for-the-PC as the geographic information system (GIS) component of our simulation model. We were successful in coupling this program with the output of the previous component (the matrix of contrast ratios) by rewriting parts of OSU-MAP-for-the-PC. Since OSU-MAP-for-the-PC is a copyrighted program, we do not present the listing here. As an overview, however, OSU-MAP-for-the-PC works by converting the numerical value in each cell of the matrix of pixels (i.e., the contrast ratio of each pixel) to a 0 if the numerical value is less than or equal to some threshold value and to a 1 if the numerical value is greater than the threshold value. We refer to this as "eliminating the pavement," since, after this step, we expected the pavement to be represented primarily by 0's and the vehicles to be represented by 1's (or vice-versa, depending on the characteristics of the pavement). The 0's could then be "eliminated" from further consideration. The program then forms clumps or clusters of all cells with values of 1 that are contiguous, and determines characteristics of the clumps, such as the number of pixels in the clumps. The number of pixels in a clump would indicate its size and would be the basis for classifying it as a certain type of vehicle or as some nonvehicle element. The output from the program can then be used to develop distributions of the clump sizes. We note that the program is flexible enough to assign 0 values to cell values above a second threshold and that with algebraic operators it is straightforward to change 0's to 1's and 1's to 0's. Therefore, it is possible to form clumps based on contrast ratios in user-specified intervals. The general logic is presented in the GIS Block and Output Block in Figure A.6.

The input to this stage, then, is the matrix of numbers representing the contrast ratios in each pixel of the grid. The outputs are distributions of the clump sizes, i.e., the number of clumps in which the number of pixels falls within a given range. Once we determine the clump sizes (number of pixels in the clumps) that would correspond to each vehicle type, the program can summarize the number of vehicles estimated for each class and compare this to the number of vehicles that the program generated in each class to obtain a measure of aggregate performance in the vehicle class. The program would allow one to investigate the effects on classification performance of pixel resolution, thresholding values for "eliminating the pavement," and ranges of clump sizes to be associated with vehicle classes. Illustrative results can be found in Appendix B. We call these results illustrative and shall not describe them here because of the arbitrary distributions (fabricated) of R_{veh} and R_{pvt} that were used as inputs.

APPENDIX B

Description and Illustrative Results of a Simulation Model
for Vehicle Imaging Performance

Appendix B. Description and Illustrative Results of a Simulation Model for Vehicle Imaging Performance

We simulated digital images on pavement background by coupling the software we developed with the OSU-MAP-for-the-PC GIS package. We ran these simulations primarily to give us a feel for the capabilities and the limitations of the analysis, since the validity of the outputs is constrained by the rather arbitrary input data used for the R_{pvt} and R_{veh} distributions. Typical images of the output are seen in Figure B.1. Although the vehicles can be seen in these images, we cannot rely on visual inspection for large scale use and must use a procedure that works in an automatic fashion. A flow chart for the simulation is given in Figure A.6.

The process basically works as follows. The user specifies the desired number of vehicles to be generated, the probabilities of generating small and large vehicles (to represent cars and trucks, respectively), the rotation angle between the pavement and the pixel grid, and the pixel resolution. The program then randomly generates the locations of the vehicles (with some constraints) with respect to the pixel array, generates (from stored distributions) reflectance values for pixels completely covered by vehicles and those completely covered by pavement, and calculates the reflectances of the pixels covered by a combination of vehicle and pavement according to the weighted average of pavement and vehicle area. The user then inputs a range of "cleaning" values meant to be representative of the anticipated pavement reflectances. The OSU-MAP-for-the-PC program deletes pixels with these values and then "clumps" or clusters the remaining pixels together. The output is a distribution of the size of the clumps, where size is measured by the number of pixels in the clump.

The results of six simulation runs are presented in Tables B.1a-B.1c and Tables B.2a-B.2c. All runs reported were for a highway rotated 45° from the pixel array. To illustrate how to read the results, consider the simulation run summarized in Table B.1a. In this run, we generated 1000 vehicles, 538 of which are "cars" and 462 of which were "trucks."

The far left column, called "Size Range," lists ranges of numbers of pixels. The 538 under "Gen Veh/Veh 1" in the 16-22 row indicates that 538 "cars" (vehicle type 1) were generated that actually covered (at least partially) between 16-22 pixels. The 538 in the 10-28 row indicates that 538 "cars" (the same 538 vehicles as above) were generated that actually covered between 10-28 pixels. The 462 values in the "Gen Veh/Veh 2" column indicate that 462 "trucks" (vehicle type 2) were generated that actually covered (at least partially) between 57-70 (and, therefore, between 51-76 and between 44-83) pixels. The next sets of columns, labeled "18-22" and "19-21," present the results when pixels with reflectances between 18-22 and between 19-21, respectively, are eliminated ("cleaned") in an attempt to eliminate the pavement from the scene. The last set of columns, labeled "No Cleaning," presents results when the cleaning step is not used.

Consider the "No Cleaning" columns first. The "No Cleaning/Veh 1" column of Table B.1a shows that if we did not first clean the pavement, we would identify 2085 groups (clumps) with between 16-22 pixels and 8507 groups with between 10-28 pixels, ranges we think would be representative of cars. Since we only input 538 cars, many of these clumps are groups of pavement. Therefore, an approach that simply says "any clumps with between 10-28 pixels or between 16-22 pixels are cars," does not work well at all. For the large vehicles, the "No Cleaning/Veh 2" column shows that when the cleaning step is not used, we identify 2, 4, and 17 groups of between 57-70, 51-76, and 44-83 pixels, respectively, ranges we think would be representative of the trucks. (The "Gen Veh/Veh 2" column shows that all 462 generated vehicles touched between 57-70 pixels, and, therefore, between 51-76 and between 44-83 pixels.) Since we input 462 trucks, identifying trucks as clumps of large number of pixels without a cleaning step is not performing well; somehow, the large vehicles are being broken into several clumps of a smaller number of pixels.

When we first clean the pavement, the performance does much better, however. The "18-22" columns, for example, present the results when we clean all pixels with reflectances between 18-22 reflectance counts. The "Veh 1" column says that 336 and 507 clumps had sizes between 16-22 and between 10-28 pixels, respectively. If we were to say that a clump falling within this range was a car, we see from the "% Gen Veh" column that we would have predicted 62.45% (=336/538) and 94.24% (=507/538), respectively, of the true number of observations. The variation in the results when cleaning pixels with reflectance counts between 19-21 (see "19-21" columns) and when classifying large vehicles (see "57-70," "51-56," and "44-83" rows under the "18-22/Veh 2" and "19-21/Veh 2" columns) show that we need to look closely at the mechanisms when trying to determine the accuracy of this approach to vehicle classification. Among other things, some of the clumps classified as cars, for example, may be clumps of pavement or portions of the generated trucks.

To investigate more closely, we repeated the exercise twice, first generating only 1000 cars and then generating only 1000 trucks. The results are presented in the same format as those in Table B.1a. Table B.1b portrays the results for the simulation with only 1000 cars, and Table B.1c portrays those for the simulation with only 1000 trucks.

As before, the "No Cleaning" method performs very poorly, leading to too many clumps in the 16-22 and 10-28 pixel ranges to allow us to identify these clumps as cars and too few in the 57-70, 51-76, and 44-83 ranges to allow us to classify these clumps as trucks.

Comparing the cleaning options in Tables B.1a and B.1b, we see that the percentages of generated vehicles in the 16-22 and 10-28 ranges are very close; the largest difference is less than 5% (67.0% for Table B.1b *vs.* 62.45% for Table B.1a in the 16-22 classification range). Moreover, in this largest difference case, we witness a higher "%GV" in the simulation when we only generated cars than in the simulation when we generated both cars and trucks. This leads us to speculate that, in the simulations leading

to Table B.1a, the algorithm was not clumping small portions of trucks in the 16-22 or 10-28 ranges to any troublesome degree.

Similarly, comparing Tables B.1a and B.1c, we see extremely similar percentages in the 57-70, 51-76, and 44-83 size ranges. This gives us confidence in the replication of the results. If we could be sure that different situations would behave like this, we would conclude that we should clean the pavement using a range of 19-21 and then identify all clumps between 44-83 as trucks. The tables say that we would find 96% or 97% of the trucks with this approach. Although we do not have good estimates of the R_{pvt} and R_{veh} inputs and our results should, thus, be illustrative only, this exercise has still forced us to realize that one must distinguish how many of these clumps are clumps of pavement and how many are truly the vehicles. We considered this phenomenon when developing the classification rules presented in Section 3.

We repeated the three sets of simulations, but using a 2 m pixel resolution. The results are presented in Tables B.2a-B.2c. The columns are the same as those in Table B.1a-B.1c. The "Size Range" rows should be read as before, but now they consider clumps with fewer pixels because the pixels are now bigger (2 m x 2 m, instead of 1 m x 1 m). Comparing Tables B.1a and B.2a, B.1b and B.2b, and B.1c and B.2c, we notice similar performances, except when trying to classify cars when cleaning with reflectance counts between 19-21. Although one would need to investigate the mechanisms leading to these results to determine whether the summary numbers are artifacts of the simulated data, they raise the possibility that there may not be any great advantage in improving the resolution from 2 m to 1 m if the vehicle reflectance was the characteristic leading to detection.

Table B.1 Summary results for simulations with 1 m pixel resolution, highway rotated 45° from pixel array. ("Veh1" is a car and "Veh2" is a truck)

a. 538 cars and 462 trucks generated

Size	Gen Veh		18-22			19-21			No Cleaning		
Range	Veh1	Veh2	Veh1	Veh2	% GV	Veh1	Veh2	% GV	Veh1	Veh2	% GV
16-22	538		336		62.45%	306		46.88%	2085		387.55%
10-28	538		507		94.24%	564		104.83%	8507		1581.23%
57-70		462		223	48.27%		331	71.65%		2	0.43%
51-76		462		405	87.66%		427	92.42%		4	0.87%
44-83		462		434	93.94%		449	97.19%		17	3.68%

b. 1000 cars and 0 trucks generated

Size	Gen Veh		18-22			19-21			No Cleaning		
Range	Veh1	Veh2	Veh1	Veh2	% GV	Veh1	Veh2	% GV	Veh1	Veh2	% GV
16-22	1000		670		67.00%	545		54.50%	3003		300.30%
10-28	1000		956		95.60%	1073		107.30%	13573		1357.30%
57-70		0		0			0			0	
51-76		0		0			0			0	
44-83		0		0			0			0	

c. 1000 trucks and 0 cars generated

Size	Gen Veh		18-22			19-21			No Cleaning		
Range	Veh1	Veh2	Veh1	Veh2	% GV	Veh1	Veh2	% GV	Veh1	Veh2	% GV
16-22	0		0			5			3400		
10-28	0		2			125			13866		
57-70		999		494	49.45%		718	71.87%		7	0.70%
51-76		1000		872	87.20%		919	91.90%		14	1.40%
44-83		1000		939	93.90%		964	96.40		26	2.60%

Table B.2 Summary results for simulations with 2 m pixel resolution, highway rotated 45° from pixel array. ("Veh1" is a car and "Veh2" is a truck)

a. 534 cars and 468 trucks generated

Size	Gen Veh		18-22			19-21			No Cleaning		
Range	Veh1	Veh2	Veh1	Veh2	% GV	Veh1	Veh2	% GV	Veh1	Veh2	% GV
16-22	534		353		66.10%	660		123.60%	30007		5619.29%
10-28	534		540		101.12%	3455		647.00%	7188		1346.07%
57-70		468		322	68.80%		311	66.45%		215	45.94%
51-76		468		424	90.60%		431	92.09%		578	123.50%
44-83		468		447	95.51%		526	112.39%		1439	307.48%

b. 1000 cars and 0 trucks generated

Size	Gen Veh		18-22			19-21			No Cleaning		
Range	Veh1	Veh2	Veh1	Veh2	% GV	Veh1	Veh2	% GV	Veh1	Veh2	% GV
16-22	1000		668		66.80%	1309		130.90%	15144		1514.40%
10-28	1000		939		93.90%	7252		725.20%	59828		5982.80%
57-70		0		0			3			485	
51-76		0		0			31			1196	
44-83		0		0			156			3027	

c. 1000 trucks and 0 cars generated

Size	Gen Veh		18-22			19-21			No Cleaning		
Range	Veh1	Veh2	Veh1	Veh2	% GV	Veh1	Veh2	% GV	Veh1	Veh2	% GV
16-22	0		14			671			14504		
10-28	0		83			6080			59573		
57-70		1000		674	67.40%		666	66.60%		438	43.80%
51-76		1000		884	88.40%		878	87.80%		1124	112.40%
44-83		1000		934	93.40%		964	96.40%		2825	282.50%

APPENDIX C

Description and Computer Listing of Geometric Modeling Program.

PIX_VEH Computer Program

The objective of this program is to compute the area covered by the vehicle in the different pixels containing parts of the vehicle. To achieve that objective, the program uses the logic that we describe in the following paragraphs. After that, we present a description of the computer program itself, showing how this logic has been programmed.

Program Logic

The vehicle is assumed to be of rectangular shape with sides of length a and b, with a < b. The pixels are square with sides of length PS. All these quantities can be specified by the user. The position of the vehicle over the grid of pixels is determined by the position of its center (xc, yc) with respect to a center of coordinates (0, 0), and the angle Theta that the longest side of the vehicle (b) forms with the vertical axis (see Figure 1). This figure also shows that for a given position of the vehicle (determined by (xc, yc) and Theta), different pixels in its vicinity are covered. The "south" corner of the pixel containing the center of the vehicle (call it center pixel) was selected to define the center of the system of coordinates. In this system of coordinates, the abscissa axis overlaps the lower side of the center pixel and the ordinate axis the left side, and the point where these two sides intercept having coordinate (0, 0), being the center (see Figure 1).

For a given position of the vehicle, characterized by Theta, xc, and yc, we determined the equations for the lines that describe the sides of the vehicle (Eqs. (1a) to (4b)), in terms of the slope mi and the interception Ii of those lines (i = 1,...,4). That is, Y = mi X + Ii. See Appendix A for details about the derivation of mi and Ii.

$$m1 = COS(Theta) / SIN(Theta) \quad (1a)$$

$$I1 = yc + a / (2 * SIN(Theta)) - xc * COS(Theta) / SIN(Theta) \quad (1b)$$

$$m2 = COS(Theta) / SIN(Theta) \quad (2a)$$

$$I2 = yc - a / (2 * SIN(Theta)) - xc * COS(Theta) / SIN(Theta) \quad (2b)$$

$$m3 = -SIN(Theta) / COS(Theta) \quad (3a)$$

$$I3 = yc + b / (2 * COS(Theta)) + xc * SIN(Theta) / COS(Theta) \quad (3b)$$

$$m4 = -SIN(Theta) / COS(Theta) \quad (4a)$$

$$I4 = yc - b / (2 * COS(Theta)) + xc * SIN(Theta) / COS(Theta) \quad (4b)$$

We also determined the location of the vehicle corners (Eqs. (5a) to (8b)) with respect to the system of coordinates defined above (see Figure 2). In these last set of equations, xcj is the abscissa of corner j and ycj is the ordinate of that corner (j = 1,...,4).

$$xc1 = xc + b / 2 * SIN(Theta) - a / 2 * COS(Theta) \quad (5a)$$

$$yc1 = yc + b / 2 * COS(Theta) + a / 2 * SIN(Theta) \quad (5b)$$

$$xc2 = xc - b / 2 * SIN(Theta) + a / 2 * COS(Theta) \quad (6a)$$

$$yc2 = yc - b / 2 * COS(Theta) - a / 2 * SIN(Theta) \quad (6b)$$

$$xc3 = xc + b / 2 * SIN(Theta) + a / 2 * COS(Theta) \quad (7a)$$

$$yc3 = yc + b / 2 * COS(Theta) - a / 2 * SIN(Theta) \quad (7b)$$

$$xc4 = xc - b / 2 * SIN(Theta) - a / 2 * COS(Theta) \quad (8a)$$

$$yc4 = yc - b / 2 * COS(Theta) + a / 2 * SIN(Theta) \quad (8b)$$

With these equations set up, we are ready to compute the area covered by the vehicle in each pixel of its surroundings. Basically, there are two cases, which depend on the position (i.e. coordinates) of the vehicle's corners. In the first case, all 4 corners of the vehicle are contained in one pixel. Therefore, the area occupied by the vehicle in that pixel Amax is the area of the vehicle. That is: Amax = ab. In the other case there is no pixel that contains all 4 corners of the vehicle. Hence, it is necessary to determine which pixels contain part of the vehicle, and then compute how much area of these pixels is occupied. Again, two sub-cases are possible. One in which the pixel in consideration is totally covered by the vehicle. For that type of pixels the area covered is also Amax (see Figure 3). That is: Amax = PS^2.

In the second subcase, which is the most general and also the most complex, the pixel is partially occupied by the vehicle (see Figure 4). In what follows we will assume that we are studying a pixel partially covered by the vehicle and we will describe how we determined that area.

Because the pixel is partially occupied by the vehicle, at least one of the lines defining the sides of the vehicle will go through this pixel. For example, Figure 4 shows that Line 1 defines one of the borders of the area CA that we are trying to compute, and that line intercepts the pixels borders at points B and C.

For any given pixel it is possible to define the equations of its border lines in the system of coordinates defined above. For example, Eqs. (9) to (12) show these lines for a pixel with its "south", "north", "", and "east" borders located at a distance PB, PT, PL, and PR, respectively, from the center of coordinates (i.e., lines BB, TB, LB, and RB in Figure 4).

$$Y = PB; \forall X \quad (9)$$

$$X = PL; \forall Y \quad (10)$$

$$Y = PT; \forall X \quad (11)$$

$$X = PR; \forall Y \quad (12)$$

The intersection points between these pixel borders and the vehicle border-lines, defined by Eqs. (1a) to (4b), are given by Eqs. (13a) to (28b). In these equations xij is the abscissa of the intersection point between pixel border i (i = 1,.....,4, where 1 ≡ BB, 2 ≡ LB, 3 ≡ TB, and 4 ≡ RB) and vehicle line j (j = 1,....,4), and yij is the ordinate of this point (see Appendix A for details about obtaining these intersection points).

$$x11 = xc + (PB - a / (2 * SIN(Theta)) - yc) * SIN(Theta) / COS(Theta) \quad (13a)$$

$$y11 = PB \quad (13b)$$

$$x12 = xc + (PB + a / (2 * SIN(Theta)) - yc) * SIN(Theta) / COS(Theta) \quad (14a)$$

$$y12 = PB \quad (14b)$$

$$x13 = xc - (PB - b / (2 * COS(Theta)) - yc) * COS(Theta) / SIN(Theta) \quad (15a)$$

$$y13 = PB \quad (15b)$$

$$x14 = xc - (PB + b / (2 * COS(Theta)) - yc) * COS(Theta) / SIN(Theta) \quad (16a)$$

$$y14 = PB \quad (16b)$$

$$x21 = PL \tag{17a}$$

$$y21 = yc + (a / (2 * COS(Theta)) + (PL - xc)) * COS(Theta) / SIN(Theta) \tag{17b}$$

$$x22 = PL \tag{18a}$$

$$y22 = yc - (a / (2 * COS(Theta)) - (PL - xc)) * COS(Theta) / SIN(Theta) \tag{18b}$$

$$x23 = PL \tag{19a}$$

$$y23 = yc + (b / (2 * SIN(Theta)) - (PL - xc)) * SIN(Theta) / COS(Theta) \tag{19b}$$

$$x24 = PL \tag{20a}$$

$$y24 = yc - (b / (2 * SIN(Theta)) + (PL - xc)) * SIN(Theta) / COS(Theta) \tag{20b}$$

$$x31 = xc + (PT - a / (2 * SIN(Theta)) - yc) * SIN(Theta) / COS(Theta) \tag{21a}$$

$$y31 = PT \tag{21b}$$

$$x32 = xc + (PT + a / (2 * SIN(Theta)) - yc) * SIN(Theta) / COS(Theta) \tag{22a}$$

$$y32 = PT \tag{22b}$$

$$x33 = xc - (PT - b / (2 * COS(Theta)) - yc) * COS(Theta) / SIN(Theta) \tag{23a}$$

$$y33 = PT \tag{23b}$$

$$x34 = xc - (PT + b / (2 * COS(Theta)) - yc) * COS(Theta) / SIN(Theta) \tag{24a}$$

$$y34 = PT \tag{24b}$$

$$x41 = PR \tag{25a}$$

$$y41 = yc + (a / (2 * COS(Theta)) + (PR - xc)) * COS(Theta) / SIN(Theta) \tag{25b}$$

$$x42 = PR \tag{26a}$$

$$y42 = yc - (a / (2 * COS(Theta)) - (PR - xc)) * COS(Theta) / SIN(Theta) \tag{26b}$$

$$x43 = PR \tag{27a}$$

$$y43 = yc + (b / (2 * SIN(Theta)) - (PR - xc)) * SIN(Theta) / COS(Theta) \tag{27b}$$

$$x44 = PR \tag{28a}$$

$$y44 = yc - (b / (2 * SIN(Theta)) + (PR - xc)) * SIN(Theta) / COS(Theta) \tag{28b}$$

In our example, only points B = (x31, y31) and C = (x21, y21) in Figure 4 are relevant for the computation of area CA. All the other intersection points between the vehicle borders and the pixel borders (marked with and X in Figure 4) are outside the pixel in consideration. To ckeck whether an intersection point is inside or outside the pixel it is necessary to determine if the

coordinates of that point are within the borders of the pixel or not.

On top of the intersection points between vehicle lines and pixel borders, there may be other relevant points in determining the perimeter of the area to be computed. In our example there are three more points that define the perimeter of area CA. These points are the corners of the pixel that are covered by the vehicle (points A, D, and E in Figure 4).

Once all the points defining the perimeter of the area to be computed are known, we are ready to calculate that area. There are basically two practical methods --integration and triangulation-- to do so. The integration method has the disadvantage that it is necessary to work with functions, which is somehow cumbersome to program. The triangulation method, on the other hand, only requires that we know the points where the lines in the perimeter of the area to be computed intersect (i.e.; points A, B, C, D, and E in Figure 4). We adopted this method. To use the triangulation methodology it is necessary to divide the area CA into non overlapping triangles that cover it entirely. The first step in defining these triangles is to find a point V to serve as vertex for these triangles. This point can be anywhere inside or outside of the area CA, but because of simplicity, we chose to have point V inside the area (see Figure 5). If point V is outside, then it is necessary to compute the area of two sets of triangles and subtract them, as it will become apparent when we explain the methodology.

After selecting point V, the area CA is divided in triangles that have as vertices point V and two adjacent[1] corner points on the perimeter of the area to be computed. Figure 5 shows that in our example we can define 5 triangles, T1 to T5, that completely tile the area CA. Notice that the number of triangles is always equal to the number of corner points defining the perimeter of the area to be computed, if point V is inside that area. The next step is to compute the area TA of each one of these triangles and add them all to have the area of CA. One way of doing this computation is to determine for each triangle the length of its sides (for example d1, d2, and d3 for triangle T1 in Figure 6) and use trigonometric relation in Eq. (29) to calculate the area of that triangle (see Appendix A for details):

[1]There will be a subroutine in the computer program which determines whether two points on the perimeter are adjacent or not.

$$TA = .25 * [4 * d_1\text{^}2 * d_2\text{^}2 - (d_1\text{^}2 + d_2\text{^}2 - d_3\text{^}2)\text{^}2]\text{^}.5 \quad (29)$$

Notice that the length of the sides d1, d2, and d3 are very easy to compute once the coordinates of points V, A, and B are known, which is our case. The lengths are just the Euclidean distances.

We have seen in the preceding paragraphs how to determine the area occupied by the vehicle in any pixel. In the next section we will introduce an overview of how we implemented these calculations in a computer program.

Computer Program

The aim of this computer program is to identify, from all the pixels occupied by the vehicle, the one that contains the maximum area. To do so the program first determines which are the pixels containing parts of the vehicle. After that it calculates the areas occupied by the vehicle in those pixels and then it determines the maximum covered area (Amax). This process is to be repeated by varying the position of the vehicle so that we can construct a probability distribution of the ratio between Amax and PS^2 (the pixel area), for a given vehicle type (represented by its sides a and b) and a pixel size PS. Therefore, the selection must be as a function of the location and orientation of the vehicle with respect to the pixel.

Since this is a spatial problem, we first need a model representing the space surrounding the vehicle in study. Due to the fact that the only relevant information at this stage is the area occupied by the vehicle in the different pixels, we decided to depict the space around the vehicle as an array in which each element represents a pixel. In this array, the position of an element defined by its row and column indices has a correspondence to the spatial position of the pixel being represented. For example, suppose we restrict the region around the vehicle to a square area of n pixels per side. In this case, the pixel located in the north position of the area would correspond to the first element (i.e.; row 1, column 1) in this array, while the southeast pixel will be represented by the element (n, n) (see Figure 7). The program starts by computing the

dimensions of this array, which is done by determining the distance, in terms of number of pixels, to the pixel that is the farthest from the vehicle center and that contains parts of the vehicle. Some slack is added (i.e., 2 is added to the computed array dimension) to be on the safe side (for some combination of the values of angle Theta and vehicle's center position (xc, yc) the vehicle may cover some pixel outside the area defined by the pixels in the original array). This array is named *MatAVeh* in the program and its dimension is (n%, n%)[2], where, as we explained above, the first index denotes the row position of a pixel and the second one its column position.

After this, the program starts three loops that vary the position of the center of the vehicle (xc, yc) between 0 and PS/2 in both the x and y dimensions, and the angle Theta between 0 and 180 degrees, to allow, ultimately, the computation of the probability distribution of the maximum pixel area covered by the vehicle. The intervals with which xc, yc, and Theta are incremented are to be provided by the user in the program (see top of page 2 of the program listing). Once Theta, xc, and yc have been assigned values, the program computes the equations for the lines that describe the sides of the vehicle and the location of the vehicle corners (see Figure 3 and Eqs. (1a) to (8b)). See page 2 of the program listing.

Much of the logic to determine the area covered by the vehicle in the different pixels is based on the observation that there is no point on lines 1 to 4 that belongs to the vehicle and for which the distance to the center is larger than d (see Figure 2), where d is the Euclidean distance from one of the vehicle corners to the center of the vehicle. The program therefore, computes this distance d, which is called *MaxDiag* (see bottom of page 2 of the program listing).

The next step is to determine if all the four corners of the vehicle are within a single pixel. This is done by a conditional clause that tests whether the four corners of the vehicle, described by Eqs. (5a) to (8b) are within the central pixel. If this is the case, then the vehicle touches only that pixel and the area covered is just Aveh = a * b. The program stores this area and increments

---

[2]In the language that the program is written (QuickBasic v 4.0), to indicate that a variable is integer the character % must be attached to the name of that variable. A double precision variable, like angle Theta, requires to attach the character # to its name.

the indexes of the three variables Theta, xc and yc. If the vehicle's corners are not located in only one pixel, then the program analyzes all the pixels in the area of (n x n) pixels around the vehicle, computing the area occupied by the vehicle in each of these cells. As we explained above, there is a direct correspondence between the space represented by the (n x n) pixels and the elements of the *MatAVeh* array. Therefore, in order to investigate systematically all the pixels in the (n x n) area the program uses two loops to control which is the pixel that is being analyzed (see page 3 of the program listing). The first loop, with index i%, controls the vertical position of the pixel in the square area of (n x n) pixels, while the second loop, with index j%, controls its horizontal position.

For a given pixel p in this (n x n) area, characterized by the value of the indices i% and j%, the program computes the position of that pixel in the absolute coordinate system defined above, determining the coordinates of the four corners of the pixel. If the four corners of the pixel p are outside the vehicle, which is determined by analyzing if the distance of the pixel's corners to the center of the vehicle is larger than *MaxDiag*, then the pixel does not contain any part of the vehicle. Figure 8 shows that the distances of the 4 corners of the north pixel to the center of the vehicle are all simultaneously larger than *MaxDiag*, implying that the pixel does not contain any part of the vehicle. In that case the program increments the indices i% and j% and goes to the following pixel. If this is not the case, then the program determines whether all four corners of the pixel are inside the vehicle. If the answer is yes, then the area occupied by the vehicle in that pixel is the area of the pixel, that is PS^2 (see Figure 3). If only some, or even none of the pixel's corners are inside the vehicle (i.e., pixel's corners are outside vehicle but distances to intersection points between vehicle lines and pixel border are all less than d), then the program computes the intersection of the vehicle lines (i.e., the lines that define the vehicle borders) and the current pixel lines (i.e., the lines that define the current pixel borders). See Eqs. (13a) to (28b) and subroutine Inter in the program listing..

After that, the program determines if the points just found belong to the vehicle and to the pixel p at the same time (for example points A, B, C, D, and E in Figure 4). Those intersection points between the lines defining the pixel borders and the vehicle border-lines that are not inside or on the border of pixel p are eliminated (intersection points marked with an X in Figure 4).

Those that remain are the ones used to compute the area covered by the vehicle in this pixel. Notice that these points always define a convex area, which we called CA in Figure 4.

The calculation of the area covered by the vehicle in the pixel p is done by triangulation. A point inside area CA is first defined by finding the middle point between any two corner points in the perimeter of CA (see subroutine CentralPoint in the computer listing). For example, point I1 in Figure 9 is the middle point between corner points A and B. Once point I1 is identified, a new middle point V between I1 and another corner point on the CA's perimeter, for example point D in Figure 9, is identified. Notice that there will always be at least three points known on the perimeter of CA, since the minimum number of sides to enclose a convex area is 3. Point V is then used as a vertex to compute the area of the triangles defined by that point and those on the perimeter of CA as we explained before.

Before computing the areas of the different triangles that make up area CA, it is necessary to order the points on the perimeter. Those points were determined as explained above and stored in two vectors (i.e., px(.) and py(.) in the program) that contain their abscissa and ordinate, respectively. However, these points may not be in a consecutive order on the perimeter of CA, which is a necessary condition to compute the correct area CA by means of the triangulation procedure. The consecutive order is accomplished by associating to each of the points on the perimeter the angle that a line passing through the point and the vertex V forms with the horizontal line. Then the points are ordered by this angle: the point with the smallest angle is assigned the first place, the point with the second smallest angle, the second place, and so on. See subroutines Arrange and dist in the program listing.

Once the area of all the triangles is computed, the area covered by the vehicle in the current pixel is the summation of these areas. This information is stored in *MatAVeh* which is later saved in a file, in which the name starts with the letter M, followed by the vehicle type, and information about the vehicle dimensions. Another file produced by the program stores the maximum pixel area covered by a vehicle. The name of this file starts with the letter S, followed by the vehicle type, and information about the vehicle dimensions. These names and the directory where these files are to be saved must be provided by the user (see page 1 of the program listing).

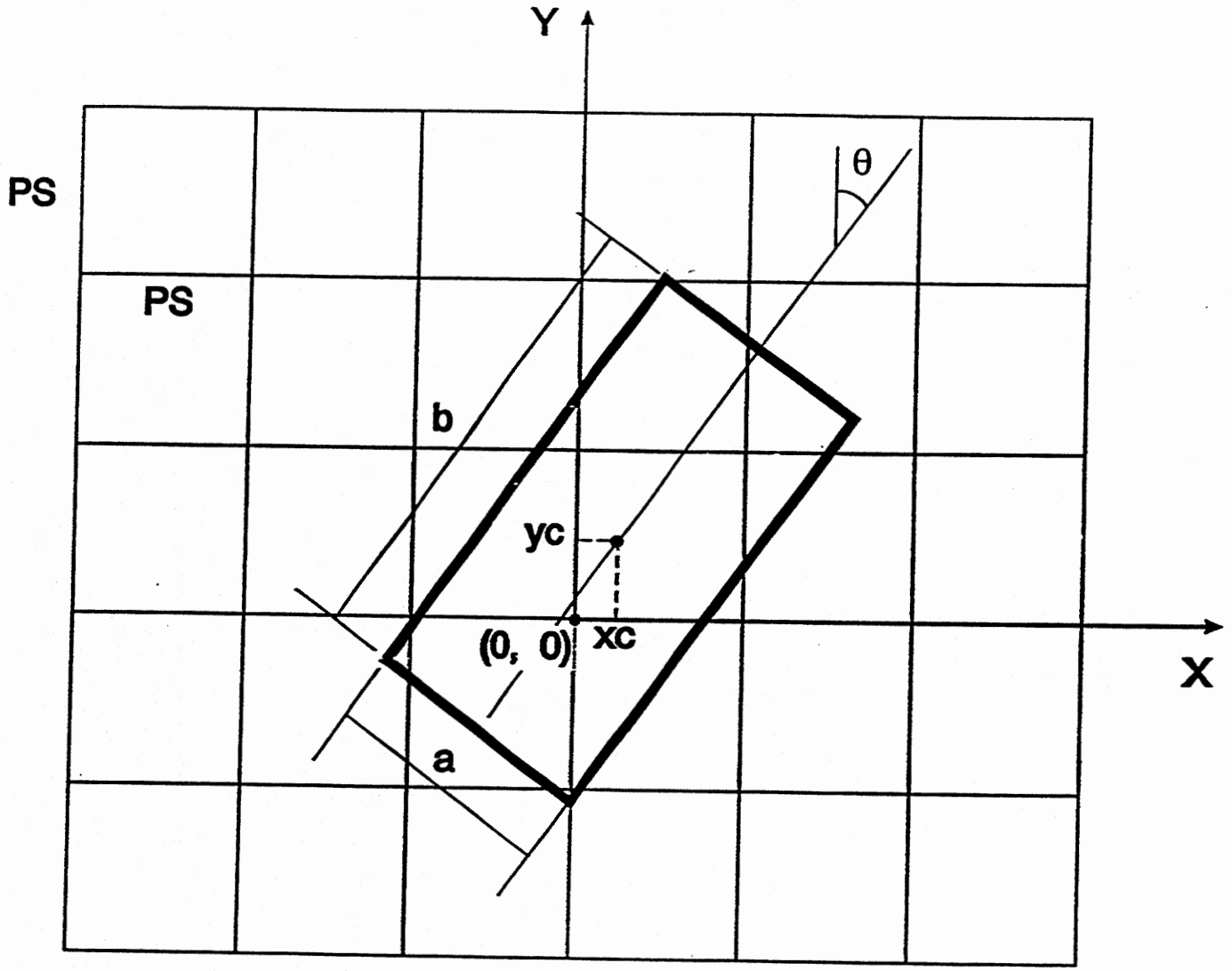

Figure 1

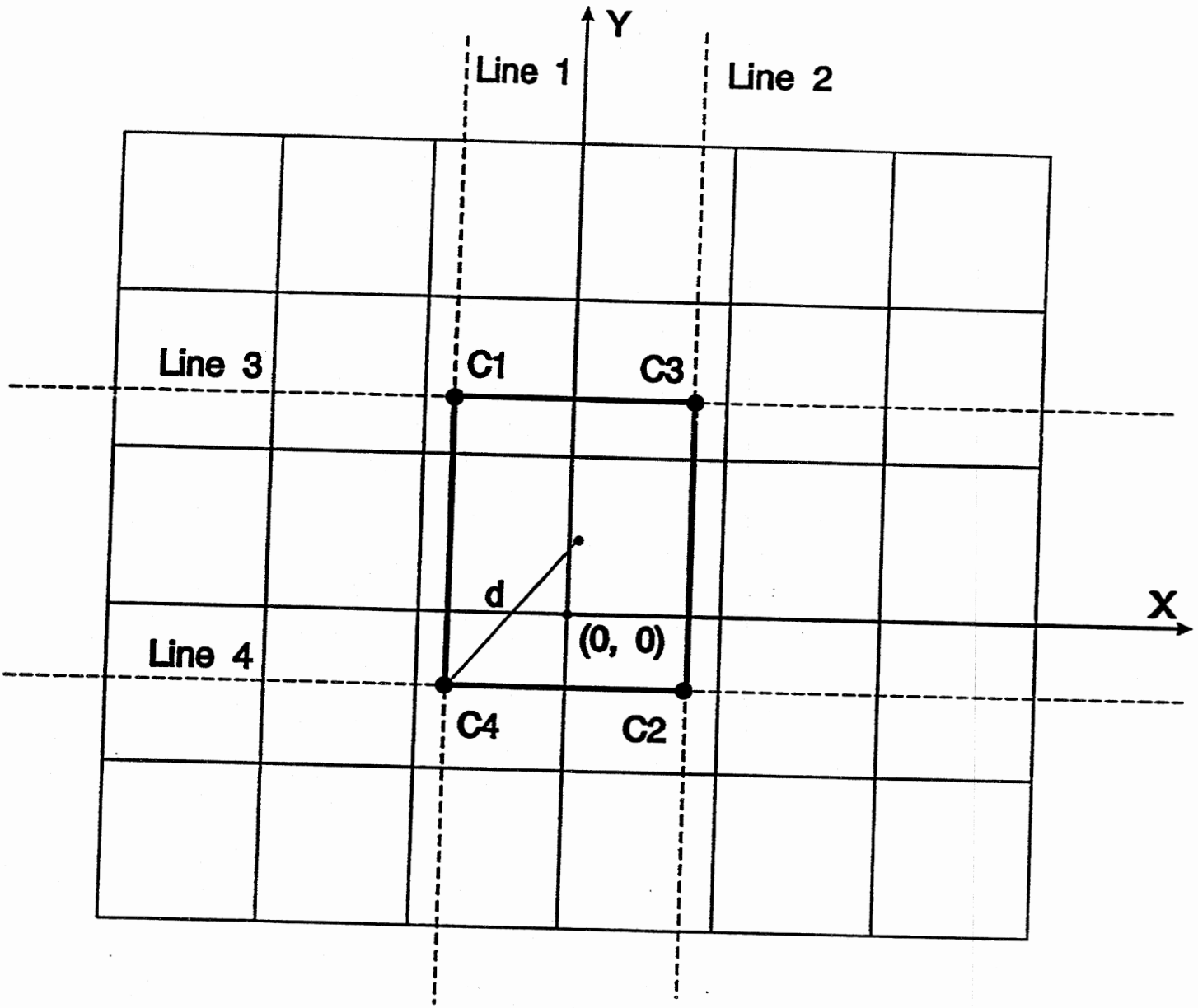

Figure 2

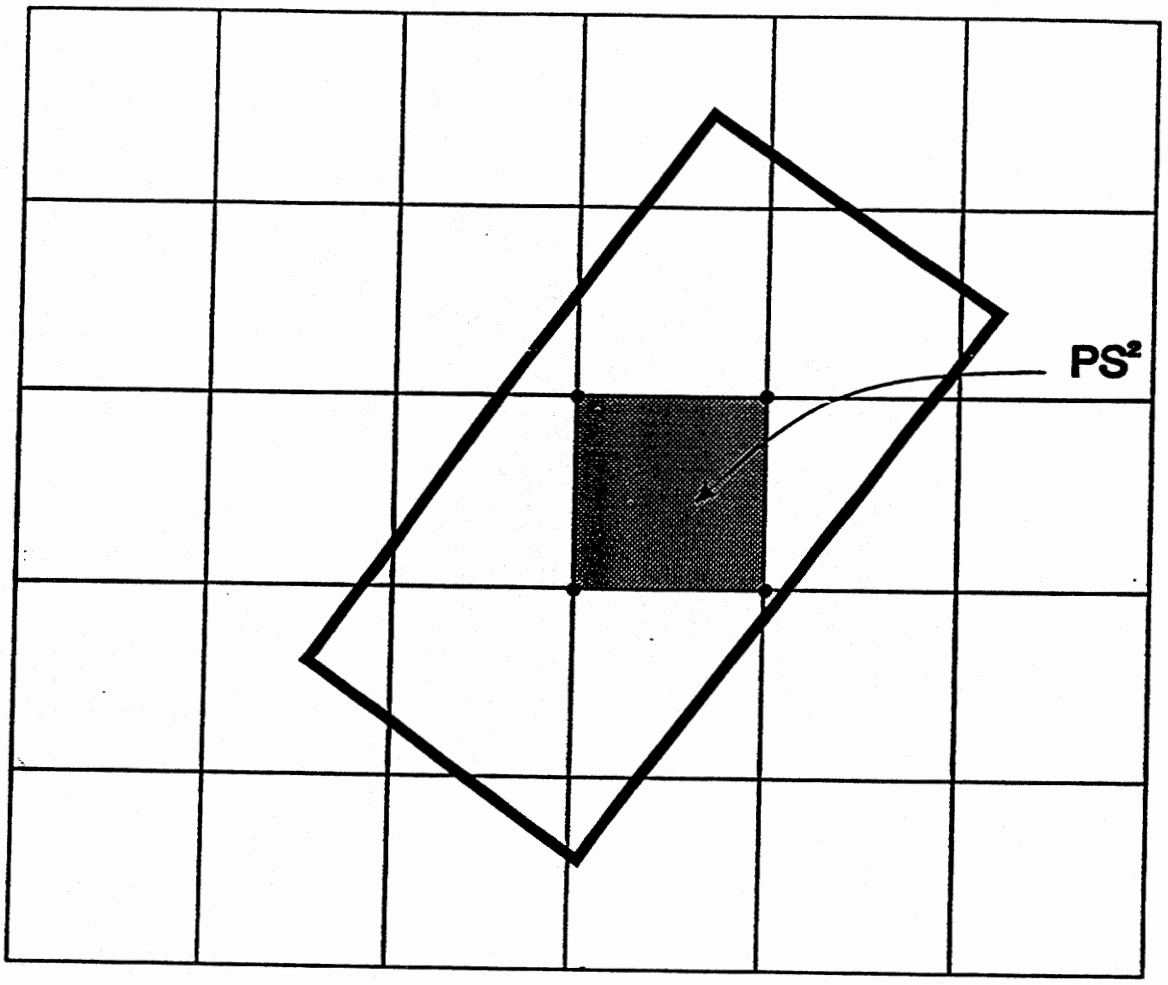

Figure 3

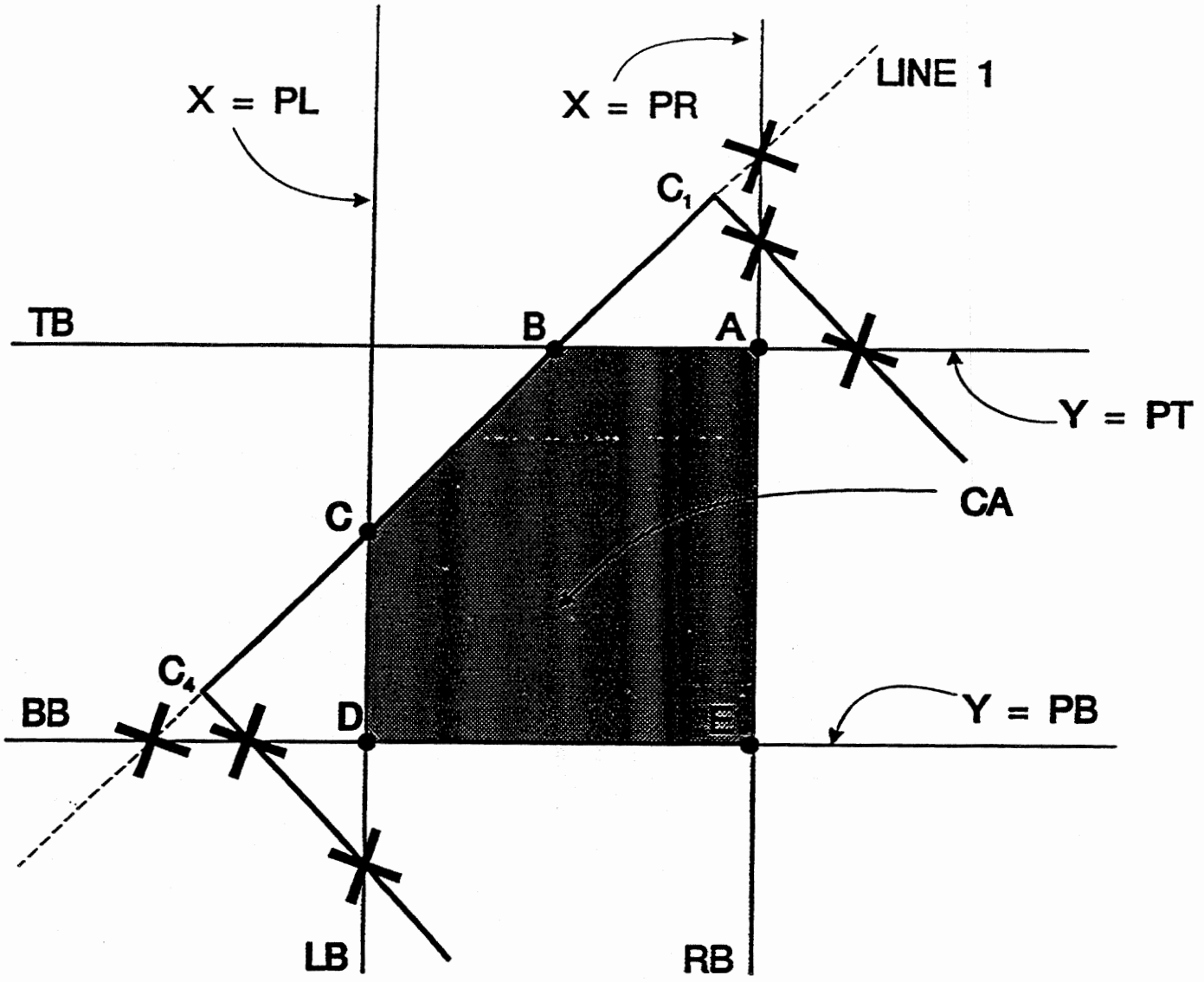

Figure 4

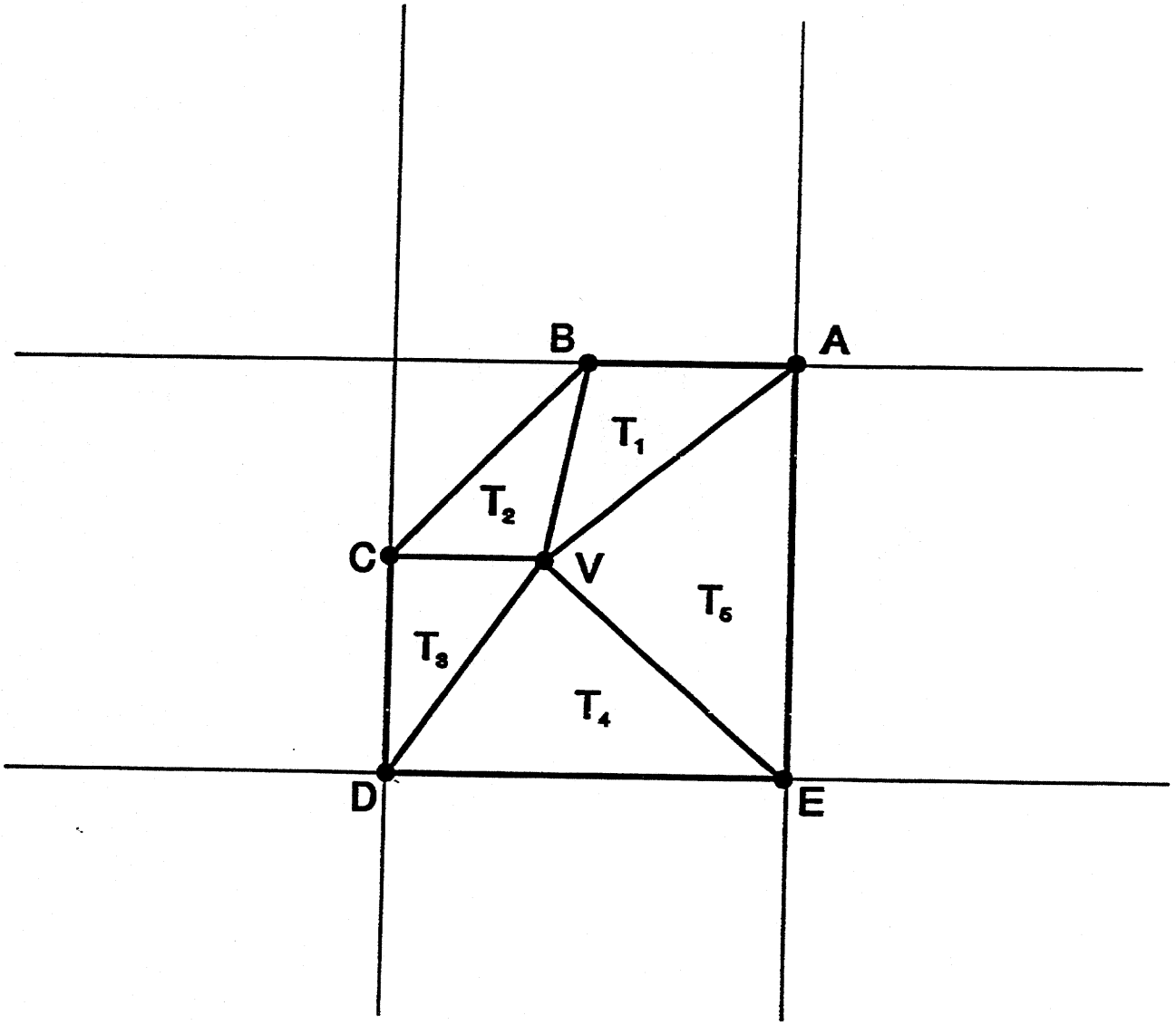

Figure 5

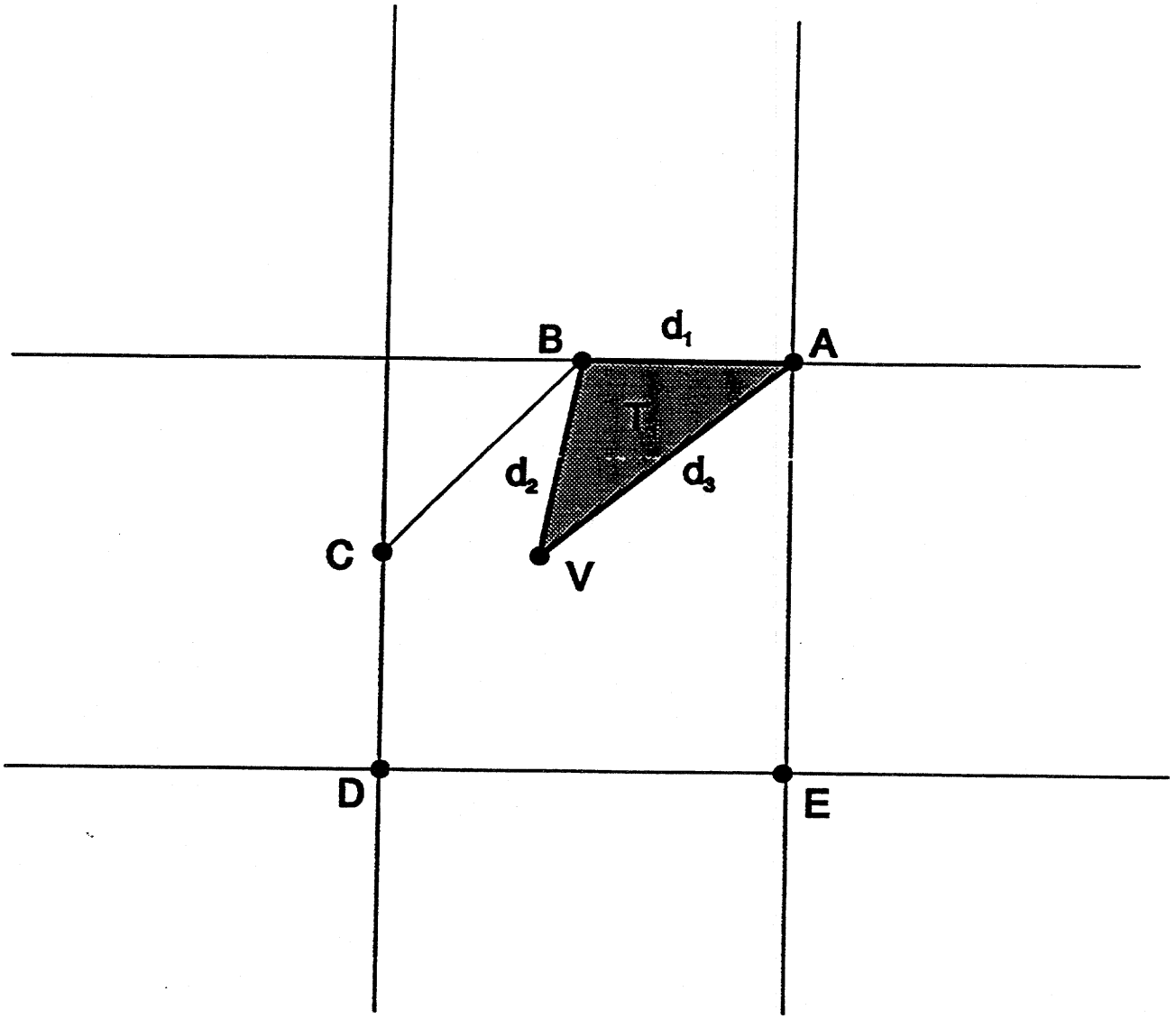

Figure 6

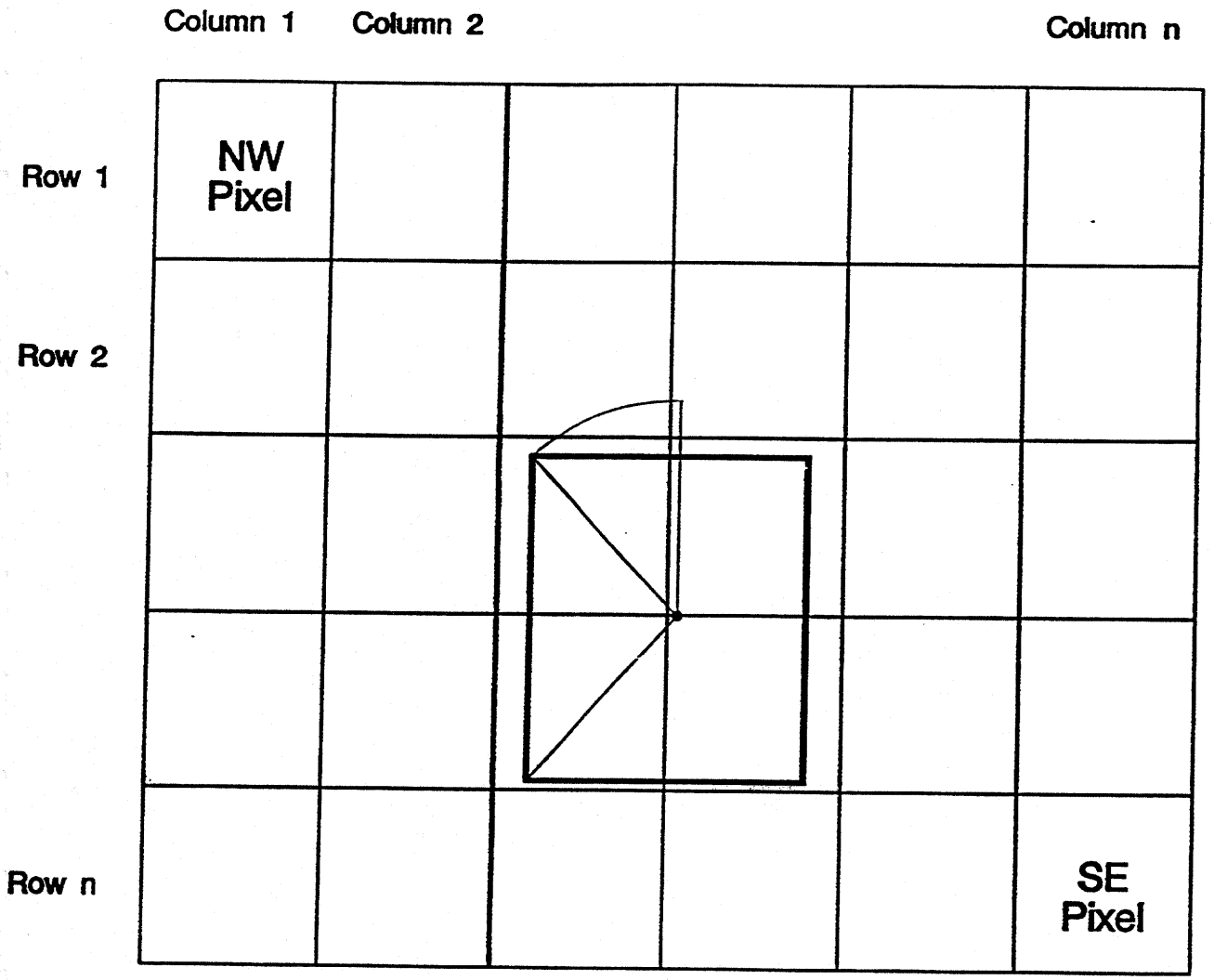

Figure 7

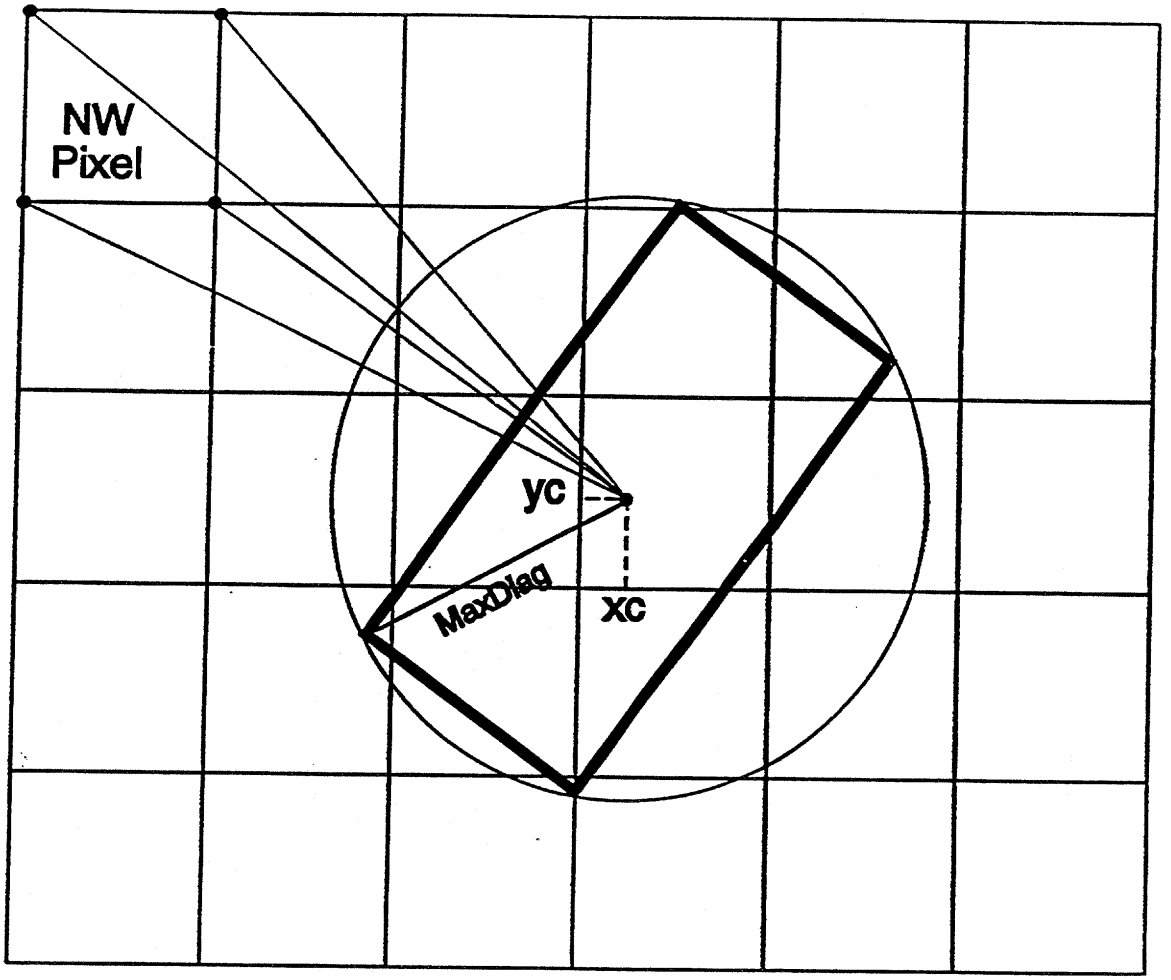

Figure 8

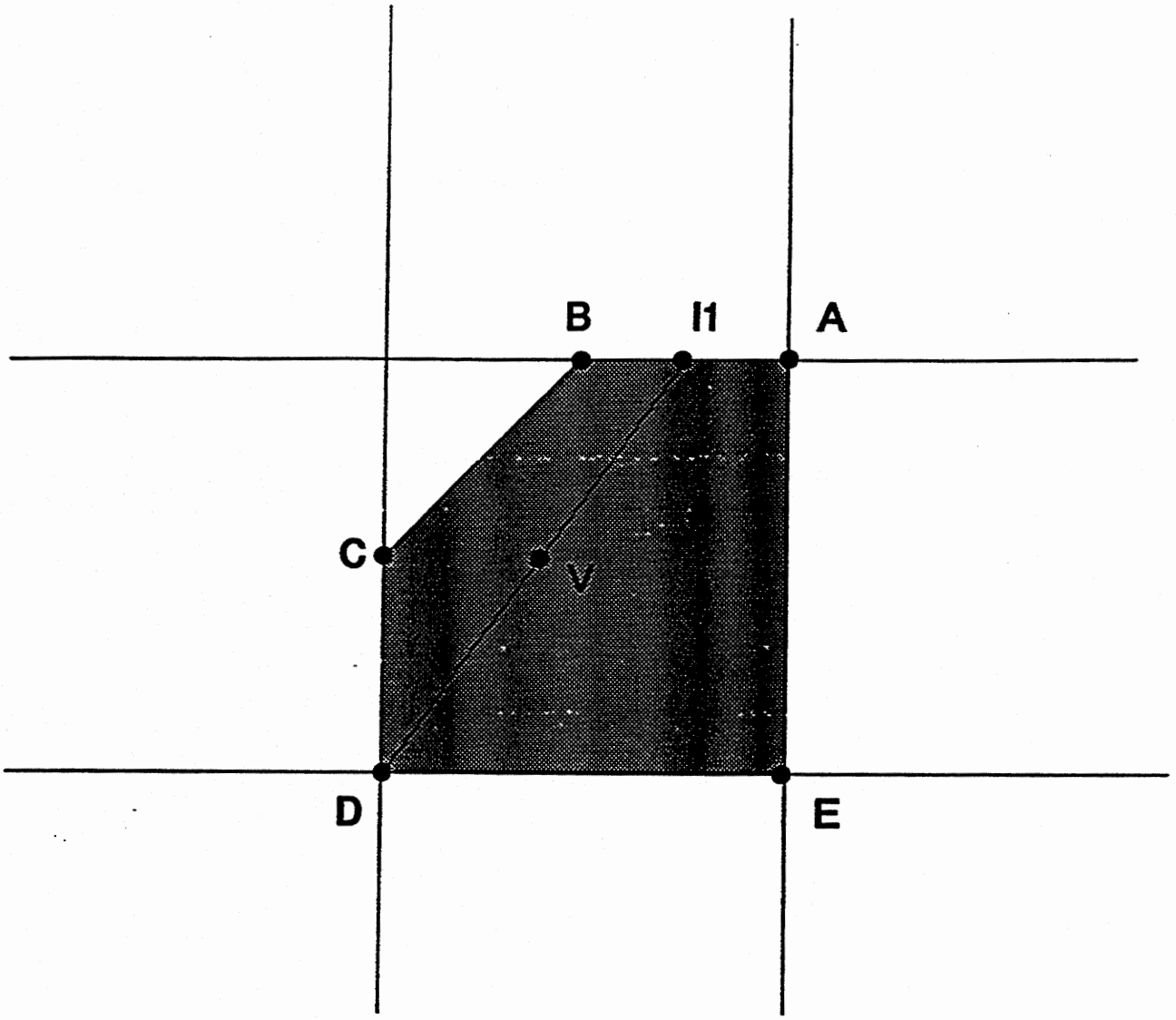

Figure 9

Vehicle Border Lines

To determine the parameters of the lines defining the borders of a vehicle of side lengths (a,b) we proceeded as follows. Consider Line 1 in Figure A1, which represents the left side of the vehicle. Generically, we can write the equation of that line as:

$$y = m1 * x + I1 \quad \text{(A1)}$$

where m1 is the slope of the line and i1 is the intersection of the line with the ordinate axis.

From Figure A1, the slope of Line 1 is:

$$m1 = tg\ \alpha = tg\ (90\text{-}\theta) = \cos\theta / \sin\theta \quad \text{(A2)}$$

Now we need a point on that line to completely specify it. Consider point A. Using triangle ACF, it is easy to see that the coordinates of that point are:

$$xA = xc - a / 2 * \cos\theta \quad \text{(A3)}$$

$$yA = yc + a / 2 * \sin\theta \quad \text{(A4)}$$

If Line 1 passes through Point A, then using Eqs. (A1) and (A2), we can write:

$$yA = \cos\theta / \sin\theta * xA + I1 \quad \text{(A5)}$$

where the only unknown is i1. Now, replacing Eqs. (A3) and (A4) in (A5), we can write:

$$yc + a / 2 * \sin\theta = \cos\theta / \sin\theta * (xc - a / 2 * \cos\theta) + I1 \quad \text{(A6)}$$

and solving for I1:

$$I1 = yc + a / 2 * \sin\theta - \cos\theta / \sin\theta * (xc - a / 2 * \cos\theta) \quad (A7)$$

which can be writen as:

$$I1 = yc + a / 2 * \sin\theta - \cos\theta / \sin\theta * xc + a / 2 * \cos^2\theta / \sin\theta \quad (A8)$$

and then

$$I1 = yc + a / 2 * (\sin^2\theta + \cos^2\theta) / \sin\theta - \cos\theta / \sin\theta * xc \quad (A9)$$

and since $\sin^2\theta + \cos^2\theta = 1$ then

$$I1 = yc + a / (2 * \sin\theta) - \cos\theta / \sin\theta * xc \quad (A10)$$

Equations (A2) and (A10) completely specify Line 1. We proceeded in the same way to determine the other three lines. Once the equations for these lines are known, then the corners of the vehicle can be easily found as the intersection between two border lines. For example, corner C4 is the intersection point between Line 1 and 2 (see Figure A1).

Intersection Between Pixel's Border Lines and Vehicle Lines

Consider for example the intersection between the south border of a given pixel, Eq. (A11) and vehicle line 1, Eq. (A12) (see Eqs. (A2) and (A10)).

$$y = PB; \ \forall x \quad (A11)$$

$$y = \cos\theta / \sin\theta \, x + yc + a / (2 * \sin\theta) - \cos\theta / \sin\theta * xc \quad (A12)$$

To find the intersection between these two lines, we simply equalize Eqs. (A11) and (A12) obtaining the abscisa of the intersection point (call it x11) as shown in Eq. (A13):

$$x11 = [PB + \cos\theta / \sin\theta * xc - yc - a / (2 * \sin\theta)] \ \sin\theta / \cos\theta \quad \text{(A13)}$$

which after some manipulation gives Eq. (A14):

$$x11 = xc + [PB - yc - a / (2 * \sin\theta)] \ \sin\theta / \cos\theta \quad \text{(A14)}$$

The ordibnate of the intersection point, which we call y11 is shown in Eq. (A15)

$$y11 = PB \quad \text{(A15)}$$

In the same way, it is possible to find the intersection points between all 4 pixel's borders and all 4 vehicle's lines.

Area of a Traingle as a Function of Its Side Lengths

The area of the triangle shown in Figure A2 can be calculated as:

$$A = d1 * d2 * \sin\alpha / 2 \quad \text{(A16)}$$

From trigonometry we can write:

$$d3^2 = d1^2 + d2^2 - 2 * d1 * d2 * \cos\alpha \quad \text{(A17)}$$

which gives

$$\cos\alpha = (d1^2 + d2^2 - d3^2) / (2 * d1 * d2) \quad \text{(A18)}$$

Squaring Eq. (A18), we have:

$$\cos^2\alpha = (d1^2 + d2^2 - d3^2)^2 / (4 * d1^2 * d2^2) \quad \text{(A19)}$$

Also from trigonometry, we can write:

$$\cos^2 \alpha + \sin^2 \alpha = 1 \qquad \text{(A20)}$$

from which

$$\sin \alpha = (1 - \cos^2 \alpha)^{.5} \qquad \text{(A21)}$$

Replacing Eq. (A19) in Eq. (A21), we have:

$$\sin \alpha = [1 - (d1^2 + d2^2 - d3^2)^2 / (4 * d1^2 * d2^2)]^{.5} \qquad \text{(A22)}$$

which replaced in Eq. (A16) gives:

$$A = d1 * d2 * [1 - (d1^2 + d2^2 - d3^2)^2 / (4 * d1^2 * d2^2)]^{.5} / 2 \qquad \text{(A23)}$$

and after some manipulation

$$A = [4 * d1^2 * d2^2 - (d1^2 + d2^2 - d3^2)^2]^{.5} / 4 \qquad \text{(A24)}$$

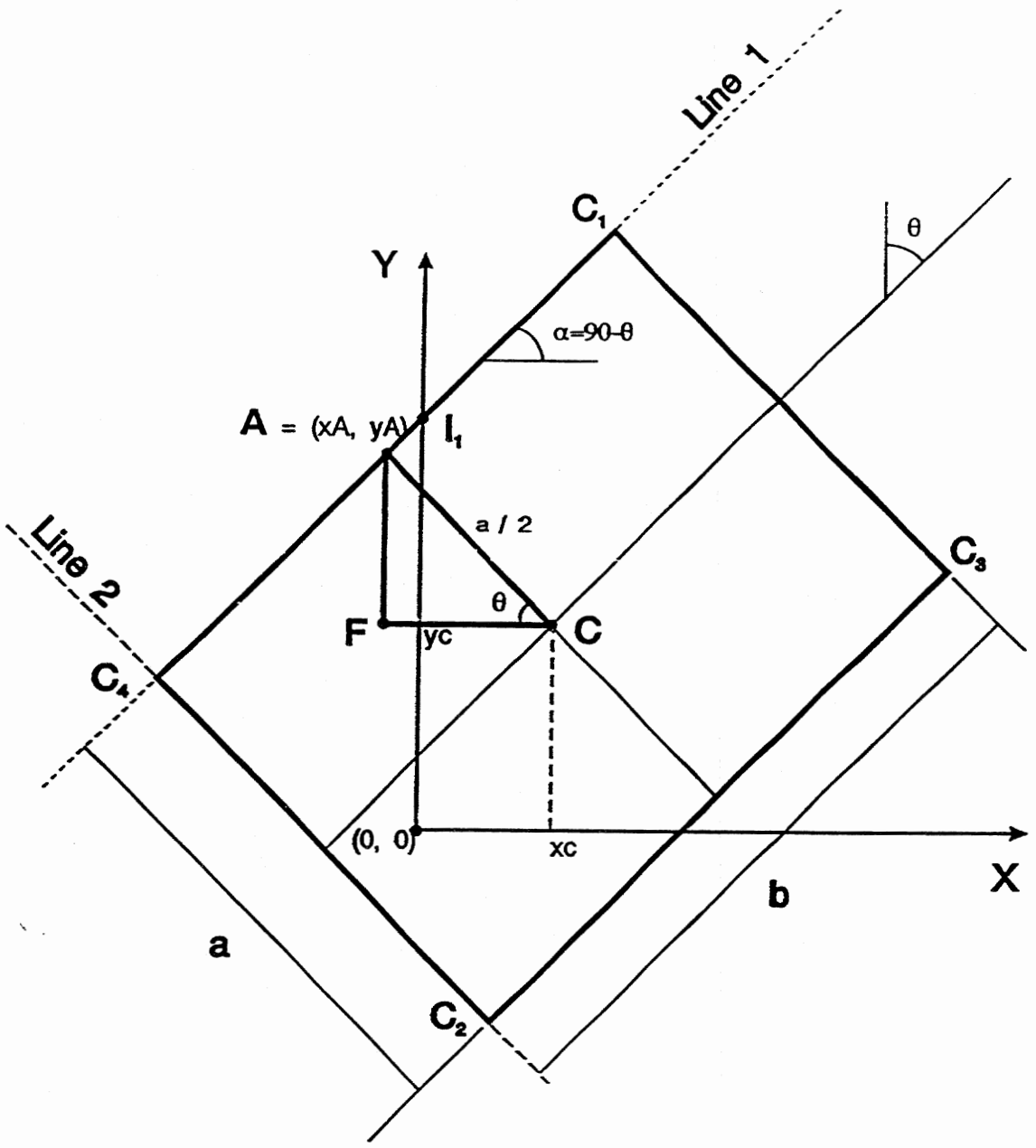

Figure A1

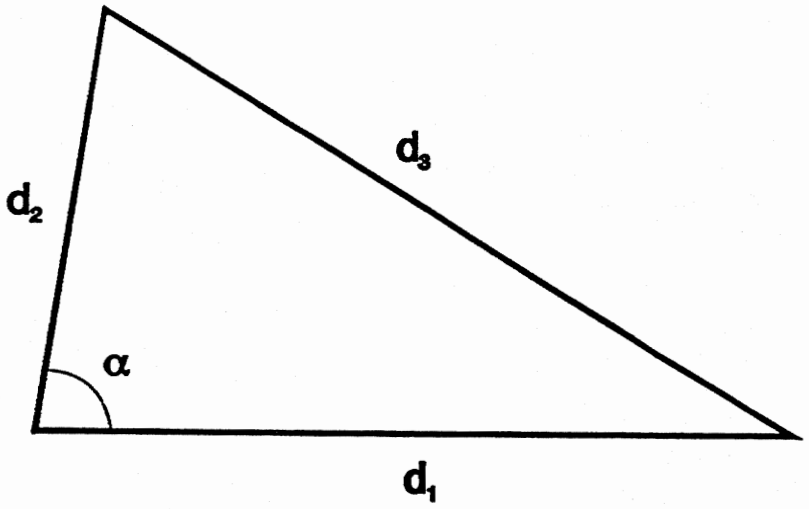

Figure A2

PIXEL-VEHICLE Computer Program

```
'Program Name: PV_PRNV1.BAS
'Program Language: QuickBasic v 4.0
'Author : Oscar Franzese
'Date: July 3, 1992

'=====================================================
'Given a grid of square pixels with side PS and a car of sides a and b, this program computes the area
'occupied by that car in the different pixels that it touches. The program permits the computation of
'these areas for different angles between the longitudinal axis of the vehicle and the grid of pixels, and
'for different positions of the center of the vehicle.
'=====================================================
'MAIN PROGRAM

DECLARE SUB CentralPoint ()
DECLARE SUB SeeIfInCell (PL!, PR!, PB!, PT!)
DECLARE SUB Arrange ()
DECLARE SUB WriteMatAVeh (n%)
DECLARE FUNCTION CompDist# (x!, y!)
DECLARE SUB IsPointIn.or.On (x!, y!)
DECLARE SUB Inter (PB!, PT!, PL!, PR!)
DECLARE SUB VerifyPix (AreaT#, Pix)
DECLARE SUB WriteMatPix (n%)
DECLARE SUB dist (i%)
COMMON SHARED MPoints(), x(), y(), PS, d(), px(), py(), Pi#, xc, yc, a, b, k%
COMMON SHARED MatAVeh(), vx, vy, NoPoints%, Theta#, MaxDiag#, Area#, MPAux()

DIM MPoints(16, 2), MPAux(16, 2), x(4, 4), y(4, 4), px(12), py(12)
DIM d(12, 7), xc(4), yc(4)

'=====================================================
'Pixel Size
PS = 1

'=====================================================
'Geometric Constants
Pi# = 3.141592654#

'=====================================================
'Vehicle Dimensions
a = .6
b = 2

'=====================================================
'Name and Location of Files (to be entered by the user)
CLS : PRINT "Start at: "; TIME$
Na0$ = "602_.PRN"
Na1$ = "F:\VEHPIX\SA" + Na0$
Na2$ = "F:\VEHPIX\MA" + Na0$
OPEN Na1$ FOR OUTPUT AS #1
OPEN Na2$ FOR OUTPUT AS #2
```

```
'=====================================================
'Dimension of array to hold pixels that get iluminated (i.e.; those in vhich vehicle's parts lie)

DIAG = (a ^ 2 + b ^ 2) ^ .5 / 2
n% = 1 + (INT(DIAG) + 1) * 2
DIM MatAVeh(n%, n%)
WRITE #2, n%

FOR yc = .00001 TO .5001 STEP .5 / 19
FOR xc = .00001 TO .5001 STEP .5 / 19
FOR Theta# = 0 TO PI# STEP PI# / 19


IF Theta# = 0 THEN Theta# = .000001
IF Theta# = PI# THEN Theta# = PI# - .000001
IF Theta# = PI# / 2 THEN Theta# = PI# / 2 + .000001

Area# = 0     'Total area of vehicle in pixel
AreaT# = 0    'Area of triangle in consideration

ERASE x, y, px, py, d
DIM x(6, 4), y(6, 4), px(12), py(12), d(12, 7)


'===VEHICLE LINES=============================================================
'---Y = ai X + bi-----------------------
'---Line 1-----------------------------
a1 = COS(Theta#) / SIN(Theta#)
b1 = yc + a / (2 * SIN(Theta#)) - xc * COS(Theta#) / SIN(Theta#)
'---Line 2-----------------------------
a2 = a1
b2 = yc - a / (2 * SIN(Theta#)) - xc * COS(Theta#) / SIN(Theta#)
'---Line 3-----------------------------
a3 = -SIN(Theta#) / COS(Theta#)
b3 = yc + b / (2 * COS(Theta#)) + xc * SIN(Theta#) / COS(Theta#)
'---Line 4-----------------------------
a4 = a3
b4 = yc - b / (2 * COS(Theta#)) + xc * SIN(Theta#) / COS(Theta#)


'===VEHICLE CORNERS===========================================================
'---Corner 1-----------------------------
xc(1) = xc + b / 2 * SIN(Theta#) - a / 2 * COS(Theta#)
yc(1) = yc + b / 2 * COS(Theta#) + a / 2 * SIN(Theta#)
'---Corner 3-----------------------------
xc(3) = xc + b / 2 * SIN(Theta#) + a / 2 * COS(Theta#)
yc(3) = yc + b / 2 * COS(Theta#) - a / 2 * SIN(Theta#)
'---Corner 2-----------------------------
xc(2) = xc - b / 2 * SIN(Theta#) + a / 2 * COS(Theta#)
yc(2) = yc - b / 2 * COS(Theta#) - a / 2 * SIN(Theta#)
'---Corner 4-----------------------------
```

```
xc(4) = xc - b / 2 * SIN(Theta#) - a / 2 * COS(Theta#)
yc(4) = yc - b / 2 * COS(Theta#) + a / 2 * SIN(Theta#)


MaxDiag# = CompDist#(xc(1), yc(1))
DistDiag# = CompDist#(xc(2), yc(2))
IF DistDiag# > MaxDiag# THEN MaxDiag# = DistDiag#
DistDiag# = CompDist#(xc(3), yc(3))
IF DistDiag# > MaxDiag# THEN MaxDiag# = DistDiag#
DistDiag# = CompDist#(xc(4), yc(4))
IF DistDiag# > MaxDiag# THEN MaxDiag# = DistDiag#

IF ((xc(1) >= 0 AND xc(1) <= PS) AND (xc(2) >= 0 AND xc(2) <= PS) AND (xc(3) >= 0 AND xc(3) <=
PS) AND (xc(4) >= 0 AND xc(4) <= PS) AND (yc(1) >= 0 AND yc(1) <= PS) AND (yc(2) >= 0 AND yc(2)
<= PS) AND (yc(3) >= 0 AND yc(3) <= PS) AND (yc(4) >= 0 _
AND yc(4) <= PS)) THEN
  Area# = a * b / PS ^ 2
  CALL VerifyPix(Area#, Pix)
  MatAVeh((n% + 1) / 2, (n% + 1) / 2) = Area#
  GOTO aaa
END IF

FOR i% = 1 TO n%
  FOR j% = 1 TO n%
    '-------Computations for pixel i%, j%:
    '-------k% = counts the number of vertices in the current pixel
    '-------Area is the area of the vehicle on the current pixel
    k% = 0
    Area# = 0

    '-------Calculates the coordinates of the current pixel's corner
    '-------PL: vertical left line in pixel (x of west side)
    '-------PR: vertical right line in pixel (x of east side)
    '-------PB: horizontal bottom line in pixel (y of south side)
    '-------PT: horizontal top line in pixel (y of north side)
    NWx% = (j% - (n% + 1) / 2) * PS
    NWy% = (-i% + (n% + 1) / 2 + 1) * PS
    PL = NWx%
    PT = NWy%
    SEx% = (j% - (n% + 1) / 2 + 1) * PS
    SEy% = (-i% + (n% + 1) / 2) * PS
    PR = SEx%
    PB = SEy%
    NEx% = SEx%
    NEy% = NWy%
    SWx% = NWx%
    SWy% = SEy%

    '------Determines if the pixel corners are outside the vehicle silhouette.
    '------If they are outside, then the area covered is null and it moves
    '------to the next pixel.
```

```
    IF (MaxDiag# > PS) THEN
      dcNW = ((xc - PL) ^ 2 + (yc - PT) ^ 2) ^ .5
      dcNE = ((xc - PR) ^ 2 + (yc - PT) ^ 2) ^ .5
      dcSW = ((xc - PL) ^ 2 + (yc - PB) ^ 2) ^ .5
      dcSE = ((xc - PR) ^ 2 + (yc - PB) ^ 2) ^ .5
      IF (dcNW > MaxDiag# AND dcNE > MaxDiag# AND dcSW > MaxDiag# AND dcSE > MaxDiag#)
GOTO EndLoop
    END IF


    '------Determines if the pixel corners are inside the vehicle silhouette.
    '------If the 4 corners are inside, then the whole pixel is cover by
    '------the vehicle (k% is incremented by 4).
    kbefore% = k%
    Y1L = a1 * NWx% + b1
    Y2L = a2 * NWx% + b2
    Y3L = a3 * NWx% + b3
    Y4L = a4 * NWx% + b4
    Y1R = a1 * SEx% + b1
    Y2R = a2 * SEx% + b2
    Y3R = a3 * SEx% + b3
    Y4R = a4 * SEx% + b4
    IF Theta# <= PI# / 2 THEN
      IF NWy% <= Y1L AND NWy% <= Y3L AND NWy% >= Y2L AND NWy% >= Y4L THEN
        k% = k% + 1
        MPoints(k%, 1) = NWx%
        MPoints(k%, 2) = NWy%
      END IF
      IF SWy% <= Y1L AND SWy% <= Y3L AND SWy% >= Y2L AND SWy% >= Y4L THEN
        k% = k% + 1
        MPoints(k%, 1) = SWx%
        MPoints(k%, 2) = SWy%
      END IF
      IF NEy% <= Y1R AND NEy% <= Y3R AND NEy% >= Y2R AND NEy% >= Y4R THEN
        k% = k% + 1
        MPoints(k%, 1) = NEx%
        MPoints(k%, 2) = NEy%
      END IF
      IF SEy% <= Y1R AND SEy% <= Y3R AND SEy% >= Y2R AND SEy% >= Y4R THEN
        k% = k% + 1
        MPoints(k%, 1) = SEx%
        MPoints(k%, 2) = SEy%
      END IF
    ELSE
      IF NWy% <= Y4L AND NWy% <= Y1L AND NWy% >= Y3L AND NWy% >= Y2L THEN
        k% = k% + 1
        MPoints(k%, 1) = NWx%
        MPoints(k%, 2) = NWy%
      END IF
      IF SWy% <= Y4L AND SWy% <= Y1L AND SWy% >= Y3L AND SWy% >= Y2L THEN
        k% = k% + 1
```

```
      MPoints(k%, 1) = SWx%
      MPoints(k%, 2) = SWy%
    END IF
    IF NEy% <= Y4R AND NEy% <= Y1R AND NEy% >= Y3R AND NEy% >= Y2R THEN
      k% = k% + 1
      MPoints(k%, 1) = NEx%
      MPoints(k%, 2) = NEy%
    END IF
    IF SEy% <= Y4R AND SEy% <= Y1R AND SEy% >= Y3R AND SEy% >= Y2R THEN
      k% = k% + 1
      MPoints(k%, 1) = SEx%
      MPoints(k%, 2) = SEy%
    END IF
  END IF
  IF k% = kbefore% + 4 THEN
    MatAVeh(i%, j%) = 1
    GOTO EndLoop
  END IF
  '------Determines if some of the vehicle's corners are inside this
  '------pixel.
  IF (xc(1) <= PR AND xc(1) >= PL AND yc(1) <= PT AND yc(1) >= PB) THEN
    k% = k% + 1
    MPoints(k%, 1) = xc(1)
    MPoints(k%, 2) = yc(1)
  END IF
  IF (xc(2) <= PR AND xc(2) >= PL AND yc(2) <= PT AND yc(2) >= PB) THEN
    k% = k% + 1
    MPoints(k%, 1) = xc(2)
    MPoints(k%, 2) = yc(2)
  END IF
  IF (xc(3) <= PR AND xc(3) >= PL AND yc(3) <= PT AND yc(3) >= PB) THEN
    k% = k% + 1
    MPoints(k%, 1) = xc(3)
    MPoints(k%, 2) = yc(3)
  END IF
  IF (xc(4) <= PR AND xc(4) >= PL AND yc(4) <= PT AND yc(4) >= PB) THEN
    k% = k% + 1
    MPoints(k%, 1) = xc(4)
    MPoints(k%, 2) = yc(4)
  END IF

  '------Determines the intersection points between the pixel lines and
  '------the vehicle lines.  Then it computes which of the intersection
  '------points, if any, belongs to the vehicle and adds it to the list
  '------of vertices.
  CALL Inter(PB, PT, PL, PR)
  FOR i1% = 1 TO 4
    FOR j1% = 1 TO 4
      CALL IsPointIn.or.On(x(i1%, j1%), y(i1%, j1%))
    NEXT j1%
  NEXT i1%
```

```
      '------Up to here we have all the points that may belong to the
      '------perimeter that we are trying to determine.  Now it is necessary
      '------to determine wether or not these points are inside the current
      '------cell.
      CALL SeeIfInCell(PL, PR, PB, PT)


      '------At this moment, all the points that are relevant in the
      '------computation of the area covered by the vehicle in the current
      '------pixel have bee n determined and stored in MPoints().
      '------The next step is to arrange these points in an orderly manner
      '------as to compute the area of the different triangles that have been
      '------defined.  All this is done by the Subroutine Arrange.  But first
      '------subroutine CentralPoint identifies a point inside the convex
      '------region in the vehicle silhouette in the current pixel.  This point
      '------is used as vertice for the computation of the triangle areas.
      CALL CentralPoint
      ERASE d
      DIM d(12, 7)
      FOR i1% = 1 TO k%
        px(i1%) = MPoints(i1%, 1)
        py(i1%) = MPoints(i1%, 2)
        CALL dist(i1%)
      NEXT i1%
      Area# = 0
      CALL Arrange
      CALL VerifyPix(Area#, Pix)
      MatAVeh(i%, j%) = Area#

EndLoop:
  NEXT j%
NEXT i%


aaa:
maxA = 0
FOR i% = 1 TO n%
  FOR j% = 1 TO n%
    IF MatAVeh(i%, j%) > maxA THEN
      maxA = MatAVeh(i%, j%)
    END IF
  NEXT j%
NEXT i%
WRITE #1, maxA

CALL WriteMatAVeh(n%)

FOR i% = 1 TO n%
  FOR j% = 1 TO n%
```

```
      MatAVeh(i%, j%) = 0
    NEXT j%
  NEXT i%

  NEXT Theta#
  PRINT "End of Theta#: "; TIME$
  NEXT xc
  PRINT "End of xc: "; TIME$
  NEXT yc
  PRINT "The End: "; TIME$

  SOUND 340, 25
  CLOSE
  END
```

```
SUB Arrange
'=====================================================
'This subroutine arranges the points on the perimeter of the area to be
'computed such that they are in the right order for the computation by
'triangles.  The order is by angle from the point used as the center or
'vertice.
'After that this subroutine calculates the total area occupied by the
'vehicle in this pixel (Area = sum of all triangle areas AreaT).
'=====================================================


FOR j% = 1 TO k%
  min# = 2 * PI#
  FOR i% = 1 TO k%
    IF (d(i%, 6) < min# AND d(i%, 7) = 0) THEN
      min# = d(i%, 6)
      mini% = i%
    END IF
  NEXT i%
  d(mini%, 7) = j%
NEXT j%


j% = 1
il:
FOR i% = 1 TO k% + 1
  IF d(i%, 7) = j% THEN
    j% = j% + 1
    d1 = d(i%, 3)
    px1 = px(i%)
    py1 = py(i%)
    FOR l% = 1 TO k% + 1
      IF d(l%, 7) = j% THEN
        d2 = d(l%, 3)
        px2 = px(l%)
        py2 = py(l%)
        l% = k% + 1
      END IF
    NEXT l%
    i% = k% + 1
  END IF
NEXT i%
d3 = ((px1 - px2) ^ 2 + (py1 - py2) ^ 2) ^ .5
Raiz = (4 * d1 ^ 2 * d2 ^ 2 - (d1 ^ 2 + d2 ^ 2 - d3 ^ 2) ^ 2)
'IF Raiz < 0 AND ABS(Raiz) < .000001 THEN Raiz = 0
IF Raiz < 0 THEN Raiz = 0
AreaT# = .25 * Raiz ^ .5
Area# = Area# + AreaT#
IF j% < k% + 1 GOTO il

j% = 1
```

```
d1 = d2
px1 = px2
py1 = py2
FOR l% = 1 TO k% + 1
  IF d(l%, 7) = j% THEN
    d2 = d(l%, 3)
    px2 = px(l%)
    py2 = py(l%)
    l% = k% + 1
  END IF
NEXT l%
d3 = ((px1 - px2) ^ 2 + (py1 - py2) ^ 2) ^ .5
Raiz = (4 * d1 ^ 2 * d2 ^ 2 - (d1 ^ 2 + d2 ^ 2 - d3 ^ 2) ^ 2)
'IF Raiz < 0 AND ABS(Raiz) < .000001 THEN Raiz = 0
IF Raiz < 0 THEN Raiz = 0
AreaT# = .25 * Raiz ^ .5
Area# = Area# + AreaT#


END SUB
```

```
SUB CentralPoint
'=====================================================
'This subroutine identifies a point inside the convex region in the vehicle
'silhouette in the current pixel.  This point is used as vertice for the
'computation of the triangle areas.
'=====================================================

x1 = MPoints(1, 1)
y1 = MPoints(1, 2)
x2 = MPoints(2, 1)
y2 = MPoints(2, 2)

xmin = x1
ymin = y1
xMAX = x2
yMAX = y2
IF x2 < x1 THEN
   xmin = x2
   ymin = y2
   xMAX = x1
   yMAX = y1
END IF

x12 = xmin + (xMAX - xmin) / 2
y12 = ymin + (yMAX - ymin) / 2
x3 = MPoints(3, 1)
y3 = MPoints(3, 2)

xmin = x12
ymin = y12
xMAX = x3
yMAX = y3
IF x3 < x12 THEN
   xmin = x3
   ymin = y3
   xMAX = x12
   yMAX = y12
END IF

vx = xmin + (xMAX - xmin) / 2
vy = ymin + (yMAX - ymin) / 2

END SUB
```

```
SUB dist (i%)
'=====================================================
'This subrroutine computes the distance from each of the points on the
'perimeter of the area to the vertice V.  It also computes the angle between
'the line passing through the point in consideration and vertice V and the
'horizontal line.  This angle is later used to order the points in a consecutive
'way for the computation of the area occupied by the vehicle in the current cell.
'=====================================================

    d(i%, 1) = px(i%) - vx
    d(i%, 2) = py(i%) - vy
    d(i%, 3) = (d(i%, 1) ^ 2 + d(i%, 2) ^ 2) ^ .5
    d(i%, 4) = d(i%, 1) / d(i%, 3)
    d(i%, 5) = d(i%, 2) / d(i%, 3)
    IF d(i%, 4) = 1 THEN
      d(i%, 6) = 0
    ELSEIF d(i%, 4) = -1 THEN
      d(i%, 6) = PI#
    ELSEIF d(i%, 4) = 0 THEN
      IF d(i%, 5) = 1 THEN
        d(i%, 6) = PI# / 2
      ELSE
        d(i%, 6) = PI# * 3 / 2
      END IF
    ELSE
      IF (d(i%, 4) > 0 AND d(i%, 5) > 0) THEN
        d(i%, 6) = ATN(d(i%, 5) / d(i%, 4))
      ELSEIF (d(i%, 4) < 0 AND d(i%, 5) > 0) THEN
        d(i%, 6) = PI# + ATN(d(i%, 5) / d(i%, 4))
      ELSEIF (d(i%, 4) < 0 AND d(i%, 5) < 0) THEN
        d(i%, 6) = PI# + ATN(d(i%, 5) / d(i%, 4))
      ELSE
        d(i%, 6) = 2 * PI# + ATN(d(i%, 5) / d(i%, 4))
      END IF
    END IF

END SUB
```

```
SUB Inter (PB, PT, PL, PR)
'=====================================================
'This subroutine computes the intersections between vehicle lines and pixel
'lines.
'x(pixel line #, vehicle line #)
'y(pixel line #, vehicle line #)
'=====================================================

'---Point PBV1-----------------------------
x(1, 1) = xc + (PB - a / (2 * SIN(Theta#)) - yc) * SIN(Theta#) / COS(Theta#)
y(1, 1) = PB
'---Point PBV2-----------------------------
x(1, 2) = xc + (PB + a / (2 * SIN(Theta#)) - yc) * SIN(Theta#) / COS(Theta#)
y(1, 2) = PB
'---Point PBV3-----------------------------
x(1, 3) = xc - (PB - b / (2 * COS(Theta#)) - yc) * COS(Theta#) / SIN(Theta#)
y(1, 3) = PB
'---Point PBV4-----------------------------
x(1, 4) = xc - (PB + b / (2 * COS(Theta#)) - yc) * COS(Theta#) / SIN(Theta#)
y(1, 4) = PB


'---Point PLV1-----------------------------
x(2, 1) = PL
y(2, 1) = yc + (a / (2 * COS(Theta#)) + (PL - xc)) * COS(Theta#) / SIN(Theta#)
'---Point PLV2-----------------------------
x(2, 2) = PL
y(2, 2) = yc - (a / (2 * COS(Theta#)) - (PL - xc)) * COS(Theta#) / SIN(Theta#)
'---Point PLV3-----------------------------
x(2, 3) = PL
y(2, 3) = yc + (b / (2 * SIN(Theta#)) - (PL - xc)) * SIN(Theta#) / COS(Theta#)
'---Point PLV4-----------------------------
x(2, 4) = PL
y(2, 4) = yc - (b / (2 * SIN(Theta#)) + (PL - xc)) * SIN(Theta#) / COS(Theta#)


'---Point PTV1-----------------------------
x(3, 1) = xc + (PT - a / (2 * SIN(Theta#)) - yc) * SIN(Theta#) / COS(Theta#)
y(3, 1) = PT
'---Point PTV2-----------------------------
x(3, 2) = xc + (PT + a / (2 * SIN(Theta#)) - yc) * SIN(Theta#) / COS(Theta#)
y(3, 2) = PT
'---Point PTV3-----------------------------
x(3, 3) = xc - (PT - b / (2 * COS(Theta#)) - yc) * COS(Theta#) / SIN(Theta#)
y(3, 3) = PT
'---Point PTV4-----------------------------
x(3, 4) = xc - (PT + b / (2 * COS(Theta#)) - yc) * COS(Theta#) / SIN(Theta#)
y(3, 4) = PT
```

```
'---Point PRV1--------------------------------
x(4, 1) = PR
y(4, 1) = yc + (a / (2 * COS(Theta#)) + (PR - xc)) * COS(Theta#) / SIN(Theta#)
'---Point PRV2--------------------------------
x(4, 2) = PR
y(4, 2) = yc - (a / (2 * COS(Theta#)) - (PR - xc)) * COS(Theta#) / SIN(Theta#)
'---Point PRV3--------------------------------
x(4, 3) = PR
y(4, 3) = yc + (b / (2 * SIN(Theta#)) - (PR - xc)) * SIN(Theta#) / COS(Theta#)
'---Point PRV4--------------------------------
x(4, 4) = PR
y(4, 4) = yc - (b / (2 * SIN(Theta#)) + (PR - xc)) * SIN(Theta#) / COS(Theta#)

END SUB
```

```
SUB IsPointIn.or.On (x, y)
'=============================================================
'This subroutine determines whether or not an intersection point between
'vehicle lines and pixel lines is on the perimeter of the vehicle or outside
'it.  If it is on that perimeter, the point is added to the set of points
'for the computation of the vehicle area covered in the current pixel.
'=============================================================

  DistDiag# = CompDist#(x, y)
  IF DistDiag# <= MaxDiag# THEN
    k% = k% + 1
    MPoints(k%, 1) = x
    MPoints(k%, 2) = y
  END IF
END SUB
```

```
SUB SeeIfInCell (PL, PR, PB, PT)
'=====================================================
'This subroutine checks if the points that have been identified belong
'to the pixel in consideration.
'=====================================================

k1% = 0
ERASE MPAux
DIM MPAux(16, 2)
FOR i% = 1 TO k%
  xaux = MPoints(i%, 1)
  yaux = MPoints(i%, 2)
  IF xaux >= PL AND xaux <= PR AND yaux >= PB AND yaux <= PT THEN
    k1% = k1% + 1
    MPAux(k1%, 1) = xaux
    MPAux(k1%, 2) = yaux
  END IF
NEXT i%
k% = k1%
FOR i% = 1 TO 16
  MPoints(i%, 1) = MPAux(i%, 1)
  MPoints(i%, 2) = MPAux(i%, 2)
NEXT i%

END SUB
```

APPENDIX D

Summary Statistics of Vehicle Identification and Classification

Appendix D. Summary Statistics of Vehicle Identification and Classification

The ability to detect and classify vehicles on the highway is summarized in the fraction correct measures. These give the number of correctly identified or classified vehicles on a highway segment divided by the total number of vehicles on the segment. Specifically, we define the Fraction of Vehicles Correctly Identified (FVCI) as the number of vehicles on the segment correctly identified as vehicles (even if misclassified as to whether they are trucks or other vehicles), divided by the total number of vehicles on the segment. Using the data elements described in Section 3:

$$FVCI = (b_{tt}+b_{to}+b_{ot}+b_{oo}) / (b_{tt}+b_{to}+b_{tn}+b_{ot}+b_{oo}+b_{on}) \quad (D.1)$$

FVCI reflects the accuracy in vehicle counting. Regarding vehicle classification, we define the Fraction of Trucks Correctly Classified (FTCC) as the number of trucks on the segment correctly classified as trucks, divided by the total number of trucks on the segment. That is:

$$FTCC = b_{tt} / (b_{tt}+b_{to}+b_{tn}) \quad (D.2)$$

Similarly, we define the Fraction of Other Vehicles Correctly Classified (FOCC) as the number of other vehicles on the segment correctly classified as other vehicles, divided by the total number of other vehicles on the segment:

$$FOCC = b_{oo} / (b_{ot}+b_{oo}+b_{on}) \quad (D.3)$$

(Since $b_{tt} = a_{tt}$ and $b_{oo} = a_{oo}$, a_{tt} and a_{oo} could be used in the numerators for FTCC and FOCC, respectively.)

The Fraction Correct indicates how well the remote sensing process (simulated by the image processing analysis) performs on the vehicles that are present. The error of omission is the complement of this measure and indicates how many vehicles are being omitted in the process.

We define the Vehicle Identification Error of Omission (VIEO) as the number of vehicles on the highway segment that were not identified as vehicles of any kind in the image processing step, divided by the total number of vehicles on the segment. Using the data elements described in Section 3:

$$VIEO = (b_{tn}+b_{on}) / (b_{tt}+b_{to}+b_{tn}+b_{ot}+b_{oo}+b_{on}) = 1 - FVCI \quad (D.4)$$

VIEO represents how many vehicles are "missed" in vehicle counting. Regarding vehicle classification, we define the Truck Classification Error of Omission (TCEO) as the number of trucks on the highway segment that were not classified as trucks in the image processing step, divided by the total number of trucks on the segment:

$$TCEO = (b_{to}+b_{tn}) / (b_{tt}+b_{to}+b_{tn}) = 1 - FTCC \quad (D.5)$$

Similarly, we define the Other vehicle Classification Error of Omission (OCEO) as the number of other vehicles on the highway segment that were not classified as other vehicles in the image processing step, divided by the total number of other vehicles on the segment:

$$OCEO = (b_{ot}+b_{on}) / (b_{ot}+b_{oo}+b_{on}) = 1 - FOCC \quad (D.6)$$

Errors of commission represent the errors that are made in counting a nonvehicle object as a vehicle, classifying a nontruck element as a truck, or classifying a non-other vehicle element as an "other" vehicle. They are based on committing errors made in the image processing step, and they are, therefore, scaled by the number of relevant elements in the clump list. We define the Vehicle Identification Error of Commission (VIEC) as the number of nonvehicle clumps that are identified as vehicles, divided by the total number of clumps identified as vehicles. That is:

$$VIEC = (a_{tn}+a_{on}) / (a_{tt}+a_{to}+a_{tn}+a_{ot}+a_{oo}+a_{on}) \quad (D.7)$$

VIEC represents the errors of commission in vehicle counting.

Regarding vehicle classification, we define the Truck Classification Error of Commission (TCEC) as the number of nontruck clumps that are classified as trucks, divided by the total number of clumps classified as trucks. That is:

$$TCEC = (a_{to}+a_{tn}) / (a_{tt}+a_{to}+a_{tn}) \quad (D.8)$$

Similarly, we define the Other vehicle Classification Error of Commission (OCEC) as the number of non-other vehicle clumps that are classified as other vehicles, divided by the total number of clumps classified as other vehicles:

$$OCEC = (a_{ot}+a_{on}) / (a_{ot}+a_{oo}+a_{on}) \quad (D.9)$$

We report all of these summary performance measures as ratios (i.e., report both numerator and denominator), as well as the decimal equivalent (see Section 3), to indicate the number of vehicles involved in the evaluation tests. These statistical measures were used to analyze the four aerial photographs that were scanned at the four spatial resolutions.

APPENDIX E

Scanned Images at 1-m Resolution for the Seven Highway Segments

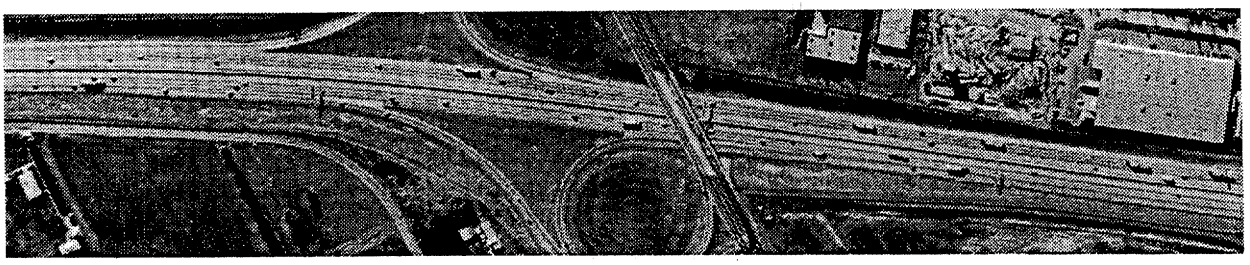

Figure E.1 Highway segment 514:E-W

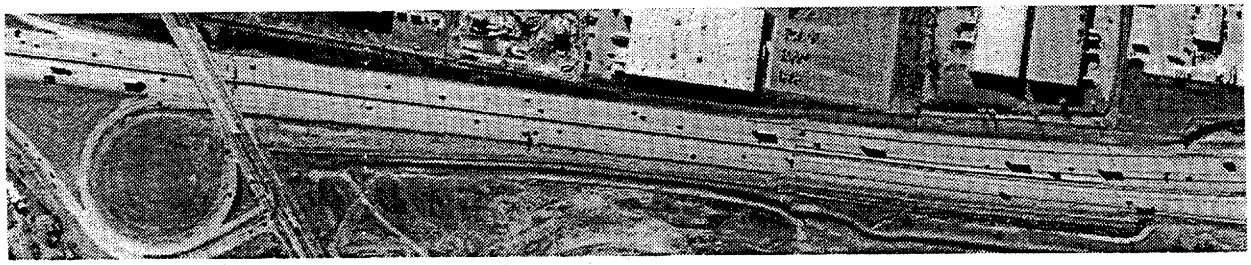

Figure E.2 Highway segment 513:E-W

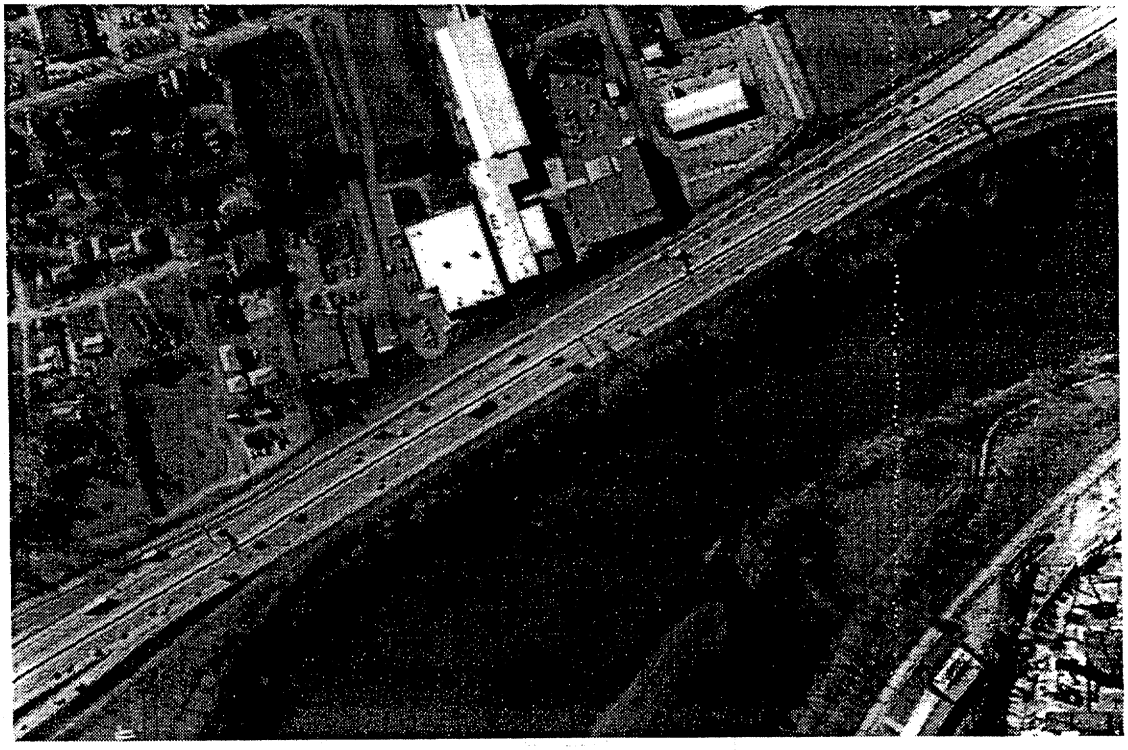

Figure E.3 Highway segment 791:NW-SE

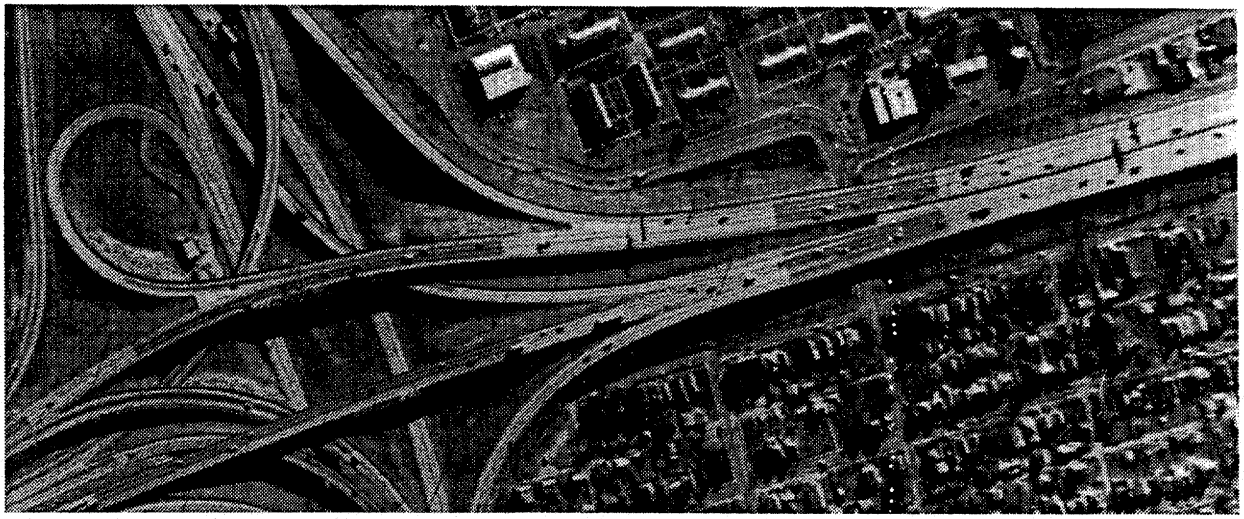

Figure E.4 Highway segment 791:E-W

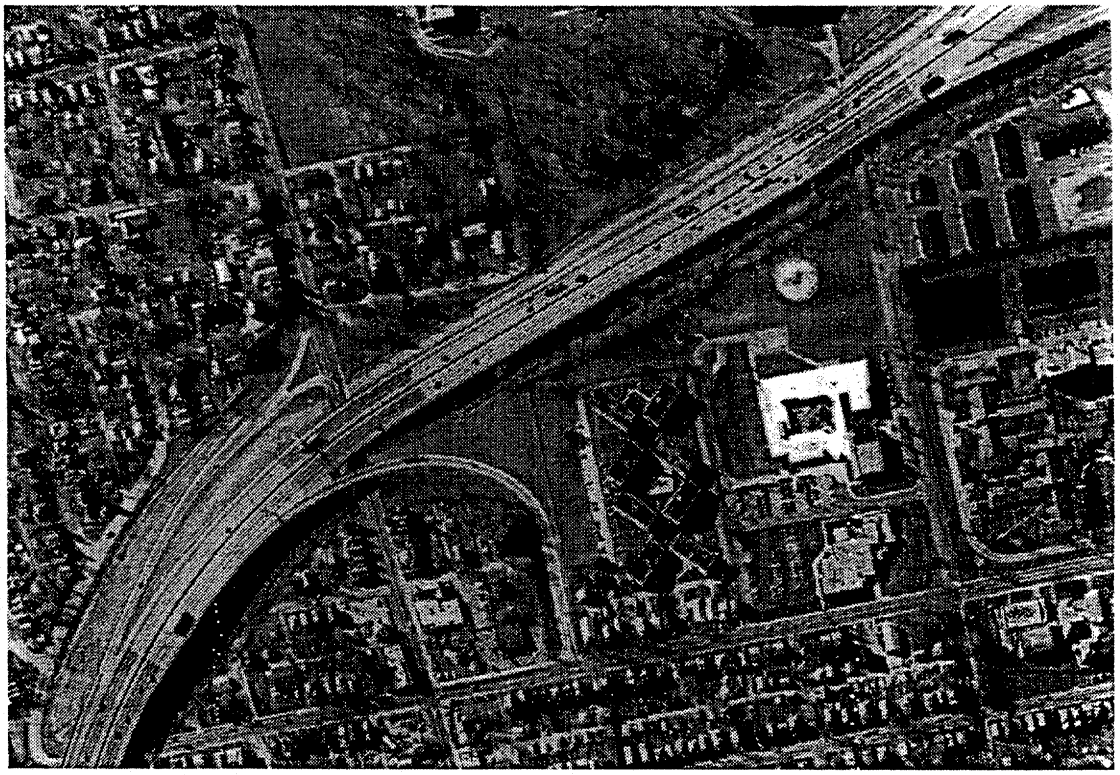

Figure E.5 Highway segment 753(1): NNW-SSE

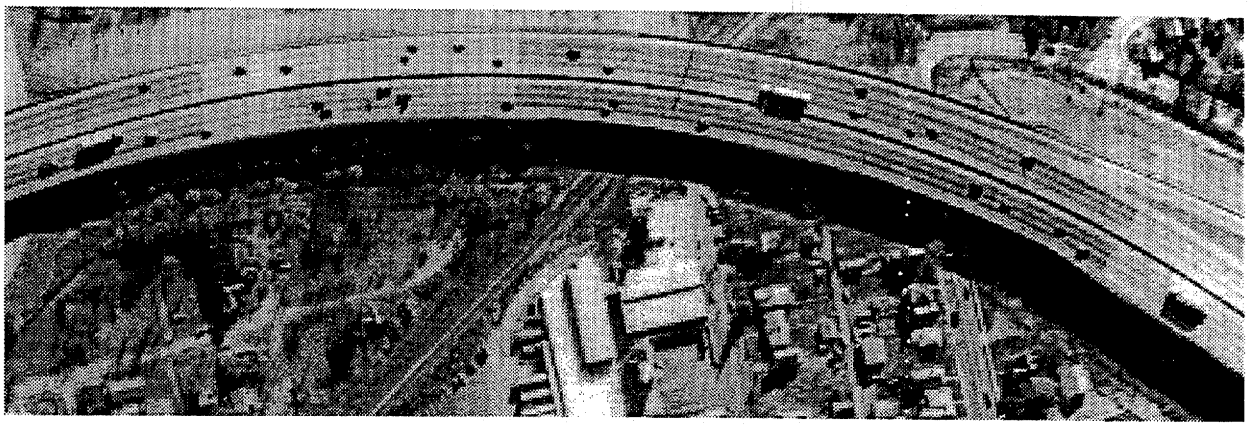

Figure E.6 Highway segment 753(2): NW-SE

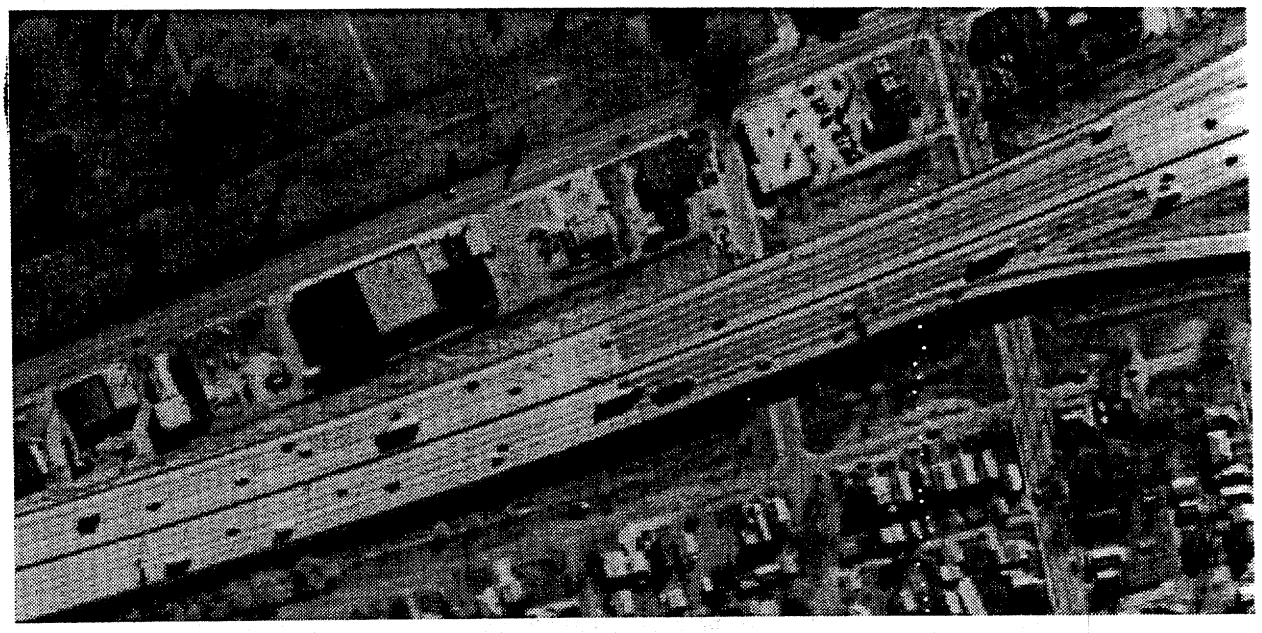

Figure E.7 Highway segment 753(3): EEN-WWS

APPENDIX F

Derivation of Orbit Parameter Equations

Appendix F. Deviation of Orbit Parameter Equations

F.1 Derivation of Equation (4.2)

A satellite at elevation H above the surface of the earth would be a distance $R+H$ from the center of the earth, where R is the distance from the center of the earth to the surface. To maintain a circular orbit of radius $R+H$, the centripetal force F_c on the satellite must be:

$$F_c = mv^2 / (R+H) \tag{F.1}$$

where m is the mass of the satellite, v^2 is the linear velocity of the satellite, and R and H are defined above.

The net force on the satellite is primarily a result of the gravitational attraction between the satellite and the earth. The gravitational force F_g exerted by the earth on the satellite would be:

$$F_g = mGM / (R+H)^2 \tag{F.2}$$

where m is again the mass of the satellite, GM is the gravitational constant at the surface of the earth, and R and H are again defined above.

To maintain the circular orbit, the net force on the satellite must equal the required centripetal force. That is, $F_g = F_c$. Equating (F.1) and (F.2), and solving for v:

$$v = [GM / (R+H)]^{1.5} \tag{F.3}$$

The length (circumference) of an orbit at radius R+H would be 2p(R+H). A satellite traveling at linear velocity v would, therefore, require a time of 2p(R+H)/v to complete one orbit. The time to complete one orbit, called the period of the satellite, is usually given in minutes. This implies that v is given in units of length corresponding to R and H (usually, kilometers) per minute. Given that there are 1440 minutes per day, the number of orbits n that the satellite would make in one day, would be:

$$n = 1440/[2p(R+H) / v] \text{ [orbits/day]} \tag{F.4}$$

where v is fixed to be in units of appropriate length per minute. We can substitute (F.3) for v, as long as v in (F.3) is guaranteed to be in units of the appropriate length per minute. This requires that the gravitational constant is in units of the length used for R and H to the third power per minute squared. Substituting (F.3) into (F.4):

$$n = 1440(GM)^{0.5} / 2p(R+H)^{0.5} \text{ [orbits/day]} \tag{F.5}$$

where the units on GM are the units of the length used for R and H to the third power per minute squared. There are several values given for GM. We used that given by Light

(1992a) – GM = 398,601 [km^3/sec^2]. Converting to [km^3/min^2] and substituting in (F.5), we get:

$$n = 8{,}681{,}665.8 / (R+H)^{1.5} \text{ [orbits/day]} \quad \text{(F.6)}$$

where the units of *R* and *H* must now be kilometers. In our analysis, we used 6,371 km as the mean radius of the earth.

F.2 Derivation of Equation (4.6)

The imaging system in a satellite works on the principle of positive lens optics (Moffitt and Mikhail, 1980). The principle leads to the proportional relation, illustrated in Figure F.1:

$$DA / SW = FL / H \quad \text{(F.7)}$$

where *DA* is the detector aperture of the instrument, *SW* is the swath width imaged on the ground, *FL* is the focal length of the instrument, and *H* is the height of the lens above the earth. As described in Section 4.2, the swath width is the number of pixels in the scan line *PPAL* times the imaging resolution of a pixel on the ground *RES* – i.e., SW = PPAL * RES. Also, the detector aperture is the width of the scan line on the instrument, which is the width of the individual sensing pixel in the instrument *PWPD* (physical width of the pixel on the detector) times the number of pixels in the scan line *PPAL* – i.e., DA = PWPD * PPAL. Substituting these relations for *DA* and *SW* in (F.7) and solving for *FL*, we find:

$$FL = H * PWPD / RES \quad \text{(F.8)}$$

Since the altitude of the satellite *H* is normally given in kilometers, the physical width of the pixel on the detector is normally given in μm (10^{-6} m), and the focal length is usually given in meters, we write (F.8) as:

$$FL = H * PWPD * 10^{-3} / RES \text{ [m]} \quad \text{(F.9)}$$

where *H* is in kilometers, *PWPD* is in μm, and *RES* and *FL* are in meters.

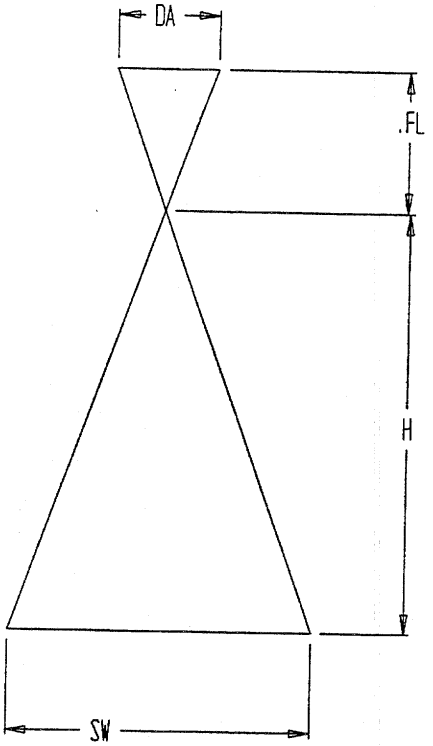

Figure F.1 Relation among detector aperature *DA*, swath width *SW*, focal length *FL*, and satellite altitude *H*

APPENDIX G

Determining Satellite Ground Track Lengths Between Two Latitudes

Appendix G. Determining Satellite Ground Track Lengths Between Two Latitudes

We are interested in determining the length of a satellite ground track between two latitudes LAT_1 and LAT_2, given that the orbit has an inclination angle i and is at an altitude that leads to n orbits per day. We denote this length $L(LAT_1,LAT_2; i,n)$.

First consider Figure G.1, which depicts the geometry of a track ascending from the southeast to the northwest, if the earth did not rotate beneath the satellite. Consider the point where the ground track crosses the equator as the reference point. Based on Snyder (1981), one can show that the longitude at which the satellite would cross some latitude LAT_j is:

$$LONG(LAT_j) = \sin^{-1} [\tan(LAT_j) \cot(p-i)] \quad (G.1)$$

where i is the inclination angle (in radians) of the orbit.

The angle $\lambda(LAT_j)$, in radians, subtended by the arc of the satellite track between the reference point at the equator and the point where the satellite crosses latitude LAT_i is (Snyder , 1981):

$$l(LAT_j) = \sin^{-1} [\sin(LAT_j) / \sin(p-i)] \quad (G.2)$$

where i is the inclination angle of the orbit. The angle $l(LAT_j,LAT_1)$, in radians, subtended by the arc of the satellite track between the points where the satellite crosses latitudes LAT_1 and LAT_j, then, is:

$$l(LAT_j,LAT_1) = l(LAT_j) - l(LAT_1) \quad (G.3)$$

where $l(LAT_j)$ and $l(LAT_1)$ can be found from equation (G.2).

We now need to consider the rotation of the earth during the time that the satellite was covering the arc of its track between LAT_1 and LAT_j. The time $t(LAT_j,LAT_1)$ that it would take the satellite to cover this arc would be the length of the arc on the ground, $l(LAT_j,LAT_1)*R$ (where R is the radius of the earth), divided by the speed of the satellite on the ground V_{sg}:

$$t(LAT_j,LAT_1) = l(LAT_j,LAT_1)*R / V_{sg} \quad (G.4)$$

Using R = 6371 km as the mean radius of the earth (Light, 1992a), and $V_{sg} = 0.4633*n$ [km/sec], where n is the number of orbits per day (see Eq. (4.5)), and converting to minutes, the time becomes:

$$t(LAT_j,LAT_1) = 229.2*l(LAT_j,LAT_1) / n \text{ [mins]} \quad (G.5)$$

At latitude LAT_j, the earth rotates at a speed:

$$v^{er}_j = 2*p*R*\cos(LAT_j) / 1440 \quad (G.6)$$

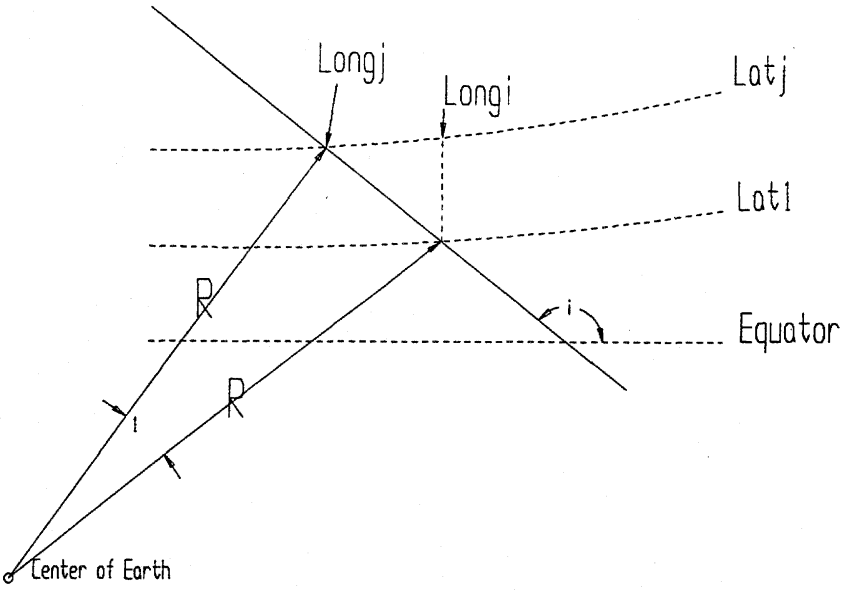

Figure G.1 Satellite track when earth does not rotate

where R is the radius of the earth, and dividing by 1440 puts v^{er}_j in units of R per minute. The distance that the earth rotates at latitude LAT_j while the satellite travels between LAT_1 and LAT_j, which we denote by $d^{er}(LAT_j; LAT_j,LAT_1)$, would be the time it took to travel this distance times the velocity of the earth's rotation. Therefore, multiplying Eq. (G.5) by Eq. (G.6), we get:

$$\begin{aligned} d^{er}(LAT_j; LAT_j,LAT_1) &= 229.2*l(LAT_j,LAT_1) * 2*p*R*\cos(LAT_j) / (1440*n) \\ &= R*\cos(LAT_j)*l(LAT_j,LAT_1) / n \end{aligned} \quad (G.7)$$

This gives the distance in units of R that would be added along LAT_j to $LONG_j$ in Figure G.1 due to the earth's rotation to determine the location where the satellite would cross latitude LAT_j. To determine the number of radians that would need to be added along LAT_j, we divide (G.7) by $R*\cos(LAT_j)$ – i.e.,. the radius at LAT_j. Calling this number of radians the "offset" at latitude LAT_j while the satellite travels from LAT_1 to LAT_j, and denoting this $OFF(LAT_j; LAT_j,LAT_1)$, we have:

$$OFF(LAT_j; LAT_j,LAT_1) = l(LAT_j,LAT_1) / n \quad (G.8)$$

We illustrate this longitudinal offset in Figure G.2.

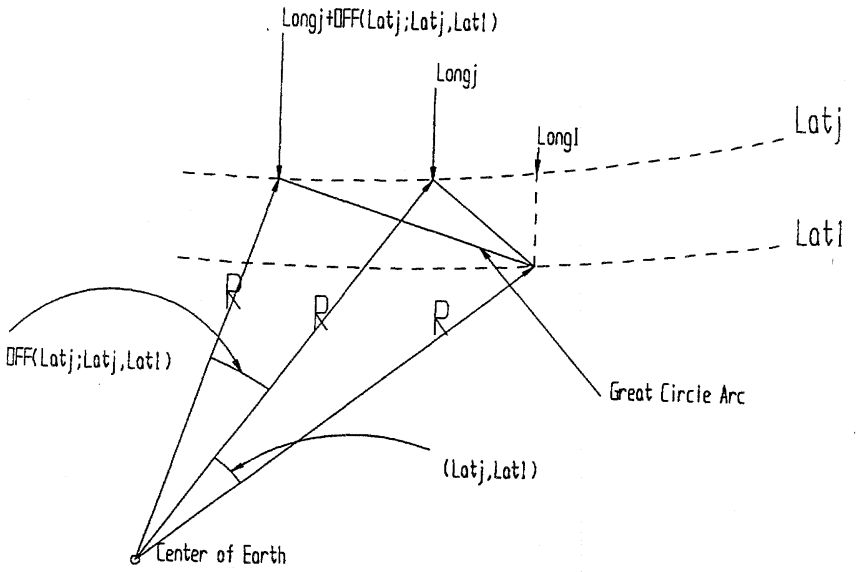

Figure G.2 Longitude offset due to earth rotation

As illustrated in Figure G.2, we can then approximate the length of the satellite track between LAT_1 and LAT_j by taking the great circle arc length between the point where the satellite would cross LAT_1 – i.e., the point whose longitude is $LONG_1$ and latitude is LAT_1 – and the point where the satellite would cross LAT_j – i.e., the point whose longitude is $LONG_j + OFF(LAT_j; LAT_j,LAT_1)$. The error in this approximation decreases as LAT_j becomes closer to LAT_1. The great circle *GC* arc length between points (X_1,Y_1) and (X_2,Y_2),where *X* depicts longitude and *Y* depicts latitude is (Robinson *et al.*, 1984):

$$GC[(X_1,Y_1),(X_2,Y_2)]=R*\cos^{-1}[\cos(Y_2)\cos(Y_1)\cos(X_2-X_1)+\sin(Y_1)\sin(Y_2)] \quad (G.9)$$

where *R* is again the radius of the earth, and the arc length is given in units of *R*.

To determine the length of the satellite track between two latitudes LAT_1 and LAT_2, then we use the following procedure:

STEP 0. Choose the inclination angle of the satellite orbit *i*. Choose the altitude of the orbit *H* and from Eq. (F.6) determine the number of orbits per day *n*. Choose a suitably small increment in latitude *DLAT*. Set $k = 0$, $L_0 = 0$ and $LAT_0 = LAT_1$.

STEP 1. Compute $LAT_{k+1} = LAT_k + DLAT$.

STEP 2. Calculate $OFF = OFF(LAT_{k+1}; LAT_{k+1},LAT_k)$ using Eq. (G.2), (G.3) and (G.8).

STEP 3. Calculate $x_1 = \text{LONG}(\text{LAT}_k)$ and $x_2 = \text{LONG}(\text{LAT}_{k+1})$ using Eq. (G.1).

STEP 4: Set $X_1 = x_1$ and $X_2 = x_2 + \text{OFF}$.

STEP 5: Calculate $\text{DL} = \text{GC}[(X_1,\text{LAT}_k),(X_2,\text{LAT}_{k+1})]$ using Eq. (G.9).

STEP 6: Set $L_k = L_k + \text{DL}$.

STEP 7: If $\text{LAT}_k \geq \text{LAT}_2$, set $L(\text{LAT}_1,\text{LAT}_2;i,n) = L_k$. If not, set $k = k+1$, and return to STEP 1.

For calculating the length of track for our approximation of the continental U.S., we used $\text{LAT}_1 = 25°\text{N}$, $\text{LAT}_2 = 50°\text{N}$, and $\text{DLAT} = 5°$. We experimented with the sensitivity of the approximation to the value of *DLAT* at various values of *i* and *n*. We used a very small increment for D*LAT*, namely $\text{DLAT} = 0.5°$ as an approximation of the true value. When we used $\text{DLAT} = 5°$, the length of the arc never differed from the approximation of the true value by more than 0.1%.

APPENDIX H

Solving Program (P2)

Appendix H. Solving Program (P2)

To approximate the maximum percentage of highways that could be imaged per day in the continental U.S. for given values of f_{npgt}, *RES, i,* $PPAL_{max}$, $(DTR*COMP)_{max}$ and FL_{max}, we saw in Section 4.4 that we could solve the following nonlinear program for given values of *RES, i,* $PPAL_{max}$, $(DTR*COMP)_{max}$, and FL_{max}:

Maximize: $PID_{US'} = n * PPAL * L(25,50; i,n)$
n, PPAL

subject to:

$$
\begin{aligned}
&PPAL \leq PPAL_{max} && \text{(a)}\\
&PPAL \leq 2.698*(DTR*COMP)_{max}*RES*10^2/n && \text{(b)}\\
&n \leq 15.6 && \text{(c)}\\
&n \geq 8{,}651{,}665.8/(FL_{max}*RES*10^2+6371)^{1.5} && \text{(d)}\\
&PPAL \geq 0 && \text{(e)}\\
&n \geq 0. && \text{(f)}
\end{aligned}
$$

(P2)

To solve (P2) first note that constraints (c) and (d) require the following condition:

$$8{,}651{,}665.8/(FL_{max}*RES*10^2+6371)^{1.5} \leq n \leq 15.6. \qquad \text{(H.1)}$$

To ensure a feasible solution, we would, therefore, need to ensure that $8{,}651{,}665.8 / (FL_{max}*RES*10^2+6371)^{1.5} \leq 15.6$, or $3.79 \leq FL_{max} * RES$. Our analysis was conducted for $FL_{max} \geq 6$ m when RES ≥ 1.0 m and $FL_{max} \geq 8$ m and RES = 0.5 m. Therefore, Condition (G.1) is satisfied. Moreover, since the right hand side of constraint (d) is strictly positive when FL_{max} and *RES* are strictly positive, which would be the case for realistic remote sensing systems, this constraint will require that *n* is greater than 0. Constraint (f) is, therefore, redundant and can be eliminated.

Next, note that the right hand side of constraint (b) – namely, $2.698*(DTR*COMP)_{max}*RES*10^2/n$ – decreases monotonically in *n*. Moreover, it is strictly positive when $(DTR*COMP)_{max}$, *RES,* and *n* are all strictly positive, which would be the case for any remote sensing system. Therefore, when considered in the *n x PPAL* decision variable space, the trace of the right hand side of constraint (b) would always lie above the PPAL = 0 axis and either: i) lie entirely above the trace of constraint (a); ii) lie entirely below the trace of constraint (a); or iii) intersect the trace of constraint (a) at exactly one point. These three possibilities, therefore, lead to the three cases for the feasible region shown in Figure H.1a-c, which we denote Cases 1-3, respectively. In Figure H.1, we use:

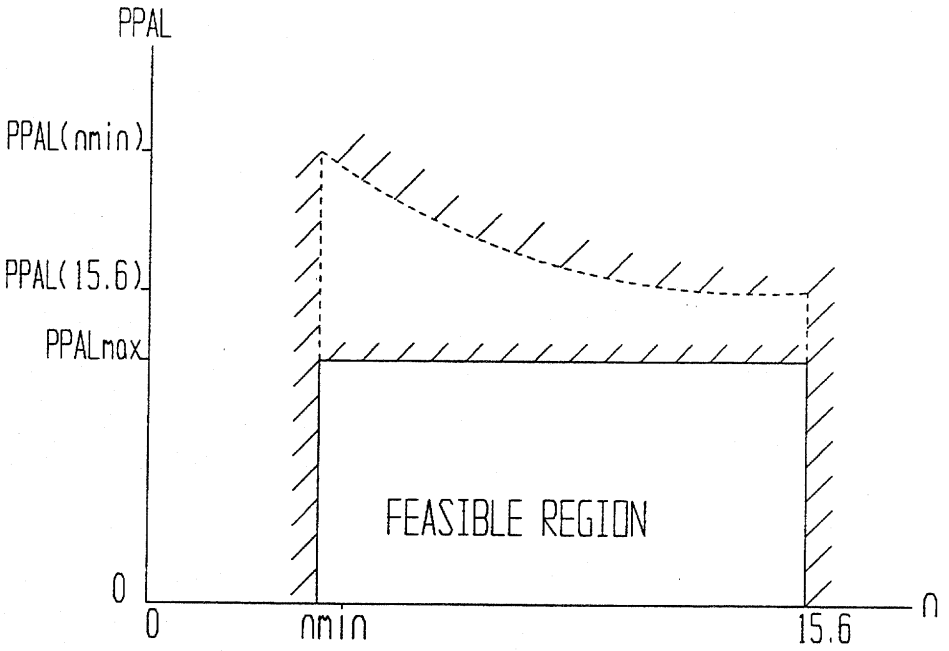

a. Case 1

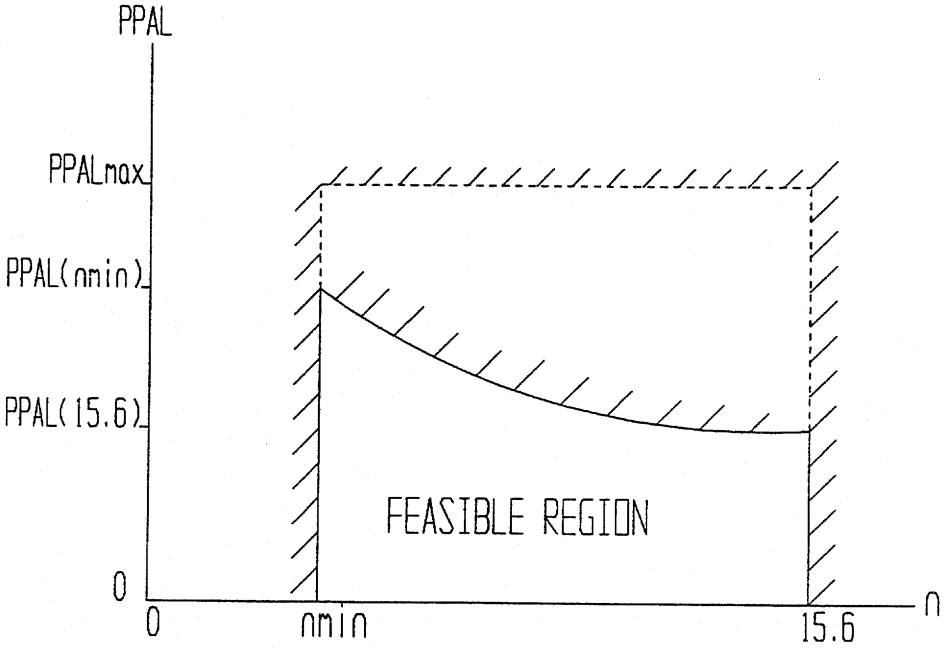

b. Case 2

Figure H.1 Possible cases for feasible region of program (P2)

Figure H.1 (continued)

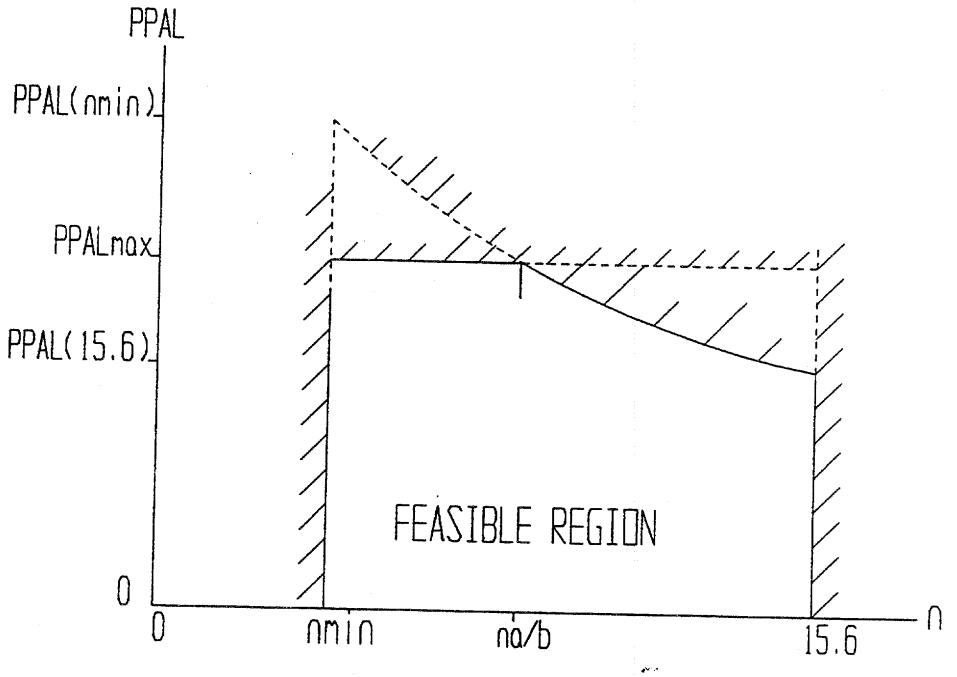

c. Case 3

i) n_{min} to denote the right hand side of constraint (d) – i.e.,
$n_{min} = 8{,}651{,}665.8 / (FL_{max}*RES*10^2+6371)^{1.5}$;

ii) $PPAL(n_{min})$ to denote the value of the right hand side of constraint (b) evaluated at $n = n_{min}$ – i.e.,
$PPAL(n_{min}) = 2.698*(DTR*COMP)_{max}*RES*10^2/n_{min}$;

iii) *PPAL(15.6)* to denote the value of the right hand side of constraint (b) evaluated at n = 15.6 – i.e.,
$PPAL(15.6)=2.698*(DTR*COMP)_{max}*RES*10^2/15.6$;

iv) $n_{a/b}$ to denote the value of *n* at which constraints (a) and (b) intersect.

Next note that for a given value of *n*, the objective function of Program (P2) is maximized by maximizing *PPAL*. This restricts the search from the two-dimensional feasible regions shown in Figure G.1a-c to one-dimensional searches along the traces of the greatest feasible *PPAL's* shown in the figures. We now consider the cases individually.

Case 1: In Case 1, constraint (b) will be nonbinding and does not need to be considered. Given that the optimal solution occurs at the greatest feasible *PPAL* value for a given *n*, (P2) becomes:

$$\text{Max: } \underset{n}{} PPAL_{max} * n * L(25,50; i,n)$$

$$\text{subject to: } n_{min} \leq n \leq 15.6. \qquad \text{(P2.1)}$$

All other things being equal, *L(25,50; i,n)* decreases in *n*. This can be shown mathematically by considering the algorithm used to determine *L(25,50; i,n)* presented in Appendix G. Intuitively, *n* increases because the speed of the satellite increases. Therefore, the time for the satellite to cover the distance between 25°N and 50°N decreases, and the earth does not rotate as far. This decreases the longitudinal offset of the satellite and, thus, the length of the ground track between the two latitudes. Since *L(25,50; i,n)* decreases in *n*, it is not obvious whether n * L(25,50; i,n) (and, therefore, the objective function) increases or decreases in *n*. Numerically, we found that this product increases in *n* for values of *n* and *i* considered in our analysis. (This means that the effect of having more orbits per day outweighs the effect of having longer tracks per orbit within the continental U.S.) This result implies that we should maximize *n*. The optimal solution in Case 1, therefore, occurs at n = 15.6, PPAL = $PPAL_{max}$, and the corresponding optimal value of $PID_{US'}$ is $PID_{US'}^* = 15.6 * PPAL_{max} * L(25,50; i,15.6)$.

Case 2: In Case 2, constraint (a) will be nonbinding and does not need to be considered. Given that the optimal solution occurs at the greatest feasible *PPAL* value for a given *n*, the solution will occur along the trace of the right hand side of constraint (b), i.e., at PPAL = $2.698 * (DTR*COMP)_{max} * RES * 10^2/n$. Substituting this for *PPAL* in the objective function, Program (P2), therefore becomes:

$$\text{Max: } \underset{n}{} n*\{2.698*(DTR*COMP)_{max}*RES*10^2/n\}*L(25,50; i,n)$$

$$= 2.698 *(DTR*COMP)_{max} * RES *10^2 * L(25,50; i,n)$$

$$\text{subject to: } n_{min} \leq n \leq 15.6. \qquad \text{(P2.2a)}$$

As explained when discussing Case 1, *L(25,50; i,n)* decreases in *n*. Therefore, the objective function is maximized at $n = n_{min}$. (This means that the effects on coverage of increasing the swath width by increasing the number of pixels per scan line and increasing the length of the ground track per orbit outweigh the effect of increasing the number of orbits per day.) The optimal solution in Case 2, therefore, occurs at $n = n_{min}$, PPAL = $PPAL(n_{min})$, and the corresponding optimal value of $PID_{US'}$ is $PID_{US'}^* = n_{min} * PPAL(n_{min}) * L(25,50; i,n_{min})$.

Case 3: In Case 3, constraint (a) will be nonbinding for $n > n_{a/b}$ and constraint (b) will be nonbinding for $n < n_{a/b}$. Given that the optimal solution occurs at the greatest feasible *PPAL* value for a given *n*, the solution will occur along the trace of constraint (a) – i.e., at PPAL = $PPAL_{max}$ – for $n \leq n_{a/b}$, and along the trace of constraint (b) – i.e., at

PPAL = 2.698 * $(DTR*COMP)_{max}$ * RES * $10^2/n$ – for $n \geq n_{a/b}$. As explained when discussing Case 1, for values of *n* and *i* considered in our analysis, the objective function increases with increasing values of *n* when *PPAL* is fixed at a constant value. Therefore, for $n_{min} \leq n \leq n_{a/b}$, the objective function is maximized at $n = n_{a/b}$ and $PPAL = PPAL_{max}$. As explained when discussing Case 2, the objective function increases with decreasing values of *n* when the solution is constrained to occur along the trace of constraint (b). Therefore, for $n_{a/b} \leq n \leq 15.6$, the objective function is also maximized at $n = n_{a/b}$ and $PPAL = PPAL_{max}$. The global maximum, therefore, occurs at this point. The optimal solution in Case 3, therefore, occurs at $n = n_{a/b}$, $PPAL = PPAL_{max}$, and the corresponding optimal value of $PID_{US'}$ is $PID_{US'}^* = PPAL_{max} * n_{a/b} * L(25,50; i,n_{a/b})$.

In summary, Program (P2) can be solved by first calculating $PPAL(n_{min})$ and PPAL(15.6) and comparing these values to $PPAL_{max}$ to determine whether the problem corresponds to Case 1, Case 2, or Case 3. If the problem corresponds to Case 1, use the algorithm presented in Appendix G to calculate *L(25,50; i,15.6)*, and find the optimal solution as $(n, PPAL, PID_{US'}) = (15.6, PPAL_{max}, 15.6 * PPAL_{max} * L(25,50; i,15.6))$. If the problem corresponds to Case 2, use the algorithm presented in Appendix G to calculate $L(25,50; i,n_{min})$, and find the optimal solution as $(n, PPAL, PID_{US'}) = (n_{min}, PPAL(n_{min}), n_{min} * PPAL(n_{min}) * L(25,50; i,n_{min}))$. If the problem corresponds to Case 3, find the value of $n_{a/b}$ ($n_{a/b} = 2.698 * (DTR*COMP)_{max} * RES * 10^2 / PPAL_{max}$), use the algorithm presented in Appendix G to calculate $L(25,50; i,n_{a/b})$, and find the optimal solution as $(n, PPAL, PID_{US'}) = (n_{a/b}, PPAL_{max}, PPAL_{max} * n_{a/b} * L(25,50; i,n_{a/b}))$.

APPENDIX I

Listing of Fortran Language Computer Code Used to Solve Program (P2)

```
!  File fl_area.f
!234567890!234567890!234567890!234567890!234567890!234567890!234567890
        program  fl_dtr_area
!234567890!234567890!234567890!234567890!234567890!234567890!234567890
      implicit none
      integer case,icase(4,3),k,j,jj,kk,ress
      double precision pi
      real  R,H,lat1,lat2,i,ppal,ppalmax,ppaln,res,delta,nmax,nmin
      real  na_b,i_r,sw,sw_p_r,a_lat1_2
      real  comp_DTR,FLmax,pwpd
      real  area_11,area_tot,p_area
      real  areat(4,3),areap(4,3),nn(4,3),hh(4,3)

      data  R,pi,j,k/ 6371.0,3.14159265358979323 85,0,0/
      data  lat1,lat2,delta,pwpd/25.,50.,5.,10./

      nmax = 15.6
      a_lat1_2=2*pi*(R**2)*(sind(lat2)-sind(lat1))
      open(unit= 3, file=  'fl.dat')

        do i = 100., 130., 15.
        if (i.le.129.99999)then
           i_r  = i*pi/180.0
        else
           i_r  = (i-.00001)*pi/180.0
        end if
        do ppalmax=15000.,30000.,5000.
        do ress=1,4
         if (ress.eq.1) Res = .5
         if (ress.eq.2) Res = 1.0
         if (ress.eq.3) Res = 2.0
         if (ress.eq.4) Res = 4.0
         write(3,200)ppalmax ,res,i
         do comp_DTR = 400.,1600.,400.
          k = k+1
          j = 0
          do FLmax = 6.,14.,4.
                j= j+1
                H =  FLmax*res*1000./pwpd
             if(H.lt.400) then
               case = 0
               area_tot = 0.
               p_area   = 0.
             else
                nmin=8681665.8*(pwpd/(FLmax*res*1000+pwpd*R))**1.5
                call  checkcase(comp_DTR,Res,ppalmax,15.6,nmin,case)
                if (case.eq.2)then
                   ppaln= comp_DTR*Res*1000/(3.7064*nmin)
                   sw_p_r=    ppaln *res/ 1000.
                   call area(lat1,lat2,delta,sw_p_r,i_r,nmin,pi,R,
     +               a_lat1_2, p_area,area_tot,area_11)
                   nn(k,j) = nmin
```

```
              else if (case.eq.1)then
                 sw_p_r=   ppalmax * res /1000.
                 call area(lat1,lat2,delta,sw_p_r,i_r,15.6,pi,R,
     +             a_lat1_2, p_area,area_tot,area_11)
                 nn(k,j) = nmin
              else if (case.eq.3)then
                 na_b = comp_DTR*Res*1000/(3.7064*ppalmax)
                 sw_p_r= ppalmax * res /1000.
                 call area(lat1,lat2,delta,sw_p_r,i_r,na_b,pi,R,
     +              a_lat1_2, p_area,area_tot,area_11)
                 nn(k,j) = na_b
              end if
            end if
              areat(k,j)=area_tot
              areap(k,j)=p_area
              icase(k,j)= case
         end do
       end do
         write(3,180)
         do kk = 1,k
          write(3,220)(areap(kk,jj),icase(kk,jj),jj=1,j)
         end do
         j = 0
         k = 0
       end do
       end do
       end do
180    format(15x,'% Area (case #)   ',
     +   //,'          FL-6          FL-10          FL-14 '/,
     +    3x  ,3('  ------------'))  ! ,2x,3(' ---'))
200    format(50('-')//,'This is for the case of ' /,
     +   'ppalmax     = ',f6.0,
     + /'Resolution  = ',f3.1,/'inclination = ',f5.1/)
220    format(4x,3(f8.4,'(',i1,')',4x))   !,2x,3(i1,3x))
       stop
       end
!234567890!234567890!234567890!234567890!234567890!234567890!234567890
       subroutine checkcase(comp_DTR,Res,ppalmax,nmax,nmin,case)
!234567890!234567890!234567890!234567890!234567890!234567890!234567890
       implicit none
       integer case
       real comp_DTR,Res,ppalmax,nmax,nmin
       real ppal_nmin,ppal_nmax,ppal,nn,r,c_dtr
       ppal_nmin = comp_DTR*Res*1000/(3.7064*nmin)
       ppal_nmax = comp_DTR*Res*1000/(3.7064*nmax)
         if(ppal_nmin.le.ppalmax)then
                 case =2
         else if(ppal_nmax.ge.ppalmax)then
                 case = 1
         else
                 case = 3
         end if
       return
       end
```

```
!234567890!234567890!234567890!234567890!234567890!234567890!234567890
      subroutine area(lat1,lat2,delta,sw,i_r,n,pi,R,
     +                a_lat1_2, p_area,area_tot,area_1l)
!234567890!234567890!234567890!234567890!234567890!234567890!234567890
      implicit none
      double precision pi
      real  lat1,lat2,delta,sw,i_r,n,R,a_lat1_2
      real  p_area,area_tot,area_1l
      real  lat,lat_2,l2_r,l_r,off
      real  lo1,lo2,theta,deltal,L
       L= 0.
      do lat =lat1,lat2-delta,delta
        lat_2= lat+delta
        l2_r= lat_2*pi/180.0
        l_r = lat*pi/180.0
        call offset(l2_r,l_r,i_r,n,pi,off)
        lo1 = asin(tan(l_r)/tan(pi-i_r))
        lo2 =(asin(tan(l2_r)/tan(pi-i_r)))+off
        theta= cos(l_r)*cos(l2_r)*cos(lo2-lo1)+sin(l_r)*sin(l2_r)
        deltal= acos(theta)*R
        L= L +deltal
      end do
      area_1l = L *sw
      area_tot = area_1l * n
       p_area  = (area_tot/a_lat1_2)*100.0
      return
      end
!234567890!234567890!234567890!234567890!234567890!234567890!234567890
      subroutine offset(latj,lati,i_r,n,pi,off)
      implicit none
      double precision pi,lambdai,lambdaj, lambda_ij
      real  latj,lati,i_r,n,off,off1
        lambdaj= asin(sin(latj)/sin(pi-i_r))
        lambdai= asin(sin(lati)/sin(pi-i_r))
        lambda_ij=(lambdaj-lambdai)
        off = lambda_ij/n
        off1 = (lambda_ij*180./pi)/n
      return
      end
!*****************************************************
```

APPENDIX J

Objective Function Values, in Terms of $PID_{US}/(1-f_c)$, for 576 Combinations of Input Combinations of Input Parameter Values in Table 4.1

This is for the case of
ppalmax = 15000.
Resolution = 0.5
inclination = 100.0

% Area (case #)

DTR*comp/	*FL-8	FL-10	FL-14
400	0.0890(1)	0.0890(2)	0.0890(2)
800	0.1779(1)	0.1780(2)	0.1781(2)
1200	0.2669(1)	0.2669(2)	0.2671(2)
1600	0.3558(1)	0.3559(2)	0.3561(2)

This is for the case of
ppalmax = 15000.
Resolution = 1.0
inclination = 100.0

% Area (case #)

DTR*comp/	FL-6	FL-10	FL-14
400	0.3560(2)	0.3565(2)	0.3569(2)
800	0.7121(2)	0.7124(3)	0.7124(3)
1200	0.7715(1)	0.7715(1)	0.7715(1)
1600	0.7715(1)	0.7715(1)	0.7715(1)

This is for the case of
ppalmax = 15000.
Resolution = 2.0
inclination = 100.0

% Area (case #)

DTR*comp/	FL-6	FL-10	FL-14
400	1.4248(3)	1.4248(3)	1.4248(3)
800	1.5430(1)	1.5430(1)	1.5430(1)
1200	1.5430(1)	1.5430(1)	1.5430(1)
1600	1.5430(1)	1.5430(1)	1.5430(1)

This is for the case of
ppalmax = 15000.
Resolution = 4.0
inclination = 100.0

% Area (case #)

DTR*comp/	FL-6	FL-10	FL-14
400	3.0859(1)	3.0859(1)	3.0859(1)
800	3.0859(1)	3.0859(1)	3.0859(1)
1200	3.0859(1)	3.0859(1)	3.0859(1)
1600	3.0859(1)	3.0859(1)	3.0859(1)

This is for the case of
ppalmax = 20000.
Resolution = 0.5
inclination = 100.0

% Area (case #)

DTR*comp/	*FL-8	FL-10	FL-14
400	0.0890(1)	0.0890(2)	0.0890(2)
800	0.1779(1)	0.1780(2)	0.1781(2)
1200	0.2669(1)	0.2669(2)	0.2671(2)
1600	0.3558(1)	0.3559(2)	0.3561(2)

This is for the case of
ppalmax = 20000.
Resolution = 1.0
inclination = 100.0

% Area (case #)

DTR*comp/	FL-6	FL-10	FL-14
400	0.3560(2)	0.3565(2)	0.3569(2)
800	0.7121(2)	0.7129(2)	0.7139(2)
1200	1.0286(1)	1.0286(1)	1.0286(1)
1600	1.0286(1)	1.0286(1)	1.0286(1)

This is for the case of
ppalmax = 20000.
Resolution = 2.0
inclination = 100.0

% Area (case #)

DTR*comp/	FL-6	FL-10	FL-14
400	1.4268(2)	1.4306(2)	1.4320(3)
800	2.0573(1)	2.0573(1)	2.0573(1)
1200	2.0573(1)	2.0573(1)	2.0573(1)
1600	2.0573(1)	2.0573(1)	2.0573(1)

This is for the case of
ppalmax = 20000.
Resolution = 4.0
inclination = 100.0

% Area (case #)

DTR*comp/	FL-6	FL-10	FL-14
400	4.1146(1)	4.1146(1)	4.1146(1)
800	4.1146(1)	4.1146(1)	4.1146(1)
1200	4.1146(1)	4.1146(1)	4.1146(1)
1600	4.1146(1)	4.1146(1)	4.1146(1)

This is for the case of
ppalmax = 25000.
Resolution = 0.5
inclination = 100.0

% Area (case #)

DTR*comp/	*FL-8	FL-10	FL-14
400	0.0890(1)	0.0890(2)	0.0890(2)
800	0.1779(1)	0.1780(2)	0.1781(2)
1200	0.2669(1)	0.2669(2)	0.2671(2)
1600	0.3558(1)	0.3559(2)	0.3561(2)

This is for the case of
ppalmax = 25000.
Resolution = 1.0
inclination = 100.0

% Area (case #)

DTR*comp/	FL-6	FL-10	FL-14
400	0.3560(2)	0.3565(2)	0.3569(2)
800	0.7121(2)	0.7129(2)	0.7139(2)
1200	1.0681(2)	1.0694(2)	1.0704(3)
1600	1.2858(1)	1.2858(1)	1.2858(1)

This is for the case of
ppalmax = 25000.
Resolution = 2.0
inclination = 100.0

% Area (case #)

DTR*comp/	FL-6	FL-10	FL-14
400	1.4268(2)	1.4306(2)	1.4348(2)
800	2.5716(1)	2.5716(1)	2.5716(1)
1200	2.5716(1)	2.5716(1)	2.5716(1)
1600	2.5716(1)	2.5716(1)	2.5716(1)

This is for the case of
ppalmax = 25000.
Resolution = 4.0
inclination = 100.0

% Area (case #)

DTR*comp/	FL-6	FL-10	FL-14
400	5.1432(1)	5.1432(1)	5.1432(1)
800	5.1432(1)	5.1432(1)	5.1432(1)
1200	5.1432(1)	5.1432(1)	5.1432(1)
1600	5.1432(1)	5.1432(1)	5.1432(1)

This is for the case of
ppalmax = 30000.
Resolution = 0.5
inclination = 100.0

% Area (case #)

DTR*comp/	*FL-8	FL-10	FL-14
400	0.0890(1)	0.0890(2)	0.0890(2)
800	0.1779(1)	0.1780(2)	0.1781(2)
1200	0.2669(1)	0.2669(2)	0.2671(2)
1600	0.3558(1)	0.3559(2)	0.3561(2)

This is for the case of
ppalmax = 30000.
Resolution = 1.0
inclination = 100.0

% Area (case #)

DTR*comp/	FL-6	FL-10	FL-14
400	0.3560(2)	0.3565(2)	0.3569(2)
800	0.7121(2)	0.7129(2)	0.7139(2)
1200	1.0681(2)	1.0694(2)	1.0708(2)
1600	1.4241(2)	1.4248(3)	1.4248(3)

This is for the case of
ppalmax = 30000.
Resolution = 2.0
inclination = 100.0

% Area (case #)

DTR*comp/	FL-6	FL-10	FL-14
400	1.4268(2)	1.4306(2)	1.4348(2)
800	2.8497(3)	2.8497(3)	2.8497(3)
1200	3.0859(1)	3.0859(1)	3.0859(1)
1600	3.0859(1)	3.0859(1)	3.0859(1)

This is for the case of
ppalmax = 30000.
Resolution = 4.0
inclination = 100.0

% Area (case #)

DTR*comp/	FL-6	FL-10	FL-14
400	5.6994(3)	5.6994(3)	5.6994(3)
800	6.1718(1)	6.1718(1)	6.1718(1)
1200	6.1718(1)	6.1718(1)	6.1718(1)
1600	6.1718(1)	6.1718(1)	6.1718(1)

This is for the case of
ppalmax = 15000.
Resolution = 0.5
inclination = 115.0

% Area (case #)

DTR*comp/	*FL-8	FL-10	FL-14
400	0.1053(1)	0.1054(2)	0.1055(2)
800	0.2106(1)	0.2107(2)	0.2110(2)
1200	0.3159(1)	0.3161(2)	0.3165(2)
1600	0.4212(1)	0.4214(2)	0.4220(2)

This is for the case of
ppalmax = 15000.
Resolution = 1.0
inclination = 115.0

% Area (case #)

DTR*comp/	FL-6	FL-10	FL-14
400	0.4217(2)	0.4228(2)	0.4239(2)
800	0.8434(2)	0.8443(3)	0.8443(3)
1200	0.9132(1)	0.9132(1)	0.9132(1)
1600	0.9132(1)	0.9132(1)	0.9132(1)

This is for the case of
ppalmax = 15000.
Resolution = 2.0
inclination = 115.0

% Area (case #)

DTR*comp/	FL-6	FL-10	FL-14
400	1.6886(3)	1.6886(3)	1.6886(3)
800	1.8264(1)	1.8264(1)	1.8264(1)
1200	1.8264(1)	1.8264(1)	1.8264(1)
1600	1.8264(1)	1.8264(1)	1.8264(1)

This is for the case of
ppalmax = 15000.
Resolution = 4.0
inclination = 115.0

% Area (case #)

DTR*comp/	FL-6	FL-10	FL-14
400	3.6527(1)	3.6527(1)	3.6527(1)
800	3.6527(1)	3.6527(1)	3.6527(1)
1200	3.6527(1)	3.6527(1)	3.6527(1)
1600	3.6527(1)	3.6527(1)	3.6527(1)

This is for the case of
ppalmax = 20000.
Resolution = 0.5
inclination = 115.0

% Area (case #)

DTR*comp/	*FL-8	FL-10	FL-14
400	0.1053(1)	0.1054(2)	0.1055(2)
800	0.2106(1)	0.2107(2)	0.2110(2)
1200	0.3159(1)	0.3161(2)	0.3165(2)
1600	0.4212(1)	0.4214(2)	0.4220(2)

This is for the case of
ppalmax = 20000.
Resolution = 1.0
inclination = 115.0

% Area (case #)

DTR*comp/	FL-6	FL-10	FL-14
400	0.4217(2)	0.4228(2)	0.4239(2)
800	0.8434(2)	0.8456(2)	0.8478(2)
1200	1.2176(1)	1.2176(1)	1.2176(1)
1600	1.2176(1)	1.2176(1)	1.2176(1)

This is for the case of
ppalmax = 20000.
Resolution = 2.0
inclination = 115.0

% Area (case #)

DTR*comp/	FL-6	FL-10	FL-14
400	1.6934(2)	1.7026(2)	1.7060(3)
800	2.4352(1)	2.4352(1)	2.4352(1)
1200	2.4352(1)	2.4352(1)	2.4352(1)
1600	2.4352(1)	2.4352(1)	2.4352(1)

This is for the case of
ppalmax = 20000.
Resolution = 4.0
inclination = 115.0

% Area (case #)

DTR*comp/	FL-6	FL-10	FL-14
400	4.8703(1)	4.8703(1)	4.8703(1)
800	4.8703(1)	4.8703(1)	4.8703(1)
1200	4.8703(1)	4.8703(1)	4.8703(1)
1600	4.8703(1)	4.8703(1)	4.8703(1)

This is for the case of
ppalmax = 25000.
Resolution = 0.5
inclination = 115.0

% Area (case #)

DTR*comp/	*FL-8	FL-10	FL-14
400	0.1053(1)	0.1054(2)	0.1055(2)
800	0.2106(1)	0.2107(2)	0.2110(2)
1200	0.3159(1)	0.3161(2)	0.3165(2)
1600	0.4212(1)	0.4214(2)	0.4220(2)

This is for the case of
ppalmax = 25000.
Resolution = 1.0
inclination = 115.0

% Area (case #)

DTR*comp/	FL-6	FL-10	FL-14
400	0.4217(2)	0.4228(2)	0.4239(2)
800	0.8434(2)	0.8456(2)	0.8478(2)
1200	1.2651(2)	1.2684(2)	1.2708(3)
1600	1.5220(1)	1.5220(1)	1.5220(1)

This is for the case of
ppalmax = 25000.
Resolution = 2.0
inclination = 115.0

% Area (case #)

DTR*comp/	FL-6	FL-10	FL-14
400	1.6934(2)	1.7026(2)	1.7124(2)
800	3.0440(1)	3.0440(1)	3.0440(1)
1200	3.0440(1)	3.0440(1)	3.0440(1)
1600	3.0440(1)	3.0440(1)	3.0440(1)

This is for the case of
ppalmax = 25000.
Resolution = 4.0
inclination = 115.0

% Area (case #)

DTR*comp/	FL-6	FL-10	FL-14
400	6.0879(1)	6.0879(1)	6.0879(1)
800	6.0879(1)	6.0879(1)	6.0879(1)
1200	6.0879(1)	6.0879(1)	6.0879(1)
1600	6.0879(1)	6.0879(1)	6.0879(1)

This is for the case of
ppalmax = 30000.
Resolution = 0.5
inclination = 115.0

% Area (case #)

DTR*comp/	*FL-8	FL-10	FL-14
400	0.1053(1)	0.1054(2)	0.1055(2)
800	0.2106(1)	0.2107(2)	0.2110(2)
1200	0.3159(1)	0.3161(2)	0.3165(2)
1600	0.4212(1)	0.4214(2)	0.4220(2)

This is for the case of
ppalmax = 30000.
Resolution = 1.0
inclination = 115.0

% Area (case #)

DTR*comp/	FL-6	FL-10	FL-14
400	0.4217(2)	0.4228(2)	0.4239(2)
800	0.8434(2)	0.8456(2)	0.8478(2)
1200	1.2651(2)	1.2684(2)	1.2717(2)
1600	1.6868(2)	1.6886(3)	1.6886(3)

This is for the case of
ppalmax = 30000.
Resolution = 2.0
inclination = 115.0

% Area (case #)

DTR*comp/	FL-6	FL-10	FL-14
400	1.6934(2)	1.7026(2)	1.7124(2)
800	3.3773(3)	3.3773(3)	3.3773(3)
1200	3.6527(1)	3.6527(1)	3.6527(1)
1600	3.6527(1)	3.6527(1)	3.6527(1)

This is for the case of
ppalmax = 30000.
Resolution = 4.0
inclination = 115.0

% Area (case #)

DTR*comp/	FL-6	FL-10	FL-14
400	6.7546(3)	6.7546(3)	6.7546(3)
800	7.3055(1)	7.3055(1)	7.3055(1)
1200	7.3055(1)	7.3055(1)	7.3055(1)
1600	7.3055(1)	7.3055(1)	7.3055(1)

This is for the case of
ppalmax = 15000.
Resolution = 0.5
inclination = 130.0

% Area (case #)

DTR*comp/	*FL-8	FL-10	FL-14
400	0.2015(1)	0.2017(2)	0.2021(2)
800	0.4030(1)	0.4034(2)	0.4041(2)
1200	0.6045(1)	0.6051(2)	0.6062(2)
1600	0.8060(1)	0.8068(2)	0.8082(2)

This is for the case of
ppalmax = 15000.
Resolution = 1.0
inclination = 130.0

% Area (case #)

DTR*comp/	FL-6	FL-10	FL-14
400	0.8075(2)	0.8104(2)	0.8135(2)
800	1.6150(2)	1.6175(3)	1.6175(3)
1200	1.7476(1)	1.7476(1)	1.7476(1)
1600	1.7476(1)	1.7476(1)	1.7476(1)

This is for the case of
ppalmax = 15000.
Resolution = 2.0
inclination = 130.0

% Area (case #)

DTR*comp/	FL-6	FL-10	FL-14
400	3.2349(3)	3.2349(3)	3.2349(3)
800	3.4953(1)	3.4953(1)	3.4953(1)
1200	3.4953(1)	3.4953(1)	3.4953(1)
1600	3.4953(1)	3.4953(1)	3.4953(1)

This is for the case of
ppalmax = 15000.
Resolution = 4.0
inclination = 130.0

% Area (case #)

DTR*comp/	FL-6	FL-10	FL-14
400	6.9905(1)	6.9905(1)	6.9905(1)
800	6.9905(1)	6.9905(1)	6.9905(1)
1200	6.9905(1)	6.9905(1)	6.9905(1)
1600	6.9905(1)	6.9905(1)	6.9905(1)

This is for the case of
ppalmax = 20000.
Resolution = 0.5
inclination = 130.0

% Area (case #)

DTR*comp/	*FL-8	FL-10	FL-14
400	0.2015(1)	0.2017(2)	0.2021(2)
800	0.4030(1)	0.4034(2)	0.4041(2)
1200	0.6045(1)	0.6051(2)	0.6062(2)
1600	0.8060(1)	0.8068(2)	0.8082(2)

This is for the case of
ppalmax = 20000.
Resolution = 1.0
inclination = 130.0

% Area (case #)

DTR*comp/	FL-6	FL-10	FL-14
400	0.8075(2)	0.8104(2)	0.8135(2)
800	1.6150(2)	1.6209(2)	1.6270(2)
1200	2.3302(1)	2.3302(1)	2.3302(1)
1600	2.3302(1)	2.3302(1)	2.3302(1)

This is for the case of
ppalmax = 20000.
Resolution = 2.0
inclination = 130.0

% Area (case #)

DTR*comp/	FL-6	FL-10	FL-14
400	3.2478(2)	3.2728(2)	3.2818(3)
800	4.6603(1)	4.6603(1)	4.6603(1)
1200	4.6603(1)	4.6603(1)	4.6603(1)
1600	4.6603(1)	4.6603(1)	4.6603(1)

This is for the case of
ppalmax = 20000.
Resolution = 4.0
inclination = 130.0

% Area (case #)

DTR*comp/	FL-6	FL-10	FL-14
400	9.3207(1)	9.3207(1)	9.3207(1)
800	9.3207(1)	9.3207(1)	9.3207(1)
1200	9.3207(1)	9.3207(1)	9.3207(1)
1600	9.3207(1)	9.3207(1)	9.3207(1)

This is for the case of
ppalmax = 25000.
Resolution = 0.5
inclination = 130.0

% Area (case #)

DTR*comp/	*FL-8	FL-10	FL-14
400	0.2015(1)	0.2017(2)	0.2021(2)
800	0.4030(1)	0.4034(2)	0.4041(2)
1200	0.6045(1)	0.6051(2)	0.6062(2)
1600	0.8060(1)	0.8068(2)	0.8082(2)

This is for the case of
ppalmax = 25000.
Resolution = 1.0
inclination = 130.0

% Area (case #)

DTR*comp/	FL-6	FL-10	FL-14
400	0.8075(2)	0.8104(2)	0.8135(2)
800	1.6150(2)	1.6209(2)	1.6270(2)
1200	2.4225(2)	2.4313(2)	2.4379(3)
1600	2.9127(1)	2.9127(1)	2.9127(1)

This is for the case of
ppalmax = 25000.
Resolution = 2.0
inclination = 130.0

% Area (case #)

DTR*comp/	FL-6	FL-10	FL-14
400	3.2478(2)	3.2728(2)	3.2990(2)
800	5.8254(1)	5.8254(1)	5.8254(1)
1200	5.8254(1)	5.8254(1)	5.8254(1)
1600	5.8254(1)	5.8254(1)	5.8254(1)

This is for the case of
ppalmax = 25000.
Resolution = 4.0
inclination = 130.0

% Area (case #)

DTR*comp/	FL-6	FL-10	FL-14
400	11.6508(1)	11.6508(1)	11.6508(1)
800	11.6508(1)	11.6508(1)	11.6508(1)
1200	11.6508(1)	11.6508(1)	11.6508(1)
1600	11.6508(1)	11.6508(1)	11.6508(1)

This is for the case of
ppalmax = 30000.
Resolution = 0.5
inclination = 130.0

% Area (case #)

DTR*comp/	*FL-8	FL-10	FL-14
400	0.2015(1)	0.2017(2)	0.2021(2)
800	0.4030(1)	0.4034(2)	0.4041(2)
1200	0.6045(1)	0.6051(2)	0.6062(2)
1600	0.8060(1)	0.8068(2)	0.8082(2)

This is for the case of
ppalmax = 30000.
Resolution = 1.0
inclination = 130.0

% Area (case #)

DTR*comp/	FL-6	FL-10	FL-14
400	0.8075(2)	0.8104(2)	0.8135(2)
800	1.6150(2)	1.6209(2)	1.6270(2)
1200	2.4225(2)	2.4313(2)	2.4404(2)
1600	3.2300(2)	3.2349(3)	3.2349(3)

This is for the case of
ppalmax = 30000.
Resolution = 2.0
inclination = 130.0

% Area (case #)

DTR*comp/	FL-6	FL-10	FL-14
400	3.2478(2)	3.2728(2)	3.2990(2)
800	6.4698(3)	6.4698(3)	6.4698(3)
1200	6.9905(1)	6.9905(1)	6.9905(1)
1600	6.9905(1)	6.9905(1)	6.9905(1)

This is for the case of
ppalmax = 30000.
Resolution = 4.0
inclination = 130.0

% Area (case #)

DTR*comp/	FL-6	FL-10	FL-14
400	12.9397(3)	12.9397(3)	12.9397(3)
800	13.9810(1)	13.9810(1)	13.9810(1)
1200	13.9810(1)	13.9810(1)	13.9810(1)
1600	13.9810(1)	13.9810(1)	13.9810(1)